Advanced source modelling with particular reference to fault transients in power systems

Shokri-Kojori, Shokrollah

Award date:
1987

Awarding institution:
University of Bath

ADVANCED SOURCE MODELLING WITH PARTICULAR REFERENCE TO FAULT TRANSIENTS IN POWER SYSTEMS

Submitted by Shokrollah Shokri Kojori, BSc, MSc

for the degree of Doctor of Philosophy of the

University of Bath

1987

COPYRIGHT

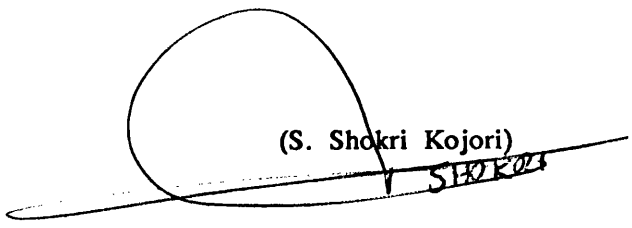

ProQuest LLC
789 East Eisenhower Parkway
P.O. Box 1346
Ann Arbor, MI 48106-1346

In the name of God,

the Compassionate, the Merciful

TO

Dr. Shaheed Mustafa Chamran

ACKNOWLEDGMENTS

The author wishes to express his deep appreciation to Dr. R. K. Aggarwal, Lecturer in Power Systems at the University of Bath. His assistance, encouragement and constant guidance, through all phases of this work is gratefully acknowledged. Invaluable advice and helpful comments from Professor A. T. Johns, of the City University, London, during the initial part of this work is also greatly appreciated. Interesting and stimulating discussion with Professor Silverman of the School of Mathematics, University of Bath, and Dr. D. Tripp of the CEGB, has contributed immensely to the work.

The author is also grateful to Professor J. F. Eastham for providing the facilities in the School of Electrical Engineering.

Thanks are also due to the staff of the Computer Centre, University of Bath, for their co-operation. The author is indebted to Mr. Dyke, Assistant Librarian of this university for doing literature search. The financial support from the Ministry of Culture and Higher Education of the Islamic Republic of Iran is gratefully acknowledged. Thanks are also due to Miss P. M. Hammond for typing the manuscript.

Finally, this thesis is dedicated to my family, without whose patience and constant encouragement it would not have been possible to complete this work.

SYNOPSIS

This study is concerned with developing simulation techniques for improving power system models so as to increase the realism with which the transients can be reproduced under a whole variety of different systems and fault conditions. Such studies are of particular importance in the development of very high speed protection schemes which utilise information a very short time after fault inception, i.e. during the period when the transients are quite pronounced.

The modelling techniques developed are based on utilising symmetrical components and frequency transforms to model a system comprising a generator, generator/transformer and a transmission line. Particular emphasis is placed on developing methods for incorporating frequency dependent parameters of the generator using frequency response data and it clearly shows that the inclusion of a realistic source side model (as opposed to an approximate source-side representation based on subtransient reactances) can have a significant effect on the fault transient waveforms both in terms of high frequency travelling wave and low frequency distortions. Furthermore, the effect on the transients of including the source side shunt capacitance is also highlighted.

Methods are also developed for modelling a complete three-phase autoreclosure sequence for faults on a double end fed system.

CONTENTS

LIST OF PRINCIPAL SYMBOLS

SYMBOLS	DESCRIPTIONS
A_f, B_f, C_f, D_f	Matrices defining fault discontinuity
$A_\ell, B_\ell, C_\ell, C_\ell$	Two port transmission line matrices
$A_{\ell 1}, B_{\ell 1}, C_{\ell 1}, D_{\ell 1}$	Matrices defining line section to point of fault
$A\ell_2, B_{\ell 2}, C_{\ell 2}, D_{\ell 2}$	Matrices defining line section beyond point of fault
AVR	Automatic voltage regulator
C_b	Capacitance to ground of bushing per-phase
C_g	Capacitance to ground of synchronous machine per-phase
CT_1	Capacitance to ground at delta-side of transformer per-phase
CT_2	Capacitance to ground at star-side of transformer per-phase
E_m	Peak value of prefault terminal voltage
E_r	Peak value of prefault voltage at infinite busbar
E_r', E_s'	Transform of superimposed voltages of breaker terminals at receiving end and sending end
e	Instantaneous value of terminal voltage
e.h.v.	Extra high voltage
F(w)	Fourier Transform of f(t)
$F(w-j\alpha)$	Modified Fourier Transform
F.F.T.	Fast Fourier Transform
g(p)	The stator to field transfer function
h(t)	Unit step function
h_1	Operator, 1 $2\pi/3$
h_2	Operator, 1 $-2\pi/3$
i	Instantaneous value of current

i_{fs}', i_{fr}'	Transform of superimposed current at fault point
i_{mc}', i_{sc}'	Transform of superimposed current of shunt capacitance at delta- and star-side of transformer
L	Self-inductance
L_d	d-axis synchronous inductance
$L_d(jw)$	d-axis frequency response function (operational inductance)
L_{ff}	Self inductance of field
L_{kk}	Self inductance of d-axis damper
L_o	Zero sequence (self) inductance
L_q	q-axis synchronous inductance
$L_q(jw)$	q-axis frequency response function (operational inductance)
L_{qq}	Self inductance of q-axis damper
L_t	Per-unit winding leakage inductance of generator/transformer
ℓ_1	Stator winding leakage inductance
M	Mutual inductance
M_{ad}	d-axis magnetising inductance
M_{aq}	q-axis magnetising inductance
m.m.f.	Magneto motive force
N	Number of samples
p	Operator, d/dt
p.u.	Per unit
P	Active power unless stated
Q	Reactive power
R	Armature resistance
r_t	Per unit winding resistance of generator/transformer
r.m.s.	Root mean square
S	The Laplace operator
s.c.l.	Short circuit level
T	Time constant unless stated

T'_d	The d-axis transient, short circuit time constant
T''_d	The d-axis subtransient, short circuit time constant
T'_{do}	The d-axis transient, open circuit time constant
T''_{do}	The subtransient open circuit time constant(d-axis)
tob	The observation time
T''_q	The q-axis short circuit subtransient time constant
T''_{qo}	The q-axis open circuit subtransient time constant
U	Unit matrix
V_m, I_m	Transform of prefault voltage and current at machine terminal
V_r, I_r	Transform of prefautl voltage and current at receiving end
V_s, I_s	Transform of prefault voltage and current at sending end
v_{ff}', e_{ff}'	Transform of superimposed voltage at fault point
v_m', i_m'	Transform of superimposed voltage and current at machine terminal
v_r', i_r'	Transform of superimposed voltage and current at receiving end
v_s', i_s'	Transform of superimposed voltage and current at sending end
w	Angular velocity
w_o	Synchronous speed
X	Line length unless stated
x	Distance to fault point from sending end unless stated
y(jw)	Shunt admittance matrix per unit length
$y_m(jw)$	Average sum of all conductor mutual admittances unless stated
$y_o(jw)$	Zero sequence admittance
$y_s(jw)$	Average sum of all conductor self admittance
$y_1(jw)$	Positive sequence admittance

$z(jw)$	Series impedance matrix per unit length
$z_m(jw)$	Average sum of all conductor mutual impedances
$z_o(jw)$	Zero sequence impedance
$z_s(jw)$	Average sum of all conductor self impedance
$z_{so}(jw), z_{s_1}(jw)$	Zero and positive phase sequence source impedances
$z_{ss}(jw), z_{sr}(jw)$	Sending end and receiving end source impedance matrices
$z_1(jw)$	Positive sequence impedance
α	Frequency shift constant
Δw	Frequency step length
Δt	Time step length
δ	Load angle with reference to terminal voltage considered positive for generator motion
ψ	Instantaneous value of flux linkage
Υ	Transmission line propagation constant
λ	Rotor angle measured from a-phase axis at time t=0
Ω	Truncation frequency
σ	Sigma factor
θ	Machine rotor direct axis angle ahead of the stator a-phase
θ_m	$\angle V_r/V_m$

SUBSCRIPTS

d	Direct axis
q	Quadrature axis
a,b,c	Phases a,b,c
f	Field unless stated
kd	Direct axis damper winding
kq	Quadrature axis damper winding
0,1,2	Symmetrical components

F	Forward components
B	Backward components
m	Machine terminal
r	Receiving end
s	Sending end

CHAPTER 1

INTRODUCTION

1.1 Background and Aim of Thesis

Protection systems on power systems use information derived from voltage and current waveforms to diagnose a fault condition and initiate the appropriate switching operations. The design and testing of a protection system requires a knowledge of voltage and current signals following any type and location of fault. Since it is not always practical to attain fault information from field tests (particularly because of the high costs involved), information derived from computer models of power systems is increasingly being used in protection relay design and developments.

In the last two decades, extensive use has been made of approximate state models in which both the transmission line and the synchronous machine are represented by an impedance or an equivalent 'π' or 'T' circuit. In the case of the machine model, refinements to include some machine transients have proved adequate for the design of low-speed electromechanical type protection relay system[36].

Modern high-speed relays often operate on information derived during the first or second half-cycle following a disturbance. Moreover, new developments in on-line digital protection as a means of further speeding fault clearance have given rise to a requirement for a more accurate simulation of fault transients. In this respect, research into methods for simulating faults on ehv transmission lines using frequency domain techniques has enabled a fair degree of realism to be obtained,

but it has nevertheless been necessary to assume simplified source networks[15]. It should be noted that simple-source side models often give acceptable accuracy in switching-surge overvoltage studies because, in terms of currents involved, such disturbances are relatively small. When dealing with system fault studies, the components of currents fed to a given fault from adjacent synchronous source can, under certain conditions, remain offset for several cycles after fault inception[42]. However, simple source side models (based upon subtransient impedances) do not produce this latter effect and, in general, the use of oversimplified source representation will give rise to some degradation in realism of any given study.

Generally speaking, the fault transients which occur in the generator and transmission line interconnection will contain high-frequency components due to travelling waves, and relatively low frequency, predominantly exponential components. It follows that in cases where a realistic predetermination of both phenomena is required, a more improved synchronous generator model connected to a distributed parameter transmission line model is essential.

In addition, when analysing the power system network, it is important to be able to accurately represent the generator/transformer. In this respect, different authors have used different methods for representing the latter. Among them, Laughton[32] achieved a good degree of accuracy by using the nodal admittance technique to solve any 3-phase transformer problem in the steady state. This was done by considering the transformer terminals as a number of nodes coupled by the appropriate admittances. The method was extended in another paper[33] to cover a number of system elements and the solution performed by an iterative technique similar to that used in system load flow studies.

In the case of transmission line modelling, during the last decade, studies of switching surge have been performed using Fourier analyses to take account of

frequency dependence of distributed transmission line parameters. The same technique has been applied to the study of travelling waves obtained during the system faults.

There are two main problems involved in developing a more improved source simulation. Firstly, the difficulty in analysing a synchronous generator and associated generator/transformer in the frequency domain and secondly, applying appropriate frequency response data to the generator and transformer models instead of representing them using analytical expressions and constant data as has been done hitherto, under transient conditions.

With regard to the machine parameters, designers of synchronous generators are increasingly being pressed to provide a whole range of generator parameters for system studies. It is normally assumed that a machine has a field winding and one damper coil on the d-axis of the rotor and a single damper coil on q-axis. While this is an appropriate model for a laminated-pole machine, however, in solid-pole turbogenerator, greater care needs to be taken particularly due to the skin effects in the rotor.

In recent years, considerable interest has been generated by questions relating to these effects and how they can be accurately modelled into solid rotor turbogenerator models. These questions have been concerned with the complexity of models required, i.e. the number and distributions of windings used to represent the rotor body, as well as with techniques for obtaining parameter values for these models. This interest has arisen due to concern that greater accuracy in the representation of turbogenerators for use in large scale digital computer studies is required as the complexity and size of power systems increases. Furthermore, a requirement has arisen for the development of very high-speed protection schemes which would permit power systems to operate closer to their stability limits. In

order to properly design such schemes, it is necessary that the relevant dynamic properties of the power system elements, of which the generator is one of the most important, be properly represented.

Whatever the accuracy of the model, a question arises as to how can the parameters be obtained. The most up-to-date technique for determining the machine parameters of interest has been outlined in a March 1987 IEE Proceeding article entitled "Standstill micromachine for turbogenerator parameter studies"(61). Of particular interest in this article is a test which is now receiving a great deal of attention. This is the "standstill frequency response test", in which relatively small currents at selected frequencies are injected in turn into the stator winding to obtain operational impedances for the d- and q-axes. The corresponding operational inductances can then be obtained.

The concept of performing frequency response tests on solid rotor turbogenerators as a means of determining their properties by direct measurements has received considerable attention in recent years, due mainly to the excellent work performed at Ontario Hydro(22,23,26,28,29,) and Northfleet(27,49) stations. In this study, a new technique for deriving the d- and q-axis operational inductances in the form of rational functions is developed. This is achieved by curve fitting the frequency response data in the complex plane to investigate the system responses.

In the case of the transformer, frequency dependence effects caused by eddy currents play an important role in the high frequency range in the transient study. The method developed in this work to analyse a transformer in the frequency domain also enables us to take account of the frequency variance of transformer parameters easily. However, because of the range of frequency of interest in this study (limited to 12KHz), the frequency dependency of transformer parameters has

not been included. In this respect it should be mentioned that the transformer parameters are more or less constant in the frequency range considered[31].

In this work, methods are extended to incorporate frequency response data when modelling the synchronous generator in the frequency domain. Symmetrical component theory is utilised. The generator model is then combined with a frequency domain model of Y/Δ transformer, which then forms the source side network of a transmission line model.

The main difficulty in proving any new technique is the shortage of comprehensive reliable field tests. For this reason, an extensive comparison of the results obtained from the new model developed here using the frequency variant data with the already verified results obtained using constant parameters has been made.

Furthermore, the system model has been developed to embrace the shunt capacitances (capacitance to ground) of generator and transformer as well as the relevant busbar capacitance to study the effect of these capacitances on the waveforms under transient conditions.

When considering the overall system model, i.e. a model comprising generator, transformer and transmission line, various researchers have adopted different approaches to the problem. For example, Slemon et al[36] in 1968 succeeded in analysing a synchronous machine connected to a distributed parameter transmission line model in the phase co-ordinate real time domain. A phase parameter model for the synchronous machine was used, while the transmission line analysis was an application of the method developed by Uram and Miller[39]. In addition to ignoring the parameter variations of the generator and transmission line the generator/transformer was not included. However, the transformer has major

influence on the generator performance and on the waveforms obtained during transmission line earth faults.

The ground effects in wave propagation which can affect the frequency dependent parameters of transmission line has been considered in reference (62) but the transformer problem has remained unsolved.

Barber and Giannini[71] studied simulation of a synchronous generator connected via a delta–star transformer and a short lumped parameter transmission line to the infinite busbar in the phase co–ordinate and the real time domain. Although the generator/transformer had been included, the parameter variations were not considered.

Owen and Lewise[57] succeeded in studying the extra delay of zero crossing at sequential faults using a large turbogenerator and its generator/transformer. However, constant parameters were applied.

In a comprehensive report by Shackshaft[24], valuable information relevant to both steady–state and transient performance of turbo–type and salient pole machine is presented. In this report the ability of frequency response tests to obtain q–axis parameters has been confirmed, while use of this data in a large disturbance and transient stability remained doubtful.

Barret and Roquefort[63] and Roquefort[64] have developed a new approach for obtaining the turboalternator operational impedances for small disturbances using frequency response information and the fast Fourier techniques. The operational impedances obtained from frequency response tests should ideally include a distributed parameter model representing the transmission line. However, this has not been done. In addition, the method utilises the d–q–o representation which

implies the study of symmetrical disturbances only.

Very recently, a similar approach has been used for a laboratory microalternator by Sriharan and Koh[65], where the faults were examined at generator terminals.

Johns and Aggarwal[15] have studied the effects of frequency variance of transmission line parameters, while more elementary source networks were used in frequency domain. However, the method uses the theory of modified Fourier transform introduced by Day, Reed and Mullinex[18] which has been implemented by applying fast Fourier Transform[66].

Bickford and Abdel-Rahman[67] have succeeded in calculation of transient-fault currents and voltages in time domain. By assuming a simple source model, the transformer influence on the generator performance and on the resulting waveforms during the fault has been neglected. Moreover, in studying the shunt capacitance effects on current and voltage waveforms, the capacitance to ground of the generator and transformer delta-side as a result of simple source assumption has not been included.

Johns and Aggarwal[68] in 1981 presented the simulation of faults and subsequent clearance in frequency domain. A simple source model connected to a distributed parameter line was used. In our study, we utilised a more complex source model to study fault and transient phenomena relevant to clearance of fault.

It can be seen that in each of the aforementioned methods of simulation, some form of approximations have been made either in the generator or transformer or transmission line, which can affect the realism with which the fault transients are produced. The work represented in this thesis is thus out to

increase the realism with which the transient can be obtained from computer models of systems.

Apart from improving the simulation technique, techniques are also developed here for applying faults at any point on the line (and not just at the machine terminals or the infinite busbar as has hitherto been done by other researchers), the line at each end being represented by realistic source models.

Finally, it is also the objective of the present investigation to develop a technique for studying the fault transient phenomena associated with three-phase autoreclosure of an uncompensated 400kV quadrature transmission system.

1.2 Summary of the Thesis

The fundamental theory of an idealised synchronous salient pole machine is presented in chapter 2. Also, a survey of conventional transforms in machine analyses is given and finally the relationships between d- and q-axes parameters and the original phase co-ordinate parameters are considered.

In chapter 3, the symmetrical component machine relationships obtained in chapter 2 are transformed into the frequency domain, where shifting techniques are applied to the positive and negative sequence components to ensure numerical stability. Furthermore, the superposition theorem is also introduced to calculate the superimposed voltages at fault point for any type of faults.

Chapter 4 describes the method of obtaining the machine d-q-o operational inductances from the Forward/Backward components which are closely related to symmetrical components. A technique to fit the frequency-response data to a fifth order polynomial function has been developed. The derived function of the

operational inductances by curve fitting procedure is then incorporated into the model to simulate any disturbance.

Chapter 5 begins by analysing the Y/Δ transformer using the nodal admittance method[32] and considers the necessary modification for transient studies. The matrix manipulations to form an economical computation technique for the generator/transformer in symmetrical components form and frequency domain are shown. In this chapter, the distributed parameter line model is also analysed by using the sequence components in frequency domain. Finally, the combination of generator, transformer and the transposed transmission line is considered.

The circuit configuration is shown in chapter 6. Besides the basic constant parameters of plant items such as generator, transformer, transmission line, shunt capacitance of generator/transformer and corresponding busbar, the data obtained by frequency response test for the generator is presented.

Chapters 7-8 cover the digital computer results of the various fault studies. Chapter 7 shows the results obtained from studies of the distortion produced due to the travelling waves associated with fault for both maximum and minimum current offsets, in the case of constant and frequency variance parameters generator model. The voltages and currents of the star and delta sides of the transformer are traced and given for each system fault. In addition, the results for the case of underexcited and overexcited machine performance for several faults at relaying point are also given. In chapter 8 the effects on the system's responses and/or model due to changing the fault point from infinite busbar to some point on the line are studied. A comprehensive digital simulation of conditions following three-phase autoreclosure fault clearance sequences are also provided.

Chapter 9 presents general conclusions and suggestions for the future work.

CHAPTER 2

SYNCHRONOUS GENERATOR MODEL

2.1 Introduction

The fundamental set of equations used here for representing the synchronous generator model are those for an idealised machine which can be approximated to the actual machine in accordance with certain well-defined assumptions[1]. In general, they are differential equations, in which an applied voltage is equated to the sum of several component voltages which in turn depend on the currents. The machine consists of several inductively coupled circuits in which the self and mutual inductances vary periodically with the angular position of the rotor, i.e. the inductances are time variant. The actual equations become more effective, considerably simple and also the corresponding inductances become independent of rotor position if they are expressed in terms of certain fictitious currents and voltages which are different from, but are related to actual values. The fictitious currents can have a physical meaning in that they can be considered to flow in fictitious windings acting along two axes at right angles, called the "direct and quadrature axes", i.e. d- and q-axes. This form of analysis is commonly known as the 'TWO-AXIS THEORY'.

Analysis based on the d-q-o method covers any steady or transient disturbance of a symmetrical nature. This transformation was developed by Blondle in 1913 for analysing steady state operation of a synchronous machine , was further examined by Doherty and Nikle[2] and Park[1] further refined it for many important practical problems. Other authors have developed transformations to determine the machine performance under asymmetrical conditions, for example,

Clark in $\alpha-\beta-o$ transformation[3] and Fortiscue in symmetrical components[4]. The latter was refined by Ku[5] to be used for symmetrical disturbances by the so-called "Forward-Backward" components transform. Symmetrical components are extensively used in power system analysis and moreover, some protective relays utilise phase sequence quantities.

This chapter considers the various transformations as applied to the machine phase co-ordinate equations. Also the steady state performance of a synchronous machine using a vector diagram, in which the machine load angle can be determined by means of d-q-o parameters under symmetrical steady state conditions, is considered.

2.2 The Ideal Synchronous Machine

The generator is assumed to be an "ideal synchronous machine" in which in accordance with Park's definition[72], the basic assumptions can be summarised as follows:

1. Saturation effects are neglected (this allows the application of the superposition principle because the model is then linear).

2. The magnetic circuit and all rotor windings are assumed to be symmetrical both with respect to the d-axis which lines up with the centre-line through the field poles, and to the q-axis, 90^0 ahead of it[6], as shown in Figure 2.1.

3. A current in any winding is assumed to set up an mmf, sinusoidally distributed in space around the air gap. Any mmf may be resolved into components along d-q axes. A sinusoidal distribution does normally

imply that only the fundamental component is considered. In making this assumption, it should be remembered that the effects of harmonics in the field distribution are small in a well-designed machine[7,8].

4. The damper windings are represented as hypothetical windings in d-q axes. The machine thus consists of three AC stator windings, one field winding on d-axis and some hypothetical windings on "d" and "q" axes.

   Practically, in a salient pole machine, amortisseur windings usually consist of a set of copper or brass bars set in pole face slots and connected together at the end of the machine but in two-pole solid-rotor turbine-generators, the solid rotor itself serves the purpose of amortisseur[9].

5. The stator slots cause no appreciable variation of any of the rotor inductances with rotor angle.

With reference to the above assumptions, a system of linear equations describes the relations between the voltages and currents in the windings of an idealised generator. For example, the voltage equation of the generator in phase co-ordinates would take the following form:

$$e = -(R)i + d(\psi)/dt \qquad \ldots (2.1)$$

where it should be noted that the direction of current is as has been shown in Figure 2.1.

2.3 The Inductance Relations

2.3.1 The armature

2.3.1.1 Self inductance

The self-inductance of the armature of the salient-pole machine depends upon machine geometry and the position of the machine rotor and varies periodically from a maximum when the pole axis is in line with the phase axis to a minimum when the inter-pole axis is in line with the phase axis[8]. Because of the symmetry of the rotor, the inductance of the armature must have a period of 180 electrical degrees and contain 'even' harmonic terms of the rotor position, and must be expressed by a series of cosines[12]. It follows that the inductance has a maximum value and is independent of rotor position. The effect of rotor slots may be taken into account by adding higher order variations in equation 2.2 below.

As shown in reference [8] the self inductances are given by:

$$
\begin{aligned}
L_{aa} &= L_{aa0} + L_{aa2} \cos 2\theta_1 + L_{aa4} \cos 4\theta_1 \\
L_{bb} &= L_{bb0} + L_{bb2} \cos 2(\theta_1 - 2\pi/3) + L_{bb4} \cos 4(\theta_1 - 2\pi/3) \\
L_{cc} &= L_{cc0} + L_{cc2} \cos 2(\theta_1 + 2\pi/3) + L_{cc4} \cos 4(\theta_1 + 2\pi/3)
\end{aligned}
\qquad \ldots (2.2)
$$

where for balanced machine design:

$$
L_{aa0} = L_{bb0} = L_{cc0} \quad , \quad L_{aa2} = L_{bb2} = L_{cc2} ,
$$

$$
L_{aa4} = L_{bb4} = L_{cc4}
$$

where 0 and 2,4 are constants and harmonic components of the inductances,

respectively.

2.3.1.2 Mutual inductance

With reference to Figure 2.1, it is evident that the mutual inductance between any phase pair is a minimum when the pole axis is midway between the phases concerned. The maximum value occurs when the rotor is advanced from its minimum position by 90^0 electrically. It follows that the mutual inductances between phases are as follows[8]:

$$\begin{aligned} M_{ab} &= M_{ab0} + M_{ab2} \cdot \cos 2\theta_3 + M_{ab4} \cdot \cos 4\theta_3 \\ M_{ac} &= M_{ac0} + M_{ac2} \cdot \cos 2\theta_2 + M_{ac4} \cdot \cos 4\theta_2 \\ M_{bc} &= M_{bc0} + M_{bc2} \cdot \cos 2\theta_1 + M_{bc4} \cdot \cos 4\theta_1 \end{aligned} \quad \ldots (2.3)$$

Again, for a balanced machine design:

$$M_{abo} = M_{ac0} = M_{bc0}, \quad M_{ab2} = M_{ac2} = M_{bc2}, \quad M_{ab4} = M_{ac4} = M_{bc4}$$

2.3.2 The armature-rotor mutual inductance

The mutual inductances between an armature coil and a field or damper coil vary periodically with period 2π. For example, 'M_{afd}' in equation 2.4 below, is maximum when phase "a" is on the d-axis and zero when phase "a" is on the q-axis. The mutual inductances contain odd harmonic terms[8]. Thus:

$$
\begin{aligned}
M_{afd} &= M_{af1} \cdot \cos\theta_1 + M_{af3} \cdot \cos 3\theta_1 + M_{af5} \cdot \cos 5\theta_1 \\
M_{akd} &= M_{ad1} \cdot \cos\theta_1 + M_{ad3} \cdot \cos 3\theta_1 + M_{ad5} \cdot \cos 5\theta_1 \\
M_{akq} &= -M_{aq1} \cdot \sin\theta_1 - M_{aq3} \cdot \sin 3\theta_1 - M_{aq5} \cdot \sin 5\theta_1 \\
M_{bfd} &= M_{bf1} \cdot \cos\theta_2 + M_{bf3} \cdot \cos 3\theta_2 + M_{bf5} \cdot \cos 5\theta_2 \\
M_{bkd} &= M_{bd1} \cdot \cos\theta_2 + M_{bd3} \cdot \cos 3\theta_2 + M_{bd5} \cdot \cos 5\theta_2 \qquad \ldots (2.4) \\
M_{bkq} &= -M_{bq1} \cdot \sin\theta_2 - M_{bq3} \cdot \sin 3\theta_2 - M_{bq5} \cdot \sin 5\theta_2 \\
M_{cfd} &= M_{cf1} \cdot \cos\theta_3 + M_{cf3} \cdot \cos 3\theta_3 + M_{cf5} \cdot \cos 5\theta_3 \\
M_{ckd} &= M_{cd1} \cdot \cos\theta_3 + M_{cd3} \cdot \cos 3\theta_3 + M_{cd5} \cdot \cos 5\theta_3 \\
M_{ckq} &= -M_{cq1} \cdot \sin\theta_3 - M_{cq3} \cdot \sin 3\theta_3 - M_{cq5} \cdot \sin 5\theta_3
\end{aligned}
$$

For a normal balanced machine design:

$$
\begin{aligned}
M_{ad1} &= M_{bd1} = M_{cd1}, \qquad M_{ad3} = M_{bd3} = M_{cd3} \\
M_{ad5} &= M_{bd5} = M_{cd5}, \qquad M_{aq1} = M_{bq1} = M_{cq1} \\
M_{aq3} &= M_{bq3} = M_{cq3}, \qquad M_{aq5} = M_{bq5} = M_{cq5} \\
M_{af1} &= M_{bf1} = M_{cf1}, \qquad M_{af3} = M_{bf3} = M_{cf3} \\
& M_{af5} = M_{bf5} = M_{cf5}
\end{aligned}
$$

In the above equations:

$$
\begin{aligned}
\theta_1 &= w_0 . t + \lambda = \theta \\
\theta_2 &= \theta_1 - 2\pi/3 \\
\theta_3 &= \theta_1 + 2\pi/3
\end{aligned}
$$

The machine parameters comprise five resistances, R (where $R_a = R_b = R_c = R$), R_{kq}, R_{fd}, R_{kd}, R_d and fourteen inductance values covering the constant, the fundamental and 2nd harmonic terms, i.e. L_{aa0}, L_{aa2}, M_{ab0}, M_{ab2}, M_{af1}, M_{af3}, M_{ad1}, M_{ad3}, L_{ff}, L_{dd}, L_{qq}, M_{aq1}, M_{aq3}, M_{fdkd}.

It should be noted that further terms in the series for the armature self and mutual inductances can be included if necessary. For many purposes, the equations can be simplified by neglecting the Fourier terms of third order and above. All of inductances would then vary sinusoidally, with an additional constant term in some cases.

2.3.3 The rotor

2.3.3.1 Self inductance

Because of neglecting the effects of stator slots and saturation, all rotor self inductances L_{ff}, L_{kk}, L_{qq}, are constant.

2.3.3.2 Mutual inductance

All mutual inductances M_{fdkd}, M_{kdfd} in the rotor are constant, since the flux linkages between the rotor windings are not a function of rotor position[8].

2.4 The Voltage Relations

With reference to equation 2.1, the relationship between each circuit voltage and current in Figure 2.1 are expressed by the general matrix form:

$$[e] = -[R].[i] + [d\psi/dt] \qquad . . (2.5)$$

These equations apply to any part of machine coils, i.e. (armature, rotor) and magnetic circuit.

2.4.1 Armature (stator voltage relationships

These are given as:

$$\begin{aligned} e_a &= p\psi_a - R.i_a \\ e_b &= p\psi_b - R.i_b \\ e_c &= p\psi_c - R.i_c \end{aligned} \qquad \ldots (2.6)$$

2.4.2 Rotor voltage relationships

2.4.2.1 Field

$$e_{fd} = p\psi_{fd} + R_{fd}.i_{fd} \qquad \ldots (2.7)$$

2.4.2.2 The damper circuit voltages

$$\begin{aligned} \text{For d-axis:} \quad 0 &= p\psi_{kd} + R_{kd}.i_{kd} \\ \text{For q-axis:} \quad 0 &= p\psi_{kq} + R_{kq}.i_{kq} \end{aligned} \qquad \ldots (2.8)$$

In the above, the zero voltages are due to the short circuiting of damper bars in each axis.

It should be noted that the symmetrical choice of the rotor circuit has the advantage of making all mutual inductances between d- and q-axis rotor circuits to be equal to zero.

2.5 Flux Linkage Relationships

The equations are defined in accordance with Figure 2.1 where the positive sign indicates current entering the plane of the paper and the arrows show the

direction of flux[6].

2.5.1 Armature flux relationships

$$\psi_a = -L_{aa}\cdot i_a - M_{ab}\cdot i_b - M_{ac}\cdot i_c + M_{afd}\cdot i_{fd} + M_{akd}\cdot i_{kd} + M_{akq}\cdot i_{kq}$$

$$\psi_b = -M_{ba}\cdot i_a - L_{bb}\cdot i_b - M_{bc}\cdot i_c + M_{bfd}\cdot i_{fd} + M_{bkd}\cdot i_{kd} + M_{bkq}\cdot i_{kq}$$

$$\psi_c = -M_{ca}\cdot i_a - M_{cb}\cdot i_b - L_{cc}\cdot i_c + M_{cfd}\cdot i_{fd} + M_{ckd}\cdot i_{kd} + M_{ckq}\cdot i_{kq} \quad \ldots (2.9)$$

2.5.2 Field flux

$$\psi_{fd} = -M_{fda}\cdot i_a - M_{fdb}\cdot i_b - M_{fdc}\cdot i_c + L_{ff}\cdot i_{fd} + M_{fdkd}\cdot i_{kd} \quad \ldots (2.10)$$

where

$$M_{fda} = M_{afd} \quad , \quad M_{fdb} = M_{bfd} \quad , \quad M_{fdc} = M_{cfd}$$

2.5.3 Amortisseur windings

a) d-axis

$$\psi_{kd} = -M_{kda}\cdot i_a - M_{kdb}\cdot i_b - M_{kdc}\cdot i_c + M_{kdfd}\cdot i_{fd} + L_{kk}\cdot i_{kd} \quad \ldots (2.11)$$

b) q-axis

$$\psi_{kq} = -M_{kqa}\cdot i_a - M_{kqb}\cdot i_b - M_{kqc}\cdot i_c + L_{qq}\cdot i_{kq} \quad \ldots (2.12)$$

where

$$M_{kdfd} = M_{fdkdq} \quad , \quad M_{kda} = M_{akd}$$

$$M_{kdb} = M_{bkd} \quad , \quad M_{kdc} = M_{ckd}$$

The equations (2.9–2.12) can be arranged in the general matrix form:

$$[\psi] = [L].[i] \qquad \ldots (2.13)$$

where $[\psi]$ and [i] are column matrices, i.e.:

$$[\psi] = [\psi_a \ \psi_b \ \psi_c \ \psi_{fd} \ \psi_{kd} \ \psi_{kq}]^t$$

$$[i] = [i_a \ i_b \ i_c \ i_{fd} \ i_{kd} \ i_{kq}]^t$$

[L] = square matrix of the form:

$$[L] = \begin{array}{c} \\ a \\ b \\ c \\ fd \\ kd \\ kq \end{array} \begin{array}{c} \begin{array}{cccccc} a & b & c & fd & kd & kq \end{array} \\ \begin{bmatrix} -L_{aa} & -M_{ab} & -M_{ac} & M_{afd} & M_{akd} & M_{akq} \\ -M_{ba} & -L_{bb} & -M_{bc} & M_{bfd} & M_{bkd} & M_{bkq} \\ -M_{ca} & -M_{cb} & -L_{cc} & M_{cfd} & M_{ckd} & M_{ckq} \\ -M_{afd} & -M_{bfd} & -M_{cfdq} & L_{ff} & M_{fdkd} & 0 \\ -M_{akd} & -M_{bkd} & -M_{ckd} & M_{kdfd} & L_{kk} & 0 \\ -M_{akq} & -M_{bkq} & -M_{ckq} & 0 & 0 & L_{qq} \end{bmatrix} \end{array}$$

$$\ldots (2.14)$$

The matrix [L] is always symmetrical, irrespective of rotor positions. Under the assumption of sinusoidal winding distribution, only the first terms of the self and mutual inductances in the above matrix are significant. Hence with reference to equations (2.2) and (2.3) we have:

$$
\begin{aligned}
L_{aa} &= L_{aa0} + L_{aa2}\ \cos 2\theta_1 \\
L_{bb} &= L_{bb0} + L_{bb2}\ \cos 2\theta_2 \\
L_{cc} &= L_{cc0} + L_{cc2}\ \cos 2\theta_3 \\
M_{ab} &= M_{ab0} + M_{ab2}\ \cos 2\theta_3 \\
M_{ac} &= M_{ac0} + M_{ac2}\ \cos 2\theta_2 \\
M_{bc} &= M_{bc0} + M_{bc2}\ \cos 2\theta_1
\end{aligned}
\qquad \ldots (2.15a)
$$

It should be noted that the variable part of the mutual inductances is of exactly the same magnitude as that of the variable part of the self inductances and that the constant part has a magnitude half the constant part of the self-inductances[12], i.e.:

$$
L_{aa0} = L_{bb0} = L_{cc0} = L_s \quad , \quad L_{aa2} = L_{bb2} = L_{cc2} = L_m
$$

$$
M_{ab0} = M_{ac0} = M_{bc0} = \frac{L_s}{2} = -M \quad , \quad M_{ab2} = M_{ac2} = M_{bc2} = L_m
$$

$$
\ldots (2.15b)
$$

and with reference to equation (2.4), for the armature-rotor mutual inductances we have:

$$
\begin{aligned}
M_{afd} &= M_{af1}.\cos\theta_1 = M_{akd} \\
M_{bfd} &= M_{bf1}.\cos\theta_2 = M_{bkd} \\
M_{cfd} &= M_{cf1}.\cos\theta_3 = M_{ckd} \\
M_{akq} &= -M_{aq1}.\sin\theta_1 \\
M_{bkq} &= -M_{bq1}.\sin\theta_2 \\
M_{ckq} &= -M_{cq1}.\sin\theta_3
\end{aligned}
\qquad \ldots (2.16)
$$

where:

$$M_{af1} - M_{bf1} - M_{cf1} - M_{af} \quad , \quad M_{aq1} - M_{bq1} - M_{cq1} - M_{aq} \quad ,$$

$$M_{afd} - M_{akd} \quad , \quad M_{bfd} - M_{bkd} \quad , \quad M_{cfd} - M_{ckd}$$

The d-axis, q-axis mutual inductances are of course zero because no flux linkage is involved here. With regard to the above relationships, the [L] matrix now takes the form as follows:

$$[L] = \begin{array}{c} \\ a \\ b \\ c \\ fd \\ kd \\ kq \end{array} \begin{array}{c} \begin{array}{ccc} a & b & c \end{array} \\ \left[\begin{array}{ccc} -L_s - L_m.\cos 2\theta_1 & M - L_m.\cos 2\theta_3 & M - L_m.\cos 2\theta_2 \\ M - L_m.\cos 2\theta_3 & -L_s - L_m.\cos 2\theta_2 & M - L_m.\cos 2\theta_1 \\ M - L_m.\cos 2\theta_2 & M - L_m.\cos 2\theta_1 & -L_s - L_m.\cos 2\theta_3 \\ -M_{af}.\cos\theta_1 & -M_{af}.\cos\theta_2 & -M_{af}.\cos\theta_3 \\ -M_{af}.\cos\theta_1 & -M_{af}.\cos\theta_2 & -M_{af}.\cos\theta_3 \\ +M_{aq}.\sin\theta_1 & +M_{aq}.\sin s\theta_2 & +M_{aq}.\sin\theta_3 \end{array} \right. \end{array} \begin{array}{c} \begin{array}{ccc} fd & kd & kq \end{array} \\ \left[\begin{array}{ccc} +M_{af}.\cos\theta_1 & M_{af}.\cos\theta_1 & -M_{aq}.\sin\theta_1 \\ +M_{af}.\cos\theta_2 & M_{af}.\cos\theta_2 & -M_{aq}.\sin\theta_2 \\ +M_{af}.\cos\theta_3 & M_{af}.\cos\theta_3 & -M_{aq}.\sin s\theta_3 \\ L_{ff} & M_{fdkd} & 0 \\ M_{kdfd} & L_{kk} & 0 \\ 0 & 0 & L_{qq} \end{array} \right] \end{array} \quad \ldots (2.17)$$

Since θ depends on the rotor position and is a function of time, hence the [L] matrix is a function of time.

2.6 Transformation

The equations of the synchronous machine can be greatly simplified by using a

proper transformation. Moreover, by applying a convenient substitution, it is possible to eliminate the time variant nature of inductances in equation (2.17). These transformations essentially depend on the type of disturbances, i.e. whether the disturbances are symmetrical or asymmetrical.

2.6.1 "d-q-o" or Park's transformation

In this method, all the armature variables are transformed to new variables relating to a rotating reference frame fixed to the field system. The d- and q-axes currents i_d, i_q are defined as the currents in fictitious coils, located on the two axes and each having the same number of turns as a phase coil which would set up the same mmf.

The relationships between the armature phase currents i_a, i_b, i_c and the new currents i_d, i_q, i_o are then given as follows[6]:

$$\begin{aligned} i_a &= i_d.\cos\theta - i_q.\sin\theta + i_o \\ i_b &= i_d.\cos(\theta - 120) - i_q.\sin(\theta - 120) + i_o \\ i_c &= i_d.\cos(\theta + 120) - i_q.\sin(\theta + 120) + i_o \end{aligned} \qquad \ldots (2.18a)$$

and similarly for voltages:

$$\begin{aligned} e_a &= e_d.\cos\theta - e_q.\sin\theta + e_o \\ e_b &= e_d.\cos(\theta - 120) - e_q.\sin(\theta - 120) + e_o \\ e_c &= e_d.\cos(\theta + 120) - e_q.\sin(\theta + 120) + e_o \end{aligned} \qquad \ldots (2.18b)$$

Similar substitution can be made for armature flux linkages.

The inverse transformation of equation (2.18a) is:

$$i_d = \frac{2}{3}.[i_a.\cos\theta + i_b.\cos(\theta - 120) + i_c.\cos(\theta + 120)]$$

$$i_q = \frac{2}{3}.[-i_a.\sin\theta - i_b.\sin(\theta - 120) - i_c.\sin(\theta + 120)]$$

$$i_o = \frac{1}{3}(i_a + i_b + i_c)$$

. . (2.19)

The above two equations can be written in matrix form as:

$$\begin{bmatrix} i_o \\ i_d \\ i_q \end{bmatrix} = [C] \begin{bmatrix} i_a \\ i_b \\ i_c \end{bmatrix} \text{ where, } [C] = (2/3)\cdot \begin{bmatrix} 1/2 & 1/2 & 1/2 \\ \cos\theta & \cos(\theta-120) & \cos(\theta+120) \\ -\sin\theta & -\sin(\theta-120) & -\sin(\theta+120) \end{bmatrix}$$

$$\begin{bmatrix} \psi_o \\ \psi_d \\ \psi_q \end{bmatrix} = [C] \begin{bmatrix} \psi_a \\ \psi_b \\ \psi_c \end{bmatrix}$$

. . (2.20a)

and:

$$\begin{bmatrix} i_a \\ i_b \\ i_c \end{bmatrix} = [C]^{-1} \begin{bmatrix} i_o \\ i_d \\ i_q \end{bmatrix} \text{ where, } [C]^{-1} = \begin{bmatrix} 1 & \cos\theta & -\sin\theta \\ 1 & \cos(\theta-120) & -\sin(\theta-120) \\ 1 & \cos(\theta+120) & -\sin(\theta+120) \end{bmatrix}$$

. . (2.20b)

With reference to equations (2.13) - (2.15) and using flux linkage transformation equation (2.20a), the d-q-o fluxes are as follows:

$$\psi_o = -(L_{aa0} + 2M_{ab0}).i_o$$

$$\psi_d = -(L_{aa0} - M_{ab0} + \frac{3}{2}L_{aa2}).i_d + M_{af}.i_{fd} + M_{af}.i_{kd}$$

$$\psi_q = -(L_{aa0} - M_{ab0} - \frac{3}{2}L_{aa2}).i_q + M_{aq}.i_{kq}$$

$$\psi_{fd} = -(3/2)M_{af}.i_d + L_{ff}.i_{fd} + M_{fdkd}.i_{kd}$$

$$\psi_{kd} = -(3/2)M_{af}.i_d + M_{fdkd}.i_{fd} + L_{kk}.i_{kd}$$

$$\psi_{kq} = -(3/2)M_{aq}.i_q + L_{qq}.i_{kq}$$

If, in the above, it is assumed that:

$$L_o = L_{aa0} + 2M_{ab0}$$

$$L_d = L_{aa0} - M_{ab0} + \frac{3}{2}L_{aa2} \qquad \text{. . (2.21a)}$$

$$L_q = L_{aa0} - M_{ab0} - \frac{3}{2}L_{aa2}$$

The matrix relationship then becomes:

$$\begin{matrix} & & o & d & q & fd & kd & kq & \\ \begin{bmatrix}\psi_o\\ \psi_d\\ \psi_q\\ \psi_{fd}\\ \psi_{kd}\\ \psi_{kq}\end{bmatrix} & = & \begin{bmatrix} -L_o & 0 & 0 & 0 & 0 & 0 \\ 0 & -L_d & 0 & M_{af} & M_{af} & 0 \\ 0 & 0 & -L_q & 0 & 0 & M_{aq} \\ 0 & -\frac{3}{2}M_{af} & 0 & L_{ff} & M_{fdkd} & 0 \\ 0 & -\frac{3}{2}M_{af} & 0 & M_{fdkd} & L_{kk} & 0 \\ 0 & 0 & -\frac{3}{2}M_{aq} & 0 & 0 & L_{qq} \end{bmatrix} & \begin{bmatrix} i_o \\ i_d \\ i_q \\ i_{fd} \\ i_{kd} \\ i_{kq} \end{bmatrix} \end{matrix}$$

. . (2.21b)

The transformed voltage equations may then be found by substituting the above flux and current relationships in equation (2.1) and are given as:

$$
\begin{aligned}
e_d &= p\,\psi_d - p\theta.\psi_q - R.i_d \\
e_q &= p\theta.\psi_d + p\,\psi_q - R.i_q \\
e_o &= p\,\psi_o - R.i_o \\
e_{fd} &= p\,\psi_{fd} + R_{fd}.i_{fd} \\
0 &= p\,\psi_{kd} + R_{kd}.i_{kd} \\
0 &= p\,\psi_{kq} + R_{kq}.i_{kq}
\end{aligned}
\qquad \ldots (2.22)
$$

where: $p\theta = w_o$

Substituting equation (2.21b) into equation (2.22) and replacing 'p' by 'jw' gives the following matrix relationship:

$$
\begin{bmatrix} e_o \\ e_d \\ e_q \\ e_{fd} \\ 0 \\ 0 \end{bmatrix} =
\begin{bmatrix}
-(R+jw.L_o) & 0 & 0 \\
0 & -(R+jw.L_d) & w_o.L_q \\
0 & -w_o.L_d & -(R+jw.L_q) \\
0 & -(3/2).jw.M_{af} & 0 \\
0 & -(3/2).jw.M_{af} & 0 \\
0 & 0 & -(3/2).jw.M_{aq}
\end{bmatrix}
$$

fd	kd	kq
0	0	0
$jw.M_{af}$	$jw.M_{af}$	$-w_o.M_{aq}$
$w_o.M_{af}$	$w_o.M_{af}$	$jw.M_{aq}$
$(R_{fd}+jw.L_{ff})$	$jw.M_{fdkd}$	0
$jw.M_{fdkd}$	$(R_{kd}+jw.L_{kk})$	0
0	0	$(R_{kq}+jw.L_{qq})$

$$
\begin{bmatrix} i_o \\ i_d \\ i_q \\ i_{fd} \\ i_{kd} \\ i_{kq} \end{bmatrix}
\qquad \ldots (2.23)
$$

It should be noted that the d–q–o transformation is rather intractable when having unbalanced disturbances.

2.6.2 The "$\alpha.\beta.o$" transformation

This transformation can be used to transform the three phase quantities into "$\alpha.\beta.o$" components on the stationary armature frame[3]. It is obtained by taking the α–axis aligned with a–phase and the β–axis aligned with the common axis of b and c–phases. Unlike the "d–q–o" transformation, such a transformation is more suitable for studying unbalanced operations of three phase systems.

The transformation between the d–q–o and α–β–o components is given as[10]:

$$\begin{bmatrix} i_o \\ i_\alpha \\ i_\beta \end{bmatrix} = \begin{bmatrix} 1 & 0 & 0 \\ 0 & \cos\theta & -\sin\theta \\ 0 & \sin\theta & \cos\theta \end{bmatrix} \begin{bmatrix} i_o \\ i_d \\ i_q \end{bmatrix} \qquad \ldots (2.24)$$

The transformation can be easily related to the phase co–ordinates as:

$$\begin{aligned} i_o &= \frac{1}{3}(i_a + i_b + i_c) \\ i_\alpha &= \frac{2}{3}.\{i_a - [(i_b + i_c)/2]\} \\ i_\beta &= (i_b - i_c)/\mathrm{sqrt}(3) \end{aligned} \qquad \ldots (2.25)$$

This transformation does not completely eliminate time variant of inductances but resulting equations are relatively easy to handle.

2.6.3 The symmetrical component transformation

The theory of symmetrical components has been used for many years in calculating steady state fault currents and voltages in a three-phase system[11].

In this method, a three-phase unbalanced system of voltages and currents is represented by three separate systems of phasors, namely, positive, negative and zero phasor systems. The well-known symmetrical component relationships for three-phase quantities are:

$$i_o = \frac{1}{3}(i_a + i_b + i_c) \qquad i_a = (i_o + i_1 + i_2)$$

$$i_1 = \frac{1}{3}(i_a + h_1.i_b + h_2.i_c) \qquad i_b = (i_o + h_2.i_1 + h_1.i_2)$$

$$i_2 = \frac{1}{3}(i_a + h_2.i_b + h_1.i_c) \qquad i_c = (i_o + h_1.i_1 + h_2.i_2)$$

. . (2.26)

The relationships between $\alpha.\beta.o$ and symmetrical components are[10]:

$$i_\alpha = (i_1 + i_2) \quad , \quad i_\beta = (i_1 - i_2)/j = -j.(i_1 - i_2)$$

The voltage equations in symmetrical components method are:

$$e_1 = p\psi_1 - R.i_1 \quad , \quad e_2 = p\psi_2 - R.i_2 \quad , \quad e_o = p\psi_o - R.i_o$$

2.6.4 Forward and Backward components transformation

As defined by Ku[10], the Forward/Backward components are related to the

symmetrical components as follows:

$$\begin{aligned} i_F &= i_1.e^{-j\theta} & \qquad i_1 &= i_F.e^{j\theta} \\ i_B &= i_2.e^{j\theta} & \qquad i_2 &= i_B.e^{-j\theta} \end{aligned} \qquad \ldots (2.27)$$

where for $\theta = w_o t = 0$, $i_1 = i_F$ and $i_2 = i_B$.

The Forward and Backward components refer to a rotating reference frame, while the symmetrical components refer to a stationary reference frame. Relationships as shown in equation (2.27) can be extended to obtain transformation between Forward and Backward and phase magnitude and vice versa, as shown below:

$$i_F = e^{-j\theta}(i_a + h_1.i_b + h_2.i_c)/3 \quad \text{or} \quad i_a = i_o + i_F.e^{j\theta} + i_B.e^{-j\theta}$$

$$i_B = e^{j\theta}(i_a + h_2.i_b + h_1.i_c)/3 \quad \text{or} \quad i_b = i_o + h_2.i_F.e^{j\theta} + h_1.i_B.e^{-j\theta}$$

$$i_c = i_o + h_1.i_F.e^{j\theta} + h_2.i_B.e^{-j\theta}$$

and in a matrix form:

$$\begin{bmatrix} e_o \\ e_F \\ e_B \end{bmatrix} = \frac{1}{3} \begin{bmatrix} 1 & 0 & 0 \\ 0 & e^{-j\theta} & 0 \\ 0 & 0 & e^{j\theta} \end{bmatrix} \begin{bmatrix} 1 & 1 & 1 \\ 1 & h_1 & h_2 \\ 1 & h_2 & h_1 \end{bmatrix} \begin{bmatrix} i_a \\ i_b \\ i_c \end{bmatrix} \qquad \ldots (2.28)$$

There is a simple relationship between the d- and q- and the Forward and Backward components as follows[10]:

$$\begin{bmatrix} i_o \\ i_d \\ i_q \end{bmatrix} = \begin{bmatrix} 1 & 0 & 0 \\ 0 & 1 & 1 \\ 0 & -j & j \end{bmatrix} \begin{bmatrix} i_o \\ i_F \\ i_B \end{bmatrix} \qquad \ldots (2.29)$$

and for the voltage equations:

$$e_F = p\,\psi_F + j(p\theta)\,\psi_B - R.i_F$$
$$e_B = p\,\psi_B - j(p\theta)\,\psi_F - R.i_B \qquad \ldots (2.30)$$

It should be noted that the Forward/Backward components of voltage are only a function of the corresponding components of flux linkage and current. This can be proved easily by substituting equation (2.29), and similar equation for the flux linkages into equation (2.22).

2.7 Classification of Different Transformations

2.7.1 According to the reference frame

2.7.1.1 Rotating reference frame

- d.q.o transformation
- F.B.o transformation

2.7.1.2 Stationary reference frame

- the original phase co-ordinates
- $\alpha.\beta$.o transformation
- the symmetrical components transformation

2.7.2 Complexity of domain

2.7.2.1 Real time domain

- the original phase co-ordinates
- $\alpha.\beta.o$ transformation
- d.q.o transformation

2.7.2.2 Complex domain

- F.B.o transformation
- the symmetrical components transformation

2.7.3 According to the type of fault study

2.7.3.1 Symmetrical disturbances

- d.q.o transformation
- F.B.o transformation

2.7.3.2 Asymmetrical disturbances

- symmetrical component transformation
- original phase co-ordinates
- $\alpha.\beta.o$ transformation

2.8 Steady State Operation of a Synchronous Machine

During normal steady AC operation, the speed of the machine is constant synchronous speed, w_o. The field voltage and current are constant, the damper

current is zero and the armature phase voltages and currents are balanced three-phase quantities. Hence, zero time is taken as the instant when a-phase is on the direct axis.

Now, for no load, $i_a = i_b = i_c = 0$, $i_{kd} = i_{kq} = 0$.

From equations (2.9), we have: $\psi_a = M_{afd}.i_{fd}$, and with reference to equation (2.16): $M_{afd} = M_{af}.COS\theta$, then: $\psi_a = M_{af}.COS\theta.i_{fd}$.

Also from equation (2.6): $e_a = p\,\psi_a - R.i_a$, and as we have defined previously: $\theta = w_o t + \lambda$ and if $\lambda = 0$ then: $\theta = wot$. We thus have: $ea = d/dt(M_{af}.COS\theta).i_{fd} = d/dt(M_{af}.COSw_o t).i_{fd}$ $e_a = - w_o.M_{af}.i_{fd}.SINw_o t = -E_{max}SINw_o t$, where: $E_{max} = w_o.M_{af}.i_{fd}$.

. . (2.31)

If the machine is loaded, armature reaction occurs and all currents, except those in the damper bars, are finite. In accordance with figure (2.2) the terminal voltage is phase shifted by δ with respect to its no-load value. As the voltage or its flux lags the no-load position by angle δ, the instantaneous angular displacement with respect to the a-phase axis becomes $(\theta - \delta)$. Equation (2.31) thus changes to:

$$e_a = -E_{max}.SIN(\theta - \delta) = - E_{max}(SIN\theta\ COS\delta - COS\theta\ SIN\delta)$$
$$= E_{max}.SIN\delta\ COS\theta - E_{max}.COS\delta\ SIN\theta \qquad . . (2.32)$$

From transformation equation (2.18), the voltage and current in a-phase are:

$e_a = e_d.COS\theta - e_q.SIN\theta$ (a) $\qquad i_a = i_d.COS\theta - i_q.SIN\theta$ (b)

Comparing equation (a) with (2.32):

$$e_d = E_{max} \cdot SIN\delta \qquad e_q = -E_{max} COS\delta \qquad \ldots (2.33)$$

For steady-state operation, it is common to use r.m.s values instead of instantaneous values. Equation (2.33) then becomes[13]:

$$e_d = sqrt(2).E_d \quad \text{and} \quad e_q = -sqrt(2)E_q \qquad \ldots (2.34)$$

and:

$$E = E_d + jE_q$$

Hence, for steady state operation at synchronous speed, the axes voltages and currents are all constant quantities independent of time. Moreover, "e_{fd}" and "i_{fd}" are constant and e_{kd}, e_{kq}, i_{kd}, i_{kq} are all zero. As shown in appendix A-1 the required expressions for the steady state currents are:

$$i_d = sqrt(2) \cdot (-E_{oc} + E_{r.m.s} \cdot COS\delta)/X_d$$
$$i_q = sqrt(2) \cdot (E_{r.m.s} \cdot SIN\delta)/X_q \qquad io = 0 \qquad \ldots (2.35)$$

where:

E_{oc} = open circuit voltage = $-X_{md} . i_{fd}/sqrt(2)$

X_{md} = magnetising reactance in direct axis

The negative sign of E_{oc} shows that with the sign convention used, a negative field voltage is required to generate a positive armature voltage.

2.9 Evaluation of Reciprocity of the Mutual Inductance Coefficients

In analysing an electrical network, an essential condition for the existence of a linear equivalent circuit is the reciprocity of the mutual-inductance coefficients and this condition is not completely satisfied in the equation (2.21), i.e. in this equation the mutual inductance coefficients between armature currents and rotor flux are $-(3/2)M_{af}$, $-(3/2)M_{af}$, $-(3/2)M_{aq}$, but the mutual inductance coefficients between armature flux and rotor currents are M_{af}, M_{af}, M_{aq}. This difficulty arises because of the transformation used for both phase currents (i_a, i_b, i_c) and fluxes (ψ_a, ψ_b, ψ_c). The difficulty can be avoided by changing the rotor currents (i_{fd}, i_{kd}, i_{kq}) in equation (2.21) by a factor of 2/3 (14).

The flux linkage relationships in equation (2.21) then become:

a) rotor

$$\begin{aligned} \psi_{fd} &= -M_{ad}\cdot i_d + L_{ff}\cdot i_{fd} + M_{ad}\cdot i_{kd} \\ \psi_{kd} &= -M_{ad}\cdot i_d + M_{ad}\cdot i_{fd} + L_{kk}\cdot i_{kd} \\ \psi_{kq} &= -M_{aq}\cdot i_q + L_{qq}\cdot i_{kq} \end{aligned} \qquad \ldots (2.36)$$

b) stator

$$\begin{aligned} \psi_d &= -L_d\cdot i_d + M_{ad}\cdot i_{fd} + M_{ad}\cdot i_{kd} \\ \psi_q &= -L_q\cdot i_q + M_{aq}\cdot i_q \\ \psi_o &= -L_o\cdot i_o \end{aligned} \qquad \ldots (2.37)$$

and the matrix form of the above relationships is as follows:

$$\begin{bmatrix} \psi_o \\ \psi_d \\ \psi_q \\ \psi_{fd} \\ \psi_{kd} \\ \psi_{kq} \end{bmatrix} = \begin{bmatrix} -L_o & 0 & 0 & 0 & 0 & 0 \\ 0 & -L_d & 0 & M_{ad} & M_{ad} & 0 \\ 0 & 0 & -L_q & 0 & 0 & M_{aq} \\ 0 & -M_{ad} & 0 & L_{ff} & M_{ad} & 0 \\ 0 & -M_{ad} & 0 & M_{ad} & L_{kk} & 0 \\ 0 & 0 & -M_{aq} & 0 & 0 & L_{qq} \end{bmatrix} \begin{bmatrix} i_o \\ i_d \\ i_q \\ i_{fd} \\ i_{kd} \\ i_{kq} \end{bmatrix} \quad \ldots (2.38)$$

2.10 Phase Values

In practice, the machine parameters are invariably quoted in d–q–o values and sometimes it is necessary to find the corresponding phase co–ordinate values. Relationships (2.15b) and (2.21a) can be usefully employed to obtain some specific equations for calculating phase parameter values as follows:

a) armature phase parameter

$$L_s + M = (L_d + L_q)/2$$
$$L_s - 2M = L_o$$

Thus:

$$L_s = (L_d + L_q + L_o)/3$$
$$M = (L_d + L_q - 2L_o)/6 \quad \ldots (2.39)$$
$$L_m = (L_d - L_q)/3$$

b) rotor phase parameter

$$
\begin{aligned}
M_{af} &= M_{fdkd} = (2/3).M_{ad} \\
M_{aq} &= (2/3).M_{aq(given)} \\
L_{ff} &= (2/3).L_{ff(given)} \\
L_{kk} &= (2/3).L_{kk(given)} \\
L_{qq} &= (2/3).L_{qq(given)}
\end{aligned}
\qquad \ldots (2.40)
$$

In addition, all rotor resistances should be multiplied by (2/3).

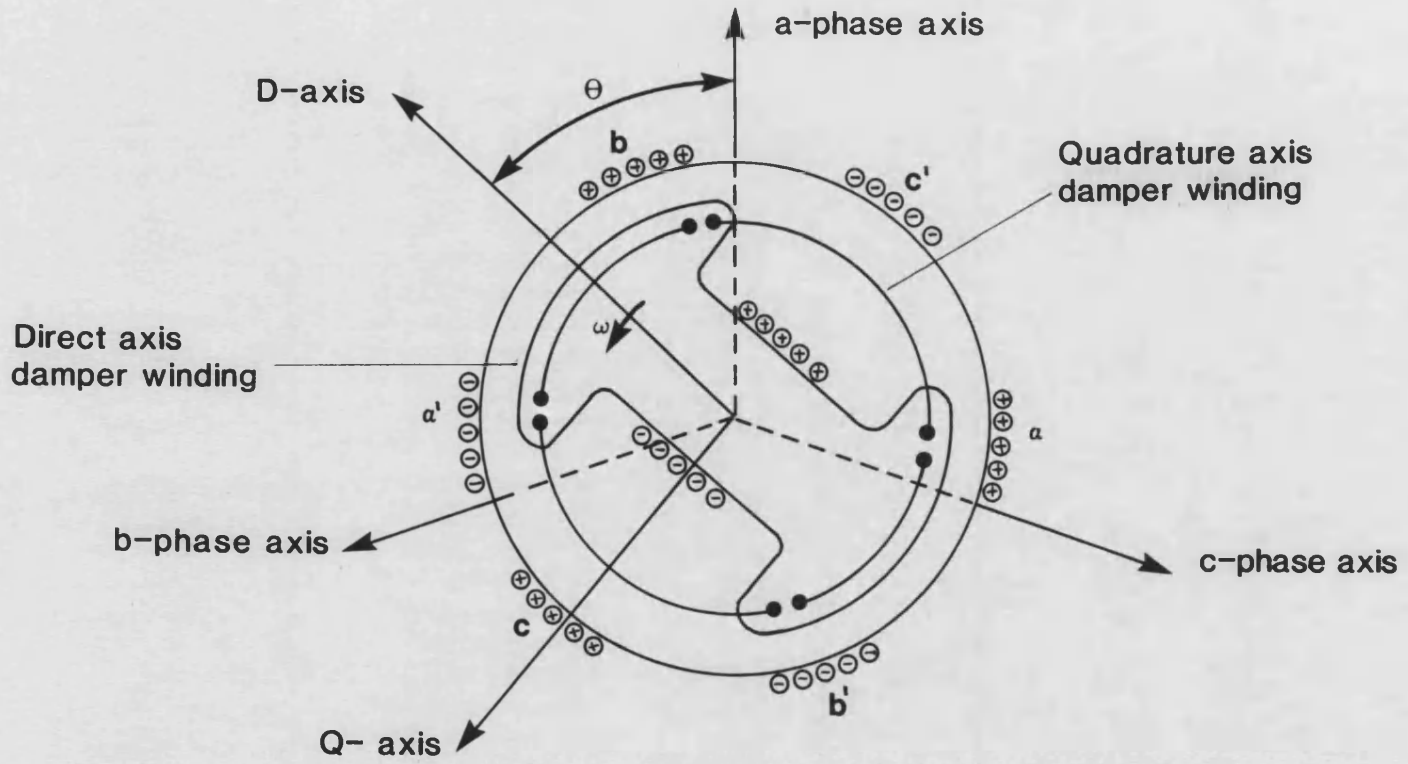

Fig 2.1 Schematic Represetation of a synchronous generator

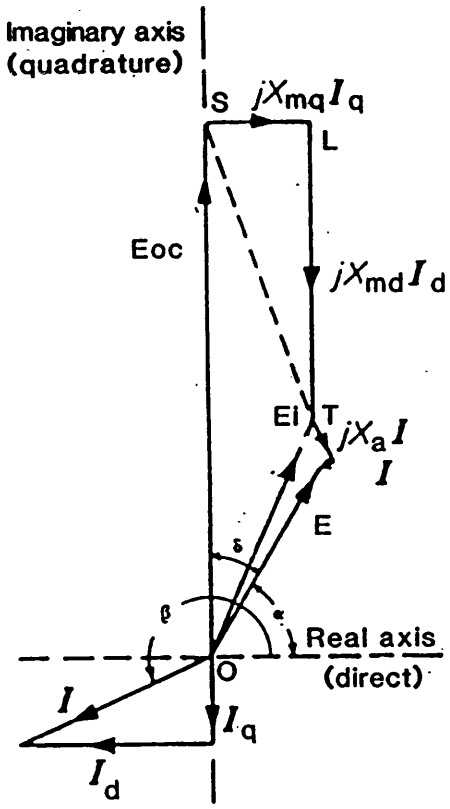

Figure 2.2 Complete machine phasor diagram for d–q–o components.

CHAPTER 3

GENERAL MACHINE EQUATIONS IN FREQUENCY DOMAIN

3.1 Introduction

As mentioned previously, in order to improve the accuracy with which the fault transient phenomena in power networks can be simulated, the frequency variance of synchronous machine parameters must also be taken into account when modelling the networks. It follows that improved frequency domain synchronous machine models, which can be relatively easily combined with the already well developed transmission line models[15], are required.

The application of Fast Fourier Transform (FFT) techniques for the simulation of transients in power systems are well-known[15,16]. Using such techniques, it has now become possible to solve the synchronous machine equations both more accurately and more efficiently (from a computational point of view) than with other numerical methods. In this study, the superposition theorem in conjunction with the FFT is used to solve the machine equations for the general case of a salient pole machine. Practical data is incorporated into the simulation to take into account the frequency variance of the machine parameters and the method developed makes use of the symmetrical components transform developed previously. Furthermore, a shifting technique is developed to facilitate both mathematical and numerical solutions to the rather complex problem.

3.2 Application of Symmetrical Components to Flux and Voltage Relationships

By applying the appropriate transformation (equation 2.26) to equation 2.17 (in the previous chapter), the flux relationships in terms of symmetrical components take the form:

$$\begin{bmatrix}\psi_0\\ \psi_1\\ \psi_2\\ \psi_{fd}\\ \psi_{kd}\\ \psi_{kq}\end{bmatrix} = \begin{bmatrix}-(L_s - 2M) & 0 & 0\\ 0 & -(L_s + M) & (-3/2).L_m.e^{j2\theta}\\ 0 & (-3/2).L_m.e^{-j2\theta} & -(L_s + M)\\ 0 & (-3/2).M_{af}.e^{-j\theta} & (-3/2).M_{af}.e^{j\theta}\\ 0 & (-3/2).M_{af}.e^{-j\theta} & (-3/2).M_{af}.e^{j\theta}\\ 0 & (-3/2j).M_{aq}.e^{-j\theta} & (+3/2j).M_{aq}.e^{j\theta}\end{bmatrix}$$

$$\begin{bmatrix}0 & 0 & 0\\ (1/2).M_{af}.e^{j\theta} & (1/2).M_{af}.e^{j\theta} & (-1/2j).M_{aq}.e^{j\theta}\\ (1/2).M_{af}.e^{-j\theta} & (1/2).M_{af}.e^{-j\theta} & (+1/2j).M_{aq}.e^{-j\theta}\\ L_{ff} & M_{fdkd} & 0\\ M_{fdkd} & L_{kk} & 0\\ 0 & 0 & L_{qq}\end{bmatrix}\begin{bmatrix}i_0\\ i_1\\ i_2\\ i_{fd}\\ i_{kd}\\ i_{kq}\end{bmatrix} \quad . . (3.1)$$

In deriving the above matrix relationship, it is assumed that:

$$i_a.\cos 2\theta + i_b.\cos(2\theta - 120) + i_c.\cos(2\theta + 120) = \frac{3}{2}(i_1.e^{-j2\theta} + i_2.e^{j2\theta})$$

$$i_a.\cos(2\theta-120)+i_b.\cos(2\theta+120)+i_c.\cos 2\theta = \frac{3}{2}(h_1.i_1.e^{-j2\theta}+h_2.i_2.e^{j2\theta})$$

$$i_a.\cos(2\theta+120)+i_b.\cos 2\theta+i_c.\cos(2\theta-120) = \frac{3}{2}(h_2.i_1.e^{-j2\theta}+h_1.i_2.e^{j2\theta})$$

and

$$i_a.SIN\theta+i_b.SIN(\theta-120)+i_c.SIN(\theta+120)=\frac{-3}{2J}(i_1.e^{-j\theta}-i_2.e^{j\theta})$$

It is interesting to note that unlike static circuits (e.g. transposed overhead lines), when the method of symmetrical components is applied to rotating circuits such as a salient pole machine, mutual coupling exists between sequence quantities as indicated in equation 3.1. With reference to equation 2.1 which is:

$$[e] = p[\psi] - [R].[i]$$

where:

$$[e] = [e_0\ e_1\ e_2\ e_{fd}\ e_{kd}\ e_{kq}]^t$$

$$[\psi] = [\psi_0\ \psi_1\ \psi_2\ \psi_{fd}\ \psi_{kd}\ \psi_{kq}]^t$$

$$[i] = [i_0\ i_1\ i_2\ i_{fd}\ i_{kd}\ i_{kq}]^t$$

$$[R[= \text{is a diagonal matrix}$$

and where $[\psi] = [L].[i]$ (as shown in equation 3.1), the above voltage relationships are now transformed into the frequency domain by applying the well-known Fourier integral:

$$F(w) = \int_{-\infty}^{\infty} f(t).e^{-jwt}.dt \qquad \ldots (3.2)$$

When this is done a transformation into frequency domain has been affected and the entire equations are:

$$
\begin{aligned}
e_0(w) &= -(R+(L_s-2M).jw).i_0(w) \\
e_1(w) &= -(R+(L_s+M).jw).i_1(w)-(3/2).L_m.jw.i_2(w-2w_0) + \\
&\quad (1/2).M_{af}.jw.i_{fd}(w-w_0) + (1/2).M_{af}.jw.i_{kd}(w-w_0) - \\
&\quad (1/2).M_{aq}.w.i_{kq}(w-w_0) \\
e_2(w) &= -(3/2)L_m.jw.i_1(w+2w_0) - (R+(L_s+M).jw).i_2(w) + \\
&\quad (1/2)M_{af}.jw.i_{fd}(w+w_0) + (1/2).M_{af}.jw.i_{kd}(w+w_0) + \\
&\quad (1/2).M_{aq}.w.i_{kq}(w+w_0) \\
e_{fd}(w) &= -(3/2).M_{af}.jw.i_1(w+w_0) - (3/2).M_{af}.jw.i_2(w-w_0) + \\
&\quad (R_{fd} + L_{ff}.jw).i_{fd}(w) + M_{fdkd}.jw.i_{kd}(w) \\
e_{kd}(w) &= 0 = -(3/2)M_{af}.jw.i_1(w+w_0) - (3/2)M_{af}.jw.i_2(w-w_0) + \\
&\quad M_{fdkd}.jw.i_{fd}(w) + (R_{kd} + L_{kk}.jw).i_{kd}(w) \\
e_{kq}(w) &= 0 = -(3/2)M_{aq}.w.i_1(w+w_0) + (3/2)M_{aq}.w.i_2(w-w_0) + \\
&\quad (R_{kq} + L_{qq}.jw).i_{kq}(w)
\end{aligned}
\qquad (3.3)
$$

It should be noted that the following transform identities have been used in the derivation of the above equations.

$f(t)$	——>	$F(w)$
$f(t).e^{\pm jwot}$	——>	$F(w \mp w_0)$
$f(t).e^{\pm j2wot}$	——>	$F(w \mp 2w_0)$
$d[f(t).e^{\pm jwot}]/dt$	——>	$jwF(w \mp w_0)$

Furthermore, in order to simplify the illustration, the fault inception angle λ has been assumed to be zero, so that θ is simply replaced by (w_0t), before the frequency transformation is applied. From a computational point of view, equations (3.3) are unacceptable as they stand because they involve several current transformations, e.g.$i_1(w)$, $i_1(w+w_0)$, $i_1(w+2w_0)$ are involved. Careful consideration

of the problem shows that by introducintg a positive frequency shift w_0 to the transformed positive phase sequence voltage component $e_1(w)$, together with a negative shift for the negative phase sequence component of voltage, the relationships take a much more convenient form. The necessary shifting is easily obtained by multiplying the original time domain equations by ($e^{\pm jw_0 t}$), as appropriate, and subsequently employing the corresponding transform pair:

$$f(t).e^{\pm jw_0 t} \longrightarrow F(w \mp w_0)$$

The foregoing technique gives rise to greatly simplified equations of the form:

$$\{e(w, w+w_0, w-w_0)\} = \{z(w, w+w_0, w-w_0)\}\ \{i(w, w+w_0, w-w_0)\} \quad \ldots (3.4)$$

The complete form of the equations involved is given in equation 3.5.

$$\begin{bmatrix} e_0(w) \\ e_1(w+w_0) \\ e_2(w-w_0) \\ e_{fd}(w) \\ 0 \\ 0 \end{bmatrix} - \begin{bmatrix} -(R+jw(L_s-2M)) & 0 & 0 \\ 0 & -(R+j(w+w_0)(L_s+M)) & -(3/2)j(w+w_0)L_m \\ 0 & -(3/2)j.(w-w_0)L_m & -(R+j(w-w_0)(L_s+M)) \\ 0 & -(3/2)j.w.M_{af} & -(3/2)jw.M_{af} \\ 0 & -(3/2)j.w.M_{af} & -(3/2)jw.M_{af} \\ 0 & -(3/2).w.M_{aq} & (3/2).w.M_{aq} \end{bmatrix}$$

$$\begin{bmatrix} 0 & 0 & 0 \\ j(w+w_0)\frac{M_{af}}{2} & j(w+w_0)\frac{M_{af}}{2} & -(w+w_0)\frac{M_{aq}}{2} \\ j(w-w_0)\frac{M_{af}}{2} & j(w-w_0)\frac{M_{af}}{2} & (w-w_0)\frac{M_{aq}}{2} \\ (R_{fd}+L_{ff}.jw) & jw.M_{fdkd} & 0 \\ jw.M_{fdkd} & (R_{kd}+jw.L_{kk}) & 0 \\ 0 & 0 & (R_{kq}+jw.L_{qq}) \end{bmatrix} \cdot \begin{bmatrix} i_0(w) \\ i_1(w+w_0) \\ i_2(w-w_0) \\ i_{fd}(w) \\ i_{kd}(w) \\ i_{kq}(w) \end{bmatrix}$$

$$[z] \longrightarrow \quad \ldots (3.5)$$

3.3 Frequency Domain Machine Equations When $\lambda \neq 0$

In equations 3.5 it has been assumed that $\lambda=0$, which gives $\theta=w_0.t$. However, if λ is finite, then $\theta=w_0t+\lambda$, and the inductance matrix of equation 3.1 is simply modified by the following substitution:

$$e^{\pm j\theta} = e^{\pm j(w_0t+\lambda)} = e^{\pm jw_0t} . e^{\pm j\lambda} \qquad . . (3.6)$$

If the load angle "δ" is also included to satisfy the loading conditions, then the terminal voltage angle of the a-phase becomes:

$$\theta = w_0t + \lambda - \delta$$

and the matrix relationship in equation 3.5 is modified to equation 3.7.

$$\begin{bmatrix} e_0(w) \\ e_1(w+w_0) \\ e_2(w-w_0) \\ e_{fd}(w) \\ 0 \\ 0 \end{bmatrix} = \begin{bmatrix} -[R+jw(L_s-2M)] & 0 & 0 \\ 0 & -[R+j(w+w_0)(L_s+M)] & (-3/2).j(w+w_0)L_m.e^{j2\lambda'} \\ 0 & (-3/2).j(w-w_0)L_m.e^{-j2\lambda'} & -[R+j(w-w_0)(L_s+m)] \\ 0 & (-3/2).jw.M_{af}.e^{-j\lambda'} & (-3/2).j.w.M_{af}.e^{j\lambda'} \\ 0 & (-3/2).jw.M_{af}.e^{-j\lambda'} & (-3/2).j.w.M_{af}.e^{j\lambda'} \\ 0 & (-3/2).w.M_{akq}.e^{-j\lambda'} & (+3/2).w.M^{akq}.e^{j\lambda'} \end{bmatrix}$$

$$\begin{bmatrix} 0 & 0 & 0 \\ (j/2)(w+w_0)M_{af}.e^{j\lambda'} & (j/2)(w+w_0)M_{af}.e^{j\lambda'} & -(1/2)(w+w_0)M_{akq}.e^{-j\lambda'} \\ (j/2)(w-w_0)M_{af}.e^{-j\lambda'} & (j/2)(w-w_0)M_{af}.e^{-j\lambda'} & (1/2)(w-w_0)M_{akq}.e^{-j\lambda'} \\ R_f+jw.L_{ff} & jw.M_{fdkd} & 0 \\ jw.M_{fdkd} & R_{kd}+jw.L_{kk} & 0 \\ 0 & 0 & R_{kq}+jw.L_{qq} \end{bmatrix} \begin{bmatrix} i_0(w) \\ i_1(w+w_0) \\ i_2(w-w_0) \\ i_{fd}(w) \\ i_{kd}(w) \\ i_{kq}(w) \end{bmatrix}$$

$$. . (3.7)$$

where:

$$\lambda' = \lambda + \delta$$

Introducing λ into [z] matrix of equation 3.5 shows that the operational impedance of the machine depends on the angle of fault inception. Also it is interesting to note that by changing the reference axis from the no-load voltage axis (q-axis) to the load terminal voltage axis, the machine time varying inductances becomes a function of $(\lambda+\delta)$.

3.4 Principle of Superposition for Fault Simulations

The application of the superposition theorem to circuit problems using instantaneous values is well-known. However, it should be mentioned that even the common symmetrical component phasor method of analysis is, in fact, an application of the superposition theorem.

To illustrate the method, let us assume that the sources of a simple system containing a generator, connected to an infinite-busbar are represented, using the source voltages e_{a1}, e_{b1}, e_{c1} (which are the voltages behind the machine operational impedances) and e_{a2}, e_{b2}, e_{c2} which are the infinte busbar voltages which by definition possess zero impedances.

The prefault voltages at the point of fault are e_a, e_b, e_c, Figure 3.1a. The prefault voltages would not affect the system if they were actual sources with the same voltages connected to the fault point. This in turn will help in simulating the fault by adding other source voltages shifted 180 electrical degrees, in series with e_a, e_b, e_c.

The addition of new voltage to the old voltage for the same phase, expresses a fault on that phase, i.e. if a solid earth fault occurs, the sum of two voltages

will be zero for the faulted phase. For example, with reference to Figure 3.1b, for a three-phase short circuit at fault point:

$$\begin{aligned} e_a + e_a' &= 0 \quad \text{i.e.} \quad e_a' = -e_a \\ e_b + e_b' &= 0 \quad \text{i.e.} \quad e_b' = -e_b \\ e_c + e_c' &= 0 \quad \text{i.e.} \quad e_c' = -e_c \end{aligned} \qquad \ldots (3.8)$$

e_a', e_b', e_c' are the superimposed voltages which are equal in magnitude and opposite in direction to e_a, e_b, e_c.

3.5 The Reduction of the Machine Equation to a 3x3 Sequence Matrix in the Frequency Domain

In practice it is often sufficient to compute only the variation of the armature currents. Furthermore, if the problem is solved by superposition and the excitation voltage "e_{fd}" is assumed to be a constant value throughout the short period of interest following a disturbance at the armature terminals, the superimposed value of the field voltage is zero. Under these conditions, the relationship shown in equation 3.7 can be reduced to the form:

$$\begin{bmatrix} i_0'(w) \\ i_1'(w+w_0) \\ i_2'(w-w_0) \end{bmatrix} = \begin{bmatrix} A_{11} & 0 & 0 \\ 0 & A_{22} & A_{23} \\ 0 & A_{32} & A_{33} \end{bmatrix} \begin{bmatrix} e_0'(w) \\ e_1'(w+w_0) \\ e_2'(w-w_0) \end{bmatrix} \qquad \ldots (3.9)$$

The admittance matrix elements (A_{11}, A_{21}, A_{22}, A_{23}, A_{32}, A_{33}) can be obtained by inversion of the full matrix given in equation 3.7 and by selecting the first three rows and columns. Such reduction reduces the computer storage and time quite significantly. Also by knowing the sequence currents, other variables such as the rotor side currents are available. Furthermore, the interconnections of

machines with external network such as generator/transformer and transmission line (as discussed latter in chapter 5) is facilitated.

3.6 Fault Simulation Using Superposition in Frequency Domain

The value of superimposed voltage components depends on the type of fault. If the rotor-angle is defined as:

$$\theta = w_0 t + \lambda - \delta,$$

then the prefault voltage of infinte busbar to which the armature of the machine is connected is given in the time domain as follows:

$$\begin{aligned} e_a &= -Em.SIN(w_0 t + \lambda - \delta) \\ e_b &= -Em.SIN(w_0 t + \lambda - \delta - 120) \\ e_c &= -Em.SIN(w_0 t + \lambda - \delta + 120) \end{aligned} \qquad \ldots (3.10)$$

3.6.1 Three phase to ground fault

As mentioned previously, for a three phase fault, the superposition voltages are suddenly applied voltages equal and opposite to the prefault value, and are given as:

$$\begin{aligned} e_a' &= E_m.SIN(w_0 t + \lambda - \delta)h(t) \\ e_b' &= E_m.SIN(w_0 t + \lambda - \delta - 120)h(t) \\ e_c' &= E_m.SIN(w_0 t + \lambda - \delta + 120)h(t) \end{aligned} \qquad \ldots (3.11)$$

The corresponding time varying symmetrical component sequence values are:

$$e_0' = (e_a' + e_b' + e_c')/3 = 0$$

$$e_1' = (e_a' + h_1.e_b' + h_2.e_c')/3 =$$

$$(E_m/2j).\exp[j(\lambda - \delta)].\exp[jw_0t]h(t) \qquad \ldots (3.12)$$

$$e_2' = (e_a' + h_2.e_b' + h_1.e_c')/3 =$$

$$(-E_m/2j).\exp[-j(\lambda - \delta)].\exp[-jw_0t]h(t)$$

To achieve the frequency domain superimposed voltage forms of above equations, it should be noted that the analogy between the modified Fourier and Laplace transforms enables us to use the two together.

Having found the "S"–domain form, a substitution for "S" with "jw" produces the frequency domain form.

From Laplace pairs we have:

$$\left[e^{\pm jw_0t} = 1/(S \mp jw_0) = 1/(jw \mp jw_0) = -j/(w \mp w_0) \right. \qquad \ldots (3.13)$$

Substituting the above into equation (3.12) will give:

$$e_o'(w) = 0.0$$

$$e_1'(w) = (-E_m/2).e^{j(\lambda-\delta)} \; . \; [1/(w-w_0)]$$

$$e_2'(w) = (+E_m/2).e^{-j(\lambda-\delta)} \; . \; [1/(w+w_0)]$$

Now by shifting positive sequence by $(w+w_0)$ and negative sequence by $(w-w_0)$ gives:

$$e_0'(w) = 0.0$$

$$e_1'(w+w_0) = (-E_m/2).e^{j(\lambda-\delta)} \; . \; [1/w] \qquad \ldots (3.14)$$

$$e_2'(w-w_0) = (+E_m/2).e^{-j(\lambda-\delta)} \; . \; [1/w]$$

3.6.2 Phase to phase fault

In this case, the b and c phases are chosen to be short circuited. It can thus be said that:

$$e_a' = 0$$

$$e_b + e_b' + \frac{e_a}{2} = 0 \quad \text{i.e.} \quad e_b' = -\left[e_b + \frac{e_a}{2}\right]$$

$$e_c + e_c' + \frac{e_a}{2} = 0 \quad \text{i.e.} \quad e_c' = -\left[e_c + \frac{e_a}{2}\right]$$

By applying equations (3.10) to the above we get:

$$e_b' = E_m.SIN(w_0t + \lambda - \delta - 120) + \left[\frac{E_m}{2}\right]SIN(w_0t + \lambda - \delta)$$

$$e_c' = E_m.SIN(wot + \lambda - \delta + 120) + \left[\frac{E_m}{2}\right]SIN(w_0t + \lambda - \delta)$$

Expansion of e_b' and e_c' above gives:

$$e_b' = -\frac{\sqrt{3}}{2}.E_m.COS(w_0t + \lambda - \delta)$$

$$e_c' = +\frac{\sqrt{3}}{2}.E_m.COS(w_0t + \lambda - \delta)$$

The corresponding time varying symmetrical components values are thus:

$$e_0' = (e_a' + e_b' + e_c')/3 = 0.0$$

$$e_1' = (e_a' + h_1.e_b' + h_2.e_c')/3 = -j.6.E_m.COS(w_0t + \lambda - \delta)/(4.3)$$

$$e_2' = (e_a' + h_2.e_b' + h_1.e_c')/3 = +j.6.E_m.COS(w_0t + \lambda - \delta)/(4.3)$$

Furthermore, by using exponential expansion and the following relationship:

$$e^{\mp jw_0t} = -j/(w \pm w_0) \quad ,$$

then the following equations can be obtained:

$$e_0'(w) = 0.0$$
$$e_1'(w) = -E_m.[A/(w-w_0) + B/(w+w_0)]/4$$
$$e_2'(w) = -e_1'(w)$$

where: $A = \exp[j(\lambda - \delta)]$ and $B = \exp[-j(\lambda - \delta)]$

Application of the shifting technique in positive and negative sequence components gives:

$$e_0'(w) = 0.0$$
$$e_1'(w+w_0) = -\frac{E_m}{4}.[A/(w)+B/(w+2w_0)] \qquad . . (3.15)$$
$$e_2'(w) = +\frac{E_m}{4}.[A/(w-2w_0) + B/w]$$

3.6.3 Phase to phase to earth fault

The b- and c-phases are chosen to be short circuited to earth. It can thus be said that:

$$e_a' = 0$$

$$e_b + e_b' = 0 \quad \text{i.e.} \quad e_b' = -e_b$$

$$e_c + e_c' = 0 \quad \text{i.e.} \quad e_c' = -e_c$$

By using equation (3.10):

$$e_b' = E_m.SIN(w_0.t + \lambda - \delta - 120)$$

$$e_c' = E_m.SIN(w_0.t + \lambda - \delta + 120)$$

Then the corresponding time varying symmetrical components values are:

$$e_0' = (e_a' + e_b' + e_c')/3 = (-E_m/3).SIN(w_0t + \lambda - \delta)$$

$$e_1' = (e_a' + h_1e_b' + h_2e_c')/3 =$$

$$\left[\frac{E_m}{6}\right]SIN(w_0t + \lambda - \delta) - j\left[\frac{E_m}{2}\right]COS(w_0t + \lambda - \delta)$$

$$e_2' = (e_a' + h_2e_b' + h_1e_c')/3 =$$

$$\left[\frac{E_m}{6}\right]SIN(w_0t + \lambda - \delta) + j\left[\frac{E_m}{2}\right]COS(w_0t + \lambda - \delta)$$

Now by using exponential expansion in conjunction with equation (3.13) in frequency domain gives:

$$e_0'(w) = \left[\frac{E_m}{6}\right][(e^{j(\lambda-\delta)}/(w-w_0)) - (e^{-j(\lambda-\delta)}/(w+w_0))]$$

$$e_1'(w) = \left[\frac{-E_m}{6}\right][(2e^{j(\lambda-\delta)}/(w-w_0)) + (e^{-j(\lambda-\delta)}/(w+w_0))]$$

$$e_2'(w) = \left[\frac{+E_m}{6}\right][(e^{j(\lambda-\delta)}/(w-w_0)) + (2e^{-j(\lambda-\delta)}/(w+w_0))]$$

Assuming $A = \exp[j(\lambda - \delta)]$ and $B = \exp[-j(\lambda - \delta)]$ and, furthermore, employing shifting technique in +ve and −ve sequences gives:

$$e_0'(w) = \left[\frac{E_m}{6}\right][A/(w-w_0) - B/(w+w_0)]$$

$$e_1'(w+w_0) = \left[\frac{-E_m}{6}\right][2A/(w) + B/(w+2w_0)] \quad \ldots (3.16)$$

$$e_2'(w-w_0) = \left[\frac{+E_m}{6}\right][A/(w-2w_0) + 2B/(w)]$$

3.6.4 Phase to earth fault

The a−phase is chosen to be short circuited to earth. The superimposed voltages are thus as follows:

$$e_a + e_a' = 0 \quad \text{i.e.} \quad e_a' = -e_a$$
$$e_b' = 0$$
$$e_c' = 0$$

Knowing the phase value of superimposed voltage, the symmetrical components with reference to equation (3.10) are:

$$e_0' = (e_a' + e_b' + e_c')/3 = (1/3).SIN(w_0t + \lambda - \delta)$$
$$e_1' = (e_a' + h_1e_b' + h_2e_c')/3 = (1/3).SIN(w_0t + \lambda - \delta)$$
$$e_2' = (e_a' + h_2e_b' + h_1e_c')/3 = (1/3).SIN(w_0t + \lambda - \delta)$$

Now, by using exponential expansion and with reference to equation (3.13), the frequency domain symmetrical components values are:

$$e_0'(w) = \left[\frac{-E_m}{6}\right][A/(w-w_0) - B/(w+w)]$$

$$e_1'(w) = e_2'(w) = e_0'(w)$$

where $A = \exp[j(\lambda - \delta)]$ and $B = \exp[-j(\lambda - \delta)$

Applying the required shift in +ve and −ve sequences gives:

$$e_0'(w) = -\left[\frac{E_m}{6}\right][A/(w-w_0) - B/(w+w_0)]$$

$$e_1'(w+w_0) = -\left[\frac{E_m}{6}\right][A/w - B/(w+2w_0)] \qquad \ldots (3.17)$$

$$e_2'(w-w_0) = -\left[\frac{E_m}{6}\right][A/(w-2w_0) - B/w]$$

The superimposed voltages for different faults in frequency domain have been summarised in Table 3.18.

3.7 The Computational Procedure

The frequency spectrum of the superimposed currents $i_0'(w)$, $i_1'(w+w_0)$, $i_2'(w-w_0)$ can be computed for any fault conditions by utilising the appropriate values of voltages from Table 3.18 in conjunction with equation (3.9). Each current is then converted into time domain by evaluating digitally the inverse relationships given in the following equations:

The Function		Fault Simulation			
		3-phase	L.L	L.G	LL.G
$e'_0(w)$		0.0	0.0	$-\frac{E_m}{6}\left[\frac{A}{w-w_0}-\frac{B}{w+w_0}\right]$	$\frac{E_m}{6}\left[\frac{A}{w-w_0}-\frac{B}{w+w_0}\right]$
Original	$e'_1(w)$	$-\frac{E_m}{2}\cdot\frac{A}{w-w_0}$	$-\frac{E_m}{4}\left[\frac{A}{w-w_0}+\frac{B}{w+w_0}\right]$	$e_0(w)$	$-\frac{E_m}{6}\left[\frac{2A}{w-w_0}+\frac{B}{w+w_0}\right]$
	$e'_2(w)$	$\frac{E_m}{2}\cdot\frac{B}{w+w_0}$	$-e_1(w)$	$e_0(w)$	$\frac{E_m}{6}\left[\frac{A}{w-w_0}+\frac{2B}{w+w_0}\right]$
Shifted	$e'_1(w+w_0)$	$-\frac{E_m}{2}\cdot\frac{A}{w}$	$-\frac{E_m}{4}\left[\frac{A}{w}+\frac{B}{w+2w_0}\right]$	$-\frac{E_m}{6}\left[\frac{A}{w}-\frac{B}{w+2w_0}\right]$	$-\frac{E_m}{6}\left[\frac{2A}{w}+\frac{B}{w+2w_0}\right]$
	$e'_2(w-w_0)$	$\frac{E_m}{2}\cdot\frac{B}{w}$	$\frac{E_m}{4}\left[\frac{A}{w-2w_0}+\frac{B}{w}\right]$	$-\frac{E_m}{6}\left[\frac{A}{w-2w_0}-\frac{B}{w}\right]$	$\frac{E_m}{6}\left[\frac{A}{w-2w_0}+\frac{2B}{w}\right]$

TABLE 3.18

$A = \exp[j(\lambda - \delta)]$ and $B = \exp[-j(\lambda - \delta)]$

$$i_0' = (1/2\pi) \int_{-\infty}^{\infty} i_0'(w).\exp(jwt)dw$$

$$i_1' = (1/2\pi) \int_{-\infty}^{\infty} i_1'(w+w_0).\exp[j(w+w_0)t]dw \quad \ldots (3.19)$$

$$i_2' = (1/2\pi) \int_{-\infty}^{\infty} i_2'(w-w_0).\exp[j(w-w_0)t]dw$$

These time-varying sequence currents are converted into phase quantities which are then added to the prefault steady-state armature currents to obtain the overall response. The theory for obtaining the prefault currents is as outlined in the previous chapter.

3.7.1 Modified Fourier Transform

The basic Fourier integrals given in equation (3.19) have to be evaluated digitally and it then becomes essential to truncate the range of integration at angular frequencies $\pm\Omega$. A modified half range form of the basic integral as shown below is then used.

$$f(t) = [\exp(\alpha t)/\pi] \int_{0}^{\Omega} \sigma F(w-j\alpha)\exp(jwt)dw \quad \ldots (3.20)$$

The finite range of integration gives rise to Gibb's oscillations, and this is overcome by introducing the σ factor given by[17]:

$$\sigma = SIN(\pi w/\Omega)/(\pi w/\Omega) \quad \ldots (3.21)$$

In addition, a frequency shift constant α is introduced to ensure numerical stability when the integral is evaluated digitally[18]. This can be simply implemented by replacing 'w' in equation 3.7 by 'w−jα'. The evaluation of 'α' depends upon the system nature and a method has been considered in (19). Furthermore, as mentioned previously, there is also shifting involved in the +ve and −ve sequence quantities. This effectively means that the original 'w−jα' in equation (3.20) is replaced by '(w+w_0)−jα' for +ve sequence and '(w−w_0)−jα' for −ve sequence.

The inverse Fourier Transform is then performed as a summation process as follows:

$$f_+(t) = \left[\frac{1}{\pi}\sum_{k=1}^{N} Fk_+ . e^{j[w-j(\alpha+jw_0)].t}\right]\Delta w$$

$$f_-(t) = \left[\frac{1}{\pi}\sum_{k=1}^{N} Fk_- . e^{j[w-j(\alpha-jw_0)].t}\right]\Delta w \qquad . . (3.22)$$

where F_k is the corresponding sequence value in frequency domain:

$$F_{k\pm} = F_\pm(w).\sigma$$

The real form of the above equations is not utilised at this stage but it is applied after the final transformation into phase co−ordinates.

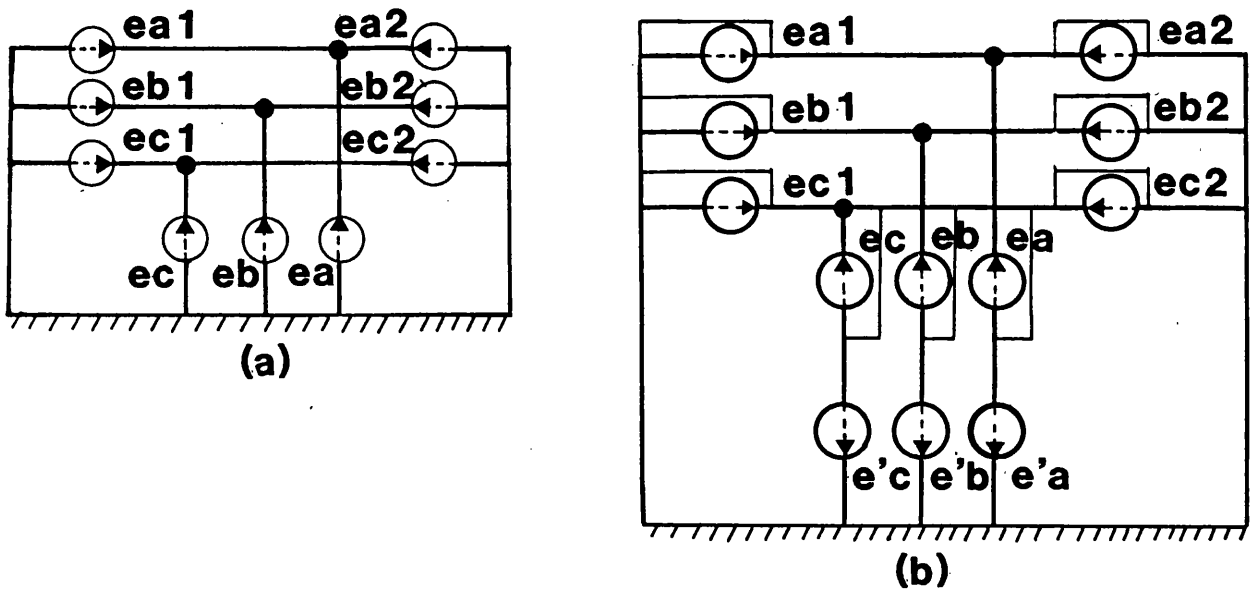

Fig 3.1: **a-Prefault Condition b-Fault Simulation**

CHAPTER 4

THE SYNCHRONOUS GENERATOR OPERATIONAL IMPEDANCES USING ANALYTICAL EXPRESSIONS AND FREQUENCY-RESPONSE DATA

4.1 Introduction

In power system fault analysis, each system state - the subtransient, transient and steady - has corresponding operational impedances according to the fault condition being studied. The methods given in chapter 2 require a knowledge of the operational parameters. In this chapter two different methods of obtaining these impedances have been considered.

In the first method, based on using analytical expression, consideration is given to some of the commonly made approximations in developing the operational impedances for frequency domain analysis. Both "d-q-o" and the Forward/Backward component methods are studied in some detail, together with using symmetrical component transformation for obtaining the final form of generator terminal equations.

In the second method, a more accurate simulation by utilising the frequency-response data obtained functions, $L_d(jw)$ and $L_q(jw)$, thus avoiding the concept of a solid rotor represented by a finite number of damper circuits, has been considered. This would, of course, enable one to do a comparison between the simulated synchronous generator with a finite number of windings, i.e. the analytical method, with that using frequency-response test results. For the latter, data is based on standstill frequency-response tests on the machine terminals and is implemented into the simulation using curve fitting techniques based on polynomials.

4.2 Operational Parameters Using Analytical Expression

In computing the generator short-circuit currents, the machine equations can be written in a more convenient form, by eliminating the rotor currents. This can be done using different methods, but care must be taken to retain the accuracy which is required for analysing the system. Here, two different methods, Adkins' approach[13] using d-q-o and Ku's method[10] using the Forward/Backward components in time domain, will be studied, and this will be followed by the development of a combination of these two approaches in the frequency domain.

4.2.1 Adkins' approach

By using equation (2.38), the d-q-o flux relationships are:

$$\begin{bmatrix}\psi_0\\ \psi_d\\ \psi_q\\ \psi_{fd}\\ \psi_{kd}\\ \psi_{kq}\end{bmatrix} = \begin{bmatrix}-L_0 & 0 & 0 & 0 & 0 & 0\\ 0 & -L_d & 0 & M_{ad} & M_{ad} & 0\\ 0 & 0 & -L_q & 0 & 0 & M_{aq}\\ 0 & -M_{ad} & 0 & L_{ff} & M_{ad} & 0\\ 0 & -M_{ad} & 0 & M_{ad} & L_{kk} & 0\\ 0 & 0 & -M_{aq} & 0 & 0 & L_{qq}\end{bmatrix} \begin{bmatrix}i_0\\ i_d\\ i_q\\ i_{fd}\\ i_{kd}\\ i_{kq}\end{bmatrix} \quad \ldots (4.1)$$

Also from equation (2.22), the voltage relationships are:

$$\begin{aligned} e_0 &= p\psi_0 - R.i_0\\ e_d &= p\psi_d - p\theta.\psi_q - R.i_d\\ e_q &= p\theta.\psi_d + p\psi_q - R.i_q\\ e_{fd} &= p\psi_{fd} + R_{fd}.i_{fd}\\ e_{kd} &= 0 = p\psi_{kd} + R_{kd}.i_{kd}\\ e_{kq} &= 0 = p\psi_{kq} + R_{kq}.i_{kq} \end{aligned} \quad \ldots (4.2)$$

4.2.1.1 Direct axis operational inductance and stator to field transfer function

The d-axis operational inductance is the ratio of d-axis armature flux linkage to d-axis current when all rotor windings are short circuited. The stator to field transfer function is the ratio of the d-axis flux linkage to field voltage when the armature is open circuited[20]. By the above definitions and with reference to equation (4.1), the flux linkage "ψ_d" depends only on the d-axis currents and is given as follows:

$$\psi_d = -L_d \cdot i_d + M_{ad} \cdot i_{fd} + M_{ad} \cdot i_{kd} \qquad \ldots (4.3)$$

By using equation (4.2), the relationship for the field and d-axis damper coils is given as:

$$\begin{aligned} e_{fd} = p\,\psi_{fd} + R_{fd} \cdot i_{fd} &= p(-M_{ad} \cdot i_d + L_{ff} \cdot i_{fd} + M_{ad} \cdot i_{kd}) + R_{fd} \cdot i_{fd} \\ &= -M_{ad} \cdot p(i_d) + (L_{ff} \cdot p + R_{fd}) \cdot i_{fd} + M_{ad} \cdot p i_{kd} \\ 0 = p\,\psi_{kd} + R_{kd} \cdot i_{kd} &= p(-M_{ad} \cdot i_d + M_{ad} \cdot i_{fd} + L_{kk} \cdot i_{kd}) + R_{kd} \cdot i_{kd} \\ &= -M_{ad} \cdot p(i_d) + M_{ad} \cdot p i_{fd} + (L_{kk} \cdot p + R_{kd}) \cdot i_{kd} \end{aligned} \qquad \ldots (4.4)$$

It can be seen that equations (4.3) and (4.4) also contain some field and damper winding currents. However, as mentioned before, in many studies such currents are not important and can be eliminated by careful manipulation of the above equations. When this is done, the resultant equation for the flux linkage takes the following form:

$$\psi_d = -L_d(p) \cdot i_d + g(p) \cdot e_{fd} \qquad \ldots (4.5)$$

where $L_d(p)$ and $g(p)$ are functions of the derivative operator (p), and are

obtainable as the quotient of two determinants each of which, when worked out, is a polynomial expression in (p). $L_d(p)$ is of the form:

$$L_d(p) = \frac{b_{(m+1)}p^{m+1} + b_m p^m + \ldots\ldots\ldots + b_0}{a_{(m+1)}p^{m+1} + a_m p^m + \ldots\ldots\ldots + a_0} \qquad \ldots (4.6)$$

In the above, both numerator and denominator are of same order. g(p) has the same denominator as $L_d(p)$ but different numerator of order "m", where m is the number of rotor circuits on d-axis.

$$g(p) = \frac{c_m p^m + c_{(m-1)}p^{m-1} + \ldots\ldots\ldots + c_0}{a_{(m+1)}p^{m+1} + a_m p^m + \ldots\ldots\ldots + a_0} \qquad \ldots (4.7)$$

In the above, the order of polynomial depends on the number of rotor circuits required in the model. Thus, for example, in the case of one damper winding on each axis of the machine we have:

$$L_d(p) = \frac{b_2p^2 + b_1p^1 + b_0}{a_2p^2 + a_1p^1 + a_0} \quad \text{and} \quad g(p) = \frac{c_1p + c_0}{a_2p^2 + a_1p^1 + a_0}$$

4.2.1.2 Quadrature-axis operational inductance

The q-axis operational inductance is the ratio of q-axis armature flux to q-axis current when all rotor windings are short circuited[20]. By this definition and with reference to equation (4.1), the flux linkage "ψ_q" depends only on the q-axis currents and is as follows:

$$\psi_q = -L_q \cdot i_q + M_{aq} \cdot i_{kq} \qquad \ldots (4.8)$$

and also by applying equations (4.2) and (4.1) we have:

$$e_{kq} = 0 = p\psi k_q + R_{kq}.i_{kq} = p(-M_{aq}.i_q + L_{qq}.i_{kq}) + R_{kq}.i_{kq}$$
$$= -M_{aq}.pi_q + (L_{qq}.p + R_{kq})i_{kq} \quad \ldots (4.9)$$

By following the previous procedure for d-axis, finally we get:

$$\psi_q = -L_q(p).i_q \quad \ldots (4.10)$$

where $L_q(p)$ is a function of (p) which is the quotient of two polynomials of order "n". For a machine with one damper winding in each axis, we have:

$$L_q(p) = \frac{k_1 p + k_0}{d_1 p + d_0}$$

It should be noted that the terms $L_d(p)$ and $L_q(p)$ which have been called the operational inductances, have phase angles which vary with frequency, because of the resistance in the rotor and iron losses in both rotor and stator. The $L_d(p)$ and $L_q(p)$ may be expressed in "Henries" or in per-unit inductances corresponding to the impedances at rated frequency[20]. At the lowest frequency, the operational inductances approach the unsaturated synchronous inductance, whereas at high frequencies they approach the stator winding leakage inductance of the machine[29].

4.2.1.3 Operational parameters as a function of time constants

The total self-inductance of each coil is the sum of the mutual and leakage inductances[13]. Hence:

$$L_d = \ell_d + M_{ad} \quad , \quad L_q = \ell_q + M_{aq}$$

$$L_{ff} = \ell_f + M_{ad} \quad , \quad L_{kk} = \ell_{kd} + M_{ad} \quad , \quad L_{qq} = \ell_{qq} + M_{aq}$$

Equations (4.3) and (4.4) now become:

$$\begin{aligned} \psi_d &= -(\ell_d + M_{ad}).i_d + M_{ad}.i_{fd} + M_{ad}.i_{kd} \\ e_{fd} &= -M_{ad}.pi_d + [R_{fd} + (\ell_f + M_{ad})p].i_{fd} + M_{ad}.pi_{kd} \\ e_{kd} &= 0 = -M_{ad}.pi_d + M_{ad}.pi_{fd} + [R_{kd} + (\ell_{kd} + M_{ad})p].i_{kd} \end{aligned} \qquad \ldots (4.11)$$

Likewise, equations (4.8) and (4.9) become:

$$\begin{aligned} \psi_q &= -(\ell_q + M_{aq}).i_q + M_{aq}.i_{kq} \\ e_{kq} &= 0 = -M_{aq}.pi_q + [R_{kq} + (\ell_{qq} + M_{aq})p].i_{kq} \end{aligned} \qquad \ldots (4.12)$$

By eliminating "i_{fd}" and i_{kd}" from equation (4.11), ψ_d can be written in a form shown in equation (4.13) below. This is an alternative form of equation (4.5):

$$\psi_d = -\left[\frac{1 + (T_4 + T_5)p + T_4.T_6.p^2}{1 + (T_1 + T_2)p + T_1T_3.p^2}\right]L_d.i_d + \left[\frac{1 + T_{kd}p}{1 + (T_1 + T_2)p + T_1T_3p^2}\right]M_{ad}.\frac{e_{fd}}{R_{fd}} \qquad \ldots (4.13)$$

The values of the time constants in the above equation are defined as follows[13]:

$$\begin{aligned} T_1 &= (L_{ff}/R_{fd}) = (1/R_{fd}) \,.\, (M_{ad} + \ell_f) \\ T_2 &= (L_{kk}/R_{kd}) = (1/R_{kd}) \,.\, (M_{ad} + \ell_{kd}) \\ T_3 &= (1/R_{kd}) \,.\, \{\ell_{kd} + [M_{ad}.\ell_f/(M_{ad} + \ell_f)]\} \\ T_4 &= (1/R_{fd}) \,.\, \{\ell_f + [M_{ad}.\ell_d/(M_{ad} + \ell_d)]\} \\ T_5 &= (1/R_{kd}) \,.\, \{\ell_{kd} + [M_{ad}.\ell_d/(M_{ad} + \ell_d)]\} \\ T_6 &= (1/R_{kd}) \,.\, \{\ell_{kd} + [M_{ad}.\ell_f.\ell_d/(M_{ad}.\ell_d + M_{ad}.\ell_f + \ell_d.\ell_f)]\} \end{aligned}$$

$$T_{kd} = (\ell_{kd}/R_{kd})$$

The values of $L_d(p)$ and $g(p)$ for a synchronous machine with one damper winding on each axis are found by comparing equation (4.5) and (4.13) and equating coefficients, then:

$$L_d(p) = \frac{(1 + T'_d.p)(1 + T''_d p)}{(1 + T'_{do}.p)(1 + T''_{do}.p)} L_d \qquad . . (4.14)$$

$$g(p) = \frac{(1 + T_{kd}.p)}{(1 + T'_{do}.p)(1 + T''_{do}.p)} \frac{M_{ad}}{R_{fd}}$$

Comparing this equation with (4.13), it follows that:

$$(1 + T_{do}'p)(1 + T_{do}"p) = 1 + (T_1 + T_2)p + T_1.T_3.p^2 \qquad . . (4.15)$$

$$(1 + T_d'p)(1 + T_d"p) = 1 + (T_4 + T_5)\,p + T_4.T_5.p^2 \qquad . . (4.16)$$

where T_{do}', $T_{do}"$ are the d-axis open circuit transient and subtransient time constants, and T_d', $T_d"$ are the d-axis short circuit transient and subtransient time constants. These new constants are the four main constants of the synchronous machine, and their values can be calculated by solving two quadratic equations (4.15) and (4.16) with a further approximation, based on the fact that the per unit value of the damper winding resistance is much larger than that of the field winding. T_2 and T_3 are then much less than T_1, and the right-hand side of equation (4.15) can be approximated to $(1 + T_1p).(1 + T_3p)$.

$$T_{do}' \cong T_1 \quad \text{and} \quad T_{do}" \cong T_3$$
$$T_d' \cong T_4 \quad \text{and} \quad T_d" \cong T_6$$

The value of $L_q(p)$ can be similarly obtained by eliminating "i_{kq}" from equations (4.12) and comparing the result with equation (4.8), i.e.:

$$L_q(p) = \frac{(1 + T''_q.p)}{(1 + T''_{qo}.p)} L_q \qquad \ldots (4.17)$$

where T''_{qo} is the q-axis open circuit subtransient time constant and T''_q is the q-axis short circuit subtransient time constant.

The fundamental machine time constants have been shown in reference (13).

4.2.1.4 The frequency domain evaluation of operational parameters

By substituting "ψ_d" and "ψ_q" from equation (4.1) into equation (4.2) we have:

$$\begin{aligned}
e_d &= p(-L_d.i_d + M_{ad}.i_{fd} + M_{ad}.i_{kd}) - w_0\,(-L_q.i_q + M_{aq}.i_{kq}) - R.i_d \\
e_q &= w_0(-L_d.i_d + M_{ad}.i_{fd} + M_{ad}.i_{kd}) + p(-L_q.i_q + M_{aq}.i_{kq}) - R.i_q \\
e_0 &= -L_0.pi_0 + R.i_0 = (-L_0p + R)i_0 \\
e_{fd} &= p(-M_{ad}.i_d + L_{ff}.i_{fd} + M_{ad}.i_{kd}) + R_{fd}.i_{fd} \\
0 &= p(-M_{ad}.i_d + M_{ad}.i_{fd} + L_{kk}.i_{kd}) + R_{kd}.i_{kd} \\
0 &= p(-M_{aq}.i_q + L_{qq}.i_{kq}) + R_{kq}.i_{kq}
\end{aligned} \qquad \ldots (4.18)$$

As an example, consider the d-axis component of the voltage given in equation (4.18), i.e:

$$e_d = p(-L_d.i_d + M_{ad}.i_{fd} + M_{ad}.i_{kd}) - w_0(-L_q.i_q + M_{aq}.i_{kq}) - R.i_d \qquad \ldots (4.19)$$

In transforming equation (4.19) by means of Fourier integral, it is useful to note that the Fourier Transform of any function of time $f(t) = f_1(p).f_2(t)$ is given by(21):

$$f(jw) = f_1(jw).f_2(jw)$$

where:

$$f_2(jw) = \int_{-\infty}^{\infty} f_2(t).\exp(-jwt).dt$$

Equation (4.19) then transforms to:

$$e_d(jw) = -(R + jwL_d) \; . \; i_d(jw) + w_0.L_q.i_q(jw) + jw.M_{ad}.i_{fd}(jw) + jw.M_{ad}.i_{kd}(jw) - w_0.M_{aq}.i_{kq}(jw)$$

Similar procedure for the other relationships given in equation (4.18) leads to the complete matrix equation relating the current and voltage components given in the following equation:

$$\begin{bmatrix} e_0(jw) \\ e_d(jw) \\ e_q(jw) \\ e_{fd}(jw) \\ 0 \\ 0 \end{bmatrix} = \begin{bmatrix} -(R + jwL_0) & 0 & 0 & 0 & 0 & 0 \\ 0 & -(R + jwL_d) & w_0.L_q & jw.M_{ad} & jw.M_{ad} & -w_0.M_{aq} \\ 0 & -w_0.L_d & -(R + jw.L_q) & w_0.M_{ad} & w_0.M_{ad} & jw.M_{aq} \\ 0 & -j.w.M_{ad} & 0 & (R_{fd} + jw.L_{ff}) & jw.M_{ad} & 0 \\ 0 & -j.w.M_{ad} & 0 & jw.M_{ad} & (R_{kd} + jw.L_{kk}) & 0 \\ 0 & 0 & -j.w.M_{aq} & 0 & 0 & (R_{kq} + jw.L_{qq}) \end{bmatrix} \begin{bmatrix} i_0(jw) \\ i_d(jw) \\ i_q(jw) \\ i_{fd}(jw) \\ i_{kd}(jw) \\ i_{kq}(jw) \end{bmatrix} \quad . \; . \; (4.20)$$

As has been mentioned previously, in similar studies, computing only the variation of armature currents and voltages for analysing the system is sufficient. Moreover, if the problem is solved by superposition and excitation voltage "e_{fd}" is constant throughout the short period of interest following a fault at armature terminals, the superimposed value of field voltage "e_{fd}" is zero.

Under this condition, equation (4.20) can be reduced to the following 3x3 matrix by eliminating the rotor circuits:

$$\begin{bmatrix} e_0'(jw) \\ e_d'(jw) \\ e_q'(jw) \end{bmatrix} = \begin{bmatrix} -(R+jwL_0) & 0 & 0 \\ 0 & -(R+jwL_d(jw)) & w_0L_q(jw) \\ 0 & -w_0L_d(jw) & -(R+jwL_q(jw)) \end{bmatrix} \begin{bmatrix} i_0'(jw) \\ i_d'(jw) \\ i_q'(jw) \end{bmatrix} \quad . . (4.21)$$

The above relationship can be obtained by inversion of the full matrix given in equation (4.20), and reinverting the 3x3 submatrix formed from the first three rows and columns.

An alternative method is to substitute for the frequency-response functions $L_d(jw)$, $L_q(jw)$ which can be obtained from d- and q-axis operational impedances $X_d(p)$, $X_q(p)$. However, expressions for the latter often involve making certain simplifying assumptions and, for this reason, the former method is preferable[20]. It should be noted that studies have also been carried out for a more complex rotor construction machine comprising two rotor windings on d-axis and three rotor windings on q-axis. The analysis for this type of machine is considered in Appendix A-2.

4.2.2 Ku's approach using Forward/Backward components

From equation (2.29), the transformation coefficients from d-q to F-B components and vice versa are given by:

$$[T_1] = \begin{matrix} \\ F \\ B \end{matrix}\begin{matrix} \begin{matrix} d & q \end{matrix} \\ \begin{bmatrix} 1/2 & j/2 \\ 1/2 & -j/2 \end{bmatrix} \end{matrix} \quad \text{and} \quad [T_1]^{-1} = \begin{matrix} \\ d \\ q \end{matrix}\begin{matrix} \begin{matrix} F & B \end{matrix} \\ \begin{bmatrix} 1 & 1 \\ -j & j \end{bmatrix} \end{matrix} \qquad \ldots (4.22)$$

Also from equation (2.27), the transformation from symmetrical components to Forward/Backward components when $\lambda = 0$ are:

$$\begin{bmatrix} e_F \\ e_B \end{bmatrix} = \begin{bmatrix} e^{-jw_0t} & 0 \\ 0 & e^{jw_0t} \end{bmatrix} \cdot \begin{bmatrix} e_1 \\ e_2 \end{bmatrix} \qquad \ldots (4.23)$$

Using the transform pairs defined in chapter 3 gives:

$$e_F(w) = e_1(w+w_0) \quad , \quad e_B(w) = e_2(w-w_0) \qquad \ldots (4.24)$$

Applying transformation coefficients $[T_1]$ and $[T_1]^{-1}$ to the d-q components of equation (4.21) yields:

$$\begin{bmatrix} e_F'(jw) \\ e_B'(jw) \end{bmatrix} = [T_1] \begin{bmatrix} -(R+jwL_d(jw)) & woL_q(jw) \\ -w_0L_d(jw) & -(R+jwL_q(jw)) \end{bmatrix} \cdot [T_1]^{-1} \begin{bmatrix} i_F'(jw) \\ i_B'(jw) \end{bmatrix}$$

$$= \begin{bmatrix} -[R+j(w+w_0)L_1(jw)] & -j(w+w_0)L_2(jw) \\ -j(w-w_0)L_2(jw) & -[R+j(w-w_0)L_1(jw)] \end{bmatrix} \begin{bmatrix} i_F'(jw) \\ i_B'(jw) \end{bmatrix}$$

$$\ldots (4.25)$$

where $L_1(jw)$ and $L_2(jw)$ are the operational inductances applicable to the Forward and Backward components, and can be calculated as follows:

$$\begin{aligned} L_1(jw) &= [L_d(jw) + L_q(jw)]/2 \\ L_2(jw) &= [L_d(jw) - L_q(jw)]/2 \end{aligned} \qquad \ldots (4.26)$$

By inversion of equation (4.25) the frequency spectrum of the currents in terms of $e_F'(jw)$, $e_B'(jw)$ will be obtained so that:

$$\begin{bmatrix} i_F'(jw) \\ i_B'(jw) \end{bmatrix} = 1/z^2 \begin{bmatrix} -R-j(w-w_0)L_1(jw) & j(w+w_0)L_2(jw) \\ j(w-w_0)L_2(jw) & -[R+j(w+w_0)L_1(jw)] \end{bmatrix} \begin{bmatrix} e_F'(jw) \\ e_B'(jw) \end{bmatrix} \qquad \ldots (4.27)$$

where:

$$z^2 = R^2 + j2wL_1(jw)\,R - (w^2 - w^2{}_0)\,[L_1{}^2(jw) - L_2{}^2(jw)]$$

It should be noted that the zero sequence relationship is unchanged throughout the calculations.

4.2.3 Using symmetrical components transformation

As we have mentioned in chapter 2, the transformation from time-varying direct phase quantities to time-varying symmetrical-component quantities is of the well-known form:

$$[T_2] = \begin{array}{c} \\ 0 \\ 1 \\ 2 \end{array} \begin{array}{c} \begin{array}{ccc} a & b & c \end{array} \\ \begin{bmatrix} 1/3 & 1/3 & 1/3 \\ 1/3 & h_1/3 & h_2/3 \\ 1/3 & h_2/3 & h_1/3 \end{bmatrix} \end{array} \qquad \ldots (4.28)$$

and the transformation from time varying phase quantities to time-varying d-q-o components is in accordance with the following:

$$[T_3] = \begin{array}{c} \\ a \\ b \\ c \end{array} \begin{array}{c} \begin{array}{ccc} o & d & q \end{array} \\ \begin{bmatrix} 1 & \cos\theta & -\sin\theta \\ 1 & \cos(\theta - 120) & -\sin(\theta - 120) \\ 1 & \cos(\theta + 120) & -\sin(\theta + 120) \end{bmatrix} \end{array} \quad \ldots (4.29)$$

Combination of the matrix relating d-q-o components to the direct-phase quantities given above with equation (4.22) and (4.28) (in which $[T_1]$ is extended to include the zero sequence), gives the connection between symmetrical components and Forward/Backward components as follows:

$$\begin{bmatrix} e_0' \\ e_1' \\ e_2' \end{bmatrix} = [T_2][T_3][T_1]^{-1} \begin{bmatrix} e_0' \\ e_F' \\ e_B' \end{bmatrix} = \begin{bmatrix} 1 & 0 & 0 \\ 0 & \exp(j\theta) & 0 \\ 0 & 0 & \exp(-j\theta) \end{bmatrix} \begin{bmatrix} e_0' \\ e_F' \\ e_B' \end{bmatrix} \quad \ldots (4.30)$$

With the assumption of constant speed, the rotor angle (θ) may be written as $\theta = w_0 t + \lambda$, and it follows that:

$$\begin{aligned} e_F'(jw) &= e_1' \exp(-jw_0 t)\exp(-j\lambda) \\ e_B'(jw) &= e_2' \exp(+jw_0 t)\exp(+j\lambda) \end{aligned} \quad \ldots (4.31)$$

Equation (4.30) can be transformed into the frequency domain by means of the following transform definition:

$$f(t)\exp(+jw_0 t) = f[j(w-w_0)] \quad \text{and} \quad f(t)\exp(-jw_0 t) = f[j(w+w_0)]$$

and it follows that:

$$e_0'(jw) = e_0'(jw)$$

$$e_F'(jw) = e_1'[j(w+w_0)]\exp(-j\lambda)$$

$$e_B'(jw) = e_2'[j(w-w_0)]\exp(+j\lambda)$$

Likewise, relationships for the frequency domain components of currents are as follows:

$$e_o'(jw) = e_o'(jw)$$

$$e_F'(jw) = e_1'[j(w+w_o)]\exp(-j\lambda)$$

$$e_B'(jw) = e_2'[j(w-w_o)]\exp(+j\lambda)$$

By using the above definitions into equation (4.27) and by including the zero sequence components, the final form of the relationships is as shown in equation (4.32).

$$\begin{bmatrix} i_0'(jw) \\ i_1'[j(w+w_0)]\exp(-j\lambda) \\ i_2'[j(w-w_0)]\exp(+j\lambda) \end{bmatrix} = [1/z^2] \begin{bmatrix} -z^2/(R+jwL_0) & 0 & 0 \\ 0 & -[R+j(w-w_0)L_1(jw)] & 0 \\ 0 & j(w-w_0)L_2(jw) & j(w+w_0)L_2(jw) \\ & & -[R+j(w+w_0)L_1(jw)] \end{bmatrix} \begin{bmatrix} e_0'(jw) \\ e_1'[j(w+w_0)]\exp(-j\lambda) \\ e_2'[j(w-w_0)]\exp(+j\lambda) \end{bmatrix}$$

. . (4.32)

Finally, it should be noted that the equation (4.26) looks similar to the following relationships which are obtained from equation (2.39):

$$L_s + M = (L_d + L_q)/2$$

$$(3/2)L_m - (L_d - L_q)/2$$

Moreover, it may be found from equation (3.7) that when the method of superposition is applied, the steady state superimposed values of i_{fd}, i_{kd}, i_{kq} are equal to zero. It is therefore clear at this stage that the operational inductances can be given as $L_1(jw) = L_s+M$ and $L_2(jw) = (3/2)L_m$ and this verifies the validity of representation.

4.3 Operational Parameters Using Curve Fitting Techniques

This section is concerned with obtaining operational parameters of the machine from practical frequency-response data which is in a discrete form. For computational purposes, since it is necessary to be able to accurately predict the parameters of any desirable freqeuncy, computer algorithms based on curve fitting techniques have thus to be applied to the practical data. The method used here is concerned with the mathematical representation of relationships between the machine parameters and the frequency. These relationships are defined by a set of data points, and it is desired to determine a mathematical function which passes satisfactorily close to these data points. The available data points cover the whole range of frequencies required in the subsequent use of the fitted function. Extrapolation of the function beyond the range of the available data is totally unreliable. To approximate the set of data points as closely as possible to the actual data, using a specified function, the function (for example, a polynomial) should be as smooth as possible. However, there is a conflict between the smoothness and closeness. For example, greater smoothness can be obtained by restricting the number of coefficients and therefore the order of the polynomials. On the other hand, to obtain greater closeness, the order of the polynomial and therefore the number of coefficients have to be increased. A compromise should thus be made between the two conflicting requirements.

In practice, the two most common fitting functions used are based on polynomials and cubic splines, because of their simplicity and ease of handling. Polynomials have long played a basic role in data fitting and their use has been extended to a wide variety of situations. Cubic spline functions have also proved themselves to be a valuable tool, particularly because of their adaptability to a wider variety of shapes than polynomials. However, in this study, because of the nature of the data which is a function of complex frequency, a curve fitting function based on polynomials is better suited to the problem.

4.3.1 General representation of polynomials

Two different forms for representing a polynomial are used in practice. One is the usual power series form (45) given by:

$$f(x) = b_0 + b_1.x + b_2.x^2 + b_3.x^3 + \ldots\ldots\ldots + b_k.x^k \qquad \ldots (4.33)$$

The other is the Chebyshev series (44) of the form:

$$f(x) = (1/2)a_0.T_0(x) + a_1.T_1(x) + a_2.T_2(x) + \ldots\ldots\ldots + a_k.T_k(x) \qquad \ldots (4.34)$$

where $T_k(x)$ is the Chebyshev polynomial of degree "k" in x, and the range of "x" has been normalised to run from −1 to +1.

Of the above two, in this study the Chebyshev form is used since it leads to much better accuracy in general, both in the computation of the coefficients and in the subsequent evaluation of the fitted polynomial at specified points (45). In equation (4.34) the term $T_k(x)$ is best defined for our purpose by its recurrence relationship (44).

$$T_{(k+1)}(x) = 2.x.T_k(x) - T_{(k-1)}(x)$$

In the above equation, starting with $T_0(x) = 1$ and $T_1(x) = x$, the next few polynomials would be:

$$T_2(x) = 2.x.x - 1 = 2x^2 - 1$$
$$T_3(x) = 4.x^3 - 3.x$$
$$T_4(x) = 8.x^4 - 8.x^2 + 1$$
$$T_5(x) = 16.x^5 - 20.x^3 + 5x \ ,$$

and so on.

The Chebyshev form of equation (4.34) is less familiar than the usual power series form of equation (4.33), but it avoids numerical problems frequently encountered with the latter, and is just as easy to implement on a computer.

4.3.2 Consideration of data form

With regard to the practical data used in this study, there are three distinct points in the frequency range (as shown in chapter 6) where there are rather abrupt changes in the machine inductances. Using just one polynomial expression to fit the entire curve would result in large unacceptable errors in the calculated points. However, this problem can be overcome by splitting the available data curve into three parts and fitting each part using a separate polynomial expression. For example, if the three frequency ranges are:

$W_x = 0 \longrightarrow W_1$
$W_y = W_1 \longrightarrow W_2$
$W_z = W_2 \longrightarrow W_3$

where 0 and W_3 are the lower and upper limits in the frequency range.

Then we can say that for a function f(w) we have:

$$f_1(w) = f(W_x) \quad \text{for} \quad 0 < w < W_1$$

$$f_2(w) = f(W_y) \quad \text{for} \quad W_1 < w < W_2$$

$$f_3(w) = f(W_z) \quad \text{for} \quad W_2 < w < W_3$$

A polynomial expression can now be written for each of the above three functions f_1, f_2 and f_3 and within the computer algorithm, the approximate function is selected depending upon frequency.

For simplicity it has been assumed that the data points are of equal weight.

4.3.3 Operational inductance in polynomial form

The operational inductances can be approximated by rational polynomials whose degree depend on the number of rotor circuits required in the model. Hurley and Schwenk[46] suggested a second order polynomial, and a third order polynomial function has also been considered[20,28,29].

However, an extensive series of studies has shown that for the type of data available for this study, a third order polynomial for a 150MVA turbogenerator used at the Northfleet station in the UK and a fifth order polynomial for a 588MVA turbogenerator at the Ontario Hydro Station in Canada gives the best fit.

The data is in the form of the d- and q-axis impedances of the machine as a function of frequency viewed from the armature terminal. With reference to the definitions which have been used in (20), they are as follows:

$$Z_d(jw) = -[\triangle e_d(jw)]/[\triangle i_d(jw)]$$
$$Z_q(jw) = -[\triangle e_q(jw)]/[\triangle i_q(jw)] \quad \ldots (4.35)$$

where the stator windings are excited and all rotor windings short circuited[47] and $\triangle e_d$, $\triangle i_d$ are small step changes. Subtracting the sum of armature and lead resistances from these operational impedances results in the d- and q-axis operational inductances being of the form:

$$L_d(jw) = [Z_d(jw) - R']/jw$$
$$L_q(jw) = [Z_q(jw) - R']/jw$$

where R' is the sum of "dc" resistance of one phase of the armature and the lead which have been used in tests. Now taking the example of say $L_d(jw)$, we can say that:

$$L_d(jw) = \text{Real}\,[L_d(jw)] + j.\text{Imag}\,[L_d(jw)]\ ,$$

in which Real and Imaginary parts can be fitted separately, thus with reference to equation (4.34):

$$L_d(jw) = (1/2)a_0.T_0(w) + a_1.T_1(w) + \ldots\ldots\ldots + a_k.T_k(w)] + j[(1/2)b_0.T_0(w) + b_1.T_1(w) + \ldots\ldots\ldots + b_k.T_k(w)] \quad \ldots (4.36)$$

Substituting "w" by "(w-jα)" for the modified Fast Fourier Transform, the function in the above equation takes the following form:

$$L_d[j(w-j\alpha)] = [(1/2)a_0T_0(w-j\alpha) + a_1T_1(w-j\alpha) + \ldots\ldots\ldots + a_kT_k(w-ja)]+ j[(1/2)b_0T_0(w-j\alpha) + b_1T_1(w-j\alpha) + \ldots\ldots\ldots + b_kT_k(w-j\alpha)]$$

Similar exprressions can be obtained for $L_q(jw)$ and $L_q[j(w-j\alpha)]$. Some effects of synchronous machine rotor construction on its operational inductance functions form have been considered in Appendix A-3.

CHAPTER 5

COMBINATION OF NETWORK ELEMENTS

5.1 Introduction

In the previous chapters a realistic model of the generator has been derived. A knowledge of the faulted responses for ehv transmission systems as a whole is, however, of considerable importance for both system design and protection-system development[41], and it is the primary purpose of this chapter to improve the realism with which faults on generator, generator/transformer and transmission-line interconnection can be simulated.

In this chapter, methods are outlined for including the previously developed synchronous machine model into an ehv transmission system.

Furthermore, a method for incorporating the transformer into the power system transient studies is also outlined. This method takes account of internal transformer voltage drops and fixes the transformer representation when various transformations are needed. Apart from the time domain phase-co-ordinate techniques, a new method using the symmetrical components in frequency domain is considered. This considerably simplifies the computational process and gives greatly improved economy of computing time.

5.2 Simulation of Generator/Transformer

5.2.1 Phase co-ordinate representation (nodal admittance method)

5.2.1.1 Single phase transformer

A single phase transformer representation is shown (Figure 5.1) with turns ratio (n):1 and equivalent leakage admittance Y(p), where:

$$Y(p) = 1/(r_t + jwL_t)$$

From Figure 5.1 it can be seen that:

$$V_s = (n).V' \qquad \ldots (5.1)$$

$$I_r = -(n).I_s \qquad \ldots (5.2)$$

Where all values are in per-unit and (n) represents the turn ratio of transformer, we also have:

$$I_r = Y(p).[V_r - V'] = Y(p).V_r - Y(p).V_s/(n) \qquad \ldots (5.3)$$

$$I_s = [-I_r/(n)] = [Y(p).V_s/(n)^2] - [Y(p).V_r/(n)] \qquad \ldots (5.4)$$

In other words, V_r and V_s may be represented by the j,k,p,q nodes as follows:

$$V_s = V_j - V_k \qquad V_r = V_p - V_q \qquad \ldots (5.5)$$

Each node will, in turn, have its own current, thus from equation (5.4) we get:

$$I_j = Y(p)/(n)^2 [V_j - V_k] - Y(p)/(n)[V_p - V_q]$$
$$= [Y(p)/n^2].V_j - [Y(p)/n^2].V_k - [Y(p)/n].V_p + [Y(p)/n].V_q \quad \ldots (5.6)$$

Since the current in transformer link "k" is opposite to the current of "j", it follows:

$$I_k = -I_j = -I_s = [-Y(p)/n^2].V_j + [Y(p)/n^2].V_k + [Y(p)/n].V_p - [Y(p)/n].V_q \quad \ldots (5.7)$$

From equations (5.2) and (5.6) we get:

$$I_p = I_r = [-Y(p)/n].V_j + [Y(p)/n].V_k + Y(p).V_p - Y(p).V_q \quad \ldots (5.8)$$

Similarly,

$$I_q = - I_p = [Y(p)/n].V_j - [Y(p)/n].V_k - Y(p).V_p + Y(p).V_q \quad \ldots (5.9)$$

From equations (5.6), (5.7), (5.8) and (5.9) the nodal admittance matrix may be written:

$$[I] = [Y].[V] \quad \ldots (5.10)$$

where:

$$[I] = [I_j \; I_k \; I_p \; I_q]^t,$$

$$[V] = [V_j \; V_k \; V_p \; V_q]^t,$$

and:

$$[Y] = \begin{array}{c} \\ j \\ k \\ p \\ q \end{array} \begin{array}{c} \begin{array}{cccc} j & k & p & q \end{array} \\ \begin{bmatrix} Y(p)/(n)^2 & -Y(p)/(n)^2 & -Y(p)/(n) & Y(p)/(n) \\ -Y(p)/(n)^2 & Y(p)/(n)^2 & Y(p)/(n) & -Y(p)/(n) \\ -Y(p)/(n) & Y(p)/(n) & Y(p) & -Y(p) \\ Y(p)/(n) & -Y(p)/(n) & -Y(p) & Y(p) \end{bmatrix} \end{array} \quad . \; . \; (5.11)$$

The topology of equation (5.10) suggests an admittance circuit (or lattice) as shown in Figure 5.2.

5.2.1.2 Three phase transformer

The extension of the lattice to form three separate bank transformers with a delta–star connection is shown in Figure 5.3, where the vector group is taken as Y_{d11} and the admittances corresponding to those between (j–q) and (k–q) in Figure 5.2, are eliminated in order to isolate the star (normally earthed) point from the delta side.

To permit Y_{d11} transformer's combination with the synchronous machine it is necessary to describe the transformer by using frequency–shifted sequence variables. The latter could, of course, be obtained from frequency response tests, but it has been shown that the inductance for a power transformer remains more or less constant up to a frequency about 12kHz[31] and drops off thereafter. Since this limit of 12kHz is well above the highest frequency of the transient components of

interest, hence it is realistic to adopt an analytical approach.

The method used here makes use of the technique which has been outlined before, for a single-phase transformer. It enables the transformer to be represented on a per-unit basis by the circuit equivalent shown in Figure 5.3b. In this particular form of representation, the magnetising impedance of the transformer has been neglected and Y(p) which is the per-unit operational leakage admittance is of equal value for positive sequence, negative sequence and zero sequence components. The circuit can, however, be modified to include the effect of magnetising impedance, in particular, to take account of the fact that, in a three-legged core-type transformer, zero-sequence components of core-flux traverse out of core-return paths. In this respect it should be noted that the delta connection effectively short-circuits the flow of zero-sequence current components, so that only relatively low components of zero sequence voltage and associated fluxes actually exist. Thus for delta-star connected three-legged core-type transformers it is possible to ignore the magnetising impedances without incurring significant errors, a fact which also applies to banked generator/transformer arrangements.

For the per-unit system, a value of 1.0 per-unit voltage on each leg of the star winding produces, under balanced conditions, $\sqrt{3}$ per-unit voltage on each leg of the delta winding (rated line to neutral voltage as base). Hence an effective tapping at $\sqrt{3}$ nominal turns ratio on the delta side is required, i.e. $n = \sqrt{3}$. Thus with reference to Figure 5.3b, a nodal analysis of equivalent circuit of the generator/transformer gives a relationship between the various voltages and currents as:

$$\begin{bmatrix} i_{ma}' \\ i_{mb}' \\ i_{mc}' \\ i_{sa}' \\ i_{sb}' \\ i_{sc}' \\ i_{n}' \end{bmatrix} = Y(p) \begin{bmatrix} 2/3 & -1/3 & -1/3 & -1/\sqrt{3} & 1/\sqrt{3} & 0 & 0 \\ -1/3 & 2/3 & -1/3 & 0 & -1/\sqrt{3} & 1/\sqrt{3} & 0 \\ -1/3 & -1/3 & 2/3 & 1/\sqrt{3} & 0 & -1/\sqrt{3} & 0 \\ 1/\sqrt{3} & 0 & -1/\sqrt{3} & -1 & 0 & 0 & -1 \\ -1/\sqrt{3} & 1/\sqrt{3} & 0 & 0 & -1 & 0 & -1 \\ 0 & -1/\sqrt{3} & 1/\sqrt{3} & 0 & 0 & -1 & -1 \\ 0 & 0 & 0 & -1 & -1 & -1 & 3 \end{bmatrix} \begin{bmatrix} v_{ma}' \\ v_{mb}' \\ v_{mc}' \\ v_{sa}' \\ v_{sb}' \\ v_{sc}' \\ v_{n}' \end{bmatrix} \quad . . (5.12)$$

where: v_{ma}', v_{mb}', v_{mc}' are delta-side (or machine terminals) voltages

i_{ma}', i_{mb}', i_{mc}' are the output currents of synchronous machine

v_{sa}', v_{sb}', v_{sc}' are the star-side voltages

i_{sa}', i_{sb}', i_{sc}' are the star-side currents

and the direction of currents is as shown in Figure 5.3a and 5.3b.

The above relationship will change to that of equation (5.13) by putting $v_n=0$ (reference to earthed point), and this permits an elimination of the seventh column and row in equation (5.12), this then gives:

$$\begin{bmatrix} i_{ma}' \\ i_{mb}' \\ i_{mc}' \\ i_{sa}' \\ i_{sb}' \\ i_{sc}' \end{bmatrix} = Y(p) \begin{bmatrix} 2/3 & -1/3 & -1/3 & -1/\sqrt{3} & 1/\sqrt{3} & 0 \\ -1/3 & 2/3 & -1/3 & 0 & -1/\sqrt{3} & 1/\sqrt{3} \\ -1/3 & -1/3 & 2/3 & 1/\sqrt{3} & 0 & -1/\sqrt{3} \\ 1/\sqrt{3} & 0 & -1/\sqrt{3} & -1 & 0 & 0 \\ -1/\sqrt{3} & 1/\sqrt{3} & 0 & 0 & -1 & 0 \\ 0 & -1/\sqrt{3} & 1/\sqrt{3} & 0 & 0 & -1 \end{bmatrix} \begin{bmatrix} v_{ma}' \\ v_{mb}' \\ v_{mc}' \\ v_{sa}' \\ v_{sb}' \\ v_{sc}' \end{bmatrix}$$

<----------[T1]---------->

. . (5.13)

5.2.2 The symmetrical component representation

As was discussed in chapters 2 and 4, the matrix form of relationships between symmetrical components and direct-phase values is as follows:

$$[I_{(sym)}] = [T_2]^{-1}.[I_{(phase)}]$$

$$\text{and } [V_{(sym)}] = [T_2]^{-1}.[V_{(phase)}]$$

$$\text{and if: } [V_{(phase)}] = [Z_{(phase)}].[I_{(phase)}]$$

$$\text{and } [I_{(phase)}] = [Y_{(phase)}].[V_{(phase)}]$$

$$\text{then: } [V_{(sym)} = [T_2]^{-1}\,[Z_{(phase)}][T_2][I_{(sym)}] = [Z_{sym}]\,[I_{(sym)}]$$

$$[I_{(sym)} = [T_2]^{-1}\,[Y_{(phase)}][T_2][V_{(sym)}] = [Y_{sym}][V_{(sym)}]$$

$$\text{where: } [Z_{sym}] = [T_2]^{-1}\,[Z_{phase}][T_2]$$

$$\text{and } [Y_{sym}] = [T_2]^{-1}\,[Y_{phase}][T_2] \qquad \ldots (5.14)$$

and:

$$[T_2] = \begin{bmatrix} 1/3 & 1/3 & 1/3 \\ 1/3 & h_1/3 & h_2/3 \\ 1/3 & h_2/3 & h_1/3 \end{bmatrix}$$

Using the principle which has been defined in equation (5.14) into equation (5.13) we get:

$$\begin{bmatrix} i_{mo}' \\ i_{m1}' \\ i_{m2}' \\ i_{so}' \\ i_{s1}' \\ i_{s2}' \end{bmatrix} - Y(p).\begin{bmatrix} T_2 & & 0 \\ & & \\ & & \\ & & \\ & & \\ 0 & & T_2 \end{bmatrix}[T_1]\begin{bmatrix} T_2 & & 0 \\ & & \\ & & \\ & & \\ & & \\ 0 & & T_2 \end{bmatrix}^{-1}\begin{bmatrix} v_{mo}' \\ v_{m1}' \\ v_{m2}' \\ v_{so}' \\ v_{s1}' \\ v_{s2}' \end{bmatrix}$$

$$- Y(p).\begin{bmatrix} 0 & 0 & 0 & 0 & 0 & 0 \\ 0 & 1 & 0 & 0 & (h_2-1)/\sqrt{3} & 0 \\ 0 & 0 & 1 & 0 & 0 & (h_1-1)/\sqrt{3} \\ 0 & 0 & 0 & -1 & 0 & 0 \\ 0 & (1-h_1)/\sqrt{3} & 0 & 0 & -1 & 0 \\ 0 & 0 & (1-h_2)/\sqrt{3} & 0 & 0 & -1 \end{bmatrix}\begin{bmatrix} v_{mo}' \\ v_{m1}' \\ v_{m2}' \\ v_{so}' \\ v_{s1}' \\ v_{s2}' \end{bmatrix}$$

. . (5.15)

It is evident from equation (5.15) that $i_{mo}' = v_{mo}' = 0$, and this thus shows the absence of the zero sequence components from the output of the delta-side.

5.2.3 Frequency-domain transformation of symmetrical components

Transformation of equation (5.15) into the frequency domain is affected by noting that the Fourier Transform of a function of time $f(t) = f_1(p)f_2(t)$ is given by:

$$f(jw) = f_1(jw).f_2(jw)$$

where:

$$f_2(jw) = \int_{-\infty}^{\infty} f_2(t).e^{-jw.t}.dt$$

It follows that equation (5.15) transforms to:

$$\begin{bmatrix} i_{mo}'(jw) \\ i_{m_1}'(jw) \\ i_{m_2}'(jw) \\ i_{so}'(jw) \\ i_{s_1}'(jw) \\ i_{s_2}'(jw) \end{bmatrix} = -Y(p) \begin{bmatrix} 0 & 0 & 0 & 0 & 0 & 0 \\ 0 & 1 & 0 & 0 & (h_2-1)//3 & 0 \\ 0 & 0 & 1 & 0 & 0 & (h_1-1)//3 \\ 0 & 0 & 0 & -1 & 0 & 0 \\ 0 & (1-h_1)//3 & 0 & 0 & -1 & 0 \\ 0 & 0 & (1-h_2)//3 & 0 & 0 & -1 \end{bmatrix} \begin{bmatrix} v_{mo}'(jw) \\ v_{m_1}'(jw) \\ v_{m_2}'(jw) \\ v_{so}'(jw) \\ v_{s_1}'(jw) \\ v_{s_2}'(jw) \end{bmatrix} \quad \ldots (5.16)$$

where, as has been defined before, $Y(p) = 1/(r_t + jwL_t)$.

Frequency-shifted variables are easily obtained by replacing "w" by $(w \pm w_o)$ in equation (5.16) as appropriate. The final form of the equation is therefore as given in equation (5.17):

$$\begin{bmatrix} i_{mo}'(jw) \\ i_{m_1}'[j(w+w_o)] \\ i_{m_2}'[j(w-w_o)] \\ i_{so}'(jw) \\ i_{s_1}'[j(w+w_o)] \\ i_{s_2}'[j(w-w_o)] \end{bmatrix} = \begin{bmatrix} 0 & 0 & 0 \\ 0 & 1/[r_t+j(w+w_o)L_t] & 0 \\ 0 & 0 & 1/[r_t+j(w-w_o)L_t] \\ 0 & 0 & 0 \\ 0 & (1-h_1)//3.[r_t+j(w+w_o)L_t] & 0 \\ 0 & 0 & (1-h_2)//3.[r_t+j(w-w_o)L_t] \end{bmatrix}$$

$$\begin{bmatrix} 0 & 0 & 0 \\ 0 & (h_2-1)/\!/\,3.[r_t+j(w+w_o)L_t] & 0 \\ 0 & 0 & (h_1-1)/\!/\,3.[r_t+j(w-w_o)L_t] \\ -1/(r_t+jwL_t) & 0 & 0 \\ 0 & -1/[r_t+j(w+w_o)L_t] & 0 \\ 0 & 0 & -1/[r_t+j(w-w_o)L_t] \end{bmatrix} \begin{bmatrix} v_{mo}'(jw) \\ v_{m_1}'[j(w+w_o)] \\ v_{m_2}'[j(w-w_o)] \\ v_{so}'(jw) \\ v_{s_1}'[j(w+w_o)] \\ v_{s_2}'[j(w-w_o)] \end{bmatrix}$$

. . (5.17)

The above equation is more conveniently handled in the form given below:

$$i_{mo}'(jw) = 0.0$$

$$i_{so}'(jw) = -v_{so}'(jw)/(r_t + jwL_t) \qquad . . (5.18a)$$

$$\begin{bmatrix} i_{m_1}'[j(w+w_o)] \\ i_{m_2}'[j(w-w_o)] \\ i_{s_1}'[j(w+w_o)] \\ i_{s_2}'[j(w-w_o)] \end{bmatrix} = \begin{bmatrix} Y_{T_{11}} & Y_{T_{12}} \\ & \\ Y_{T_{21}} & Y_{T_{22}} \end{bmatrix} \begin{bmatrix} v_{m_1}'[j(w+w_o)] \\ v_{m_2}'[j(w-w_o)] \\ v_{s_1}'[j(w+w_o)] \\ v_{s_2}'[j(w-w_o)] \end{bmatrix} \qquad . . (5.18b)$$

where:

$$[Y_{T_{11}}] = \begin{bmatrix} 1/[r_t+j(w+w_o)L_t] & 0 \\ 0 & 1/[r_t+j(w-w_o)L_t] \end{bmatrix}$$

$$[Y_{T_{12}}] = \begin{bmatrix} (h_2-1)/\!/\,3.[r_t+j(w+w_o)L_t] & 0 \\ 0 & (h_1-1)/\!/\,3.[r_t+j(w-w_o)L_t] \end{bmatrix}$$

$$[Y_{T_{21}}] = \begin{bmatrix} (1-h_1/\!/\,3.[r_t+j(w+w_o)L_t] & 0 \\ 0 & (1-h_2)/\!/\,3.[r_t+j(w-w_o)L_t] \end{bmatrix}$$

$$[Y_{T_{22}}] = \begin{bmatrix} -1/[r_t+j(w+w_o)L_t] & 0 \\ 0 & -1/[r_t+j(w-w_o)L_t] \end{bmatrix}$$

5.3 Simulation of Transmission Line

5.3.1 Introduction

A practical transmission line is a complex arrangement of conductors, all of which are mutually coupled not only to each other but also to earth. It is often the practice to minimise the effects of line unbalance by transposing phase conductors at regular intervals to achieve some averaging of the line parameters. For lines which are short, electrically speaking, the net unbalance can be ignored.

In this chapter, the distributed parameter line model is analysed using the frequency-domain method of solution in the sequence components form. To complete the analysis, the transmission line is fed by the generator through the generator/transformer, from one side and an infinite busbar or another generator/transformer from the other side.

5.3.2 Basic equations

Consider a homogenous line containing "n" conductors and taking an element of infinitesimal length Δx, when current "i_j" flows in the 'jth' conductor (where j=1,2,3,.....,n), the voltage developed in length "Δx" of the 'kth' conductor is:

$$\Delta v_k = \sum_{j=1}^{n} z_{kj} \cdot i_j \cdot \Delta x$$

where k goes from 1 to 'n' to include all conductors and z_{jk} is the mutual impedance per-unit length of the 'kth' conductor for current in the 'jth' conductor. Similarly, there is a shunt displacement current due to the potential applied to the 'jth' conductor which is:

$$\Delta I_k = \sum_{j=1}^{n} Y_{kj} \cdot V_j \cdot \Delta x$$

Alternatively, in matrix form and for $\Delta x \longrightarrow 0$ the following definitive equations are appropriate:

$$\begin{aligned} dv/dx &= z(p).i \quad (a) \\ di/dx &= y(p).v \quad (b) \end{aligned} \qquad \ldots (5.19)$$

where z and y are the series impedance and shunt admittance matrices respectively for the line on a per-unit basis. From equation (5.19) the following relationships can be obtained:

$$\begin{aligned} dv^2/dx^2 &= z(p).y(p).v \\ di^2/dx^2 &= y(p).z(p).i \end{aligned} \qquad \ldots (5.20)$$

5.3.3 Symmetrical components representation in frequency domain

With reference to equation (5.20), at any point x from the sending end of the line, the frequency-transformed voltages and currents are related by the well-known differential equations (5.21)[34] as shown below. The equations form the starting point in the simulation of transmission-line transients and, where necessary, the series impedance and shunt admittance matrices z(jw) and y(jw) can be evaluated at any frequency (where p is replaced by jw) and include the effect of overhead shielding earth wires by using the method developed by Golloway et al[35].

$$[dv^2_{abc}(jw)]/dx^2 = [z_{abc}(jw)].[y_{abc}(jw)].[v_{abc}(jw)] \quad (a)$$

$$[di^2_{abc}(jw)]/dx^2 = [y_{abc}(jw)].[z_{abc}(jw)].[i_{abc}(jw)] \quad (b)$$

. . (5.21)

where:

$$[v_{abc}(jw)] = [v_a(jw)\ v_b(jw)\ v_c(jw)]^t$$

$$\text{and } [i_{abc}(jw)] = [i_a(jw)\ i_b(jw)\ i_c(jw)]^t$$

For the frequency-invariant transformation from a,b,c phase co-ordinates to 0,1,2 symmetrical components values, [T2] transformation matrix (equation 4.28) may be applied directly to equations (5.21) and with reference to equation (5.14), we get:

$$[dv^2_{012}(jw)]/dx^2 = [T_2].[z_{abc}(jw)].[y_{abc}(jw)].[T_2]^{-1}.[v_{012}(jw)]$$

. . (5.22a)

$$[di^2_{012}(jw)]/dx^2 = [T_2].[y_{abc}(jw)].[z_{abc}(jw)].[T_2]^{-1}.[i_{012}(jw)]$$

. . (5.22b)

where:

$$[v_{012}(jw)] = [v_o(jw)\ v_1(jw)\ v_2(jw)]^t$$

$$[i_{012}(jw)] = [i_o(jw)\ i_1(jw)\ i_2(jw)]^t$$

5.3.4 Distributed parameter representation for transmission line

With reference to equation (5.19a), the transmission line voltage measured from the receiving end varies from point to point along the line, due to the series voltage drop. In this equation:

$$z(p) = r + pl$$

is the operational impedance, where r, l are the resistance and inductance in per-unit length of the line.

The current (i) at any point in accordance with equation (5.19b) also varies on account of the shunt current. The shunt current results from shunt voltage (v) being impressed on the shunt capacitance and conductance and in this equation:

$$y(p) = g + pc$$

is the shunt operational admittance, per-unit length of the line. The apparent shunt conductance (g) is the result of the combined effects of leakage current through the insulation and over its surface, dielectric loss, and corona. However, the shunt conductance of power transmission lines is very small and may be safely neglected. Figure 5.4 shows transmission line parameters in terms of sequence components[36].

Equations (5.21) are the well-known partial differential equation of transmission lines. The solution of such equations suggests diagonalising the products[34], [z(jw)][y(jw] and [y(jw)][z(jw)]. This may be done by finding the eigenvalues and eigenvectors appropriate to each product and applying the theory of matrix functions to yield a phase co-ordinate set of equations. However, the alternative method investiaged here which is based on the symmetrical component method can be used provided transposition of the line conductors is assumed, since the effects of nontransposition are not marked on short lines. However, in the case of untransposed lines, the necessity for computing eigenvalues cannot be avoided even if the symmetrical component transform is then used subsequently.

In the case of transposed transmission line, the series and shunt admittance matrix take the well-known form given in equation (5.23)[35].

$$[z(jw)] = \begin{bmatrix} z_s(jw) & z_m(jw) & z_m(jw) \\ z_m(jw) & z_s(jw) & z_m(jw) \\ z_m(jw) & z_m(jw) & z_s(jw) \end{bmatrix} \quad \ldots (5.23a)$$

$$[y(jw)] = \begin{bmatrix} y_s(jw) & -y_m(jw) & -y_m(jw) \\ -y_m(jw) & y_s(jw) & -y_m(jw) \\ -y_m(jw) & -y_m(jw) & y_s(jw) \end{bmatrix} \quad \ldots (5.23b)$$

where:

$$z_s(jw) = r + jwl_s$$

$$z_m(jw) = r_m + jwl_m$$

$$y_s(jw) = jwc_s$$

$$y_m(jw) = jwc_m$$

Substituting equations (5.23) into equation (5.22) gives a set of independent linear differential equations of the form:

$$\left[\frac{d_2 V'_{012}(jw)}{dx^2}\right] = \begin{bmatrix} [z_s(jw)+2z_m(jw)][y_s(jw)-2y_m(jw)] & 0 & 0 \\ 0 & [z_s(jw)-z_m(jw)][y_s(jw)+y_m(jw)] & 0 \\ 0 & 0 & [z_s(jw)-z_m(jw)][y_s(jw)+y_m)jw)] \end{bmatrix} [.V'_{012}(jw)] \quad \ldots (5.24)$$

The sequence components of impedance and admittance have been defined in equation (5.25)[34,35,39]:

$$z_0(jw) = z_s(jw) + 2z_m(jw), \quad y_0(jw) = y_s(jw) - 2y_m(jw)$$
$$z_1(jw) = z_s(jw) - z_m(jw), \quad y_1(jw) = y_s(jw) + y_m(jw)$$
$$z_2(jw) = z_1(jw), \quad y_2(jw) = y_1(jw) \qquad \ldots (5.25)$$

Substituting equations (5.25) into equation (5.24) gives:

$$[d^2v'_{012}jw)]/dx^2 = \begin{bmatrix} z_0(jw)y_0(jw) & 0 & 0 \\ 0 & z_1(jw)y_1(jw) & 0 \\ 0 & 0 & z_1(jw)y_1(jw) \end{bmatrix} [v'_{012}(jw)] \qquad \ldots (5.26)$$

The impedances $z_0(jw)$, $z_1(jw)$ and admittances $y_0(jw)$, $y_1(jw)$ are readily realised as the sequence component parameters of the line, and an identical expression to equation (5.26) can be obtained for the sequence currents at any point on the line. Equations (5.26) are seen to form a set of independent differential equations in which their solution takes the usual exponential form. For example, the zero sequence voltage will vary with "x" according to:

$$v_0(jw) = A.\exp[\Upsilon_0.x] + B.\exp[\Upsilon_0.x] \quad (a)$$
$$i_0(jw) = C.\exp[\Upsilon_0.x] + D.\exp[\Upsilon_0.x] \quad (b) \qquad \ldots (5.27)$$

where:

$$\Upsilon_0 = [z_0(jw).y_0(jw)]^{\frac{1}{2}}$$

also:

$$\Upsilon_1 = [z_1(jw).y_1(jw)]^{\frac{1}{2}} \qquad \Upsilon_2 = [z_2(jw).y_2(jw)]^{\frac{1}{2}}$$

Similar expressions exist for the positive and negative-sequence components of currents and voltages. The constants A, B, C, D for both voltage and current components are derived from a knowledge of the boundary values of voltage and current given in equation (5.28a), and the final form of the two-port matrices relating current and voltage components at either end of the line are then given in equation (5.28b).

$$
\begin{aligned}
[v(jw)]_{012} &= [v_s(jw)]_{012} \quad \text{for } x = 0 \\
[i(jw)]_{012} &= [i_s(jw)]_{012} \quad \text{for } x = 0 \\
[v(jw)]_{012} &= [v_r(jw)]_{012} \quad \text{for } x = x \\
[i(jw)]_{012} &= [i_r(jw)]_{012} \quad \text{for } x = x
\end{aligned}
\qquad \ldots (5.28a)
$$

$$
\begin{bmatrix} v_{so}'(jw) \\ v_{s1}'(jw) \\ v_{s2}'(jw) \\ i_{so}'(jw) \\ i_{s1}'(jw) \\ i_{s2}'(jw) \end{bmatrix}
\begin{bmatrix} A_{\ell 0} & 0 & 0 & B_{\ell 0} & 0 & 0 \\ 0 & A_{\ell 1} & 0 & 0 & B_{\ell 1} & 0 \\ 0 & 0 & A_{\ell 1} & 0 & 0 & B_{\ell 1} \\ C_{\ell 0} & 0 & 0 & D_{\ell 0} & 0 & 0 \\ 0 & C_{\ell 1} & 0 & 0 & D_{\ell 1} & 0 \\ 0 & 0 & C_{\ell 1} & 0 & 0 & D_{\ell 1} \end{bmatrix}
\begin{bmatrix} v_{ro}'(jw) \\ v_{r1}'(jw) \\ v_{r2}'(jw) \\ i_{ro}'(jw) \\ i_{r1}'(jw) \\ i_{r2}'(jw) \end{bmatrix}
\qquad \ldots (5.28b)
$$

where:

$$
\begin{aligned}
A_{\ell 0} &= \text{COSh}[\Upsilon_0.x] \\
A_{\ell 1} &= \text{COSh}[\Upsilon_1.x] \\
B_{\ell 0} &= [z_0(jw)/y_0(jw)]^{\frac{1}{2}}.\text{SINh}[\Upsilon_0.x] \\
B_{\ell 1} &= [z_1(jw)/y_1(jw)]^{\frac{1}{2}}.\text{SINh}[\Upsilon_1.x] \\
C_{\ell 0} &= [y_0(jw)/z_0(jw)]^{\frac{1}{2}}.\text{SINh}[\Upsilon_0.x]
\end{aligned}
$$

$$C_{\ell 1} = [y_1(jw)/z_1(jw)]^{\frac{1}{2}} . SINh[\Upsilon_0 . x]$$

$$D_{\ell 0} = A_{\ell 0} \quad \text{and} \quad D_{\ell 1} = A_{\ell 1}$$

It will be recalled from chapter 3, that the analysis of the synchronous generator in the frequency domain requires the use of frequency shifted constants and these may be applied also to the line (as has been applied to the transformer) equations before the analysis can be completed. In equation (5.28) by substituting "w" by $(w \pm w_0)$ where appropriate, the following equations are obtained:

$$\begin{bmatrix} v_{so}'(jw) \\ i_{so}'(jw) \end{bmatrix} = \begin{bmatrix} A_{\ell 0} & B_{\ell 0} \\ C_{\ell 0} & A_{\ell 0} \end{bmatrix} \begin{bmatrix} v_{ro}'(jw) \\ i_{ro}'(jw) \end{bmatrix} \qquad (a)$$

$$\begin{bmatrix} v_{s1}'[j(w+w_o)] \\ v_{s2}'[j(w-w_o)] \\ i_{s1}'[j(w+w_o)] \\ i_{s2}'[j(w-w_o)] \end{bmatrix} = \begin{bmatrix} A_{\ell 12} & B_{\ell 12} \\ & \\ & \\ C_{\ell 12} & A_{\ell 12} \end{bmatrix} \begin{bmatrix} v_{r1}'(j(w+w_o)] \\ v_{r2}'[j(w-w_o)] \\ i_{r1}'[j(w+w_o)] \\ i_{r2}'[j(w-w_o)] \end{bmatrix} \qquad (b)$$

. . (5.29)

With reference to equation (5.28) we have:

$$A_{\ell 12} = \begin{bmatrix} A_{\ell 11} & 0 \\ 0 & A_{\ell 22} \end{bmatrix} , \quad B_{\ell 12} = \begin{bmatrix} B_{\ell 11} & 0 \\ 0 & B_{\ell 22} \end{bmatrix} ,$$

$$C_{\ell 12} = \begin{bmatrix} C_{\ell 11} & 0 \\ 0 & C_{\ell 22} \end{bmatrix} , \quad D_{\ell 12} = A_{\ell 12}$$

where:

$$\Upsilon_1 = \{z_1[j(w+w_o)] . y_1[j(w+w_o)]\}^{\frac{1}{2}}$$

$$\Upsilon_2 = (z_1[j(w-w_o)].y_1[j(w-w_o)])^{\frac{1}{2}}$$

and:

$$A_{\ell 11} = \text{COSh}[\Upsilon_1.x]$$

$$A_{\ell 22} = \text{COSh}[\Upsilon_2.x]$$

$$B_{\ell 11} = (z_1[j(w+w_o)]/y_1[j(w+w_o)])^{\frac{1}{2}}.\text{SINh}[\Upsilon_1.x]$$

$$B_{\ell 22} = (z_1[j(w-w_o)]/y_1[j(w-w_o)])^{\frac{1}{2}}.\text{SINh}[\Upsilon_2.x]$$

$$C_{\ell 11} = (y_1[j(w+w_o)]/z_1[j(w+w_o)])^{\frac{1}{2}}.\text{SINh}[\Upsilon_1.x]$$

$$C_{\ell 22} = (y_1[j(w-w_o)]/z_1[j(w-w_o)])^{\frac{1}{2}}.\text{SINh}[\Upsilon_2.x]$$

and where:

$$z_1 = z_2 \quad \text{and} \quad y_1 = y_2$$

$$z_1(j(w+w_o)) = r_1 + j(w+w_o).1_1$$

$$z_1(j(w-w_o)) = r_1+j(w-w_o).1_1$$

$$y_1(j(w+w_o)) = j(w+w_o).c_1$$

$$y_1(j(w-w_o)) = j(w-w_o).c_1$$

It should be noted that the line parameters taken for the purpose of evaluating transmission line constants are applicable to the whole line length. Additionally, the method which has been used is inherently more accurate than the approach developed in reference (39), in which losses have been neglected. Another advantage of this technique is that it is possible to take into acocunt the frequency variant nature of transmission line parameters[40], which can significantly affect fault transient waveforms.

5.4 The Generator, Generator/Transformer and Transmission Line Combination

As has been shown previously in chapter 3, when modelling a faulted system comprising a generator connected to an infinite busbar, the faults are simulated by applying a set of superimposed voltages so that the addition of the prefault steady-state variations and superimposed values represents the total response. Likewise, in this study which is for a system comprising generator, generator/transformer and transmission line, it is necessary to proceed from a knowledge of the prefault voltages at fault point. It is thus necessary to combine the equations representing the generator, generator/transformer and transmission line so that by applying an appropriate set of superimposed voltages at the fault point, the variations of both currents and voltages at any point in the system considered can be obtained. In chapter 4 and also in the preceding sections of this chapter, equations describing each element were considered. With reference to equation (4.32) the positive and negative frequency-shifted currents at generator terminals (by substituting i_1', i_2' by i_{m1}', i_{m2}' and e_1', e_2' by v_{m1}', v_{m2}') are as follows:

$$\begin{bmatrix} i_{m1}'[j(w+w_o)] \\ i_{m2}'[j(w-w_o)] \end{bmatrix} = [Y_m] \begin{bmatrix} v_{m1}'[j(w+w_o)] \\ v_{m2}'[j(w-w_o)] \end{bmatrix} \qquad . . \quad (5.30)$$

where:

$$[Y_m] = (1/z^2) \begin{bmatrix} -[R+j(w-w_o)L_1(jw)] & j(w+w_o)L_2(jw).\exp(j2\lambda) \\ j(w-w_o)L_2(jw).\exp(-j2\lambda) & -[R+j(w+w_o)L_1(jw)] \end{bmatrix}$$

The equations relating positive- and negative-sequence frequency-shifted currents at generator terminals of the generator/transformer are given by equation (5.18).

$$\begin{bmatrix} i_{m_1}'\{j(w+w_o)\} \\ i_{m_2}'\{j(w-w_o)\} \end{bmatrix} = [Y_{T_{11}}] \begin{bmatrix} v_{m_1}'\{j(w+w_o)\} \\ v_{m_2}'\{j(w-w_o)\} \end{bmatrix} + [Y_{T_{12}}] \begin{bmatrix} v_{s_1}'\{j(w+w_o)\} \\ v_{s_2}'\{j(w-w_o)\} \end{bmatrix} \quad . . (5.31)$$

$$\begin{bmatrix} i_{s_1}'\{j(w+w_o)\} \\ i_{s_2}'\{j(w-w_o)\} \end{bmatrix} = [Y_{T_{21}}] \begin{bmatrix} v_{m_1}'\{j(w+w_o)\} \\ v_{m_2}'\{j(w-w_o)\} \end{bmatrix} + [Y_{T_{22}}] \begin{bmatrix} v_{s_1}'\{j(w+w_o)\} \\ v_{s_2}'\{j(w-w_o)\} \end{bmatrix} \quad . . (5.32)$$

Now by equating equations (5.31) and (5.30) we get:

$$\begin{bmatrix} v_{m_1}'\{j(w+w_o)\} \\ v_{m_2}'\{j(w-w_o)\} \end{bmatrix} = [Y_m - Y_{T_{11}}]^{-1} . Y_{T_{12}} . \begin{bmatrix} v_{s_1}'\{j(w+w_o)\} \\ v_{s_2}'\{j(w-w_o)\} \end{bmatrix} \quad . . (5.33)$$

Substituting equation (5.33) into equation (5.32), the following line–side relationship will be obtained:

$$\begin{bmatrix} i_{s_1}'\{j(w+w_o)\} \\ i_{s_2}'\{j(w-w_o)\} \end{bmatrix} = [Y_{T_{21}} . [Y_m - Y_{T_{11}}]^{-1} . Y_{T_{12}} + Y_{T_{22}}] . \begin{bmatrix} v_{s_1}'\{j(w+w_o)\} \\ v_{s_2}'\{j(w-w_o)\} \end{bmatrix} \quad . . (5.34)$$

With reference to equation (5.29) which describes the transmission lines, this equation may be rearranged as follows:

$$\begin{bmatrix} v_{s_1}'\{j(w+w_o)\} \\ v_{s_2}'\{j(w-w_o)\} \end{bmatrix} = [A_{\ell_{12}}] \begin{bmatrix} v_{r_1}'\{j(w+w_o)\} \\ v_{r_2}'\{j(w-w_o)\} \end{bmatrix} + [B_{\ell_{12}}] \begin{bmatrix} i_{r_1}'\{j(w+w_o)\} \\ i_{r_2}'\{j(w-w_o)\} \end{bmatrix} \quad . . (5.35)$$

$$\begin{bmatrix} i_{s1}'(j(w+w_o)) \\ i_{s2}'(j(w-w_o)) \end{bmatrix} - [C_{\ell 12}] \begin{bmatrix} v_{r1}'(j(w+w_o)) \\ v_{r2}'(j(w-w_o)) \end{bmatrix} + [A_{\ell 12}] \begin{bmatrix} i_{r1}'(j(w+w_o)) \\ i_{r2}'(j(w-w_o)) \end{bmatrix}$$

. . (5.36)

Now by equating equation (5.34) to equation (5.36) and rearranging the result, the positive and negative frequency-shifted sequence voltages at the sending end of the line are given by equation (5.37):

$$\begin{bmatrix} v_{s1}'(j(w+w_o)) \\ v_{s2}'(j(w-w_o)) \end{bmatrix} = \left\{ [Y_{T21} \cdot [Y_m - Y_{T11}]^{-1} \cdot Y_{T12} + Y_{T22}] \right\}^{-1}$$

$$\left\{ [C_{\ell 12}] \cdot \begin{bmatrix} v_{r1}'(j(w+w_o)) \\ v_{r2}'(j(w-w_o)) \end{bmatrix} + [A_{\ell 12}] \begin{bmatrix} i_{r1}'(j(w+w_o)) \\ i_{r2}'(j(w-w_o)) \end{bmatrix} \right\}$$

. . (5.37)

Equating this to equation (5.35) and rearranging the result gives a final relationship between the variation of voltage and current at receiving end of transmission line:

$$\begin{bmatrix} i_{r1}'(j(w+w_o)) \\ i_{r2}'(j(w-w_o)) \end{bmatrix} = \left\{ [Y_{T21} \cdot [Y_m - Y_{T11}]^{-1} \cdot Y_{T12} + Y_{T22}]^{-1} \cdot A_{\ell 12} - B_{\ell 12} \right\}^{-1}$$

$$\left\{ [A_{\ell 12} - [Y_{T21} \cdot [Y_m - Y_{T11}]^{-1} \cdot Y_{T12} + Y_{T22}]^{-1} \cdot C_{\ell 12}] \right\} \begin{bmatrix} v_{r1}'(j(w+w_o)) \\ v_{r2}'(j(w-w_o)) \end{bmatrix}$$

. . (5.38a)

Also, with reference to equations (5.18a) and (5.29a), we get:

$$i_{ro}'(jw) = - [A_{\ell 0} + (r_t + jwL_t) C_{\ell 0}] \cdot v_{ro}'(jw) / [B_{\ell 0} + (r_t + jwL_t) \cdot A_{\ell 0}]$$

. . (5.38b)

With reference to the above equation, the frequency spectrum of the superimposed voltage components at the fault point enables the corresponding spectrum of currents to be computed. By knowing the latter this then enables the spectrum of voltage and current components at the sending end of the line and that at the machine terminals to be determined by means of equations (5.29) and (5.18). The determination of the frequency spectrum of the superimposed fault point voltage is considered in section (5.5). It should be noted that the foregoing theory is also applicable to studies of fault at some intermediate point on a line which is fed from the remote end by any arbitrary remote-source configuration. In this case the line parameters ($A_{\ell 12}$, $B_{\ell 12}$, $C_{\ell 12}$, $D_{\ell 12}$) defining the various matrices in equation (5.38a,b) are evaluated for the length up to the point of fault, and superimposed voltage components will be pre-evaluated from a knowledge of the remote-source configuration. This aspect of the work will be discussed in more detail in chapter 8.

5.5 Evaluation of Superimposed Voltage at Fault Point

As has been considered in chapter 2, the steady-state variations of voltage and current corresponding to any pre-fault loading condition are easily obtained using the symmetrical steady state power frequency equations for the generator[43], transformer and transmission line. For any given load angle "δ" measured with reference to the prefault terminal voltage, the terminal voltages of machine will be given by equation (5.39).

$$\begin{aligned} V_{ma} &= -E_m.SIN(w_o t + \lambda - \delta) \\ V_{mb} &= -E_m.SIN(w_o t + \lambda - \delta - 2\pi/3) \\ V_{mc} &= -E_m.SIN(w_o t + \lambda - \delta + 2\pi/3) \end{aligned} \qquad \ldots (5.39)$$

With regard to the prefault voltage relations at machine terminal, the prefault

voltage relations at the infinite-busbar (or fault point) are as follows:

$$\begin{aligned} v_{ra} &= -E_r.SIN(w_o t + \lambda - \delta + \theta_m) \\ v_{rb} &= -E_r.SIN(w_o t + \lambda - \delta + \theta_m - 2\pi/3) \\ v_{rc} &= -E_r.SIN(w_o t + \lambda - \delta + \theta_m + 2\pi/3) \end{aligned} \quad . . (5.40)$$

The angle "θ_m" is the angle by which the prefault voltage at fault point leads that at machine terminals and is readily evaluated from a knowledge of per-unit phasor values of prefault voltage and current at machine terminals.

In the steady-state case, a transposed line will possess only positive sequence components and in accordance with the previous theory and using equation (5.28) we have:

$$\begin{aligned} V_s &= A\ell_1.V_r + B\ell_1.I_r \\ I_s &= C\ell_1.V_r + A\ell_1.I_r \end{aligned} \quad . . (5.41)$$

With reference to equation (5.41) the voltage at the receiving end is related to the current and voltage at the sending end by equation (5.42).

$$V_r = A\ell_1.V_s - B\ell_1.I_s \quad . . (5.42)$$

For the $Y_{d_{11}}$ transformer, the prefault current on the machine terminal leads that on the line side by "$\pi/6$", and this is expressed as $I_m = I_s \angle \pi/6$. Additionally, equation (5.43) expresses the steady-state phasor value of the machine terminal voltage in terms of phasor values I_m, V_s.

$$V_m = [(r_t + jw_oL_t).I_m + V_s] \angle \pi/6 \quad . . (5.43)$$

By substituting equation (5.43) into equation (5.42) it can be shown that voltage at the remote end of the line in terms of the prefault variations at the machine terminals is as follows:

$$V_r = [A_{\ell_1}.V_m - (B_{\ell_1} + A_{\ell_1}(r_t + jwL_t)).I_m] \angle -\frac{\pi}{6} \quad . . (5.44)$$

With the prefault machine voltage taken as reference, the argument of equation (5.44), thus represents the angle "θ_m" and its magnitude is related to the peak of the prefault voltage at the remote end of the line by:

$$E_r = \sqrt{2}\,|V_r|.$$

The actual determination of the frequency-shifted superimposed voltages from a knowledge of the prefault time variation of voltage at the point of fault was considered in detail in chapter 3. Moreover, in that chapter, the machine directly connected to an infinite-busbar was considered and the spectra of superimposed voltages were derived via prefault variations of equation (5.39).

A comparison of equations (5.39 and (5.40) show that to evaluate the spectra of superimposed voltages at remote end, as required in the present study, it is necessary simply to replace "E_m" by the appropriate value of "E_r" and λ by $\lambda+\theta_m$ in the equations for a machine operating directly into infinite busbars. The latter are given for various fault conditions in Table 3.18.

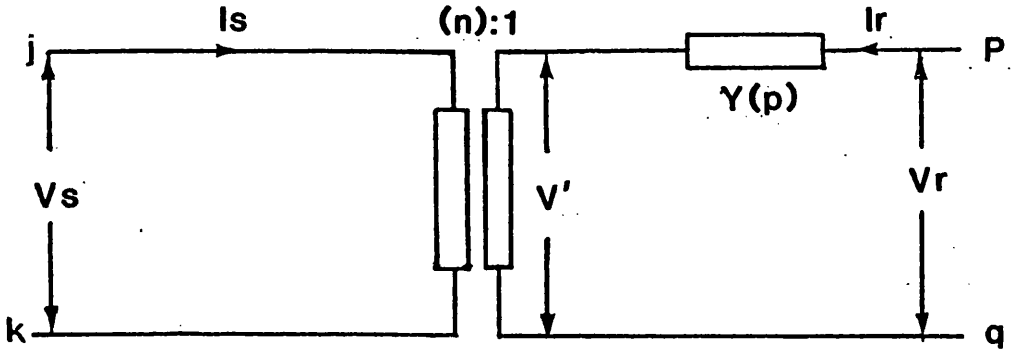

Fig. 5.1 Single Phase Ideal Transformer

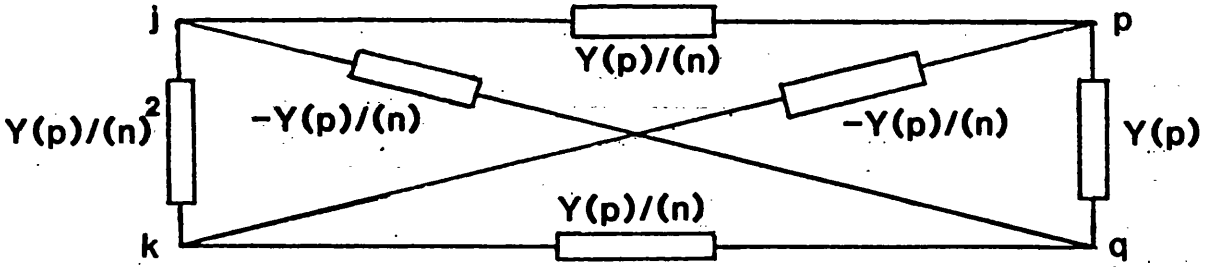

Fig. 5.2 Single Phase Ideal Transformer Representation Using the Nodal Admittance Method

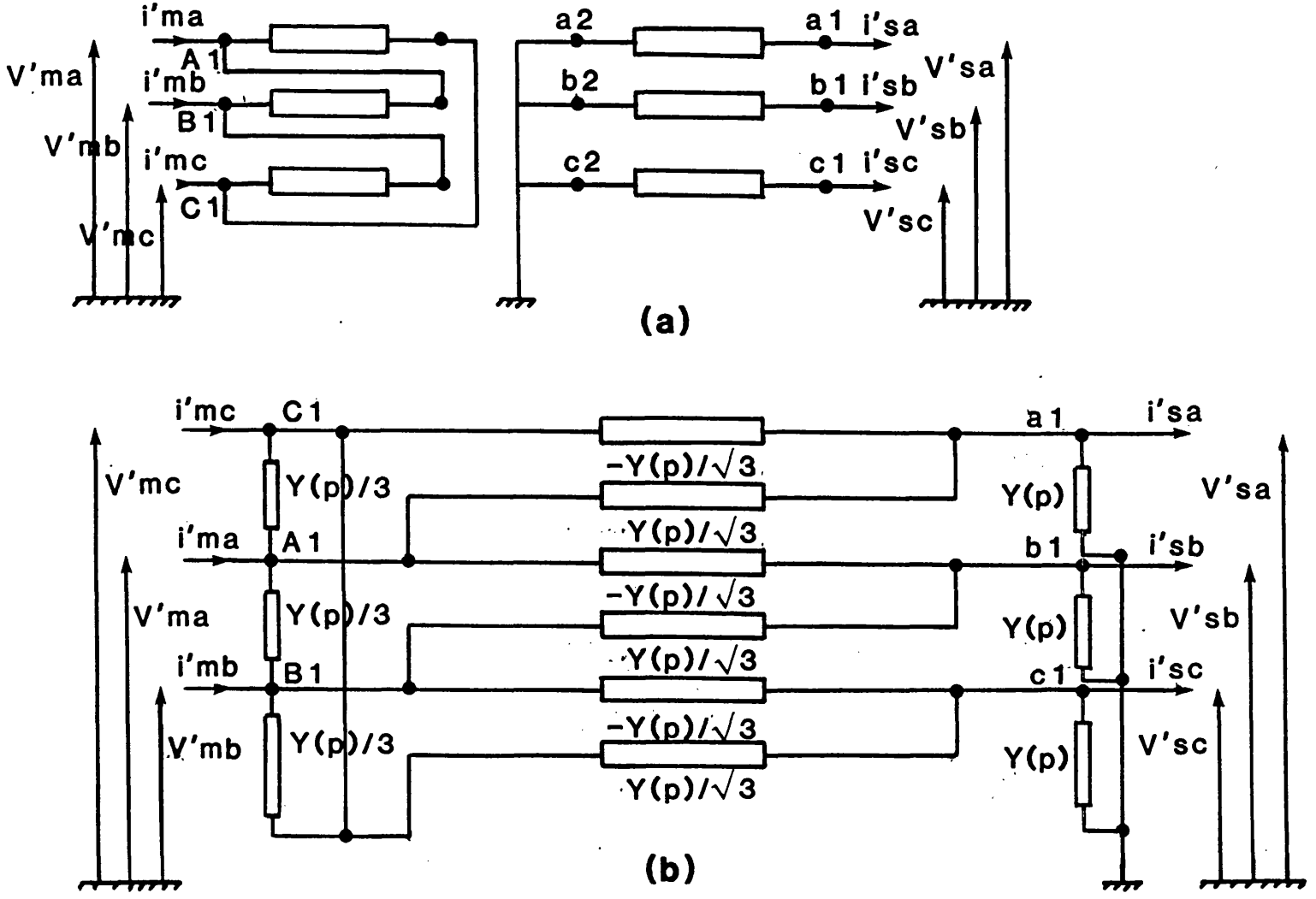

Fig. 5.3 Yd11 Generator Transformer Arrangements

(a)- Circuit arrangements

(b)- Equivalent phase-frame circuit

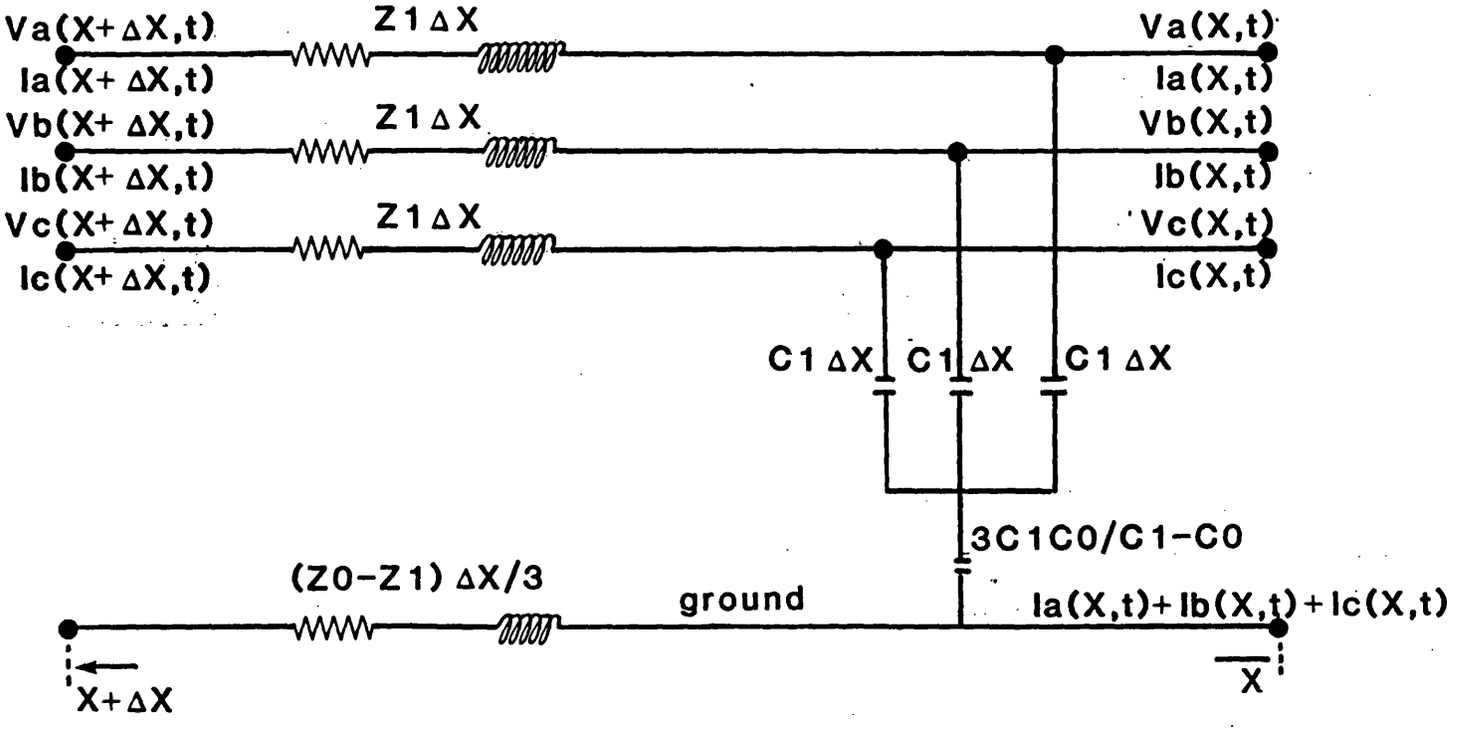

Fig.5.4 Distributed Paremeter Line Representation

CHAPTER 6

SYSTEM PARAMETERS

6.1 Introduction

The simulation results presented in this work are for two different systems. One is for the lower 132kV single circuit system and the other is for an ehv system comprising a 400kV single circuit line. Both systems have their own complex source side networks and the transmission lines are transposed. As shown in chapter 4, the synchronous generators used here are modelled with greater complexity, and therefore with more realism, by considering damping effects and frequency variant operational inductances. The latter have been obtained by standstill frequency response tests, on the Northfleet station in UK and the Ontario Hydro station in Canada.

The transformer model for system studies as has been derived in chapter 5, is without taking into account the frequency dependency of its parameters and the magnetising impedance has been neglected. Furthermore, the frequency bandwidth of interest is such that the transformer can be represented by an analytical expression instead of test results. Likewise in the transient calculations the inter-turn capacitances of both the generator and its associated transformer are also neglected. However, the capacitance to ground of both the plant items and the connected busbar are calculated and included in the simulation.

This chapter summarises the parameters of the synchronous generators, transformers and transmission lines.

6.2 Synchronous Generator Parameters

It has been general practice in the past to represent transient and subtransient effects in generator simulations by a constant parameters model, i.e. a model with constant resistances and leakage inductances. However, it is well-known that both resistances and inductances are frequency dependent (skin effect) and that inductances are current dependent (saturation effects in leakage flux paths). As has been mentioned previously in chapter 2 in this study, the saturation effects have been neglected and the generator resistances are assumed to be constant, but, the frequency dependency of operational inductances is included.

6.2.1 150MVA synchronous generator

This machine (turbo alternator) is of the one studied in the Northfleet Exercise[25,48,49], with the following basic data:

stator terminal voltage = 13.8kV

machine rating = 120MW

nominal frequency = 50Hz

speed = 3000rpm

6.2.1.1 Frequency dependent parameters

As is normal practice, frequency-response measurements were made (at standstill) of impedance looking into the stator terminals with the machine in the following positions:

a) Rotor aligned in direct axis, field winding short circuited.

b) Rotor aligned in quadrature axis.

Knowing the impedances looking into the stator terminals, the operational inductances are calculated at different frequencies (as shown in chapter 4) and these are shown in Figures 6.1 and 6.2.

6.2.1.2 Manufacturer's data (constant parameters)

The following is the manufacturer's data, and the p.u. quantities are expressed to 150MVA and 13.8kV base values:

a) Stator

R	= 0.0014	L_q	= 1.76
L_d	= 1.850	L_o	= 0.095

b) Rotor

R_{fd}	= 0.0009	L_{kk}	= 1.693
R_{kd}	= 0.011	L_{qq}	= 1.603
R_{kq}	= 0.0055	M_{ad}	= 1.675
L_{ff}	= 1.775	M_{aq}	= 1.585

6.2.2 588MVA synchronous generator

This turbogenerator which has been a subject of study at Ontario Hydro[29], is a 2-pole, 3600 rpm machine rated at 500MW, 0.85 power factor, and 22kV line to line stator voltage. The stator winding is a direct, water-cooled type; the rotor is directly cooled with hydrogen.

6.2.2.1 Frequency dependent parameters

The stator impedances were measured by standstill frequency-response tests. The d-axis operational impedances were determined with the field winding shorted through a shunt resistance. The d- and q-axis operational inductances were computed from the corresponding impedances (see chapter 4). The results are presented in Figures 6.3 and 6.4.

6.2.2.2 Manufacturer's data (constant parameters)

This data in p.u. form to 588MVA and 22kV base values is as follows:

a) Stator

R	= 0.0027	L_q	= 2.242
L_d	= 2.36	L_o	= 0.195

b) Rotor

R_{fd}	= 0.00076	L_{kk}	= 2.210
R_{kd}	= 0.00703	L_{qq_1}	= 2.203
R_{kq_1}	= 0.0039	L_{qq_2}	= 2.085
R_{kq_2}	= 0.0014	M_{ad}	= 2.165
L_{ff}	= 2.256	M_{aq}	= 2.047

6.3 The Generator/Transformer Parameters

It has been realised that under transient conditions, transformer equivalent high frequency reactances have a lower value than the normal 50Hz values[50].

Gosland[51] found that at a natural frequency of about 20kHz the transformer equivalent inductances was approximately 85% of its 50Hz value. Li[31] reported that the response is more or less flat for a frequency below 12kHz, but when the frequency exceeds 12kHz, the inductance drops at a rapid rate. However, as has been mentioned previously in this study, because the frequency bandwidth is limited to less than 12kHz, the transformer's parameeters are assumed to be constant.

6.3.1 150MVA generator/transformer

150MVA 132/13.8kV Y/Δ

Basic Insulation Level = 650/110

15 taps vector group Yd11

When neglecting magnetising components, the equivalent resistance and leakage reactance per phase p.u. to base values of 150MVA and 132kV are:

r_t = 0.0073

L_t = 0.1795

6.3.2 600MVA generator/transformer

600MVA 400/22kV Y/Δ

Basic Insulation Level = 1750/150

18 taps vector group Yd11

Again, by neglecting magnetising impedances, the equivalent resistance and leakage inductance per phase p.u. to base values of 600MVA and 400kV are:

r_t = 0.001773

L_t = 0.16319

6.4 Generator/Transformer Capacitances

It should be noted that the capacitances of plant items such as generators and transformers which have been hitherto neglected in the previous studies, can significantly influence the transient waveforms. Each turn of a generator or transformer winding has a capacitance to ground (ground in this context is a core or a tank).

6.4.1 Transformer capacitance to ground

Although the interturn capacitances have been neglected, there are, however, significant capacitances between the winding and ground. Like any other capacitors, their capacitance values depend upon the area of the plates, the separation of the plates, and permittivity of the materials separating them. One would expect, therefore, that transformers of high MVA would have higher capacitance than those of low MVA, simply because they are physically bigger. It should be also noted that the capacitance of high-voltage transformer would tend to be less than a low-voltage transformer of comparable rating, since a high voltage demands more separation between the windings, and between windings and core. It is also reasonable to expect that a so-called "dry type" transformer has less capacitance than corresponding transformer, where the interstices of the windings are filled with oil or some similar fluid of higher permittivity.

Figures 6.5(a)(b)(c) provide values of the total capacitance to ground on a per phase basis[52]. With reference to Figures 6.5(a)(b)(c), for a 150MVA, 132/13.8kV transformer, the capacitance to ground of the low and high voltage sides of transformer are as follows:

C_{T1} (low voltage) = 14200 pF/phase

C_{T2} (high voltage) = 6000 pF/phase

Referring to Figures 6.5(a)(b)(c) the capacitances to ground of a 600MVA, 400/22kV transformer are:

C_{T1} (low voltage) = 15000 pF/phase

C_{T2} (high voltage) = 3750 pF/phase

It should be mentioned that for a Y-connected bank, half the capacitance values are taken in each terminal and for a Δ-connected bank, the full phase values are used because there are two windings providing lumped terminal capacitances.

Furthermore, in addition to the capacitance of the winding, there is also the capacitance of bushing to which it is connected and this should also be added to the terminal to ground capacitance of transformer. For a delta connected bank of a single-phase transformer, the capacitance of two bushings must be added, and the total transformer terminal capacitances are then:

a) 150MVA transformer

$$C_{\Delta} = C_{T1} + 2C_b = 14200 + 600 = 14800 \text{ pF/phase} = 0.0188\text{x}10^{-6}\text{p.u.}$$

$$C_Y = C_{T2}/2 + C_b = 3000 + 300 = 3300 \text{ pF/phase} = 0.384\text{x}10^{-6}\text{p.u.}$$

b) 600MVA transformer

$$C_{\Delta} = C_{T1} + 2C_b = 15000 + 1500 = 16500 \text{ pF/phase} = 0.0133\text{x}10^{-6}\text{p.u.}$$

$$C_Y = C_{T2}/2 + C_b = 1875 + 750 = 2625 \text{ pF/phase} = 0.70\text{x}10^{-6}\text{p.u.}$$

6.4.2 Generator terminal capacitance to ground

The capacitance between coils is very low (negligible), since each coil is embedded in a slot which acts as an earthed boundary(53). On the other hand, due to the fact that coil is embedded in the slot, the coil-to-earth capacitance in comparison with a transformer is higher. Generally speaking, the capacitance of generators increases with size but there can be a considerable spread in a given rating, because of design. This is apparent from Figure 6.6, which shows capacitance values for 2-pole generators.

This capacitance is the total capacitance-to-ground of the 3-phase stator winding. Using the "Π" model again for each phase, each of the "Π" model capacitors would be 1/6 of the value in the figure. Forced cooled machines tend to have smaller capacitance because the conductors can be smaller, and the slower rpm machines, particularly hydro-machines, tend to have higher capacitances(52).

With reference to Figure 6.6 the capacitances to ground at generator terminal are:

a) for 150MVA generator

$C_g = 0.4/6\mu\text{F/phase} = 0.067\text{x}10^{-6}$ F/phase

Using base values of 150MVA and 13.8kV give:

$C_g = 0.085\text{x}10^{-6}\text{p.u.}$

b) for 600MVA generator

C_g = 0.6/6μF/phase = 0.1×10^{-6} F/phase

While to base values of 588MVA and 22kV give:

$C_g = 0.08 \times 10^{-6}$p.u.

6.4.3 Busbar capacitance to ground

Bus runs comprising parallel bars, usually of rectangular cross section, are commonplace in industrial power circuits. A typical configuration is as shown in Figure 6.7. The equivalent capacitance to ground for such a configuration is:

C(busbar) = 0.1×10^{-6} F

6.5 Transmission Line Parameters

6.5.1 400kV quad conductor

The fault studies apply to a typical quadrature construction (4 conductor per phase), 400kV single circuit, transposed line as shown in Figure 6.8. The data which applies to the line model is as follows:

a) Phase conductors are 4x54/7/0.33cm s.c.a. with 0.305m bundle spacing.

b) Earth wires are 54/7/0.33cm s.c.a.

c) Earth resistivity is 100Ω/m.

d) Conductor resistance = 0.0169Ω/km (at power frequency).

e) Earth wire resistance = 0.0677Ω/km (at power frequency).

f) Conductor reactance = 0.0039Ω/km (at power frequency).

g) Earth wire reactance = 0.0157Ω/km (at power frequency).

h) Conductor overall radius = 0.1338 meter.

i) Earth wire overall radius = 0.0115 meter.

j) Line length = 160km.

6.5.1.1 Basic computed parameters

The power frquency parameters of the line models presented here are necessary for steady state calculations,. These computeed parameters are based on the p.u. length of impedance and admittance matrices of the line. They are evaluated using the same principles as suggested by Galloway et al[35].

Impedance matrix [z]:

$$[z] = \begin{bmatrix} 0.47 + j5.0 & 0.30 + j2.20 & 0.29 + j1.60 \\ 0.30 + j2.2 & 0.46 + j4.90 & 0.28 + j1.90 \\ 0.29 + j1.6 & 0.28 + j1.90 & 0.45 + j4.60 \end{bmatrix} \times 10^{-4}\Omega/m$$

Admittance matrix [Y]:

$$[Y] = \begin{bmatrix} j3.6 & -j0.73 & -j0.26 \\ -j0.73 & j3.4 & -j0.72 \\ -j0.26 & -j0.72 & j3.2 \end{bmatrix} \times 10^{-9} \text{ mho/m}$$

6.5.2 Symmetrical components value

a) For 400kV transmission line:

The positive sequence parameters:

r_1 = 0.02335 Ω/km

l_1 = 0.95108 m.h./km

c_1 = 1.23792 x 10^{-2} μ.F/km

It should be noted that the negative sequence parameters are equal to positive sequence parameters.

The zero sequence parameters:

r_0 = 0.38848Ω/km

l_0 = 3.225079 m.h./km

c_0 = 0.84541 x 10^{-2} μ.F/km

The above values in per unit to 588MVA base are:

r_1 = 0.00876x10^{-2} p.u./km r_0 = 0.14568x10^{-2} p.u./km

l_1 = 0.11204x10^{-2} p.u./km l_0 = 0.38298x10^{-2} p.u./km

c_1 = 0.10371x10^{-2} p.u./km c_0 = 0.07083x10^{-2} p.u./km

b) For 132kV transmissionline:

r_1 = 0.0388x10^{-2} p.u./km r_0 = 0.167x10^{-2} p.u./km

l_1 = 0.3180x10^{-2} p.u./km l_0 = 1.170x10^{-2} p.u./km

c_1 = 0.0350x10^{-2} p.u./km c_0 = 0.0175x10^{-2} p.u./km

6.6 Simple Source Parameters

As mentioned previously, studies have also been performed by terminating a transmission line by simple lumped sources, short circuit levels s.c.l. The source parameters under these conditions are:

s.c.l	machine reactance
5 GVA	0.12 p.u.
1.25 GVA	0.475 p.u.

X:R for source = 30

In every case, the zero sequence to positive sequence reactance ratio z_{s0}/z_{s1}, for the source is taken as = 1.0.

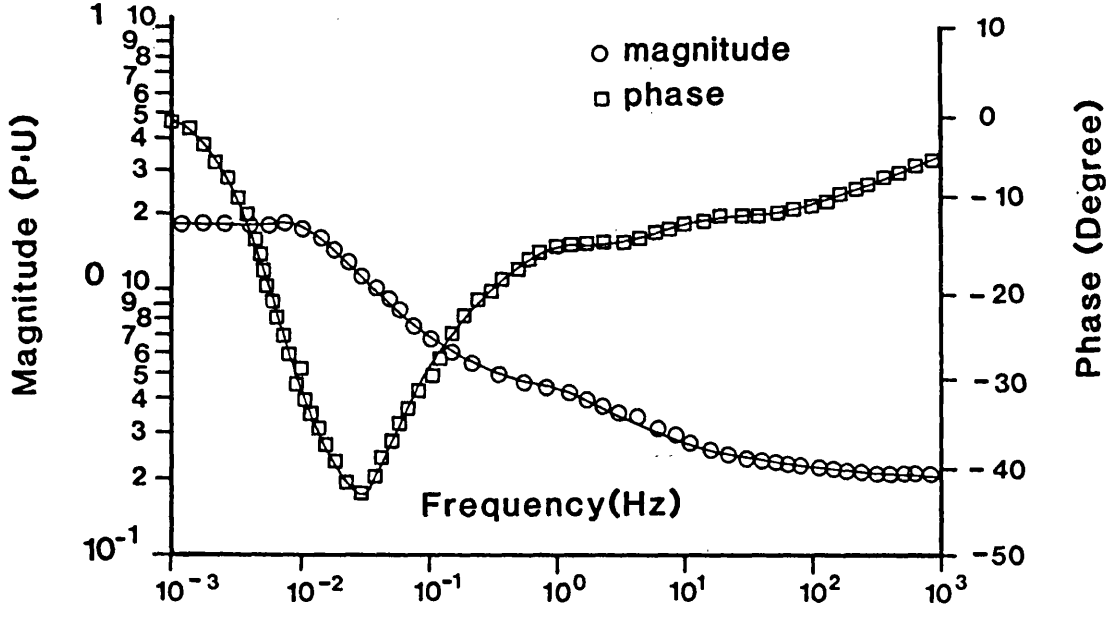

Figre 6.1 Northfleet machine direct axis operational inductance

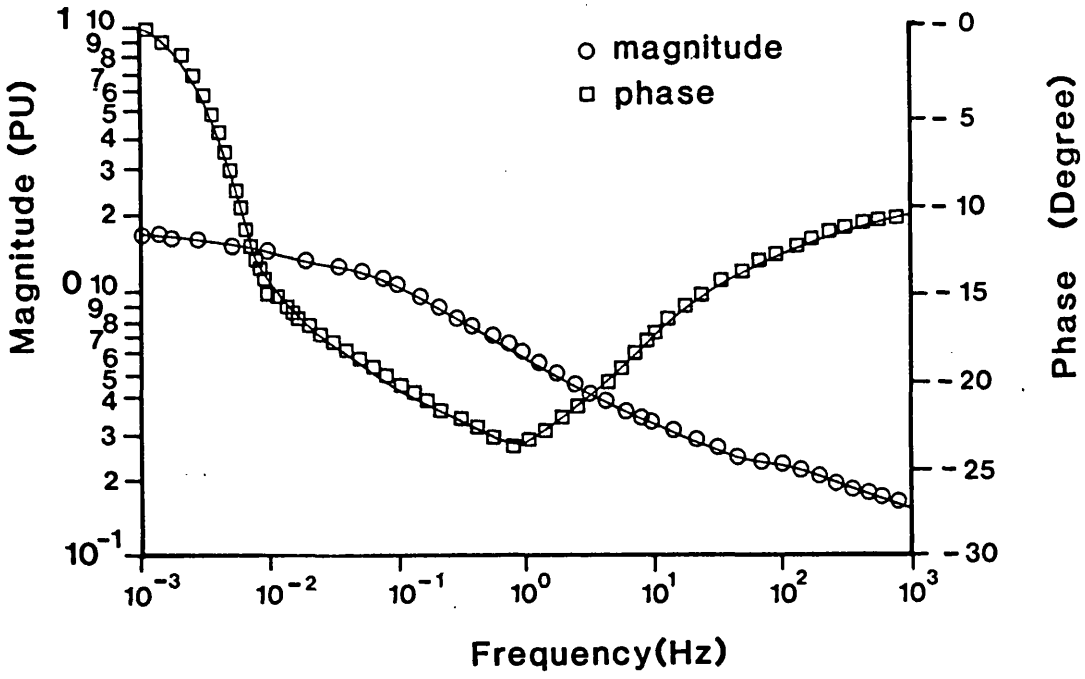

Figure 6.2 Northfleet machine Avadrature axis operational inductance

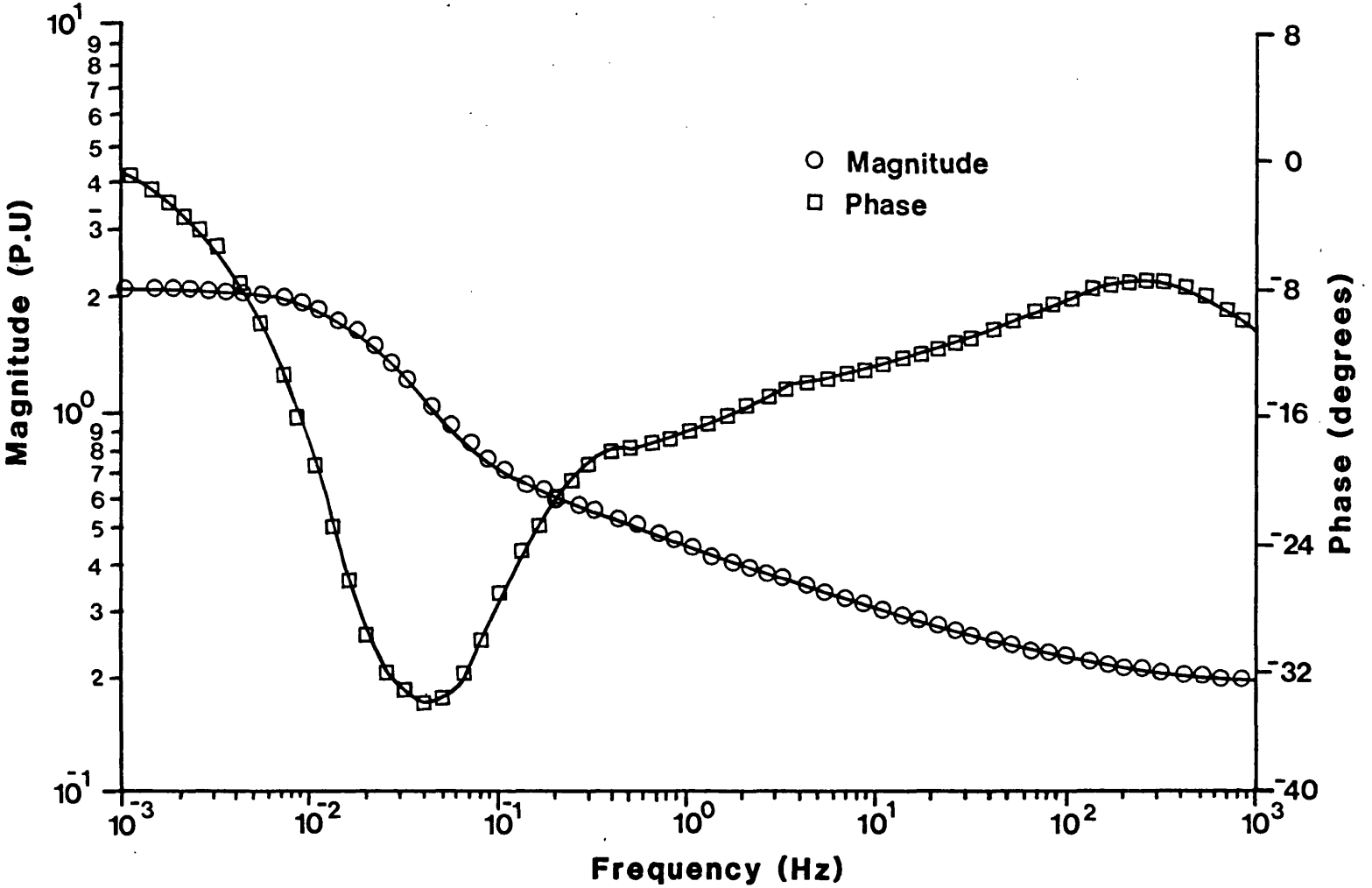

FIGURE 6.3 Nanticoke Direct Axis Operational Inductance.

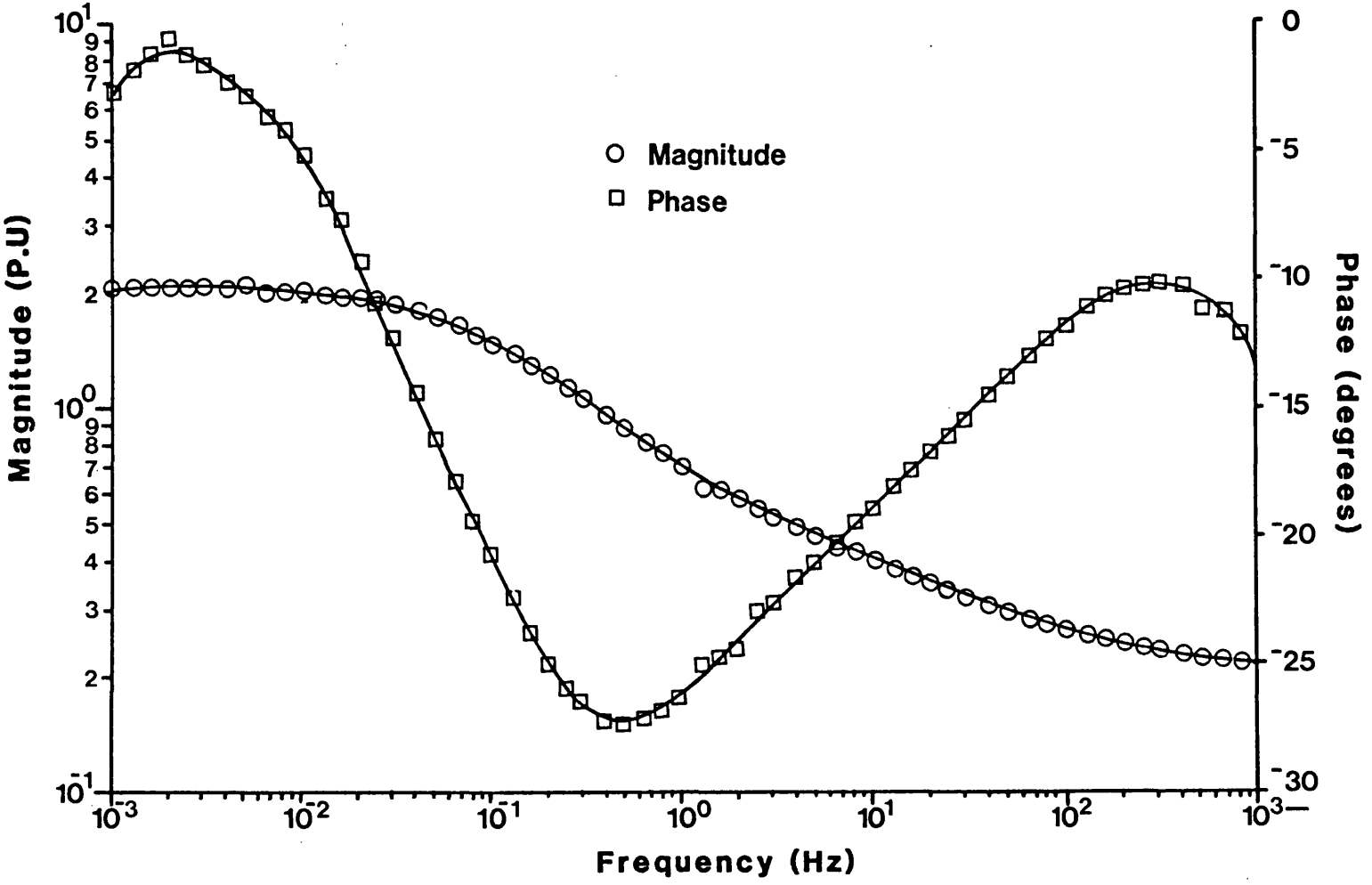

FIGURE 6·4 **Nanticoke Quadrature Axis Operational Inductance.**

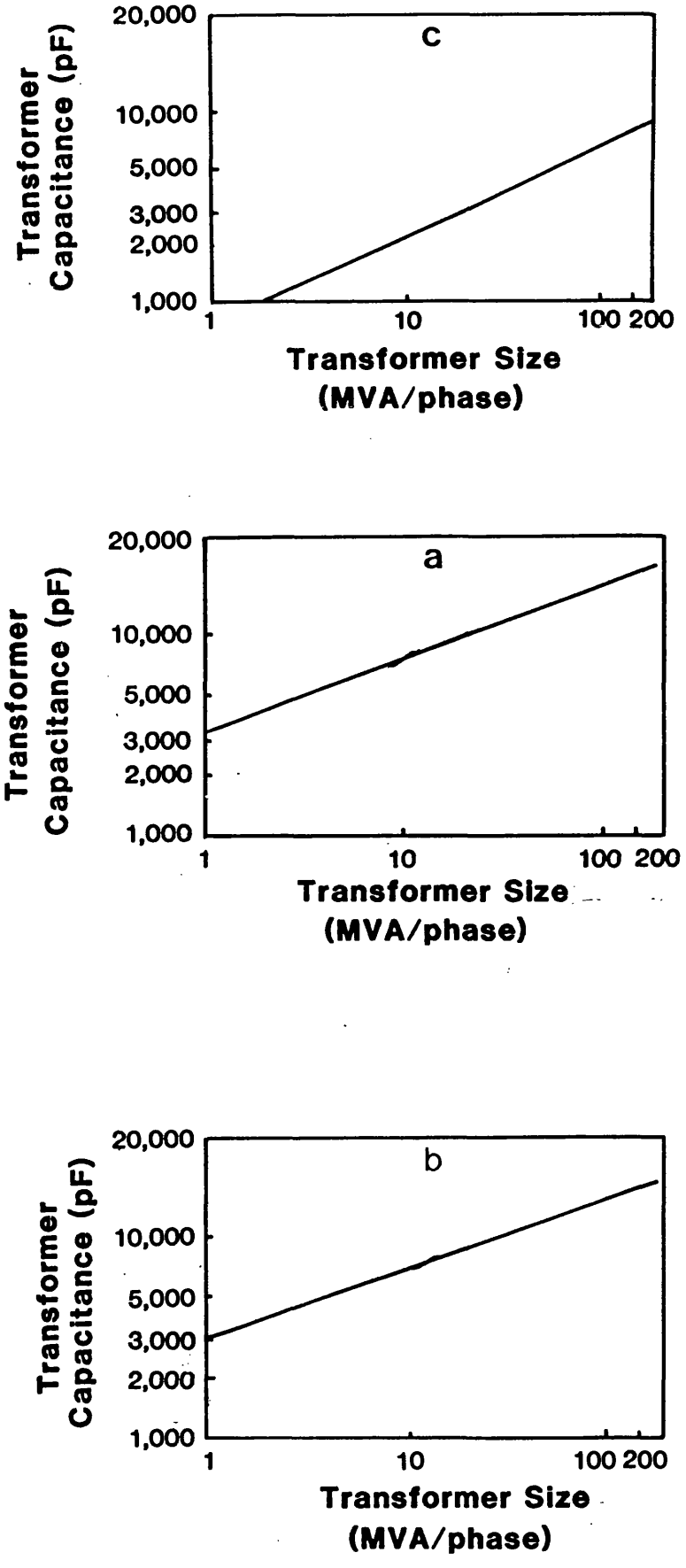

Figure 6.5 Transformer winding capacitance to ground range of values for various BIL of highest voltage winding

(a) 110 kv BIL (b) 150 kv BIL (c) 650 kv BIL

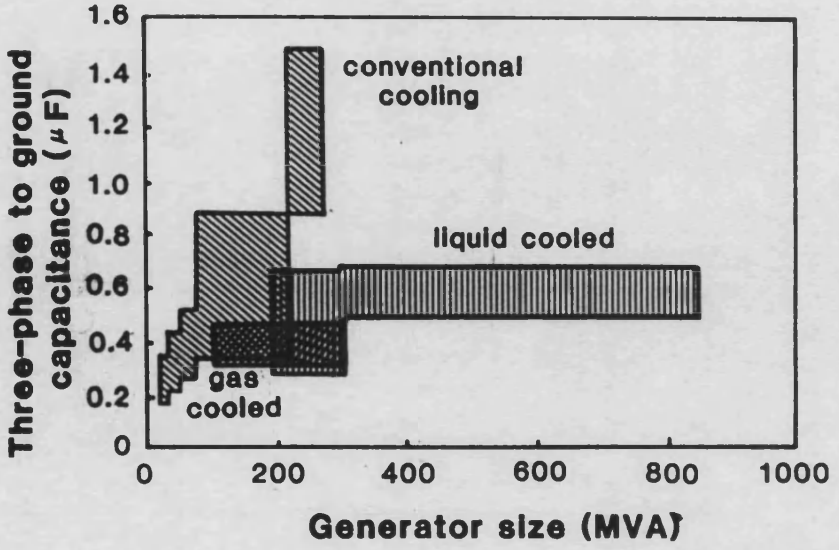

Figure 6.6 Capacitance to ground of synchronous generators

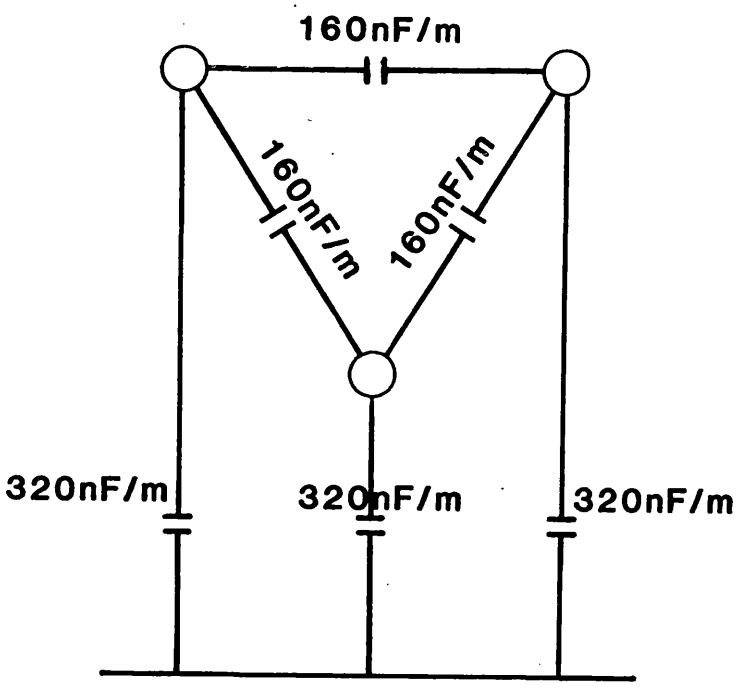

Fig. 6.7 Busbar Configuration

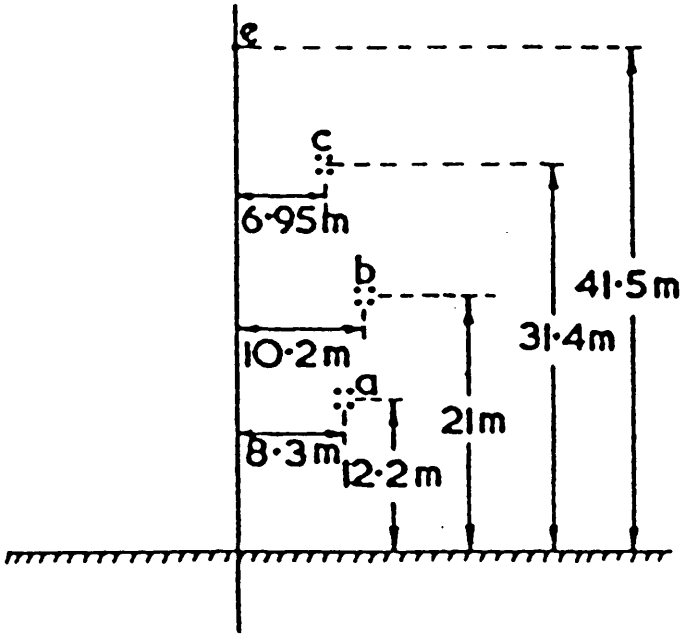

Fig. 6.8 400kV Quad Conductor Line Configuration

CHAPTER 7

EVALUATION OF THE GENERAL SYSTEM WAVEFORMS UNDER FAULT CONDITIONS

7.1 Introduction

The results presented here are associated with faults on infinite busbar of a system comprising transmission line and a turboalternator connected to its separate banked generator/transformer ($Y_{d_{1,1}}$). The turboalternator whose xd≠xq is analysed in a similar manner to the salient pole machine discussed in the preceding chapters. For this analysis, the two types of data used are the constant data as supplied by the manufacturer and the frequency-response data obtained from standstill frequency response tests. The transmission lines is represented by its distributed parameters and frequency variance of these parameters is taken into account.

It should be mentioned that a number of factors, namely, fault inception angle, type of fault and fault position considerably affect travelling wave distortion of both current and voltage waveforms at the star- and delta-side of the generator/transformer. Apart from these factors, the assumption of the frequency invariance of the transmission line parameters, which although it reduces computational times, can significantly affect the realism with which both the high and low frequency distortion in voltage and current waveforms is produced[15]. Hence it is important also to include frequency variance of transmission line parameters in the simulation.

Furthermore, the shunt capacitance (capacitance to ground) of the source side

(generator, transformer and busbar) can considerably affect the system waveforms.

As mentioned before, a major part of this work is concerned with a comparison of results obtained between representing the generator by an analytical expression using constant frequency-invariant machine parameters and a more realistic model using frequency variant machine data. Hence it is also necessary to consider in more detail the effects of the aforementioned factors on the voltage and current waveforms, in particular, how they are affected by the two types of machine models.

Some results are also presented which show a comparison between waveforms, in particular, current waveforms, for a system model comprising a simple source representation based on subtransient impedance with waveforms for a system comprising a realistic generator model.

The system model, as has been developed in chapter 5, is used to obtain the system responses. The system configuration considered is as shown in Figure 7.1.

Different types of solid faults, namely, three-phase, two-phase to earth, phase-to-phase and phase-to-earth have been considered. The parameters used here are as described in chapter 6. The prefault loading conditions are assumed to be at approximately full load, unity power factor and one per unit voltage at infinite busbar.

7.2 Effect of Source Side Capacitance to Ground (Shunt Capacitance)

As mentioned before, the voltage and current waveforms of the transformer star- and delta-sides can be significantly affected by the shunt capacitance of the generator transformer and busbar. Since the transferred voltage at the generator

terminal may also be affected by shunt capacitance of the cable connnected between generator/transformer[54,55], this latter has also been included in the relevant capacitances at transformer delta-side.

It should be noted that here, the effects of internal oscillations of the machine and transformer winding (due to the interaction between mutual inductance and capacitance between turns) has been neglected. The mathematical analysis for inclusion of the capacitance in the system model and the final form of resultant equations is as shown in Appendix A4.

The results shown here are a comparison between the waveforms obtained for a system which includes shunt capacitance and those obtained in which this capacitance is neglected, for different types of fault.

7.2.1 Solid three phase fault

Figure 7.2 shows the transformer star-side waveforms (voltage and current) for a three-phase fault without the shunt capacitance. As can be seen from Figure 7.2a, for a fault which occurs near zero voltage of the a-phase, complete offsetting of the current in this phase is seen to occur. Moreover, with reference to Figure 7.2b, the a-phase voltage being close to zero at applied fault inception, does not as expected contain a significant proportion of travelling wave distortion. The b- and c-phases, however, due to the phase angle difference with the a-phase, are subjected to significant overvoltages caused by travelling-waves which are, in turn, initiated by the abrupt collapse of relatively large voltages at the remote end of the line, for this type of fault.

When considering an identical 3-phase fault on a system in which the shunt capacitance is included, Figure 7.3a shows an increased distortion in the current

waveforms, particularly in the b- and c-phases. The transients on the voltage waveforms are, however, slightly reduced as can be seen by comparing Figures 7.3b and 7.2b.

Figure 7.4 shows the transformer delta-side current and voltage waveforms, when the shunt capacitance is neglected. It can be seen from Figure 7.4b that transformation of the star-side voltages to the delta-side causes the three-phase voltages to become almost equally distorted. A comparison between Figures 7.4 and 7.5 (the latter of which is for the system with shunt capacitance), shows that on the delta-side, inclusion of shunt capacitance has no important effect on current and voltage waveforms.

7.2.2 Solid line-to-line-to-earth fault (b-c-earth)

Figure 7.6 shows the waveforms (current and voltage) at star-side following a fault which occurs at maximum of the prefault interphase voltage. The shunt capacitances are not presented. For this particular fault condition, the aerial modes of travelling-wave voltage are of a large and almost equal and opposite magnitude, and since they are additive in the a-phase (sound phase), the voltage of this phase is relatively distortion free. On the other hand, the large valued aerial-mode components give rise to significant overvoltages on the faulted phases.

Figure 7.7 shows the current and voltage waveforms at the star-side of transformer when the shunt capacitance is included. Here again a comparison with Figure 7.6 shows that inclusion of shunt capacitance in the system causes the current waveforms to be more distorted (particularly for the faulted phases) and, at the same time, reduces the overvoltage levels at the star-side of the transformer.

The delta-side current and voltage wavefroms for this fault type are shown in

Figures 7.8 and 7.9, which corresponds to a system with and without shunt capacitance respectively. A comparison of the waveforms at machine terminals (delta-side) with that at star-side of transformer, shows that the delta-star connection reduces the overvoltages level at machine terminals[55], but nevertheless causes overvoltages to appear on all three phases. As before, for the three-phase fault, the inclusion of the shunt capacitance has a negligible effect on both the voltage and current waveforms on the delta-side.

7.2.3 Pure interphase fault (b-c-phase)

Figure 7.10 shows the waveforms (current and voltage) at the star-side of the transformer for a voltage minimum phase to phase fault. There is no shunt capacitance in the system. As expected, the level of high-frequency distortion is relatively low, but as can be seen from Figure 7.10a, complete offsetting of the c-phase current is produced. Since, in an interphase fault, the faulted phase superimposed currents are almost equal and opposite, the healthy a-phase voltage is distortion free, as shown by Figure 7.10b.

The waveforms resulting from the above-mentioned fault in a system comprising shunt capacitance at star-side of the transformer are shown in Figure 7.11. A comparison between Figures 7.10 and 7.11 shows that, as expected, because of the nature of the fault, which is a voltage minimum fault, inclusion of capacitance to ground has no significant effect on both current and voltage waveforms. A voltage maximum fault on the other hand, results in an accentuation of the high frequency spikes by the presence of the shunt capacitance, as shown by comparing Figures 7.12 and 7.13. The delta-side waveforms for the minimum interphase prefault voltage (former case) condition are shown in Figures 7.14 and 7.15. As can be seen in comparison with star-side voltages (Figures 7.10 and 7.11) the faulted phases are less distorted, but the healthy phase is not as

smooth as it is on the star-side. It should be noted that these effects are due to the presence of delta-star connection which is a further point of discontinuity.

Comparison of figures 7.14 and 7.15 shows that the waveforms at the delta-side, as for the two previously considered types of fault, are not significantly affected by inclusion of shunt capacitance in the system under study.

7.2.4 Phase to earth fault (a-phase to earth fault)

The waveforms at star-side of the transformer, when shunt capacitances are neglected, are shown in Figures 7.16a and b. The fault occurs at approximately 20^0 before the positive to negative zero-crossing of the fault point voltage. As can be seen from Figure 16, since the line is assumed transposed and the fault is applied at the infinite busbar, similar distortion is superimposed on the healthy phases. For the case when the shunt capacitance is included, the waveforms on the star-side are as shown in Figure 7.17. Comparing these with Figure 7.16, it can be seen when shunt capacitance is included, the high-frequency spikes appear in the current waveforms (Figure 7.17) each time a travelling-wave arrives from the faulted end of the line. Conversely, the inclusion of the capacitance has the effect of slightly reducing the spikes on the voltage waveforms (Figures 7.16 and 7.17).

For the delta-side, as before, the inclusion of the capacitance has a negligible effect on the voltage and current waveforms.

7.3 Effect of Frequency Variance of Operational Parameters of the Generator

The techniques for attaining the frequency variant operational parameters of the generators from a knowledge of frequency response data have been outlined in

chapter 4.

The result presented in this section considers the effects of incorporating frequency variant of generator parameters on the voltage and current waveforms, when firstly the system shown in Figure 7.1 is faulted at the infinite busbar, and secondly, for faults at the generator terminals for no load prefault conditions. The waveform observations are at the transformer star-side (i.e. sending end). For this study the frequency variant of transmission line parameters is also included.

7.3.1 Faults on the infinite busbar

7.3.1.1 Three phase (solid) fault

Figures 7.18 and 7.19 show simulation of conditions following a three phase to earth fault which occurs near voltage zero of the prefault a-phase, the former being for constant generator parameters and the latter in which the frequency-response data has been included. First of all, looking at the current waveforms, it is evident from Figures 7.18a and 7.19a that for the system with frquency variant generator parameters, there is a complete offset of the current in the a-phase, whereas, in the case of constant parameter generator model, an earlier zero crossing is seen to occur. Furthermore, magnitudes of currents in all the three phases are reduced and the b- and c-phase currents are also relatively more distorted for this case. In the case of voltage waveforms (Figures 7.18b and 7.19b), the waveforms for the system with frequency variant parameters are less distorted.

7.3.1.2 Line to line fault (b-c)

For this fault study, the results shown by Figures 7.20 and 7.21 are for a

fault which occurs at voltage minimum of the prefault interphase voltage between b- and c-phases. First of all, comparing the current waveforms between the frequency variant and frequency invariant models, as expected, the waveforms are relatively distortion free in both cases. The c-phase currents in both cases are fully offset; this is clearly shown by Figures 7.20a and 7.21a. However, when observing the current waveforms for longer observation time, Figure 7.20b and 7.21b quite distinctly show that whilst in the case of constant parameters model, the zero crossing on the c-phase current occurs approximately three cycles after fault inceptions, nonetheless, the zero crossing on the c-phase does not occur even after five cycles after fault inception in the case of the frequency variant parameters model. This can be attributed to the lower X/R ratio of the source for the former case which also accounts for the slightly larger magnitude of the currents for the case of the constant parameter model. As before, the voltage waveforms are more or less identical in the two cases, as shown by Figures 7.20c and 7.21c.

7.3.1.3 Line to ground fault (a-phase to earth)

7.3.1.3.1 General observations

Figure 7.22 shows a comparison of the results for the two models with a prefault voltage condition as Figure 7.16, for a-phase-earth fault. Since the line is assumed transposed and the fault is applied at infinite busbar, it can be seen from Figures 7.22b, d, f, that similar distortion is superimposed on the healthy phases (b and c). In the case of the current waveforms (Figures 7.22a, c and e) it can be seen that there is a reduction in the magnitudes for the frequency dependent parameter generator model and this is so by virtue of the fact that the machine operational inductances are generally larger when considering frequency response data. The a-phase current waveforms for a larger observation time

(Figure 7.23) clearly show the difference in magnitude between the two cases. As before, the voltage waveforms are more or less the same in the two cases.

7.3.1.3.2 Effect of line length

Considering voltage maximum faults at the infinite busbars, Figures 7.24 - 7.27 show the current and voltage waveforms (at the sending end) for two different line lengths of 50Km and 160Km respectively. The figures clearly show that because the currents are relatively distortion free, there is little difference in the waveforms between frequency dependent and frequency independent generator models. This is the case irrespective of the line length considered (Figures 7.24a - 7.27a). However, in the case of the voltage waveforms, there are very significant transients presented and, as mentioned before, the apparent frequency of these transients is lower for the longer line length. Comparing the waveforms for the two generator models, it is clearly evident that the magnitudes of the transients are lower when frequency variance of the parameters of the generator model is taken into account, this being so for both line lengths considered (Figures 7.24b - 7.27b). An extensive series of studies have shown that when considering the effect of frequency variance of the generator parameters, the difference in magnitude between the maximum spikes between the two models, is at its highest for longer line length and gradually reduces as the line length goes down. This effect is summarised in the graph shown in Figure 7.28.

7.3.1.3.3 Effect of fault inception angle

Fault inception angle affects the travelling wave distortion (particularly in voltage waveforms), this being minimum for faults near voltage zero and maximum for voltage maximum faults. Here again, the differences in the magnitudes of the transients obtained when considering frequency variant and frequency invariant

parameters of the generator is a function of the fault inception angle. Figure 7.29 summarises this effect and it can be seen that as the fault inception angle approaches zero, the approximations involved in considering frequency invariant generator model become less.

7.3.2 Generator terminal fault studies for no load prefault conditions

Figures 7.30 - 7.32 compare the waveforms of short circuit currents obtained between the machine represented by analytical expressions using constant data and those obtained for a machine represented by using frequency response data for operational inductances. As can be seen, very significant differences, particularly in magnitude, are observed between two studies for different types of faults. For example, in the three phase fault case (Figure 7.30), in which the fault occurs at maximum voltage of a-phase, the magnitude of the currents for the frequency variant model are significantly smaller than for those for the frequency invariant model, particularly in the initial period after fault inception. However, for other types of faults (phase to earth and two phase to earth) shown in Figure 7.31 and 7.32, there are not such discernible differences between magnitudes of the currents attained for the two models.

These studies again clearly show the importance of including frequency variant parameters of the machine particularly at the design stage of the machine.

It should be mentioned that all the aforementioned differences in the results between frequency variant and frequency invariant 588MVA generator model, are also observed when considering a system comprising 150MVA generator.

7.4 Effect of Complexity of Source Model

The developments in generator design and the associated trends in machine parameters, have resulted in higher X:R ratios at the hv terminals of the generator/transformer. This increase, coupled with developments to reduce the copper losses and the use of multiple conductor transmission lines, has resulted in a general raising of the network X:R level. These high X:R values indicate that high fault current asymmetry can occur for faults under the worst case conditions and that slow decay of the dc component will occur[57].

In this work when studying fault conditions on the system comprising 588MVA turbogenerator (with a realistic model), generator/transformer and transmission line indicate that even at lagging power factors, for voltage minimum faults dc offset can be so high that the fault current in the phase with the highest asymmetry at the sending end may not exhibit a zero crossing for some 30ms after fault. Such problems show a possible requirement to delay the opening of circuit breakers under such conditions. On the other hand, as has been mentioned previously in chapter 5, a simple source model based upon subtransient impedance does not produce the same degree of offset and, as such, using such a source model will cause a significant inaccuracy in the realism of any obtained results.

In this section, a comparison of results in particular for the current waveforms, is made for faults on a system comprising simple source and that in which the source is represented by a more realistic model.

7.4.1 Three phase solid fault

Figure 7.33a shows the current waveforms, following a three phase fault in a system comprising a realistic generator model. The fault occurs near zero voltage

in the a-phase and as can be seen a complete offset of the current in this phase has occurred. It should be mentioned here that the fault resistance can also affect the dc components[58,59] in that, if it is neglected, it can prolong the time at which the zero crossing occurs.

The current waveforms for a simple source model, with an identical fault conditon are shown in Figure 7.33b. A comparison between these two figures shows, as expected, an earlier zero crossing occurs when using a simple source model.

7.4.2 Pure interphase fault (b-c-phases)

The current waveforms for a system with a more realistic machine model and that of simple source model are shown in Figures 7.34a and b, the fault being a pure interphase fault occurring at voltage minimum of the pre-interphase voltage. For this type of fault, although the probability of a large asymmetry occurring is much slimmer and the necessary time for zero crossing is shorter than a three phase fault[58], but, nonetheless, with reference to Figure 7.34 it can be seen that complete offsetting of the c-phase current has occurred. This latter effect is not seen when a realistic source model is substituted by a simple model and, as can be seen from Figure 7.34b, an earlier zero crossing has occurred for the c-phase.

7.5 General Fault Transient Waveforms for a System with a Realistic Generator Model

7.5.1 Effect of power factor

For a generator, a lagging power factor causes the armature mmf to weaken the flux and the field current must be increased to maintain the voltage, i.e. an

overexcited generator exports lagging MVAR to the system connected to its terminals. On the other hand, a leading power factor causes the armature mmf to strengthen the flux and the field current must therefore be reduced, i.e. an underexcited generator exports leading MVAR to the system. With regard to these facts the stator short circuit current which comprises steady state, transient, subtransient and asymmetrical components, is high for an underexcited generator and corresponding asymmetrical component is much more severe than the case of an overexcited generator[60]. Such an asymmetrical component, which is a significant part of the total short circuit current and because of its nature (i.e. exponential) delays the zero crossing for the underexcited generator.

This effect can be seen by comparing the current waveforms in Figures 7.35a and 7.35b, these being for overexcited and underexcited generators respectively. In both cases, the fault is a three phase type occurring near the zero voltage of the a-phase and, as expected, in the case of an underexcited generator more severe short circuit current can be seen. Also it is necessary to wait for a longer time for the first actual zero transition to ensure safe interruption.

7.5.2 The behaviour of an underexcited alternator for various types of fault

7.5.2.1 588MVA generator

Two cases of 0.94 leading power factor, 1.065p.u. voltage and 0.98 leading power factor, 1.02p.u. voltage (in which in both cases full load at the infinite busbar is assumed) are studied. This study shows the severe dc component which is expected in very large machines. Such conditions would delay the zero crossing of faulty phase current which in turn can affect the operation of certain protective equipment. With reference to the above initial conditions, the results for the transformer star- and delta-side output currents are traced for several types of

fault and are given in Figures 7.36 - 7.41. For more details, the delay for the first zero crossing of star-side a-phase current of the 3-phase and line to ground faults (which are given in Figure 7.36, 7.39, 7.37 and 7.40) and the b-phase current of the line to line to ground fault (which are given in Figures 7.38 and 7.41) for two above-mentioned cases are compared in the following table:

Type of fault	20^0 leading p.f.	11^0 leading p.f.
3-phase fault	137ms	158ms
Line-to-line earth fault	37ms	56ms
Line-to-earth fault	18ms	18ms

Table 1

It should be noted that the above delays are obtained considering zero arc fault resistances.

7.5.2.2 150MVA generator

The two different power factors which have been used previously in section 7.5.2.1 are also applied to a system comprising 150MVA generator. Due to high resistance of the transformer winding associated with this generator and its lower reactance (which results in a lower X/R ratio) in comparison with a 588MVA generator/transformer, an early zero crossing is expected to occur in the faulted phase currents. Figure 7.42 show a comparison of the faulted phase current waveforms between the star and delta sides of the transformer for three types of fault.

As expected, a comparison between Tables 1 and 2 confirms that because of the much lower X/R ratio associated with a system comprising a 150MVA generator and 132/13.8kV transformer, the zero crossing occurs much earlier on in this system.

Type of fault	20^0 leading p.f.	11^0 leading p.f.
3-phase fault	18.5ms	18.5ms
Line-to-line earth fault	14ms	14ms
Line-to-earth fault	17.5ms	17.5ms

Table 2

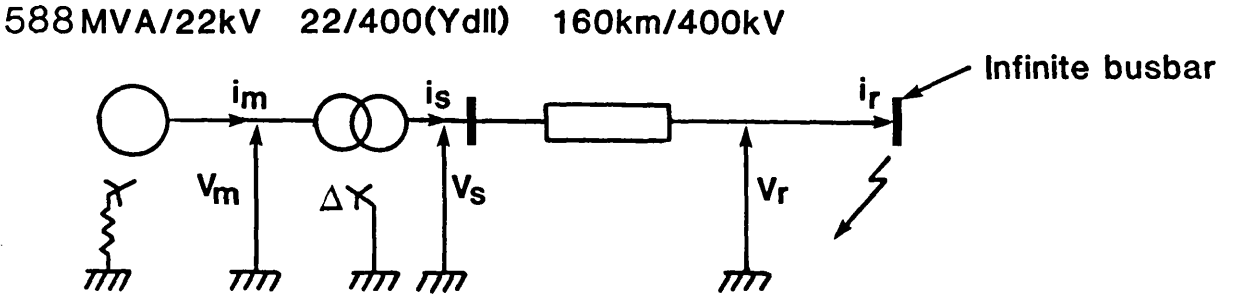

Fig 7.1 Single-line diagram of configuration studied

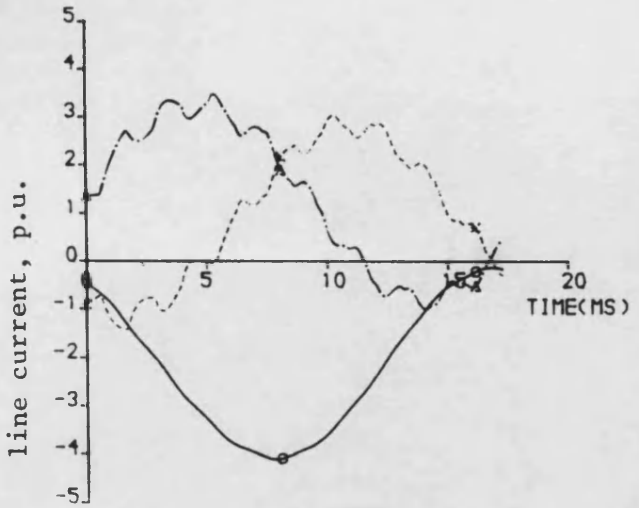

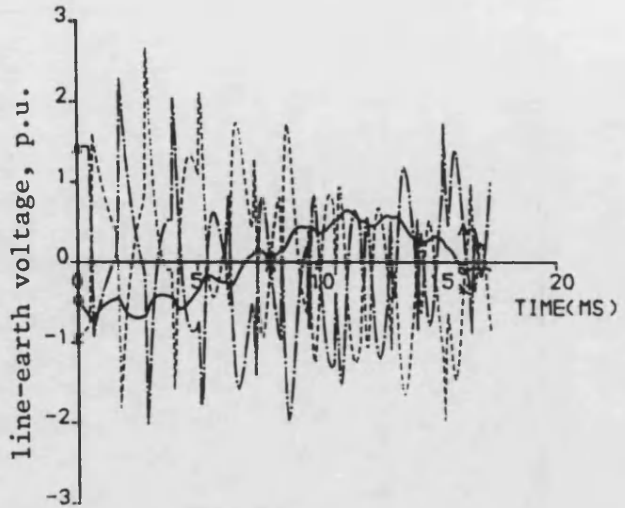

Figure 7.2 Waveforms on the star-side of transformer for a solid three phase fault source side shunt capacitances neglected

$\delta = 66°$ $\lambda = 114°$ $\theta_m = -50°$

——— a-phase
—.— b-phase
----- c-phase

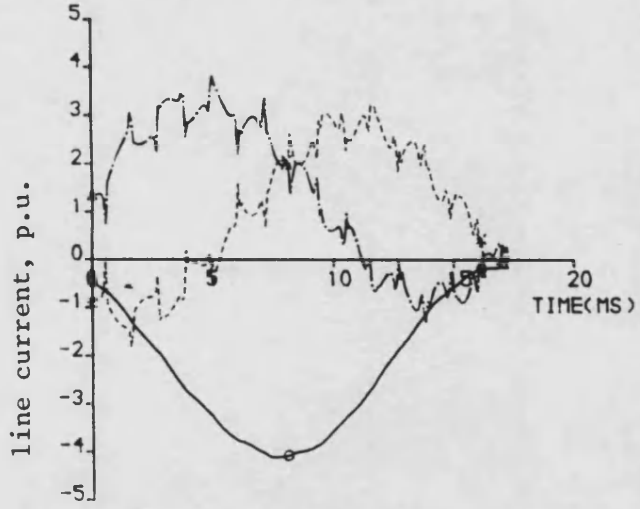

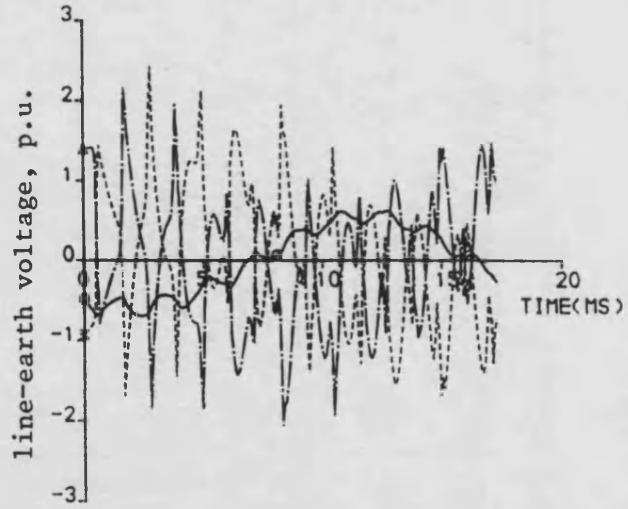

Figure 7.3 Waveforms on the star-side of transformer for a solid three phase fault, source side shunt capacitances included

$\delta = 66°$ $\lambda = 114°$ $\theta_m = -50°$

——— a-phase
—.— b-phase
----- c-phase

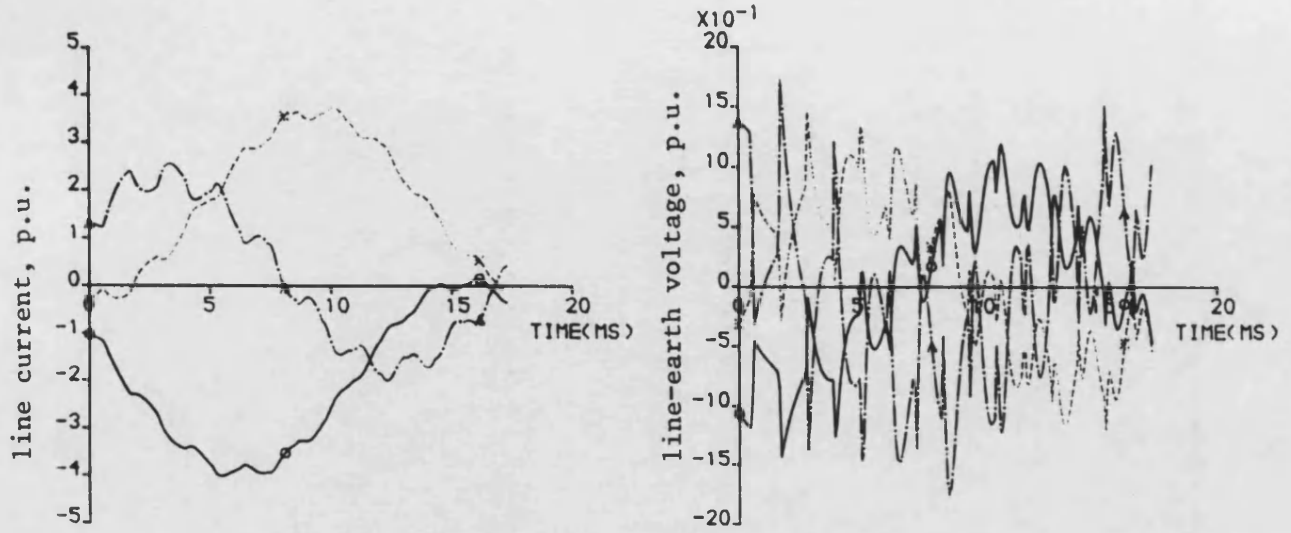

Figure 7.4 Waveforms on the delta-side of transformer for a solid three phase fault, source side shunt capacitances neglected

$\delta = 66°$ $\lambda = 114°$ $\theta_m = -50°$

——— a-phase
—.— b-phase
----- c-phase

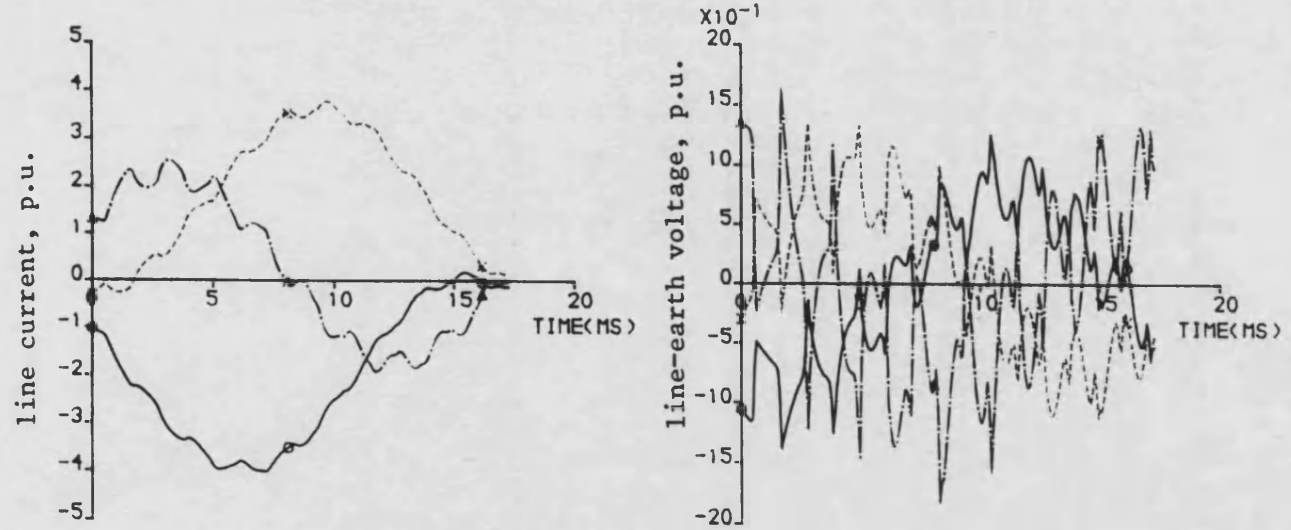

Figure 7.5 Waveforms on the delta-side of transformer for a solid three phase fault, source side shunt capacitances included

$\delta = 66°$ $\lambda = 114°$ $\theta_m = -50°$

——— a-phase
—.— b-phase
----- c-phase

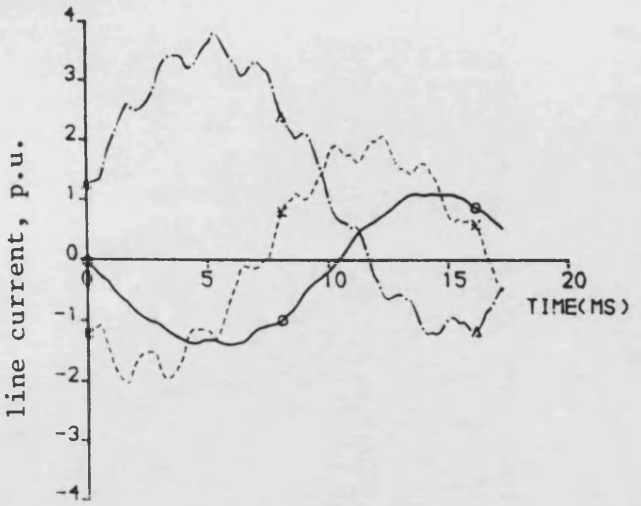

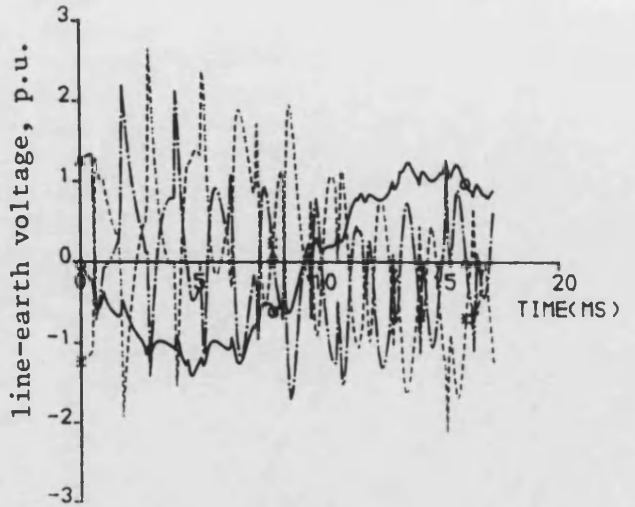

Figure 7.6 Waveforms on the star-side of transformer for a solid two-phase-to-earth fault (b-c-earth), source side shunt capacitances neglected

$\delta = 64°$ $\lambda = 96°$ $\theta_m = -50°$

——— a-phase
—.— b-phase
----- c-phase

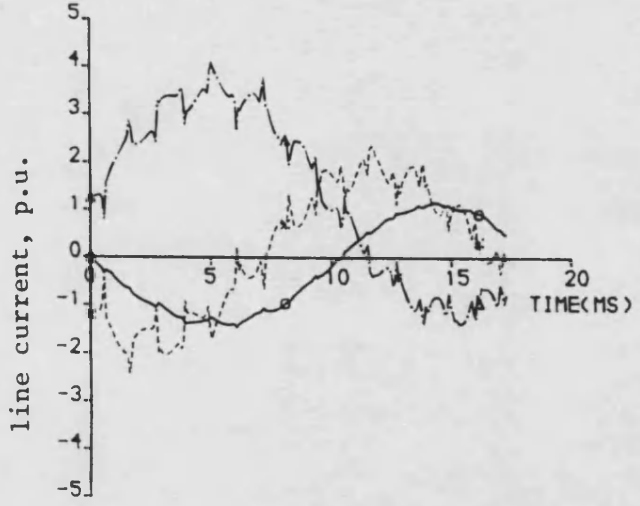

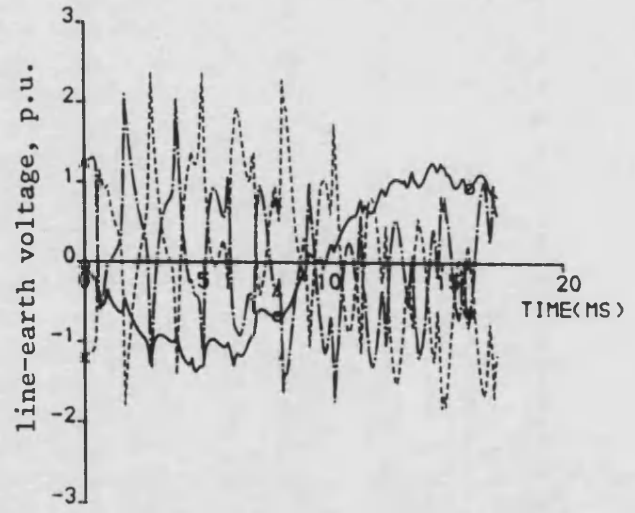

Figure 7.7 Waveforms on the star-side of transformer for a solid two-phase-to-earth fault (b-c-earth), source side shunt capacitances included

$\delta = 64°$ $\lambda = 96°$ $\theta_m = -50°$

——— a-phase
—.— b-phase
----- c-phase

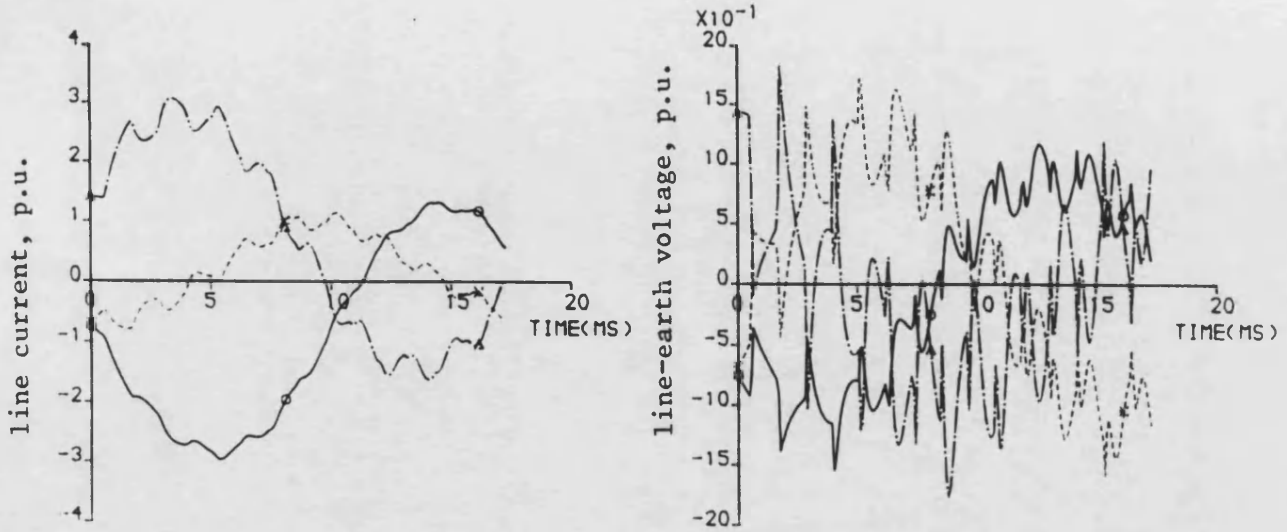

Figure 7.8 Waveforms on the delta-side of transformer for solid two-phase-to-earth fault (b-c-earth), source side shunt capacitances neglected

$\delta = 64°$ $\lambda = 96°$ $\theta_m = -50°$

——— a-phase
—.— b-phase
----- c-phase

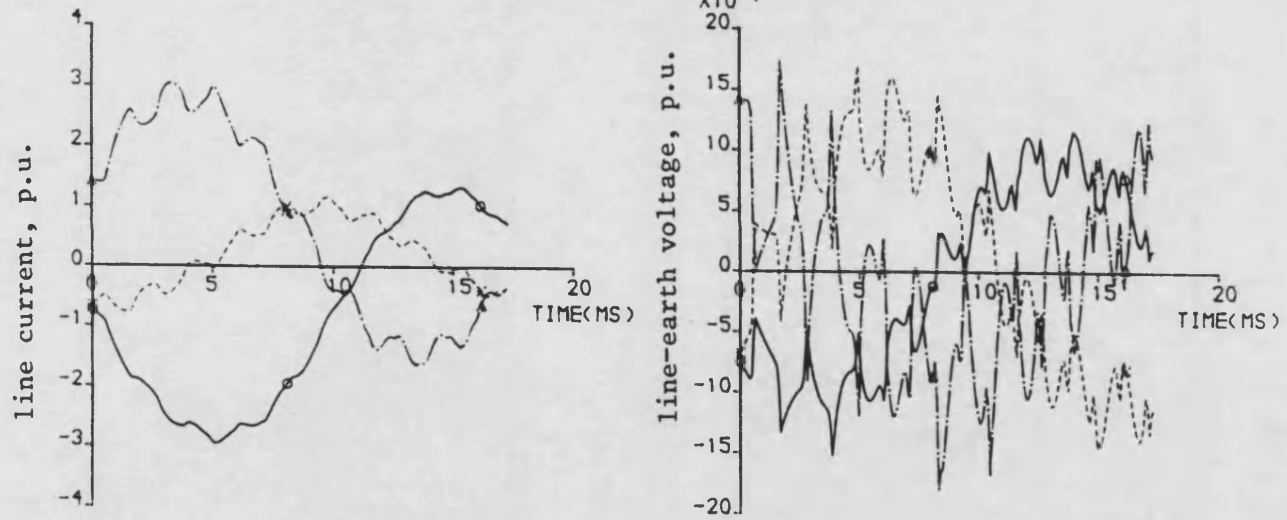

Figure 7.9 Waveforms on the delta-side of transformer for solid two-phase-earth fault (b-c-earth), source side shunt capacitances included

$\delta = 64°$ $\lambda = 96°$ $\theta_m = -50°$

——— a-phase
—.— b-phase
----- c-phase

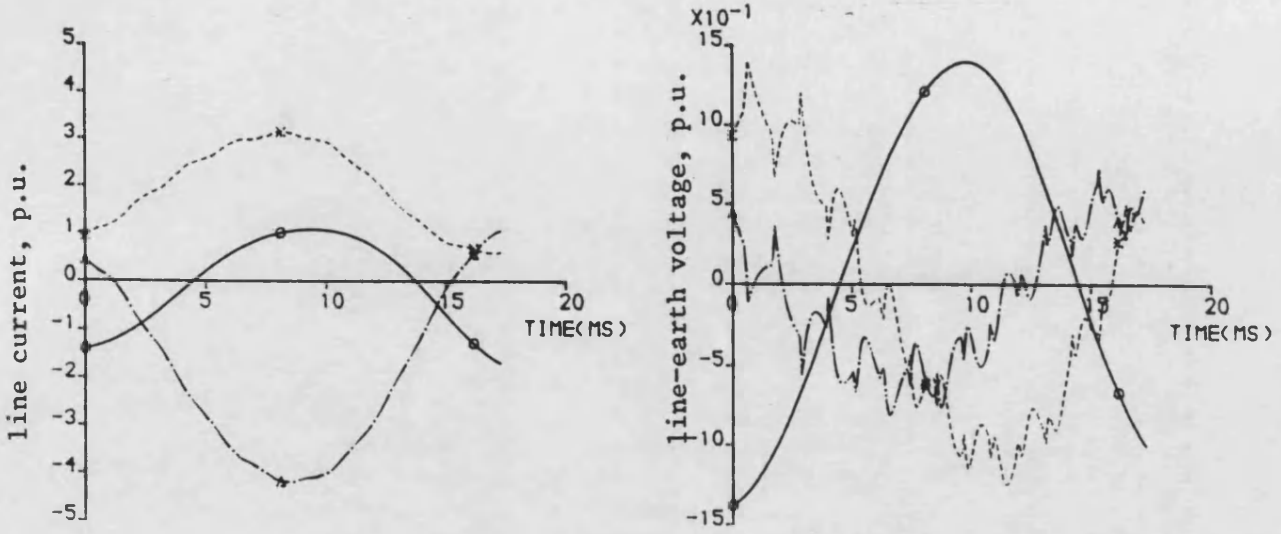

Figure 7.10 Waveforms on the star-side of transformer for a pure interphase fault, (b-c), source side shunt capacitances neglected

$\delta = 60°$ $\lambda = 192°$ $\theta_m = -50°$

——— a-phase
—.— b-phase
----- c-phase

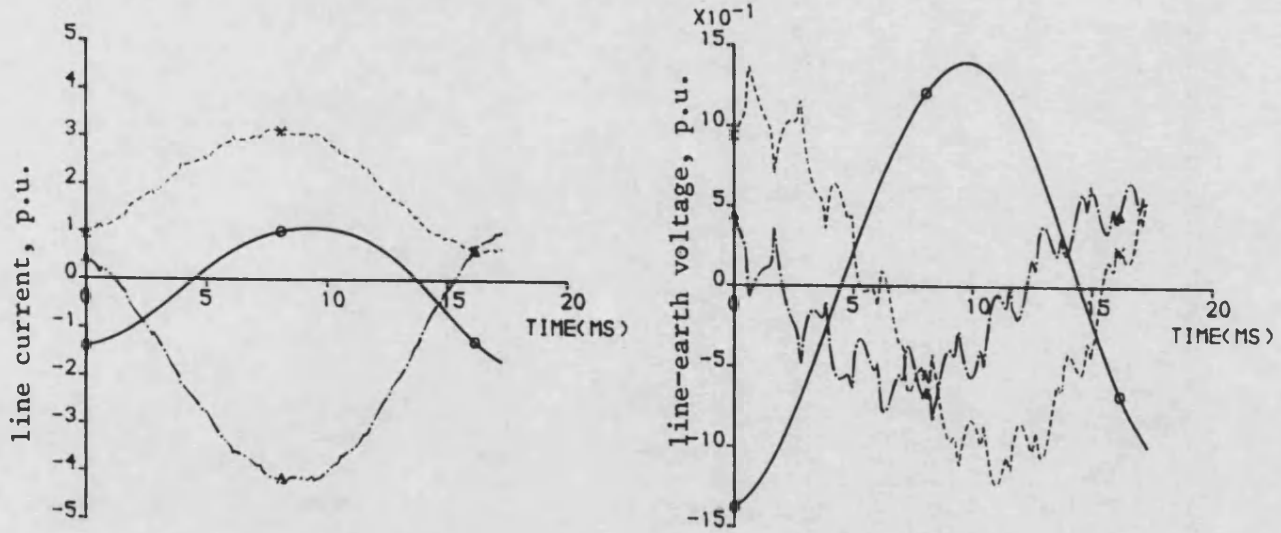

Figure 7.11 Waveforms on the star-side of transformer for a pure interphase fault, (b-c), source side shunt capacitances included

$\delta = 60°$ $\lambda = 192°$ $\theta_m = -50°$

——— a-phase
—.— b-phase
----- c-phase

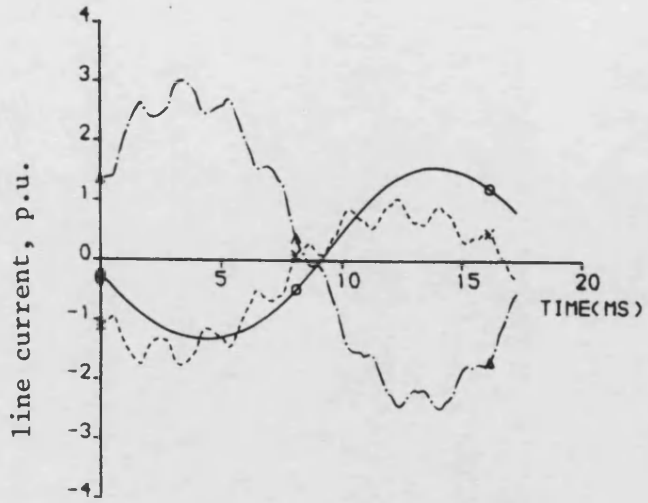

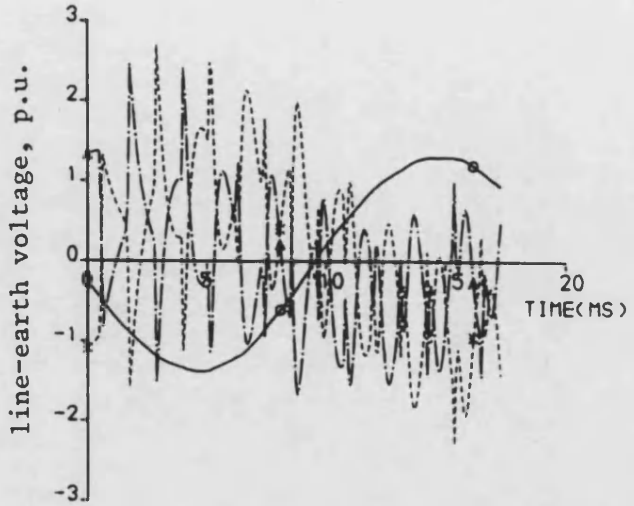

Figure 7.12 Waveforms on the star-side of transformer for a pure interphase fault (b-c) for maximum prefault voltage, source-side shunt capacitances neglected

$\delta = 60°$ $\lambda = 92°$ $\theta_m = -50°$

——— a-phase
—.— b-phase
----- c-phase

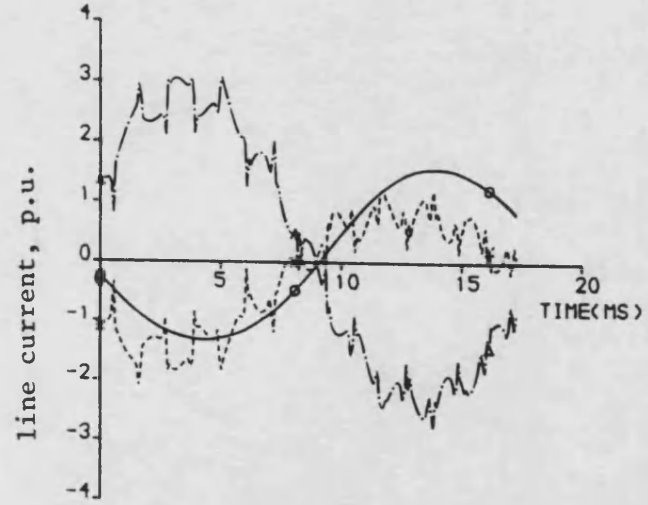

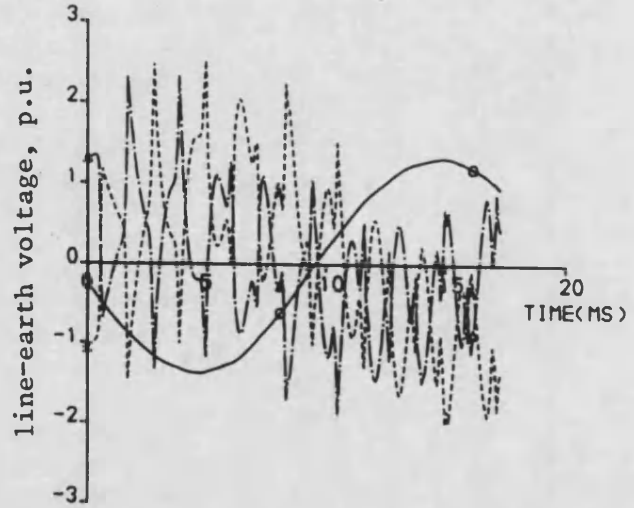

Figure 7.13 Waveforms on the star-side of transformer for a pure interphase fault (b-c), for maximum prefault voltage, source side shunt capacitances included

$\delta = 60°$ $\lambda = 92°$ $\theta_m = -50°$

-——— a-phase
—.— b-phase
----- c-phase

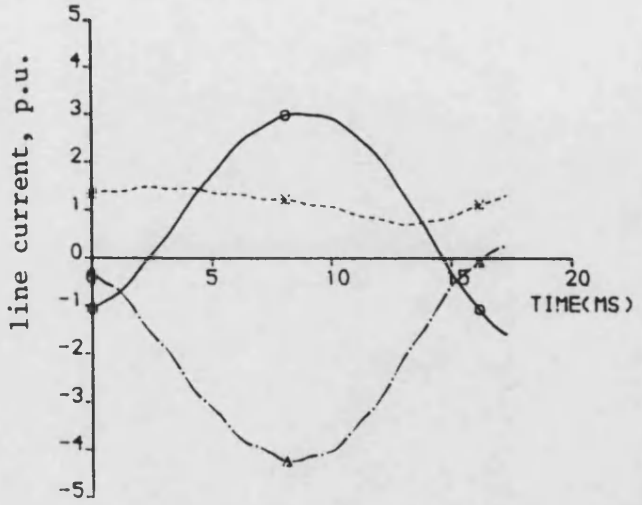

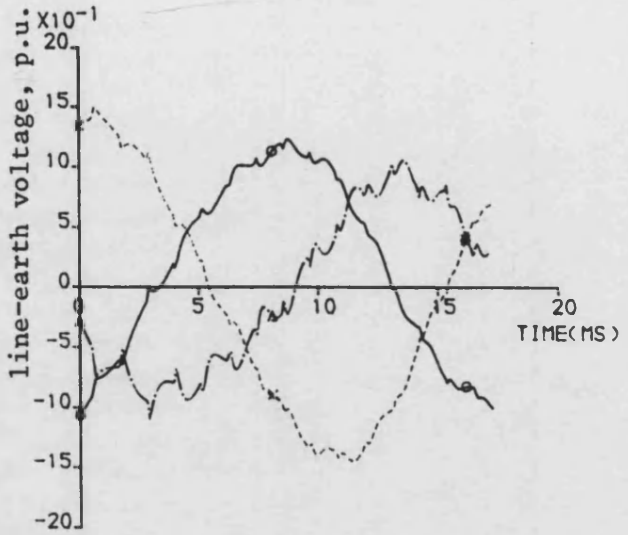

Figure 7.14 Waveforms on the delta-side of transformer for a pure interphase fault (b-c), source side shunt capacitance neglected

$\delta = 60°$ $\lambda = 192°$ $\theta_m = -50°$

——— a-phase
—.— b-phase
----- c-phase

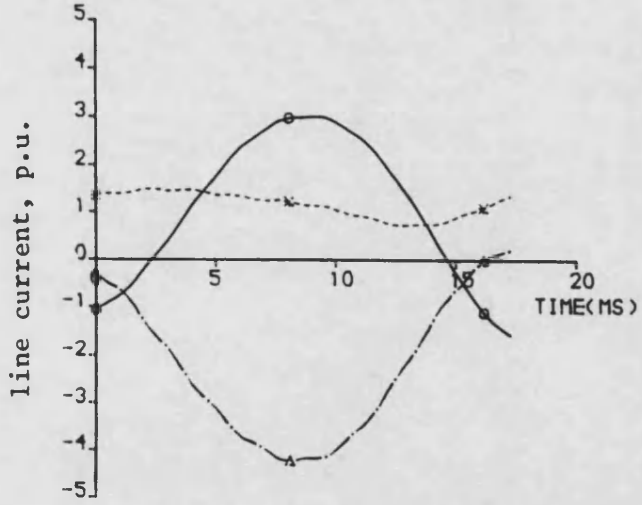

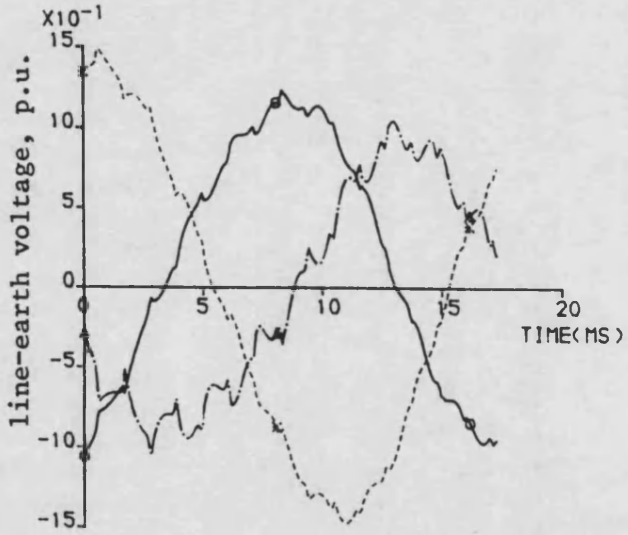

Figure 7.15 Waveforms onthe delta-side of transformer for a pure interphase fault (b-c), source side shunt capacitance included

$\delta = 60°$ $\lambda = 192°$ $\theta_m = -50°$

——— a-phase
—.— b-phase
----- c-phase

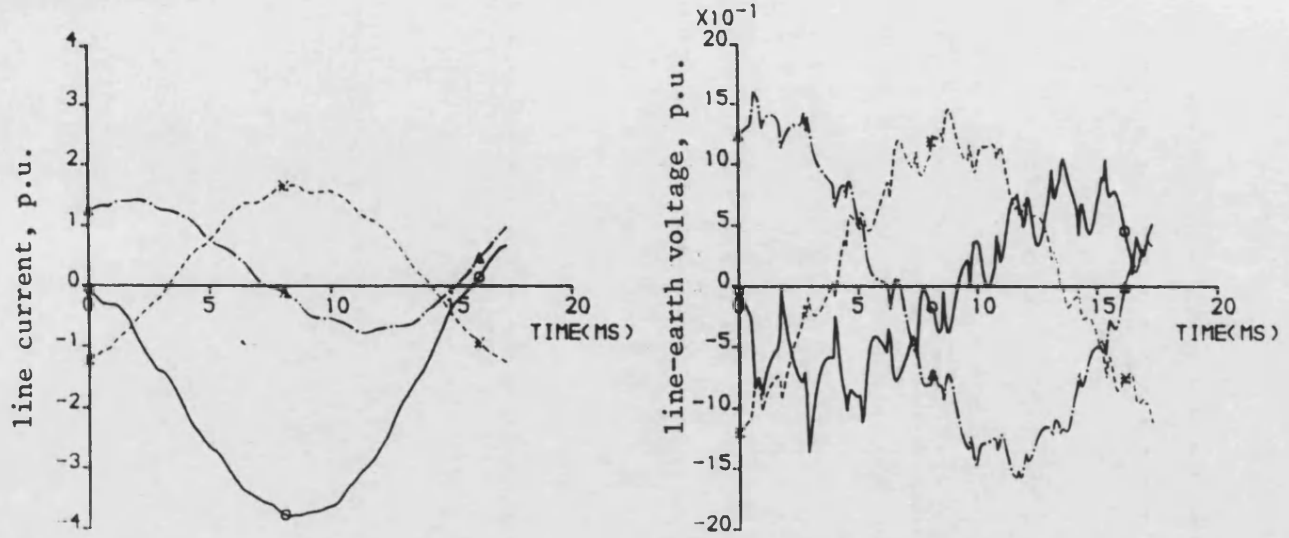

Figure 7.16 Waveforms on the star-side of transformer, for an a-phase to earth fault, source side shunt capacitances neglected

$\delta = 64°$ $\lambda = 96°$ $\theta_m = -50°$

——— a-phase
—.— b-phase
----- c-phase

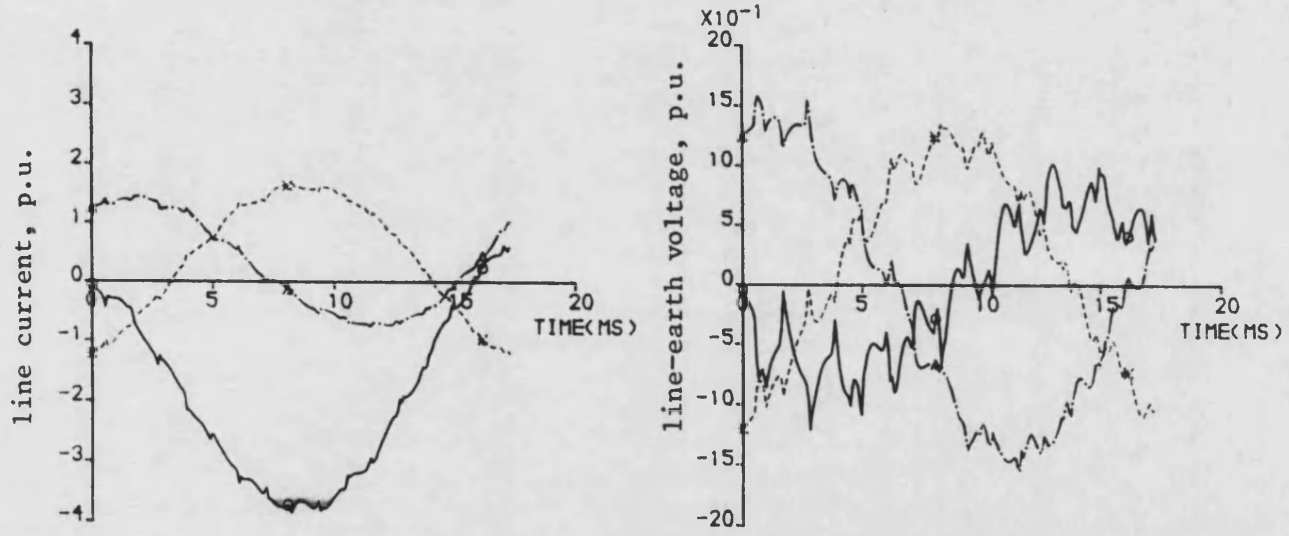

Figure 7.17 Waveforms on the star-side of transformer, for an a-phase to earth fault, source side shunt capacitance included

$\delta = 64°$ $\lambda = 96°$ $\theta_m = -50°$

——— a-phase
—.— b-phase
----- c-phase

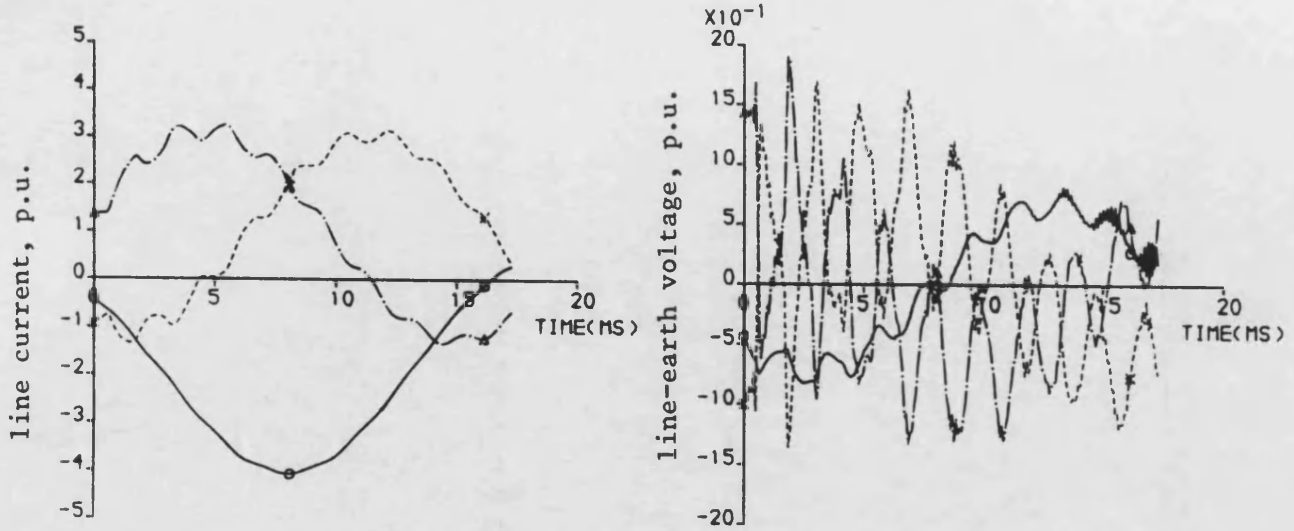

Figure 7.18 Waveforms on the star-side of transformer for a solid three phase fault, for frequency invariant parameters generator model

——— a-phase
—.— b-phase
----- c-phase

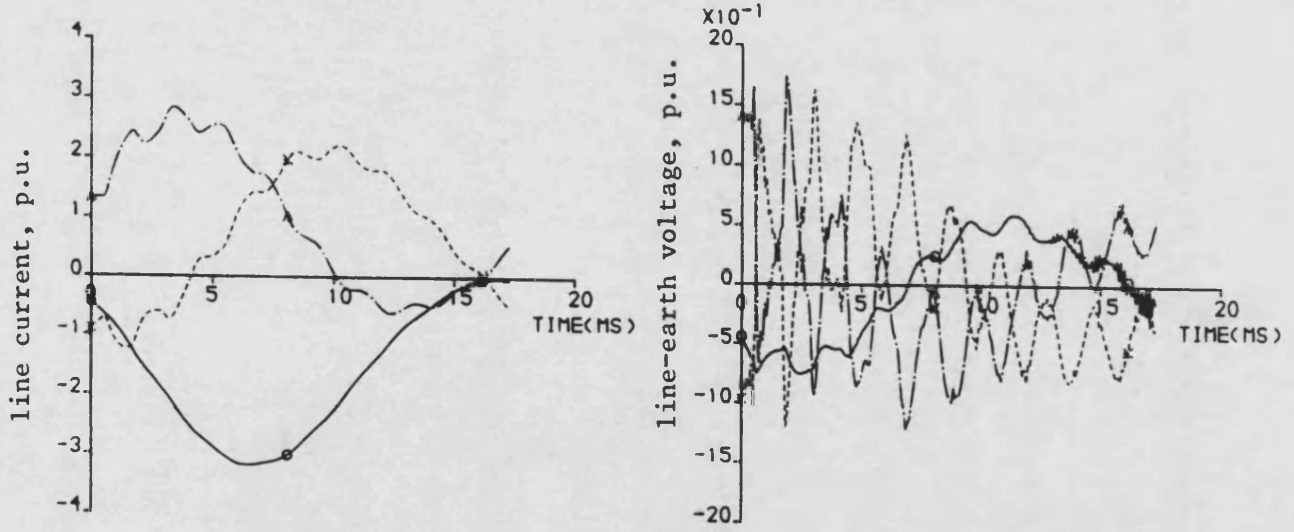

Figure 7.19 Waveforms on the star-side of transformer for a solid three phase fault for frequency variant parameters generator model

——— a-phase
—.— b-phase
----- c-phase

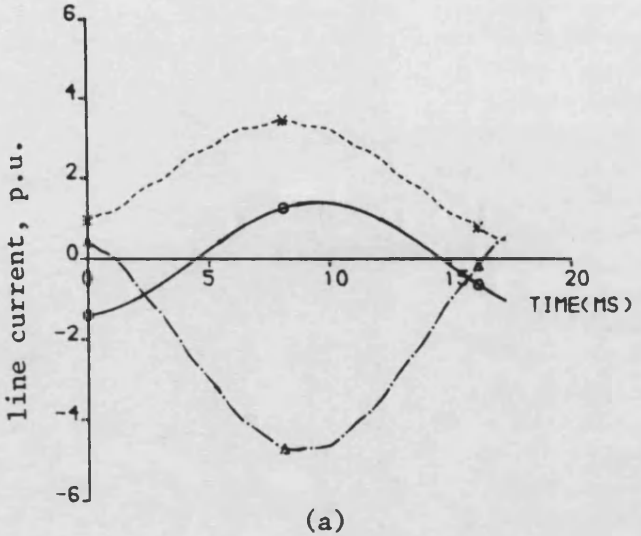

(a)

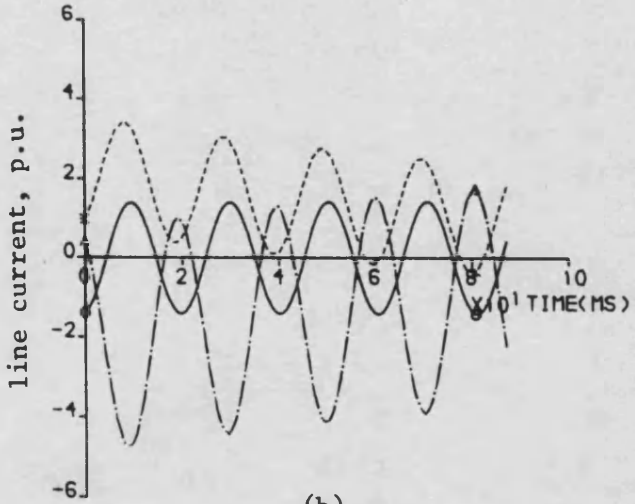

(b)

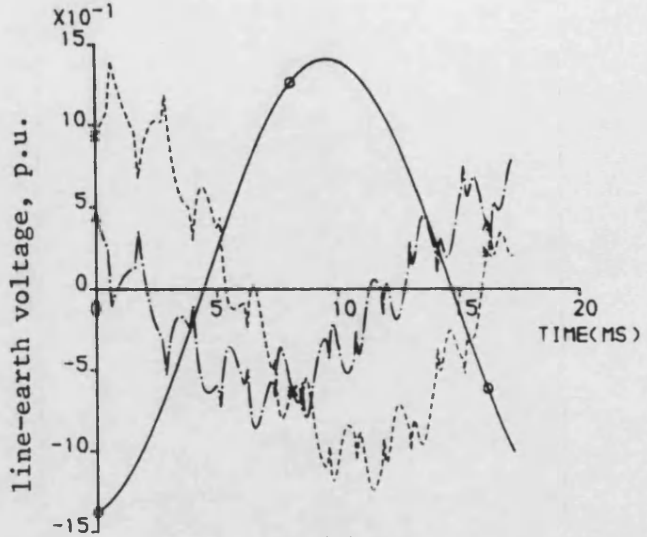

(c)

Figure 7.20 Waveforms on the star-side of transformer for a pure interphase fault (b-c), for frequency invariant parameters generator model

(a) Current for a short observation time
(b) Current for a longer observation time
(c) Voltage for a short observation time

P = 1.0 Q = 0.2 (lag)

——— a-phase

—.— b-phase

----- c-phase

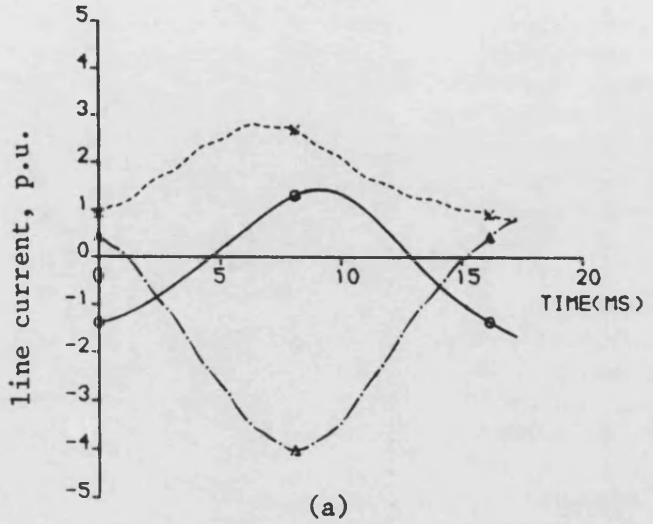

(a)

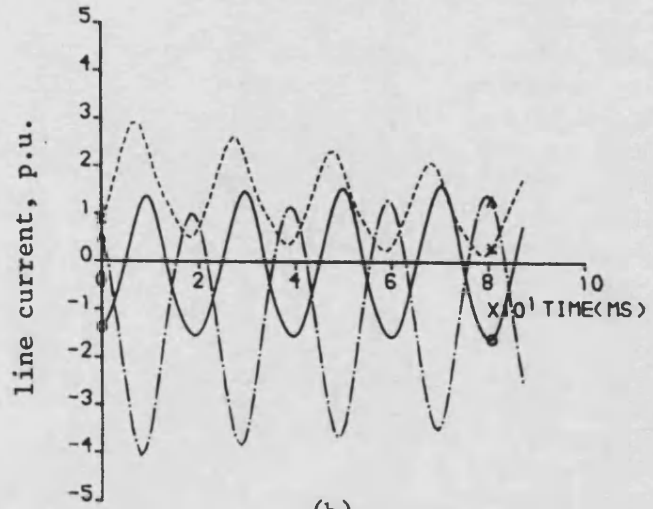

(b)

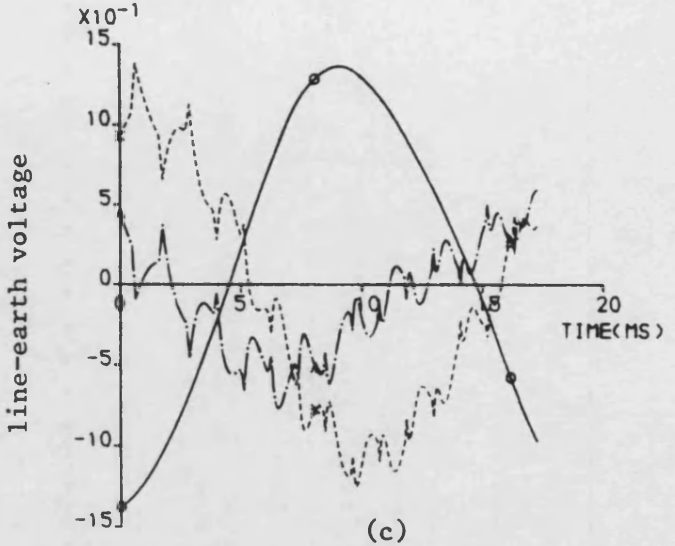

(c)

Figure 7.21 Waveforms on the star-side of transformer for a pure interphase fault (b-c), for frequency variant parameters generator model

(a) Current for a short observation time
(b) Current for a longer observation time
(c) Voltage for a short observation time

P = 1.0 Q = 0.2 (lag)

——— a-phase
—.— b-phase
----- c-phase

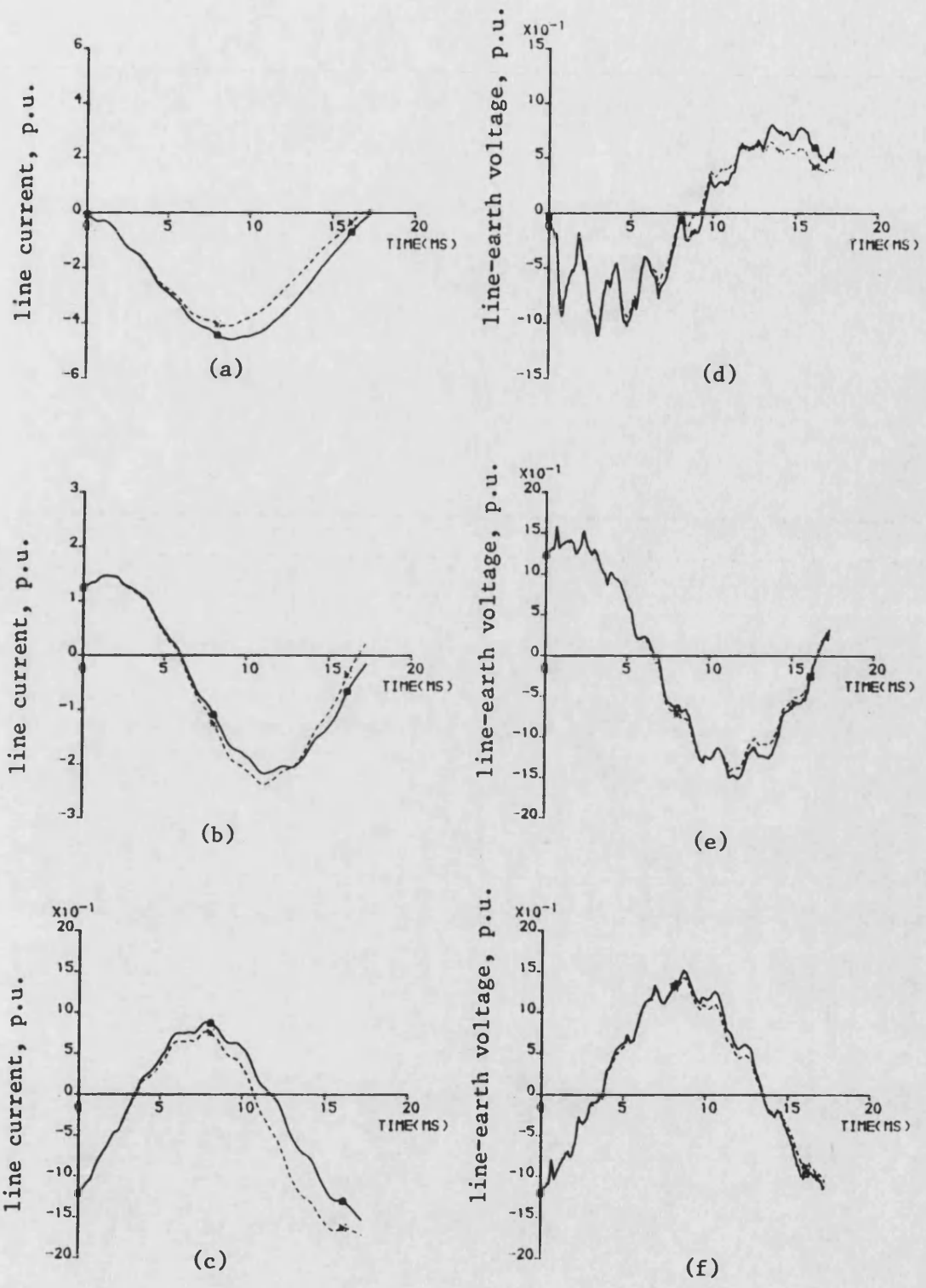

Figure 7.22 Waveforms on the star-side of transformer, for an a-phase to earth fault

(a) a-phase current
(b) b-phase current
(c) c-phase current
(d) a-phase voltage
(e) b-phase voltage
(f) c-phase voltage

——— frequency invariant generator model
----- frequency variant generator model

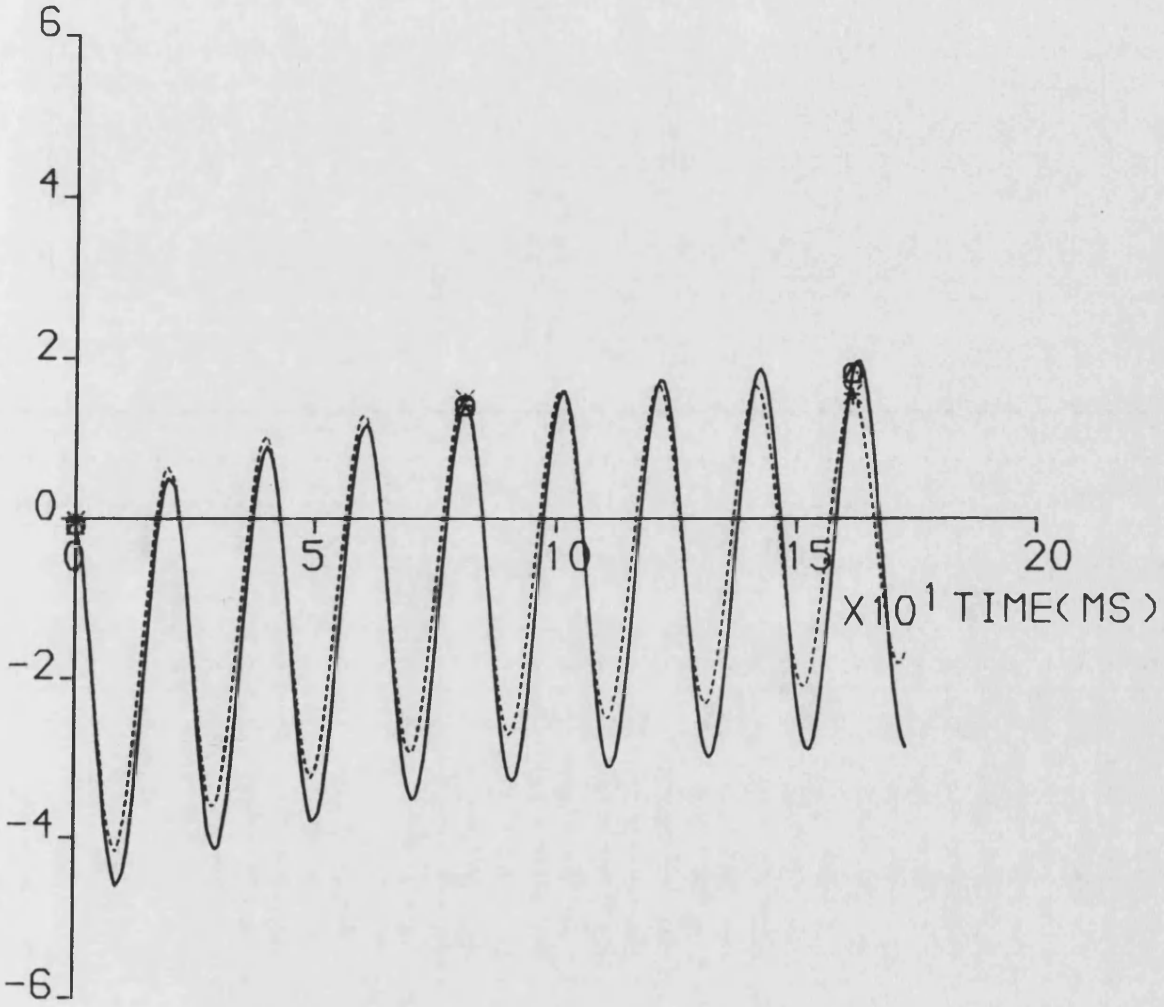

Figure 7.23 a-phase current waveforms on the star-side of transformer, for an a-phase to earth fault, for a long observation time

——— frequency invariant generator model
----- frequency variant generator model

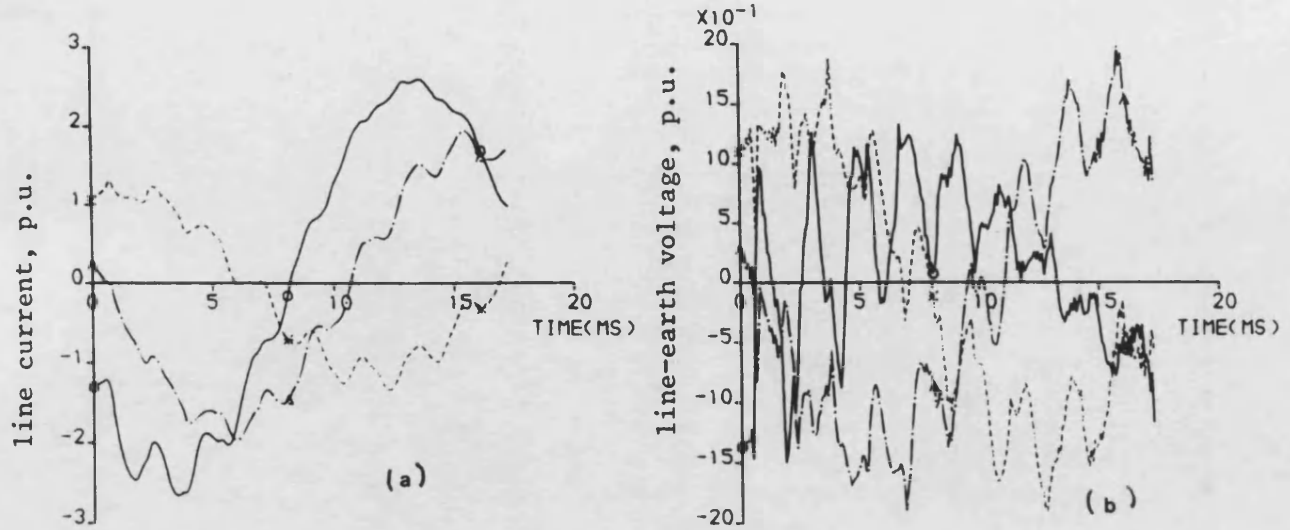

Figure 7.24 Waveforms on the star-side of transformer for a maximum prefault voltage a-phase to earth fault, for frequency invariant parameters generator model (x = 160Km)

——— a-phase
—.— b-phase
----- c-phase

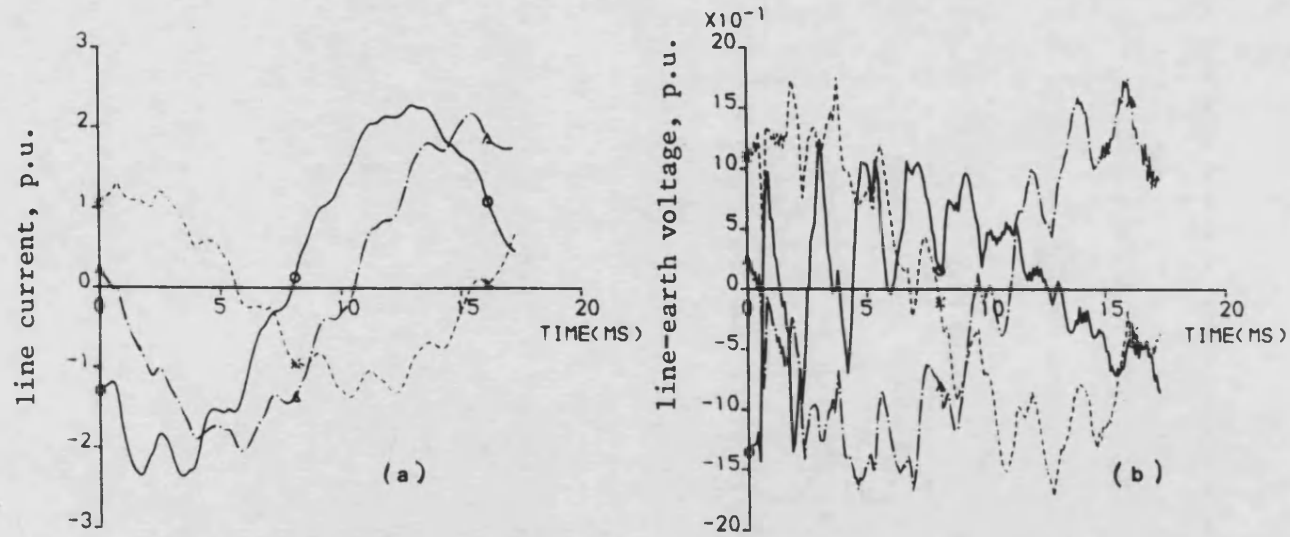

Figure 7.25 Waveforms on the star-side of transformer for a maximum prefault voltage a-phase to earth fault, for frequency variant parameters generator model (x = 160Km)

——— a-phase
—.— b-phase
----- c-phase

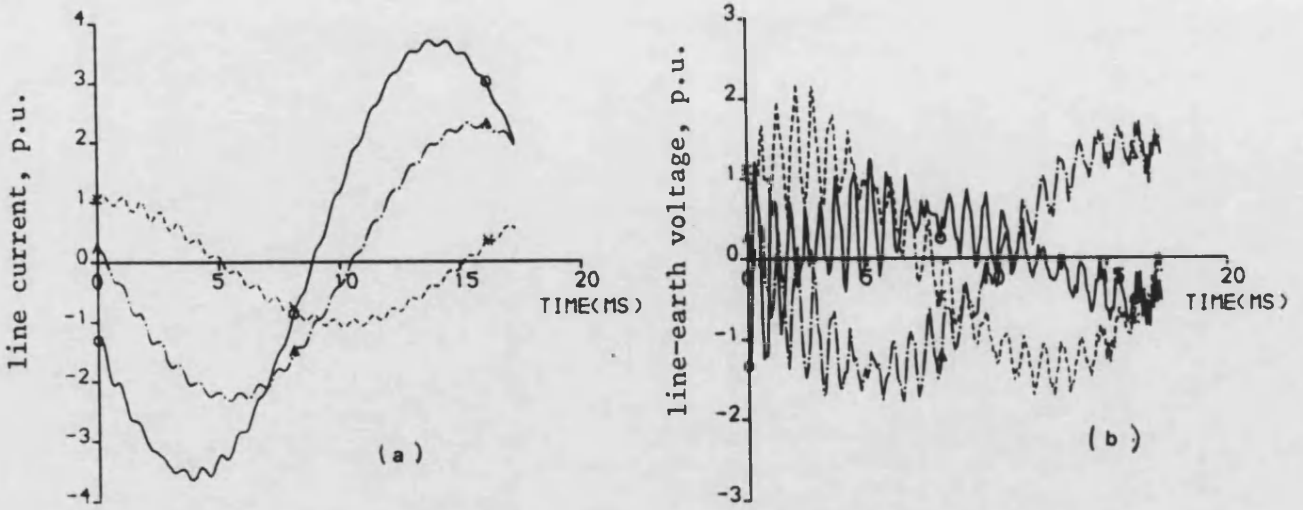

Figure 7.26 Waveforms on the star-side of the transformer, for a maximum prefault voltage a-phase to earth fault, for frequency invariant generator model (x = 50Km)

——— a-phase
—.— b-phase
----- c-phase

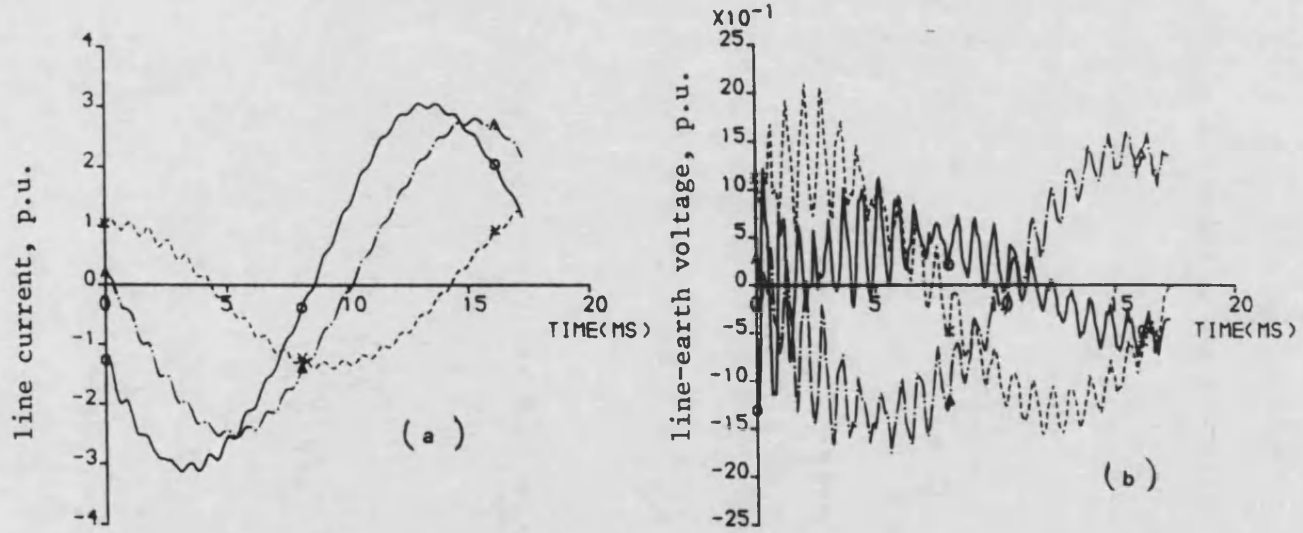

Figure 7.27 Waveforms on the star-side of the transformer, for a maximum prefault voltage a-phase to earth fault, for frequency variant generator model (x = 50Km)

——— a-phase
—.— b-phase
----- c-phase

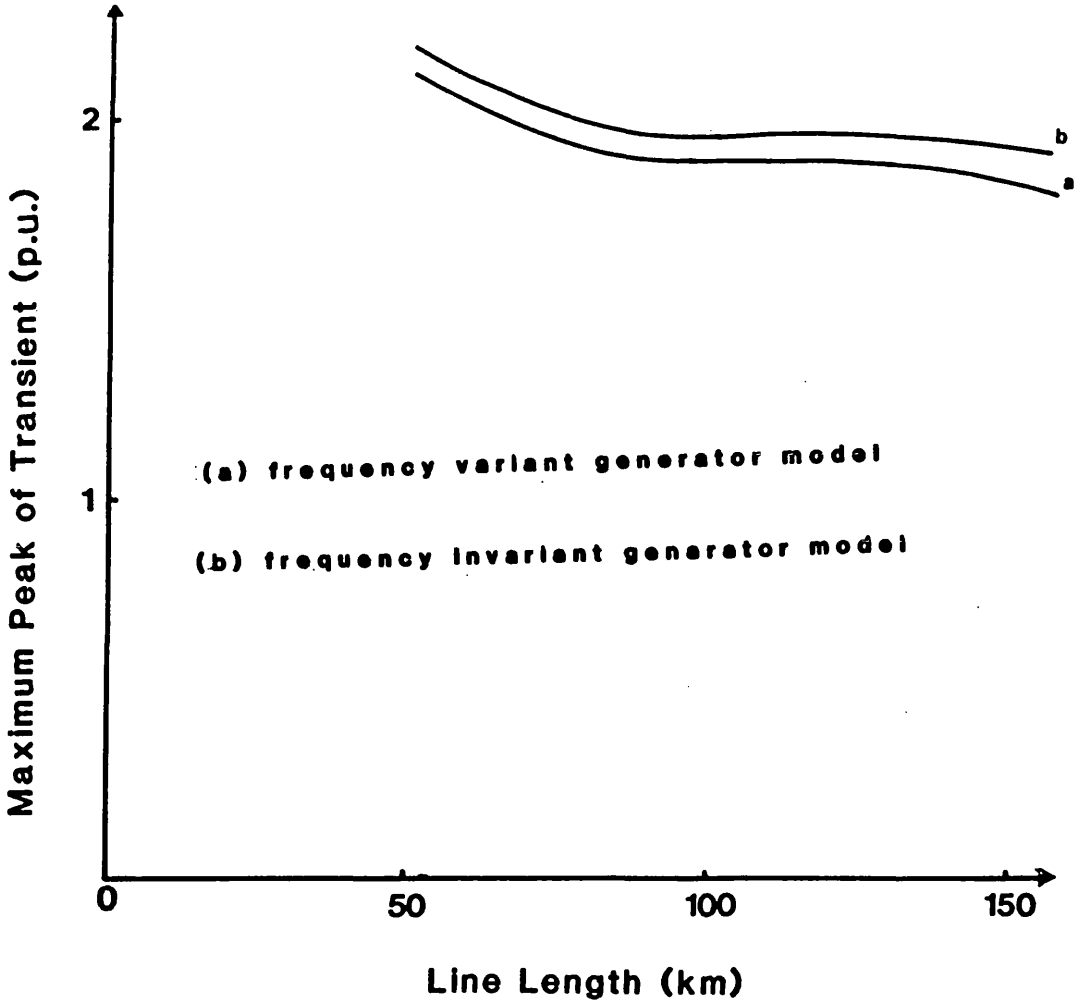

Fig. 7.28 Effect of Line Length on Maximum Peak Transient Magnitude

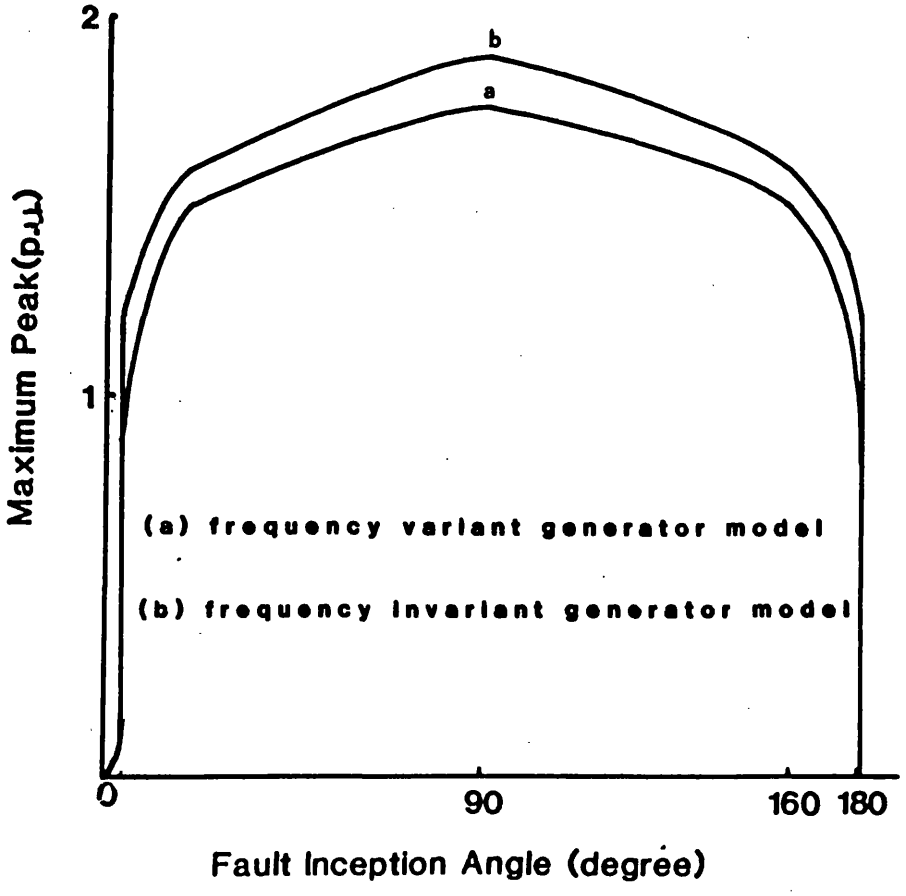

Fig. 7.29 Effect of Fault Inception Angle on Maximum Transient Magnitude

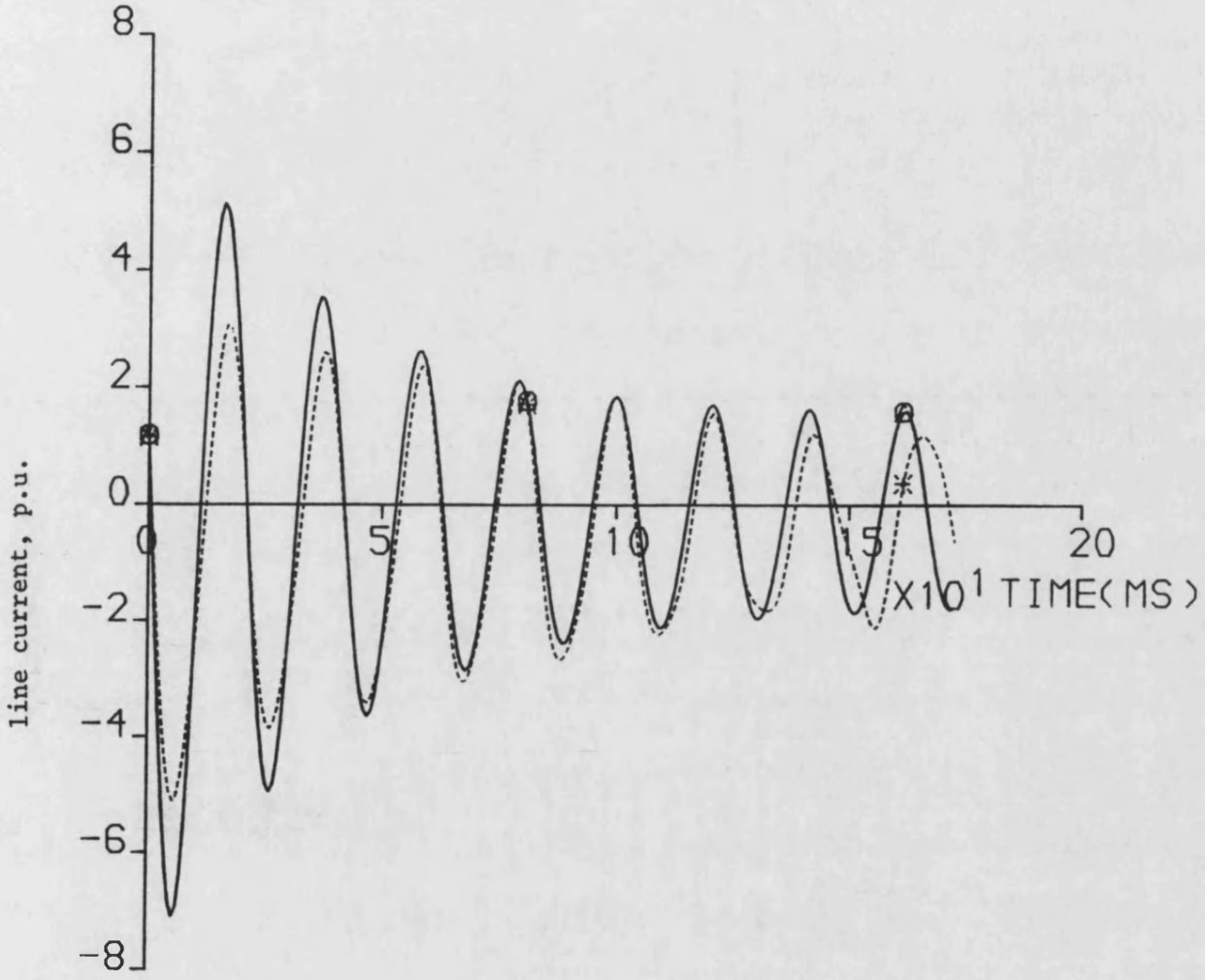

Figure 7.30 a-phase current waveforms on the machine terminals, for a three phase fault, with maximum prefault voltage condition for a-phase in a no load condition

——— frequency invariant parameters generator model
----- frequency variant parameters generator model

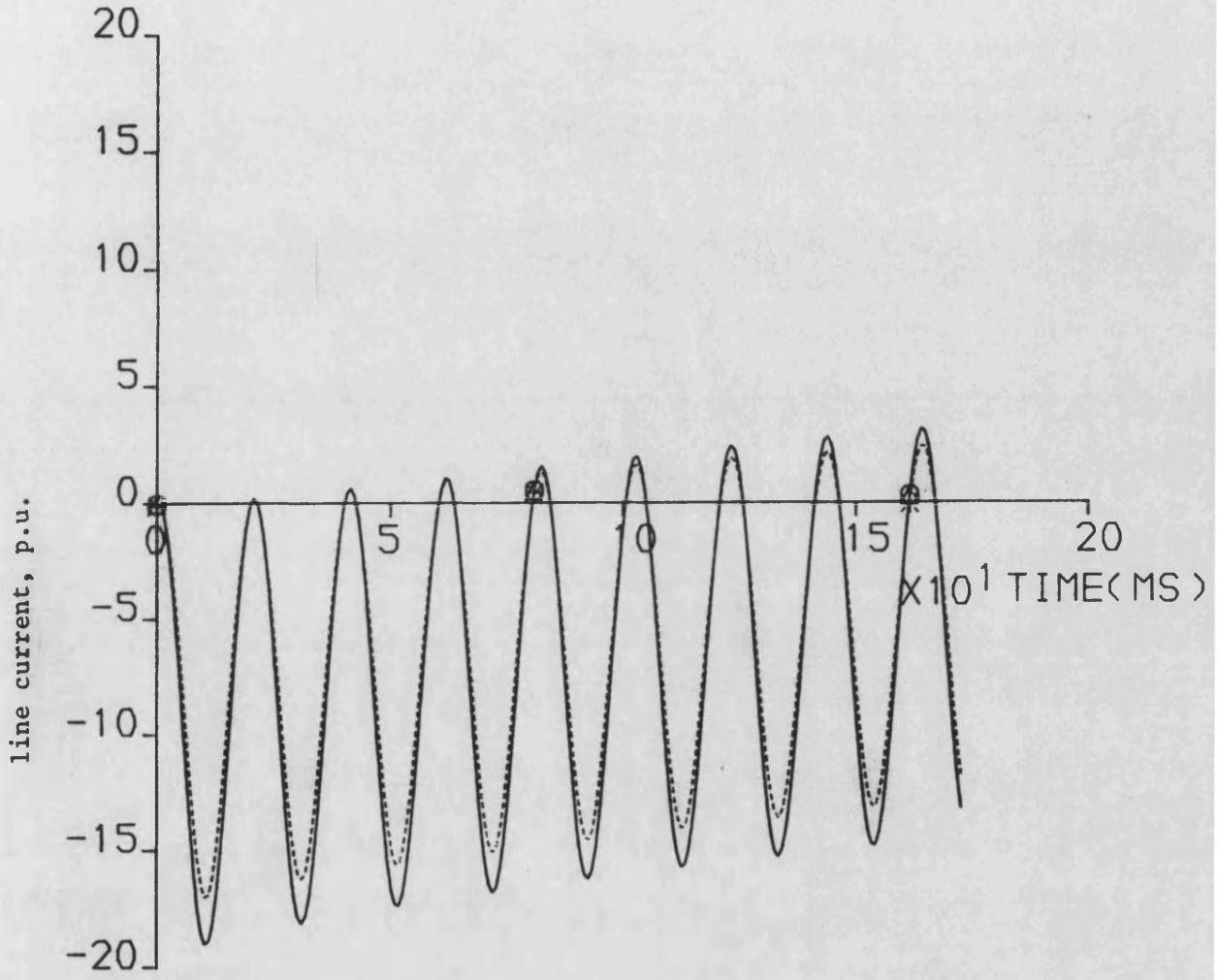

Figure 7.31 a-phase current waveforms, on the machine terminals, for a minimum prefault voltage a-phase to earth fault in a no-load condition

——— frequency invariant generator model
----- frequency variant generator model

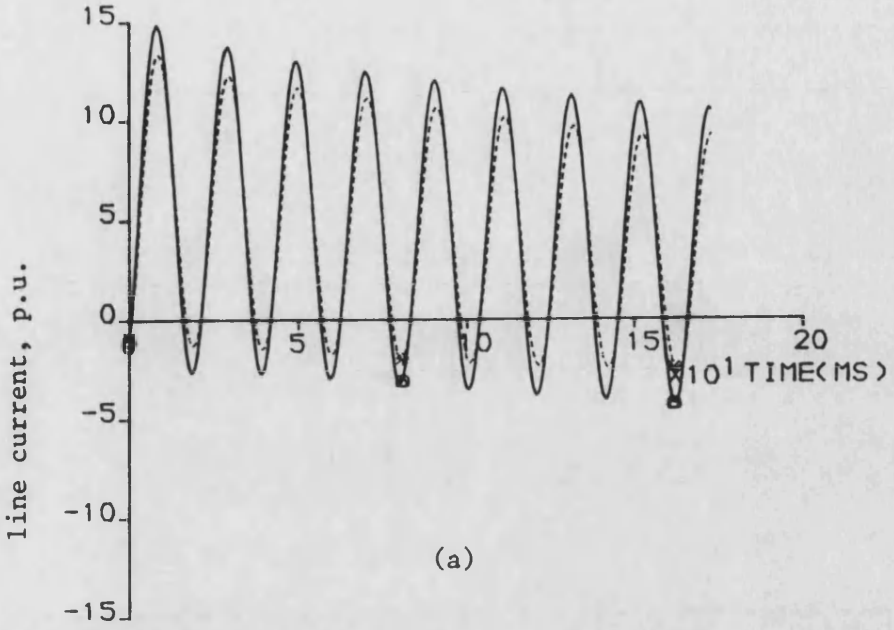

(a)

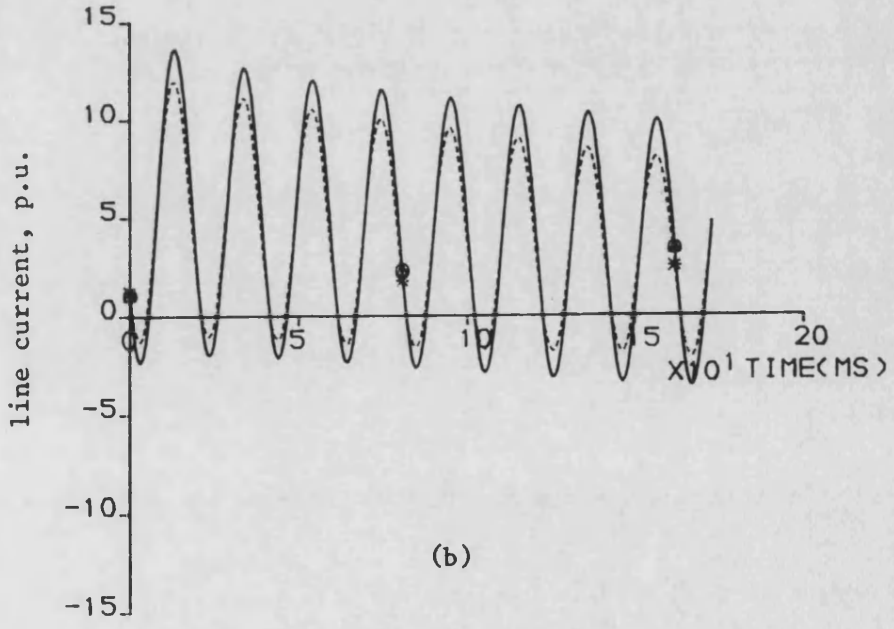

(b)

Figure 7.32 Current waveforms on the machine terminals for two-phase-to-earth fault (b-c-earth) with minimum prefault voltage between faulty phases, in a no load condition

(a) b-phase current
(b) c-phase current

——— frequency invariant parameters generator model
----- frequency variant parameters generator model

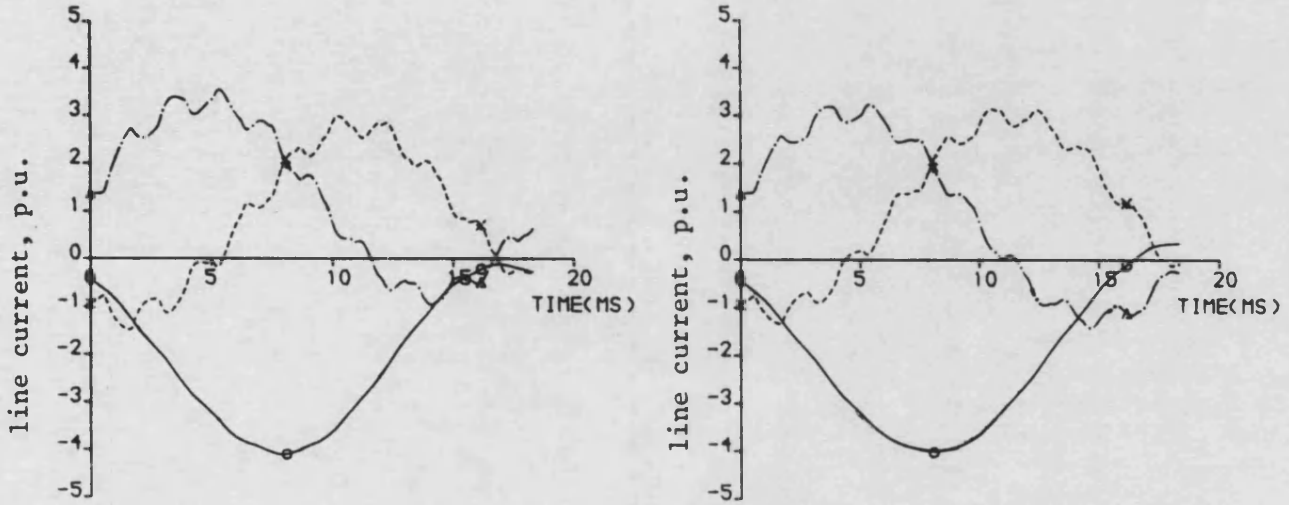

Figure 7.33 Current waveforms on the star-side of the transformer, for a three-phase fault

(a) for a complex source model
(b) for a simple source model

——— a-phase
—.— b-phase
----- c-phase

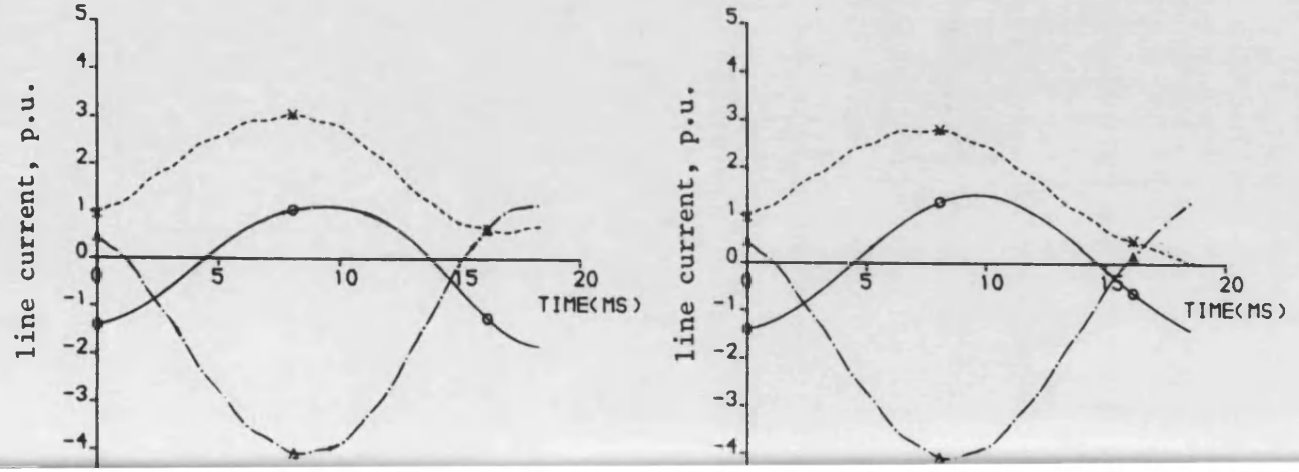

Figure 7.34 Current waveforms on the star-side of the transformer, for an interphase fault (b-c)

(a) for a complex source model
(b) for a simple source model

——— a-phase
—.— b-phase
----- c-phase

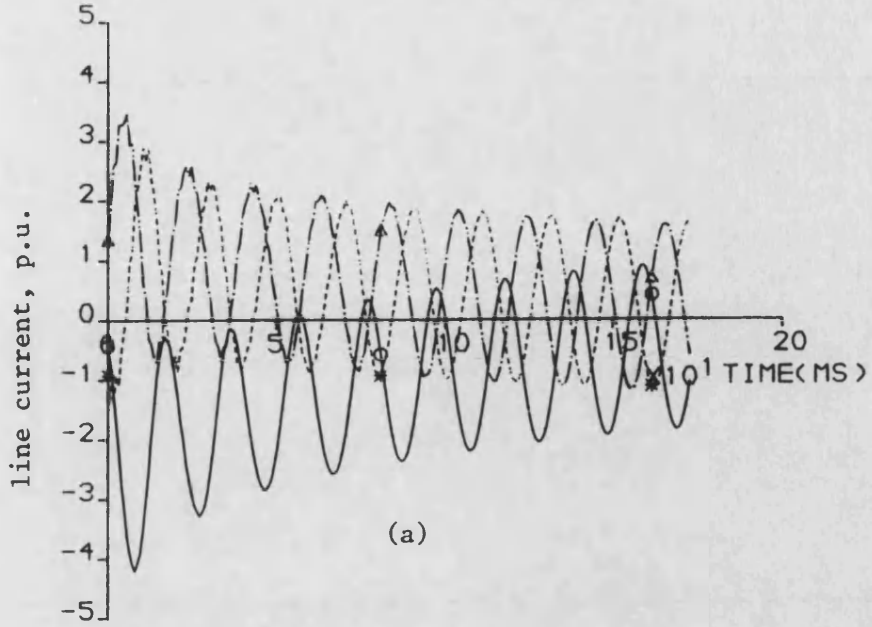

(a)

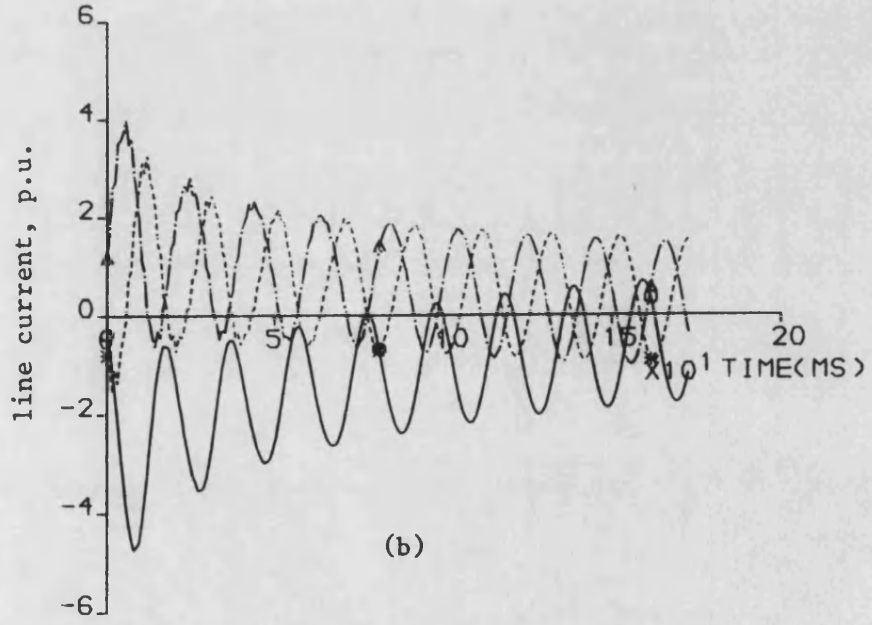

(b)

Figure 7.35 Current waveforms on the star-side of the transformer for a three phase fault with minimum prefault voltage for a-phase conditions

(a) for overexcited generator (lagging power factor)
(b) for underexcited generator (leading power factor)

——— a-phase
—.— b-phase
----- c-phase

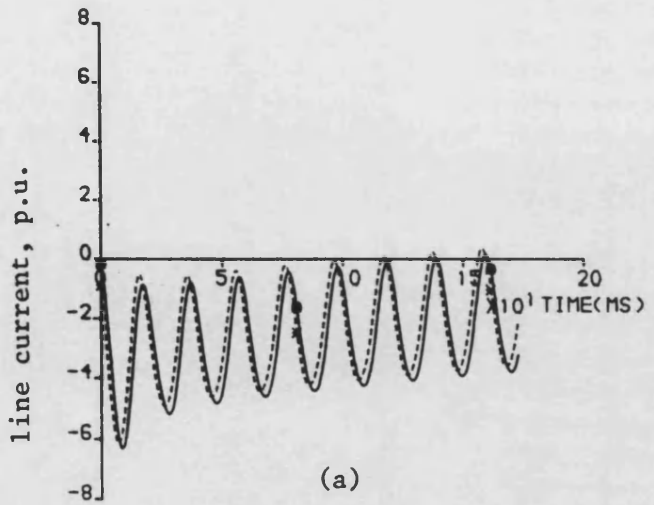

(a)

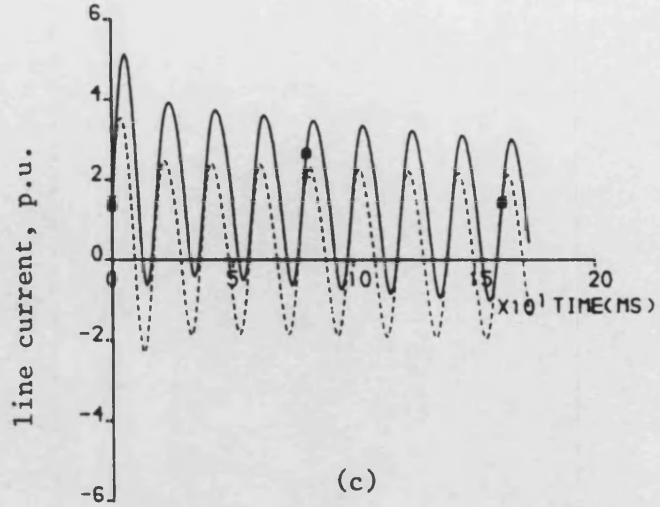

(c)

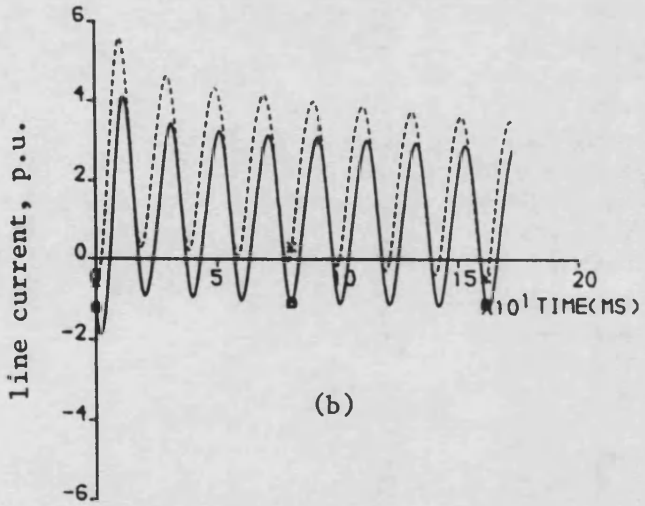

(b)

Figure 7.36 Current waveforms on the delta- and star-sides of transformer, for a three phase fault, in the case of underexcited 588MVA generator (20° leading power factor), fault is at relaying point and is to produce maximum offset for the a-phase current

(a) a-phase current on the delta- and star-sides
(b) b-phase current on the delta- and star-sides
(c) c-phase current on the delta- and star-sides

——— star-side
----- delta-side

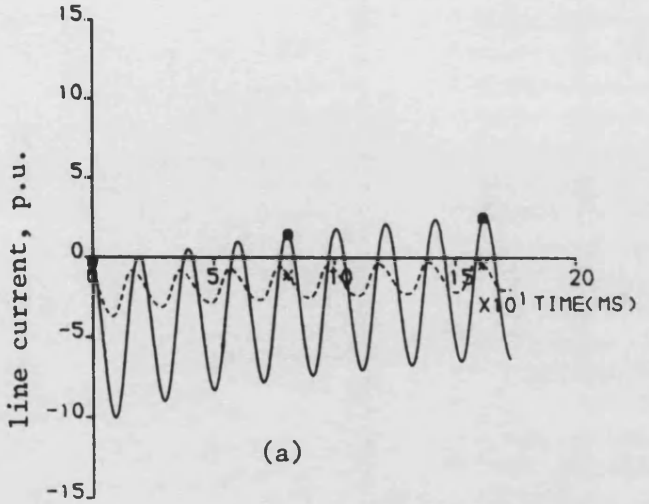

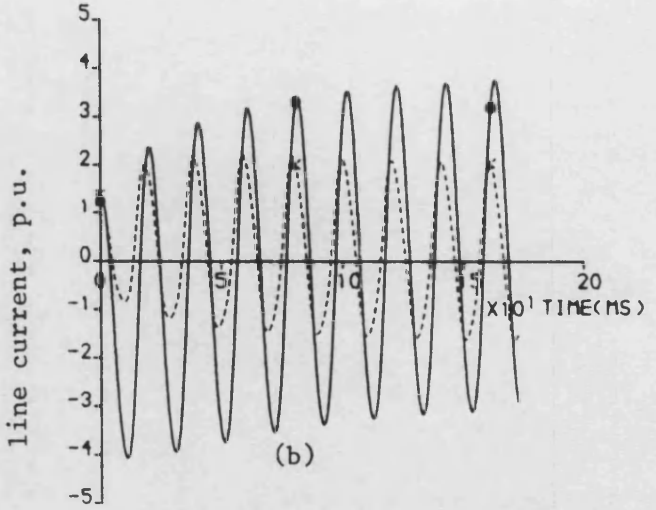

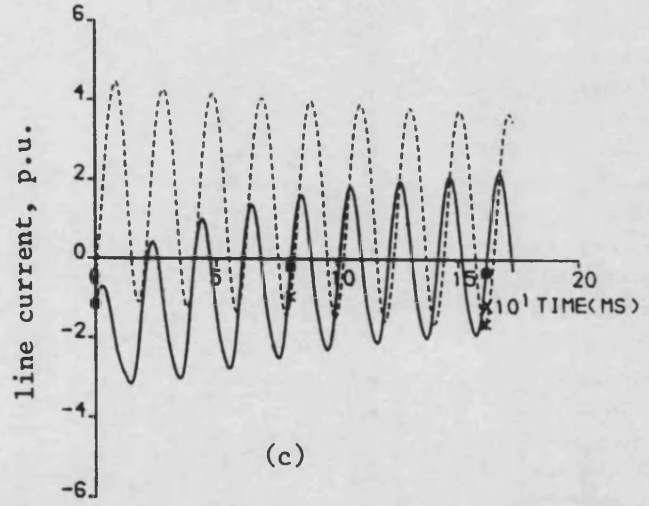

Figure 7.37 The same conditions as Figure 7.36 but for line to ground fault (a-earth)

(a) a-phase current on the delta- and star-sides
(b) b-phase current on the delta- and star-sides
(c) c-phase current on the delta- and star-sides

——— star-side
----- delta-side

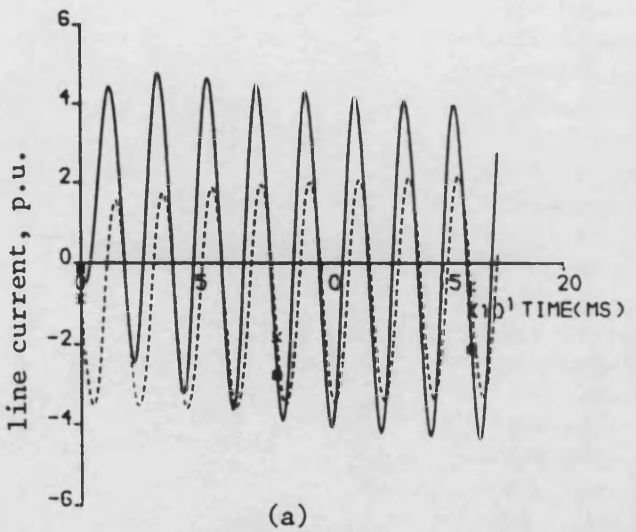

(a)

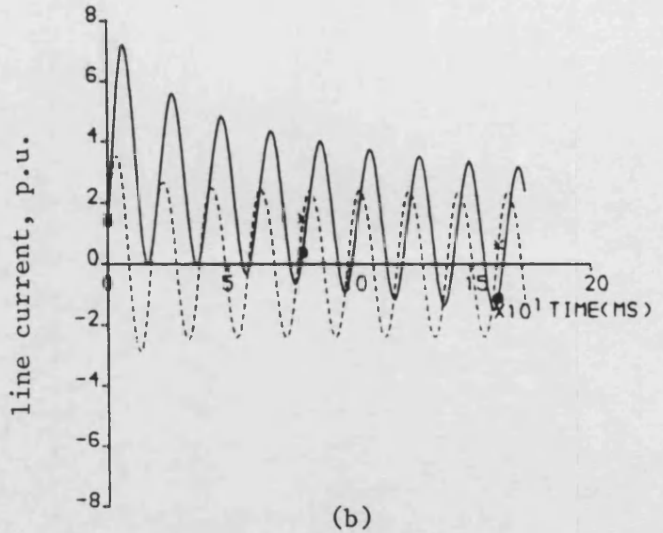

(b)

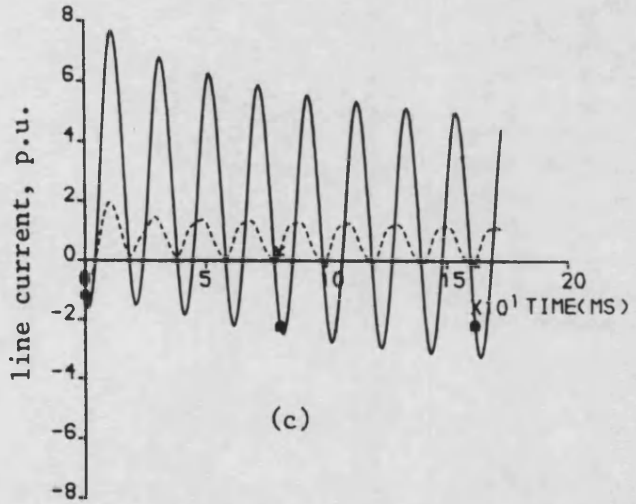

(c)

Figure 7.38 Current waveforms on the delta- and star-sides of transformer, for a two-phase-earth fault (b-c-earth), in the case of underexcited 588MVA generator (20° leading power factor), fault is at relaying point, is to produce maximum offset for the b-phase current

(a) a-phase current on the delta- and star-sides
(b) b-phase current on the delta- and star-sides
(c) c-phase current on the delta- and star-sides

——— star-side ----- delta-side

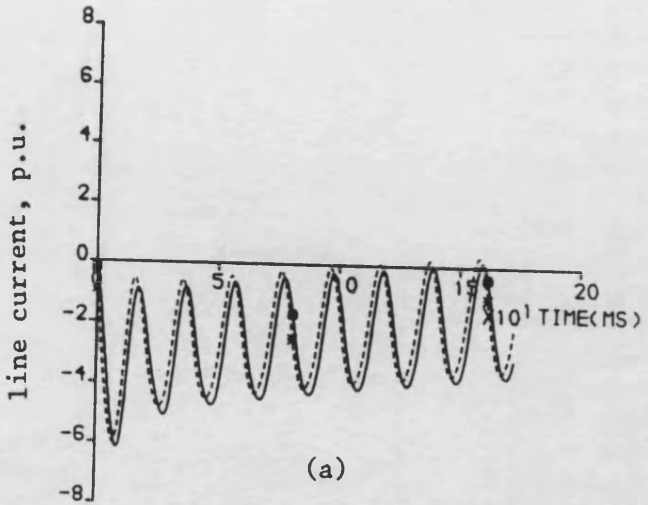

(a)

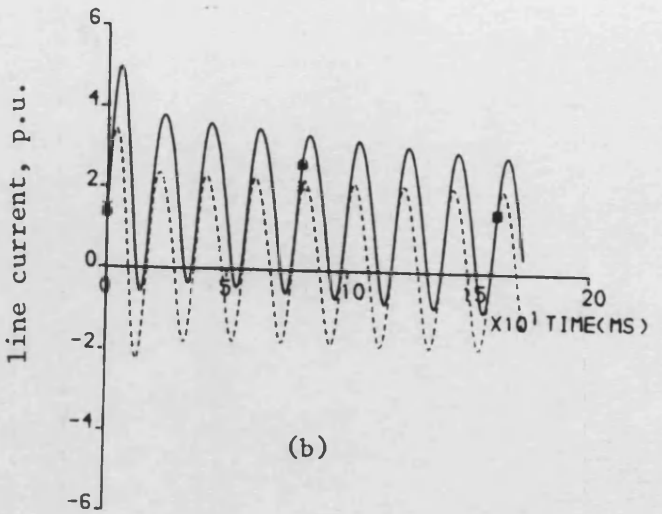

(b)

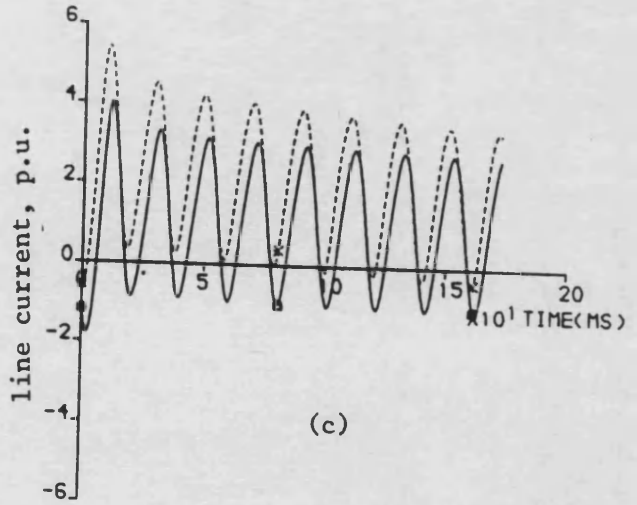

(c)

Figure 7.39 The same conditions as Figure 7.36 but for different power factor (11° leading power factor)

(a) a-phase current on delta- and star-sides
(b) b-phase current on delta- and star-sides
(c) c-phase current on delta- and star-sides

——— star-side
----- delta-side

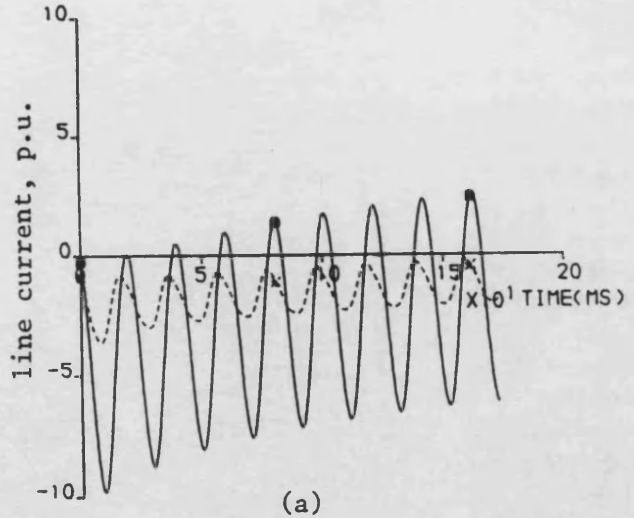

(a)

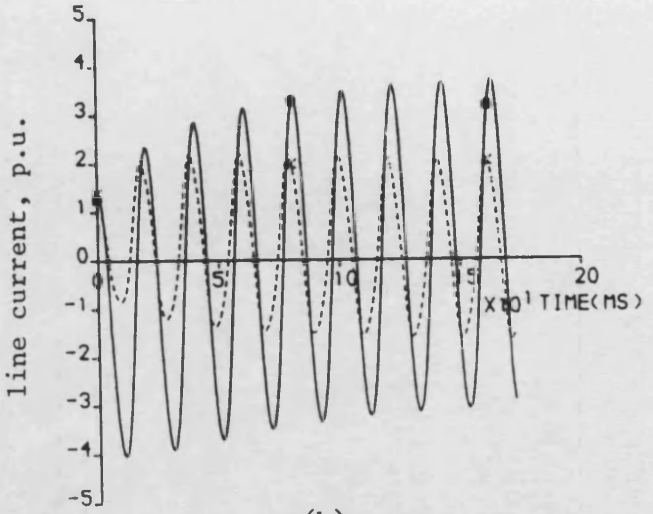

(b)

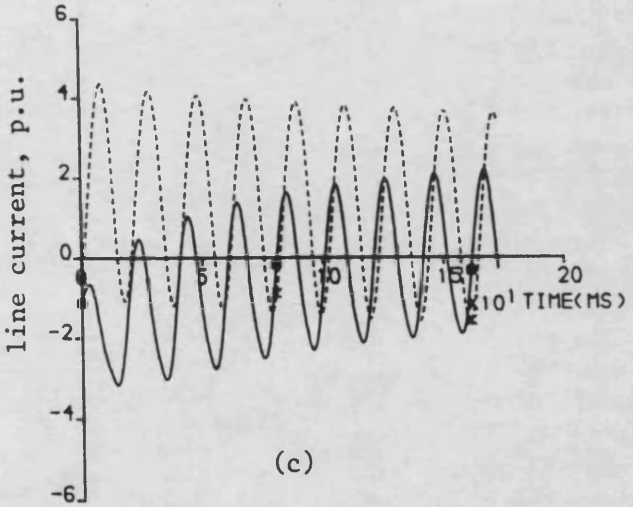

(c)

Figure 7.40 The same conditions as Figure 7.37, but for different power factor (11° leading power factor)

(a) a-phase current on the delta- and star-sides
(b) b-phase current on the delta- and star-sides
(c) c-phase current on the delta- and star-sides

——— star-side
----- delta-side

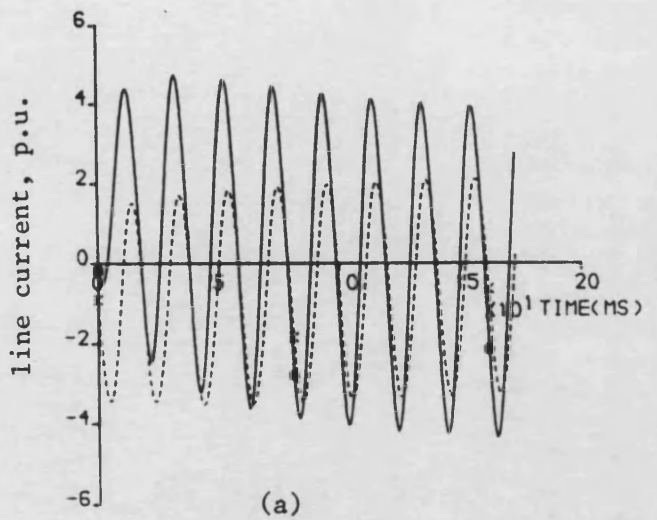

(a)

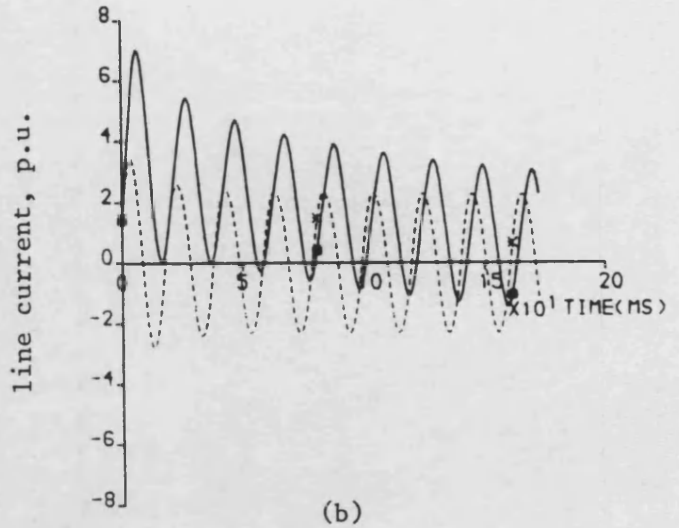

(b)

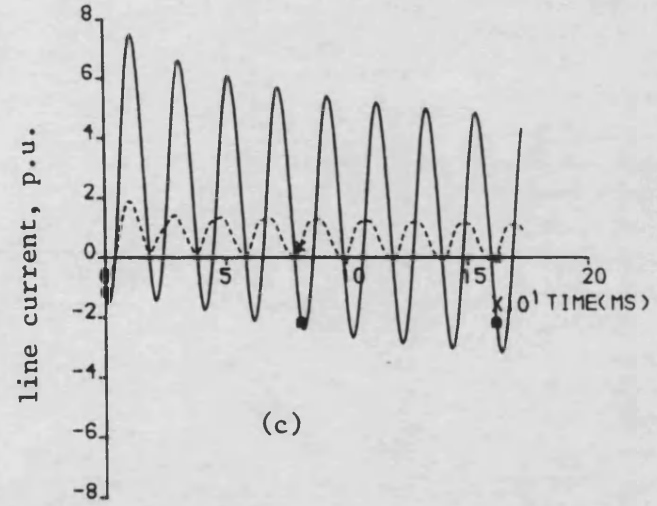

(c)

Figure 7.41 The same conditions as Figure 7.38, but for different power factor (11° leading power factor)

(a) a-phase current on the delta- and star-sides
(b) b-phase current on the delta- and star-sides
(c) c-phase current on the delta- and star-sides

——— star-side
----- delta-side

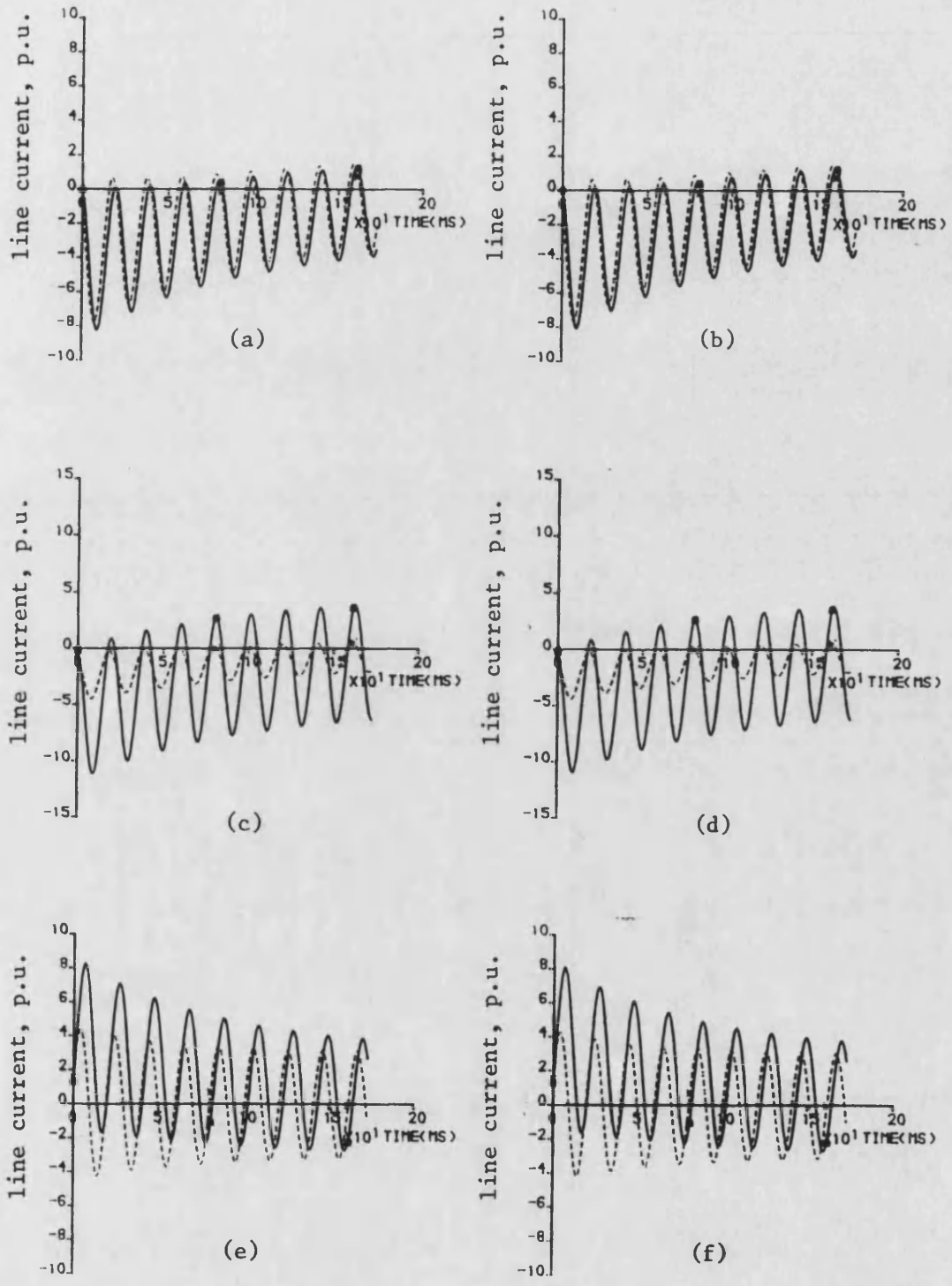

Figure 7.42 Current waveforms on the delta- and star-sides of transformer for different types of fault, in the case of 150MVA underexcited generator

(a) a-phase currents for 20° leading power factor (three-phase fault)
(b) a-phase currents for 11° leading power factor (three-phase fault)
(c) a-phase currents for 20° leading power factor (a-phase to earth fault)
(d) a-phase currents for 11° leading power factor (a-phase to earth fault)
(e) b-phase currents for 20° leading power factor (two-phase to earth fault)
(f) b-phase currents for 11° leading power factor (two-phase to earth fault)

——— star-side
----- delta-side

CHAPTER 8

MODELLING TECHNIQUE FOR SIMULATING FAULTS AND ASSOCIATED 3-PHASE AUTORECLOSURE SEQUENCES ON A DOUBLE-END FED SYSTEM

8.1 Introduction

So far, the mathematical analysis, the system modelling techniques and hence the fault studies outlined in the previous chapters have been only concerned with fault studies either at the infinite busbar of the system (as shown in Figure 7.1) or at the machine terminals under no load conditions. This is primarily so because with the introduction of the symmetrical component theory and associated frequency shift techniques necessary for machine modelling, it becomes somewhat easier, both from modelling and computational points of view, to consider only such fault conditions. In this respect, it should be mentioned that a consideration of only such faults more than adequately helps to illustrate all the important differences and salient points between the results obtained for different systems models (in particular the effect of source side representation in terms of approximations) under faults (as shown in chapter 7).

However, when considering the inaccuracies obtained in the results due to simplified and therefore approximate models of particular equipments in a system (especially at the system design and equipments development stages), it is also important to know to what degree the accuracy is affected under a whole variety of practically encountered different system and fault conditions.

In this chapter methods are outlined for simulating faults at different points on the transmission line for the system shown in Figure 8.1, which is essentially the

same as that shown in Figure 7.1, except that there is now a source at the other end, i.e. it is a double-end fed system. Some results are then presented to essentially illustrate the voltage and current waveforms at the sending end for some typical fault conditions.

Furthermore, computer techniques are also outlined for simulating conditions following the complete sequences associated with 3-phase autoreclosure for the system shown in Figure 8.1. In this respect it should be mentioned that when developing new equipments (such as protection relays) it is important to be able to test their performances throughout the full sequence of events and not just the initial measurement period prior to fault clearance. A brief study is presented to illustrate the effect of the discontinuities associated with the autoreclosure sequences on voltage and current waveforms.

8.2 Simulation of Faults at Different Points on the Transmission Line

Unlike the case for an infinite busbar fault simulation (the theory of which has been developed in chapter 5), when a fault occurs somewhere on a transmission line, the diagonal nature of the transmission line matrix [z].[y] (equation (5.20)) is lost because the fault is now fed from the two ends as opposed to the just one end in the former case. Under these conditions, whilst it is relatively easy to define the voltages, in particular the sound phase voltages, at the fault point when using phase co-ordinates[15], however, when employing frequency shifted symmetrical components, the problem of determining such voltages becomes relatively more difficult. A trial and error method, coupled with the use of transmission line eigenvalues and vectors, has thus to be employed.

8.2.1 Simulation of double end-fed feeders

A faulted transmission system essentially consists of a network of cascaded sections as shown in Figure 8.2. As mentioned previously in chapter 5, two-port transfer matrices are particularly useful in the solution of such problems. For example, the transfer matrix representing the line section up to the point of fault is given by equation (8.1), and this can be used in combination with the corresponding matrices representing the fault discontinuity and the line section between the fault and the receiving busbar, to yield a relationship between the currents and voltages at either end of the line. Equation (8.2) shows the multiplication process involved to yield the latter relationship.

With reference to equations (5.28) and (5.29) and knowing that the fault has been applied at any point on the transmission line, the relationships between the sending end and the fault point can be defined as:

$$\begin{bmatrix} v_{so}'(jw) \\ i_{so}'(jw) \end{bmatrix} = \begin{bmatrix} A_{\ell 10} & B_{\ell 10} \\ C_{\ell 10} & A_{\ell 10} \end{bmatrix} \cdot \begin{bmatrix} e_{fo}'(jw) \\ i_{fo}'(jw) \end{bmatrix} \qquad \text{(a)}$$

$$\begin{bmatrix} v_{s1}'[j(w+w_o)] \\ v_{s2}'[j(w-w_o)] \\ i_{s1}'[j(w+w_o)] \\ i_{s2}'[j(w-w_o)] \end{bmatrix} = \begin{bmatrix} A_{\ell 112} & B_{\ell 112} \\ & \\ & \\ C_{\ell 112} & A_{\ell 112} \end{bmatrix} \begin{bmatrix} e_{f1}'[j(w+w_o)] \\ e_{f2}'[j(w-w_o)] \\ i_{f1}'[j(w+w_o)] \\ i_{f2}'[j(w-w_o)] \end{bmatrix} \qquad \text{(b)}$$

. . (8.1)

where $A_{\ell 10}$, $B_{\ell 10}$, $C_{\ell 10}$ and $A_{\ell 112}$, $B_{\ell 112}$, $C_{\ell 112}$ which are the line parameters up to fault point, can be obtained by applying the theory as outlined in chapter 5. The general form of equations which relate the sending end to the receiving end are:

$$\begin{bmatrix} v_{so}'(jw) \\ i_{so}'(jw) \end{bmatrix} - \begin{bmatrix} A_{\ell 10} & B_{\ell 10} \\ C_{\ell 10} & A_{\ell 10} \end{bmatrix} \cdot \begin{bmatrix} A_{fo} & B_{fo} \\ C_{fo} & A_{fo} \end{bmatrix} \cdot \begin{bmatrix} A_{\ell 20} & B_{\ell 20} \\ C_{\ell 20} & A_{\ell 20} \end{bmatrix} \cdot \begin{bmatrix} v_{ro}'(jw) \\ i_{ro}'(jw) \end{bmatrix} \quad \text{(a)}$$

$$\begin{bmatrix} v_{s1}'[j(w+w_o)] \\ v_{s2}'[j(w-w_o)] \\ i_{s1}'[j(w+w_o)] \\ i_{s2}'[j(w-w_o)] \end{bmatrix} - \begin{bmatrix} A_{\ell 112} & B_{\ell 112} \\ C_{\ell 112} & A_{\ell 112} \end{bmatrix} \cdot \begin{bmatrix} A_{f12} & B_{f12} \\ C_{f12} & A_{f12} \end{bmatrix} \cdot \begin{bmatrix} A_{\ell 212} & B_{\ell 212} \\ C_{\ell 212} & A_{\ell 212} \end{bmatrix} \cdot \begin{bmatrix} v_{r1}'[j(w+w_o)] \\ v_{r2}'[j(w-w_o)] \\ i_{r1}'[j(w+w_o)] \\ i_{r2}'[j(w-w_o)] \end{bmatrix} \quad \text{(b)}$$

. . (8.2)

Here again, the submatrices ($A_{\ell 212}$, $B_{\ell 212}$, $C_{\ell 212}$, $A_{\ell 20}$, $B_{\ell 20}$, $C_{\ell 20}$) which define the line between fault and receiving end can be easily defined. The matrix defining the fault discontinuity is formulated according to the type of fault simulated. Source side networks (as have been simulated in chapter 4) can be relatively easily incorporated into the system equations.

8.2.2 General system equations under fault conditions

With reference to Figure 8.3, and equations (8.1) and (8.2), if homogeneous line sections are assumed, two principal relationships (equations (8.3) and (8.4) emerge:

$$\begin{bmatrix} e_{ffo}'(jw) \\ -i_{fso}'(jw) \end{bmatrix} = \begin{bmatrix} A_{\ell 10} & B_{\ell 10} \\ C_{\ell 10} & A_{\ell 10} \end{bmatrix} \cdot \begin{bmatrix} v_{so}'(jw) \\ -i_{so}'(jw) \end{bmatrix} \qquad \text{(a)}$$

$$\begin{bmatrix} e_{ff_1}'[j(w+w_o)] \\ e_{ff_2}'[j(w-w_o)] \\ -i_{fs_1}'[j(w+w_o)] \\ -i_{fs_2}'[j(w-w_o)] \end{bmatrix} \begin{bmatrix} A_{\ell 112} & B_{\ell 112} \\ & \\ & \\ C_{\ell 112} & A_{\ell 112} \end{bmatrix} \begin{bmatrix} v_{s_1}'[j(w+w_o)] \\ v_{s_2}'[j(w-w_o)] \\ -i_{s_1}'[j(w+w_o)] \\ -i_{s_2}'[j(w-w_o)] \end{bmatrix} \qquad \text{(b)}$$

. . (8.3)

$$\begin{bmatrix} e_{ffo}'(jw) \\ i_{fro}'(jw) \end{bmatrix} = \begin{bmatrix} A_{\ell 20} & B_{\ell 20} \\ C_{\ell 20} & A_{\ell 20} \end{bmatrix} \cdot \begin{bmatrix} v_{ro}'(jw) \\ i_{ro}'(jw) \end{bmatrix} \qquad \text{(a)}$$

$$\begin{bmatrix} e_{ff_1}'[j(w+w_o)] \\ e_{ff_2}'[j(w-w_o)] \\ i_{fr_1}'[j(w+w_o)] \\ i_{fr_2}'[j(w-w_o)] \end{bmatrix} \begin{bmatrix} A_{\ell 212} & B_{\ell 212} \\ & \\ & \\ C_{\ell 212} & A_{\ell 212} \end{bmatrix} \begin{bmatrix} v_{r_1}'[j(w+w_o)] \\ v_{r_2}'[j(w-w_o)] \\ i_{r_1}'[j(w+w_o)] \\ i_{r_2}'[j(w-w_o)] \end{bmatrix} \qquad \text{(b)}$$

. . (8.4)

With reference to equation (5.18a) and knowing that the voltages and currents at each end are related to the source impedance, we then have:

$$v_{so}'(jw) = -(z_{sso}).i_{so}'(jw) \qquad \text{(a)}$$

$$\begin{bmatrix} v_{s_1}'[j(w+w_o)] \\ v_{s_2}'[j(w-w_o)] \end{bmatrix} = -[z_{ss}]_{12} \begin{bmatrix} i_{s_1}'[j(w+w_o)] \\ i_{s_2}'[j(w-w_o)] \end{bmatrix} \qquad \text{(b)}$$

. . (8.5)

and likewise at the receiving end we have:

$$v_{ro}'(jw) = (z_{sro}).i_{ro}'(jw) \qquad \text{(a)}$$

$$\begin{bmatrix} v_{r_1}'[j(w+w_o)] \\ v_{r_2}'[j(w-w_o)] \end{bmatrix} = [z_{sr}]_{12} \begin{bmatrix} i_{r_1}'[j(w+w_o)] \\ i_{r_2}'[j(w-w_o)] \end{bmatrix} \qquad \text{(b)}$$

. . (8.6)

As can be seen in Appendix A5, by substituting equation (8.6) into equation (8.4) and equation (8.5) into equation (8.3) gives:

$$i_{fro}'(jw) = \underset{\text{<----------}}{\left[\left[C_{\ell 20}(z_{sro})+A_{\ell 20}\right]\right.} \underset{\text{----------}u_{22}\text{----------}>}{\left.\left[\left[A_{\ell 20}(z_{sro})+B_{\ell 20}\right]\right]^{-1}\right.} e_{ffo}'(jw)$$

$$i_{fso}'(jw) = -\underset{\text{<----------}}{\left[\left[C_{\ell 10}(z_{sso})+A_{\ell 10}\right]\right.} \underset{\text{----------}u_{11}\text{----------}>}{\left.\left[\left[A_{\ell 10}(z_{sso})+B_{\ell 10}\right]\right]^{-1}\right.} e_{ffo}'(jw)$$

The fault point sequence components with regard to directions of currents shown in Figure 8.3 are as follows:

$$i_{fo}'(jw) = i_{fso}'(jw) - i_{fro}'(jw) = -(u_{11} + u_{22}).e_{ffo}'(jw) \quad \ldots (8.7)$$

and:

$$\begin{bmatrix} i_{fr_1}'[j(w+w_o)] \\ i_{fr_2}'[j(w-w_o)] \end{bmatrix} = \underset{\text{----------}v_{22}\text{----------}}{\left[\left[C_{\ell 212}(z_{sr})+A_{\ell 212}\right]\right.} \left.\left[\left[A_{\ell 212}(z_{sr})+B_{\ell 212}\right]\right]^{-1}\right. \begin{bmatrix} e_{ff_1}'[j(w+w_o)] \\ e_{ff_2}'[j(w-w_o)] \end{bmatrix} \quad (a)$$

$$\begin{bmatrix} i_{fs_1}'[j(w+w_o)] \\ i_{fs_2}'[j(w-w_o)] \end{bmatrix} = -\underset{\text{----------}v_{11}\text{----------}}{\left[\left[C_{\ell 112}(z_{ss})-A_{\ell 112}\right]\right.} \left.\left[\left[A_{\ell 112}(z_{ss})-B_{\ell 112}\right]\right]^{-1}\right. \begin{bmatrix} e_{ff_1}'[j(w+w_o)] \\ e_{ff_2}'[j(w-w_o)] \end{bmatrix} \quad (b)$$

Now defining:

$$i_{f_1}' = i_{fs_1} - i_{fr_1} \quad , \quad i_{f_2}' = i_{fs_2} - i_{fr_2}$$

we then have:

$$\begin{bmatrix} i_{f_1}'[j(w+w_o)] \\ i_{f_2}'[j(w-w_o)] \end{bmatrix} = -(v_{11}+v_{22}) \cdot \begin{bmatrix} e_{ff_1}'[j(w+w_o)] \\ e_{ff_2}'[j(w-w_o)] \end{bmatrix} \qquad . . (8.8)$$

As can be seen in this case the currents and voltages at the sending end and receiving end are also related to the fault point variables and can be determined by using the same procedure as outlined in chapter 5.

8.2.3 Techniques for obtaining the superimposed voltages

When determining superimposed voltages for faults at any point on a transmission line, a symmetrical fault, i.e. a three-phase fault, poses no problems as such since, for such a fault, all the three phase voltages are known at the outset, an essential prerequisite in the application of the symmetrical component theory. However, when considering asymmetrical faults such as single phase to earth fault, problems arise because at the outset, the sound phase voltages are unknown. This problem can be solved by using a trial and error method. In this method, when calculating the prefault superimposed voltages at the fault point using symmetrical component theory, the sound phase voltages can be assumed to be known quantities to start with. The injection of voltage(s) at the fault point would therefore inevitably lead to an error, in that small current(s) would also flow through the fault path(s) of the healthy phase(s). An injection of these residual current(s) in an equal and opposite direction with an assumed value of current(s) in the actual faulted conductor(s), would lead to small voltages being developed at

the fault point for the now solidly grounded faulted phase(s) for phase to earth faults or between faulted phases for phase-phase faults. The idea is to attain a situation where, for example, for an a-phase to earth fault the a-phase voltage at the fault point and the two sound phases fault point superimposed currents are zero. This can be achieved by the process of repeatedly injecting voltages and currents alternatively at the fault point and it may take several injections before satisfactory results can be attained. An extensive series of studies have shown that four injections (two voltages and two currents) are more than adequate to produce a satisfactory result.

8.2.4 Evaluation of fault responses for the double end fed feeder

8.2.4.1 Verification of fault responses for the double end fed feeder

When developing new modelling techniques, it is vitally important to be able to verify the validity of the new methods developed. Figure 8.4 shows the voltage and current waveforms at the sending end when a fault occurs close to the receiving end of the system shown in Figure 8.1, the source at the receiving end being considered to be very large ($\simeq$ infinite) in this instance. The results attained are using the aforementioned trial and error methods. When comparing these results with those attained for an identical infinite busbar fault on the system shown in Figure 7.1 (the modelling techniques in this instance being those outlined in chapter 5) Figure 8.5 clearly shows that the waveforms in the two cases are identical. This study thus confirms the accuracy of the new technique developed.

8.2.4.2 Effect of prefault load

Figures 8.6 and 8.7 show a comparison of the waveforms when there is prefault loading ($\angle V_S/V_R = 20^0$), on the line. First of all comparing the voltages

(Figures 8.6b and 8.7b), it can be seen that these are not significantly affected by the load. This is so because for the short line considered, prefault voltage at any point on the line is almost independent of the circuit loading, as therefore is the magnitude of the voltage collapse which initates the travelling-wave pattern. However, comparing Figure 8.6a with Figure 8.7a, it can be seen that the current waveforms are significantly different in the two cases, especially the sound phase currents whose magnitudes become comparable to the faulted phase current (Figure 8.6a).

When comparing the waveforms at the receiving end for the same power transfer, i.e. exporting from sending end to receiving end, similar observation as at the sending end can be made and these are shown in Figures 8.8 and 8.9. However, as expected, the waveforms, in particular the voltage waveforms at the receiving end, are slightly more distorted than the corresponding sending end waveforms, this being so because the fault is closer to the receiving end (Figures 8.7b and 8.8b).

8.2.4.3 Effect of fault position

As already mentioned in chapter 7, when the fault position becomes more distant from the observation point, the frequency of the superimposed components decreases due to essentially the transit time between the source discontinuities and fault point increasing. This phenomena can be seen by comparing Figure 8.6b with the Figure 8.5b, the former being for a fault which occurs at x = 100km. Figure 8.6a shows the corresponding current waveforms at the sending end and, as can be seen, although the magnitude of the currents is larger (due to a reduction in impedance) than the corresponding current magnitudes for a remote end fault, however, the transients on the current waveforms are more or less unaffected.

8.2.4.4 Effect of source configuration at receiving end

The source side representation of the receiving end has little effect on the waveforms at the sending end. Figures 8.10–8.13 clearly show that factors such as the accuracy of the receiving end source representation or the capacity has insignificant effect on both the sending voltage and current waveforms.

8.3 Evaluation of System Responses Associated with Three-Phase Autoreclosures

A power system network, including e.h.v. transmission lines may be subjected to different faults of which the majority are transient in nature. An autoreclosure sequence which involves opening and reclosing the faulted phase or phases to clear the fault in a relatively short time after fault can therefore be used to advantage. In practice, the main schemes employed are the single-pole and three-phase autoreclosure. Of these, the former is primarily used in long line applications employing shunt compensation and in systems in which stability problems can ensue following a fault, due to the weakness of the system. Three-phase autoreclosure schemes which are relatively cheaper to install are employed in systems comprising short lines and with large capacities, e.g. the British system.

In this section, methods are outlined for modelling the fault transient phenomena during the complete three-phase autoreclosure sequences following a fault on the system shown in Figure 8.1. This is followed by a limited study of the results obtained for the system following three-phase faults.

8.3.1 Simulation technique

The system shown in Figure 8.1 is simulated on a digital computer, the theory of symmetrical components developed previously being used for system

representation. In order to simplify the rather difficult problem of transient phenomena associated with three-phase autoreclosure schemes, the analysis is split into several distinct stages.

In the first part, a knowledge of the transient response due to the application of a fault on the line is obtained and the theory used for this part of the analysis is essentially that developed in section 8.2.

The faulted-phase currents at both the sending and receiving ends are then checked for zero crossing to determine the pole opening times. The subsequent parts of the response are then determined by a series of current and voltage injections at appropriate points in the circuit coupled with the principle of superposition. In the case of fault inception or breaker closure, the injection is specified in terms of a suddenly applied voltage equal and opposite to the sum of all previously computed superimpoed and steady state voltages at the points of discontinuity. Where breaker opening or fault break off is involved, the injection is conversely specified in terms of suddenly applied currents which are, likewise, equal and opposite to the sum of all previously determined superimposed and steady state currents at the point of discontinuity.

This can be best explained with reference to Figure 8.14 which shows the system model for a three-phase to earth fault. This shows the six total instantaneous phase currents i_{sa1}, i_{ra1}, etc., where suffix '$_1$' refers to the circuit change due to fault. For the next circuit change, the variations are referred to by the suffix '$_2$' (pole opening). Thus having determined the zero crossing of the first circuit breaker current, for example, the sending end a-phase breaker, the opening of the breaker is invoked by injecting a current i_{sa2} (Figure 8.15) which is zero up to the time of breaker opening but equal and opposite to 'i_{sa1}' thereafter.

Using equation A.6.5 (Appendix 6), the sending end, receiving end and the fault point quantities after first breaker opening are obtained and these are then transformed back into the time domain using the Fast Fourier Transform technique[15]. The five remaining breaker path currents are next checked for zero crossing to determine which pole opens next. The whole process as outlined above is then repeated to determine the total responses of the voltages and currents at the points of interest, in the time domain. The opening of the remaining poles is simulated in a similar manner. Having obtained the total time variation of the fault current, which is the sum of all the components that arise during each circuit change, it is now possible finally to inject an equal and opposite current to the latter, to break-off the fault (Figure 8.16).

In the case of breaker closure, it is assumed that the three sending end breakers close simultaneously followed by the simultaneous closure of the three receiving end breakers. Having determined the total time varying responses of the voltages across the sending-end breakers, these voltages should be injected into the opposite direction to simulate reclosing of sending-end breakers. The simultaneous reclosing of the receiving-end breakers can be simulated in a similar manner. Thus when the full sequence of events has been completed, the total time domain responses of the voltages and currents at the point of interest can be obtained. The whole sequence of events can be summarised as follows:

Time t (with respect to any arbitrary datum)	T_1	T_2	T_3	T_4
Event	Fault inception	Breaker interrupts	Fault break-off (or release)	Breaker reclosure

Table I Simple transient sequence

It should be mentioned that application of the three-phase autoreclosure sequences to system models based on symmetrical components is not as straightforward as for that based on phase co-ordinates[68]. The problems that arise are similar to those mentioned in previous sections when considering faults at different points on the line and the techniques to overcome them are therefore similar to those outlined before.

The mathematical analysis and the simulation developed for applying three-phase autoreclosure to a faulted short uncompensated line have been discussed in some detail in Appendix 6.

8.3.2 The system responses during complete autoreclosure sequences

A mid-point three-phase solid fault occurs at voltage maximum of the a-phase on the system shown in Figure 8.1, in which both the sending and receiving ends are represented by realistic source. In this study a circuit breaker opening time of typically two cycles has been allowed for and it is assumed that

the sending end breaker poles open first, followed by the receiving end breaker poles opening.

Figure 8.18 shows the effect of breakers opening on the current waveforms. First of all, considering the sending end waveforms, Figure 8.18a shows the three currents collapsing to zero on breaker poles opening. As expected, the magnitude of the fault path currents are quite significantly reduced (Figure 8.18b), because the fault path is now only fed from the receiving end. Figure 8.18c shows the current waveforms at the receiving end here again, the currents collapse to zero on receiving end pole opening. The fault path currents are now reduced to near zero (Figure 8.18d), the small ripple being due to the trapped charge in the circuit. However, this disappears on fault break-off, again as shown in Figure 8.18d.

Figure 8.19 shows some results for a typical transient fault sequence. With reference to Figures 8.19a and b, which show the line side voltages at the sending and receiving ends of the line on fault inception, distortion appears on all the three phases and is enhanced by breakers opening. The transients, however, gradually die out after fault break-off. Because of the nature of the fault which is a three-phase fault, there is no significant trapped charge and the voltages at line side during fault break-off and up to reclosing time are very small. As expected on breaker reclosure, some overvoltages result and these again can be seen from Figures 8.19a and b. The source side voltages at sending end are shown in Figure 8.19c. These are, of course, identical to the line-side values (Figure 8.19a) prior to the opening of the breakers at time T_2. However, on breaker opening, the source side voltages, as expected, return to near normal prefault steady state levels. Furthermore, as expected, again after reclosing the system at time T_4, the waveforms are the same as line side voltage waveforms (Figure 8.19a).

The behaviour of fault path voltage during the complete sequences is as shown in Figure 8.19d. As expected, the voltages collapse to near zero on fault inception. Furthermore, it can be seen that the voltage levels in all the three phases stay near zero. This is so by virtue of the fact that as this is a solid three phase fault, the residual current on breaker opening does not cause any significant voltages to develop across the fault path. Again, as expected, the voltages across the transient fault path, subsequently recover to near normal after reclosure of the breakers at two ends.

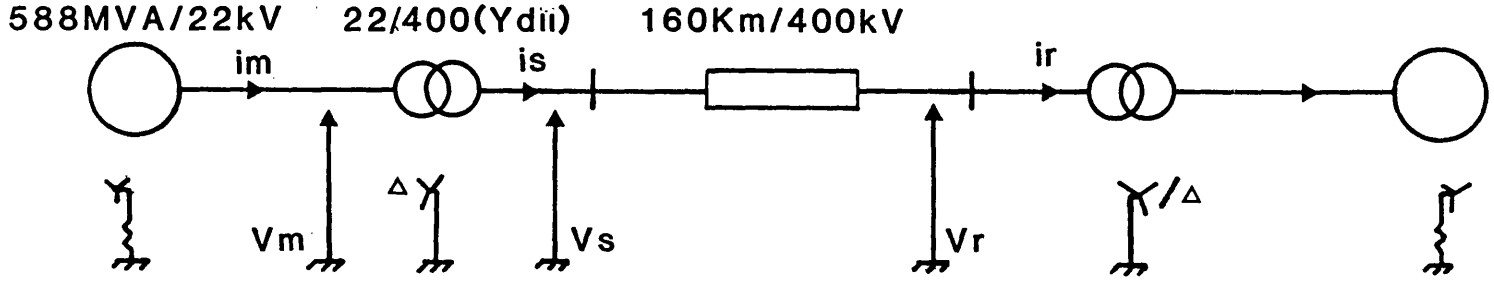

Fig. 8.1 Single Line Diagram of Configuration Studied

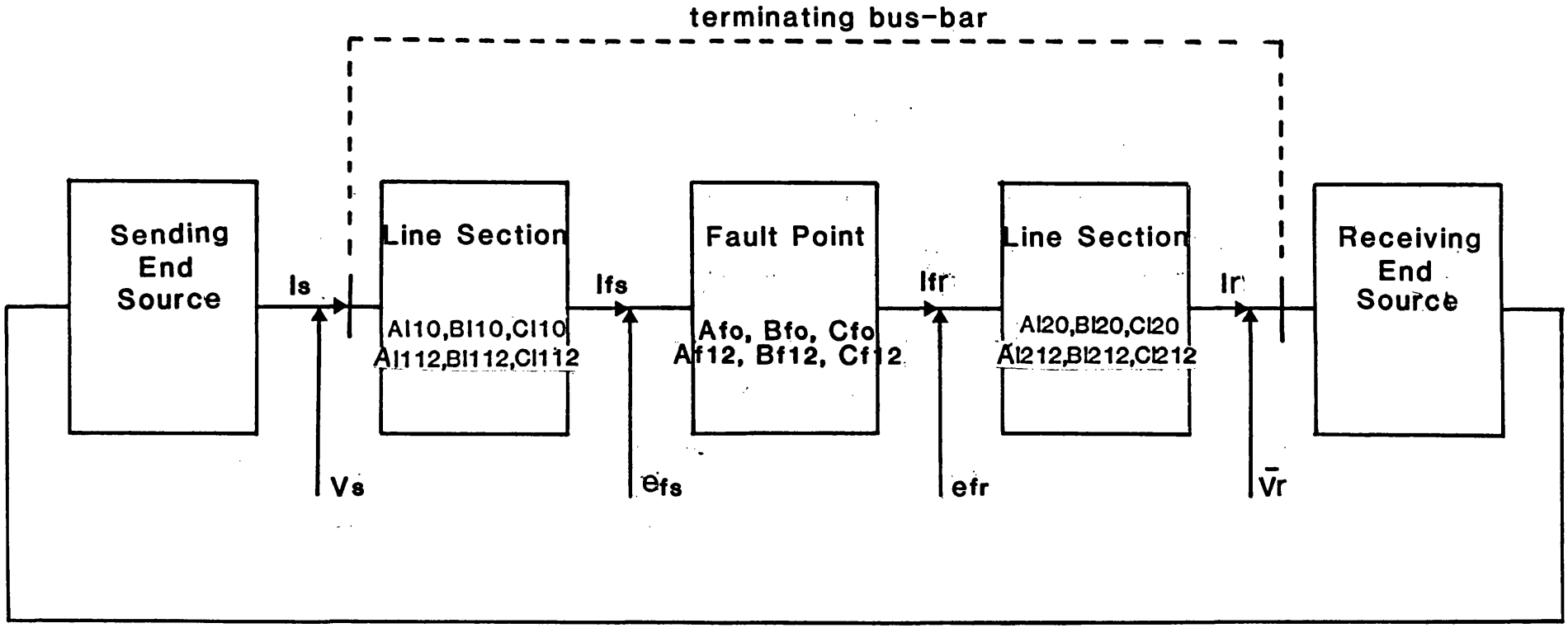

Fig. 8.2 Basic 2-ended Fault-transient Model

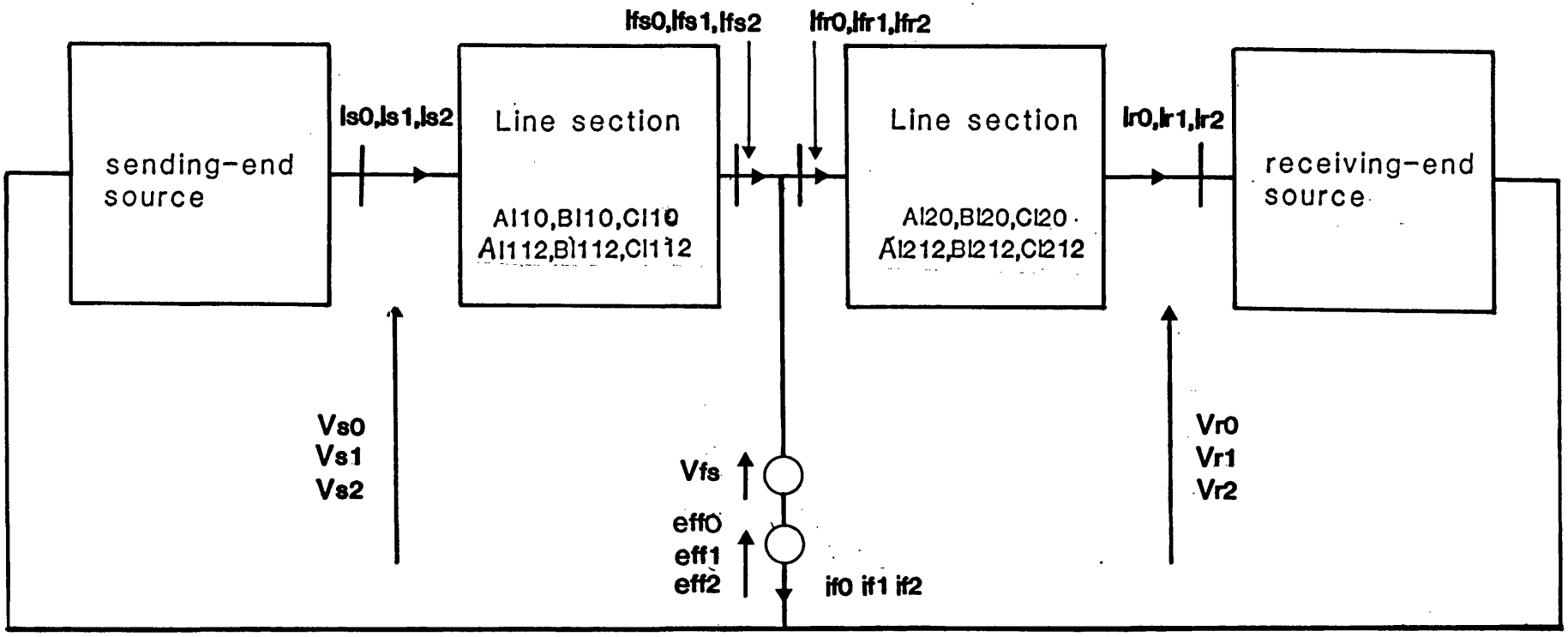

Fig. 8.3 Fault Transient Model Utilising Superimposed Voltage for Solid Faults

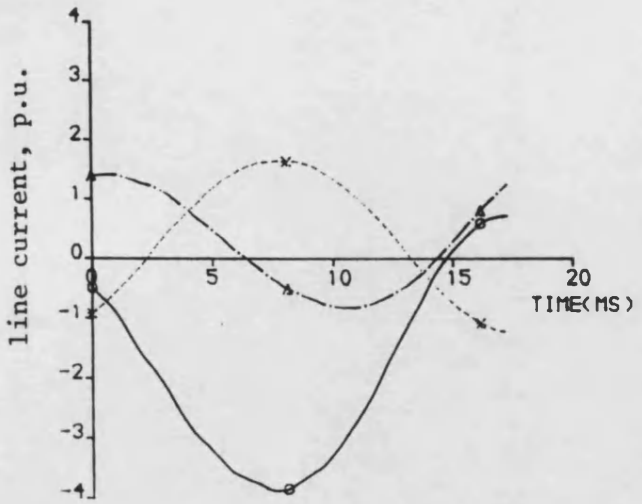

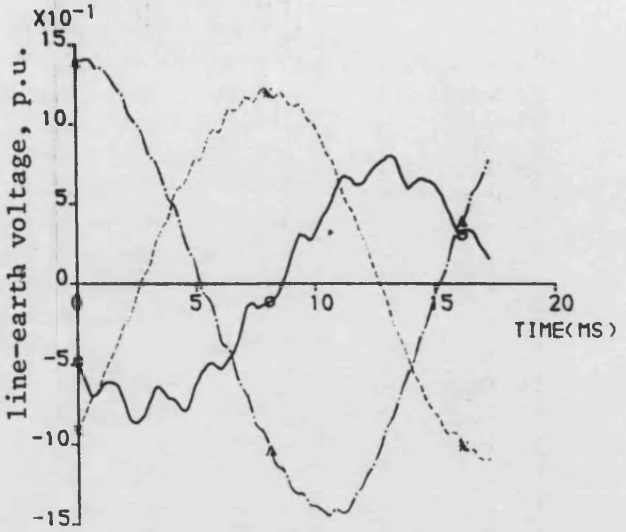

Figure 8.4 Waveforms on the star-side of the transformer, for a solid a-phase to earth fault, when the fault is near the receiving end for minimum prefault voltage in a double end fed system (X = 160Km)

——— a-phase
—.— b-phase
----- c-phase

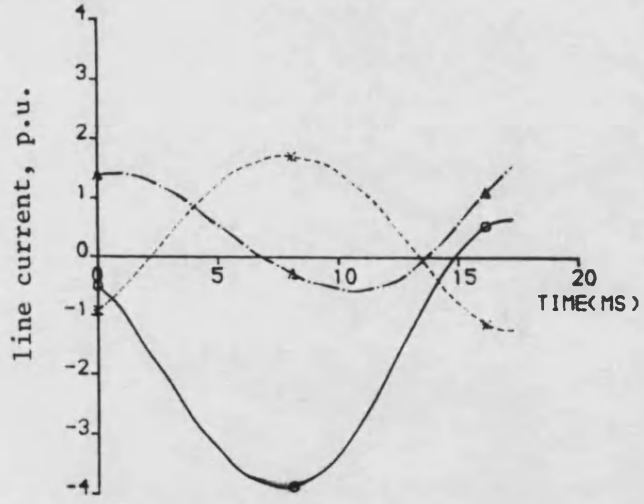

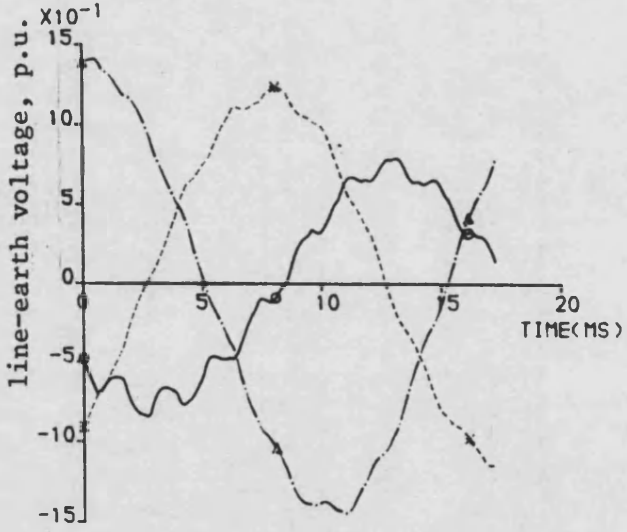

Figure 8.5 Waveforms on the star-side of the transformer, for a solid a-phase to earth fault, whenthe fault is at infinite busbar, for minimum prefault voltage (X = 160Km)

——— a-phase
—.— b-phase
----- c-phase

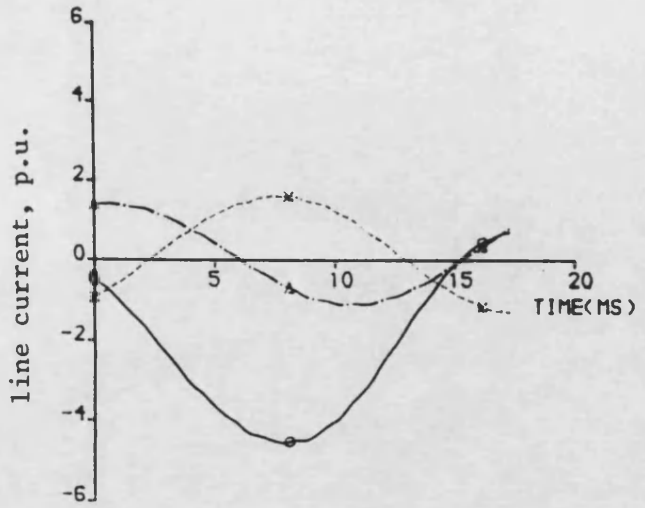

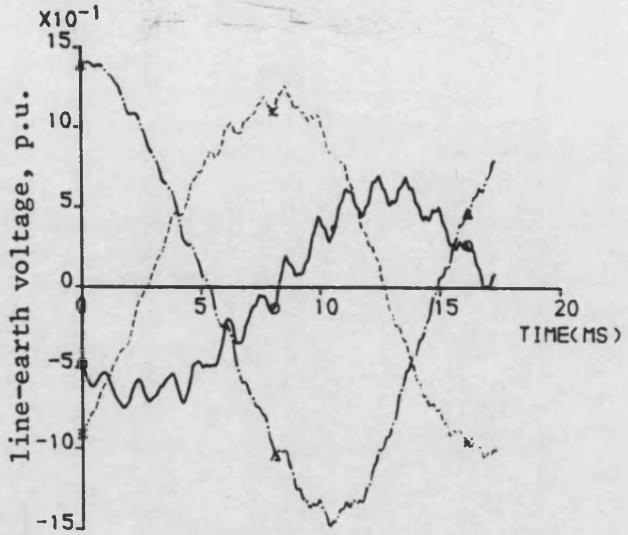

Figure 8.6 Waveforms on the star-side of the transformer, for a solid a-phase to earth fault, when the fault is at x = 100Km, for minimum prefault voltage and $V_s/V_r = \underline{/\ 20°}$

——— a-phase
—.— b-phase
----- c-phase

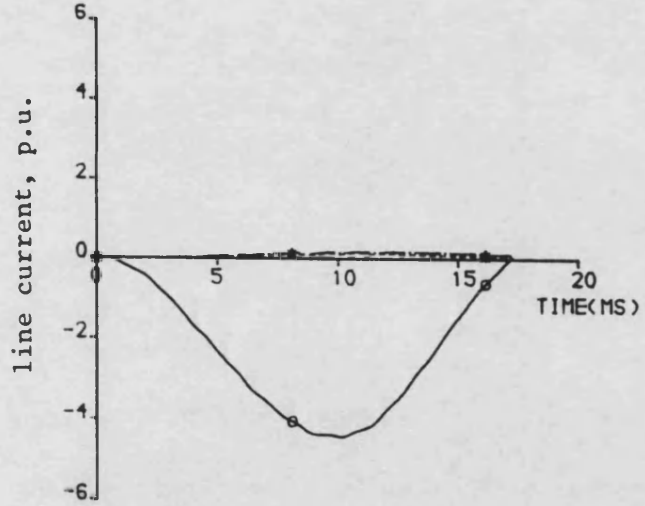

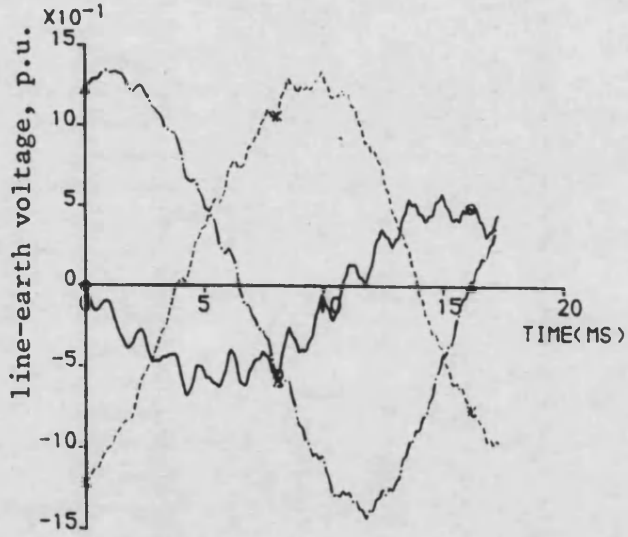

Figure 8.7 Waveforms on the star-side of the transformer, for a solid a-phase to earth fault when the fault is at x = 100Km, for minimum prefault voltage and $V_s/V_r = \underline{/\ 0.0}$

——— a-phase
—.— b-phase
----- c-phase

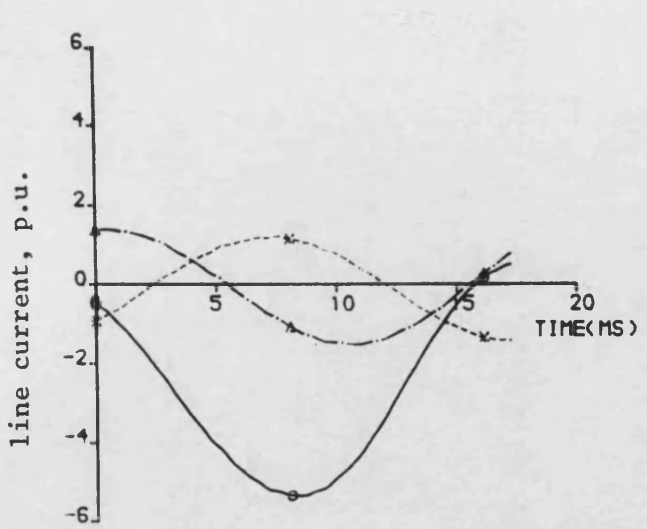

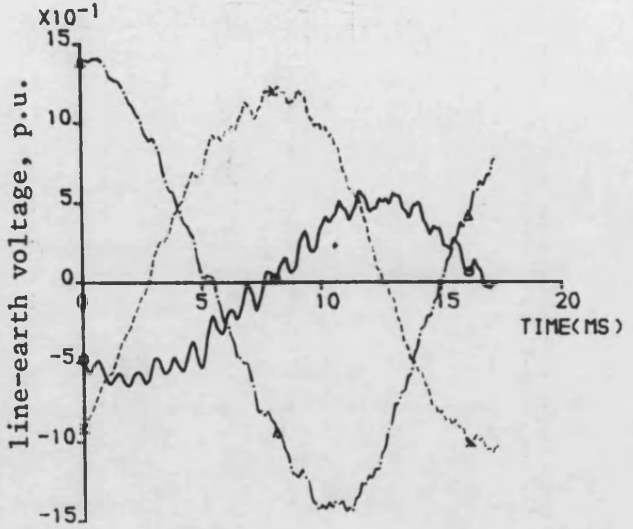

Figure 8.8 Waveforms on the receiving end of the line, for a solid a-phase to earth fault, when fault is at x = 100Km from sending end, for minimum prefault voltage, and V_s/V_r = $\underline{/\ 20°}$

——— a-phase
—.— b-phase
----- c-phase

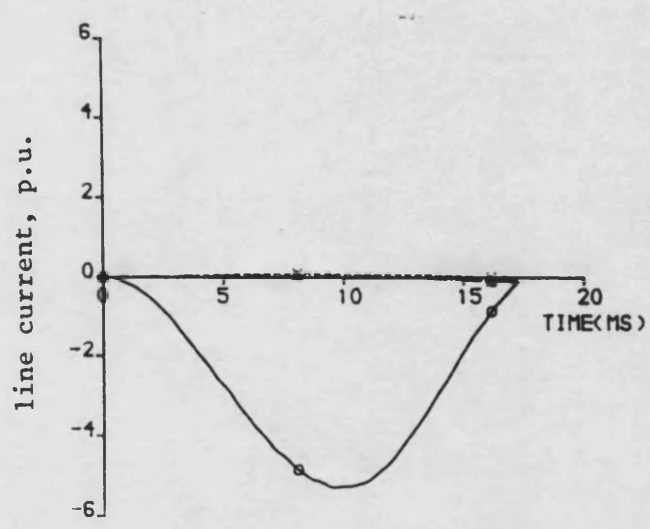

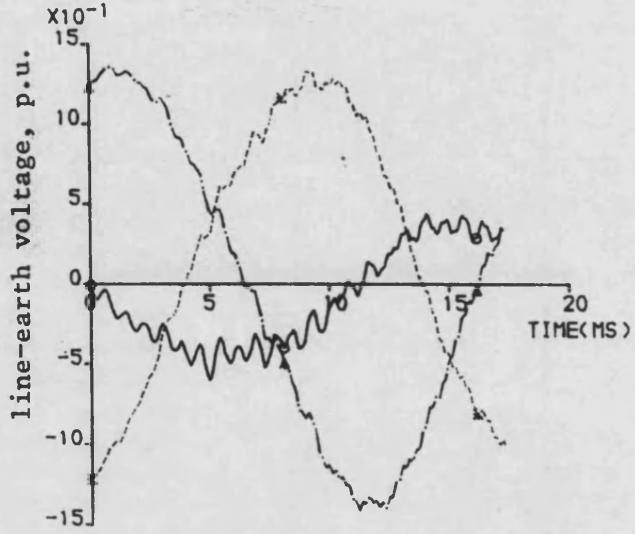

Figure 8.9 Waveforms on the receiving end of the line, for a solid a-phase to earth fault, when fault is at x = 100Km from sending end, for minimum prefault voltage, and V_s/V_r = $\underline{/\ 0.0°}$

——— a-phase
—.— b-phase
----- c-phase

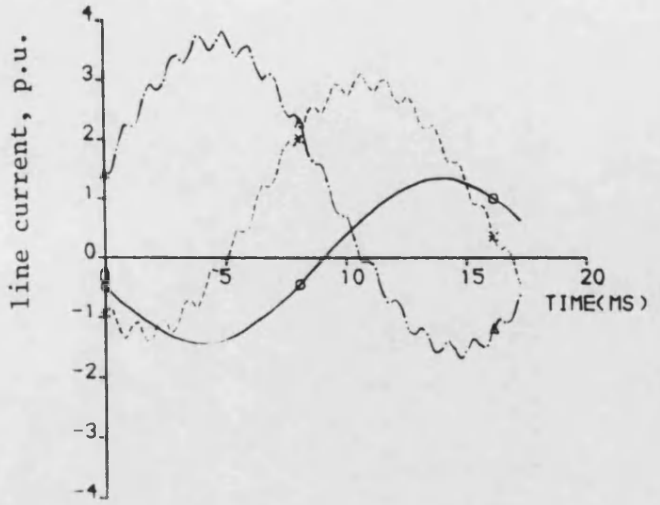

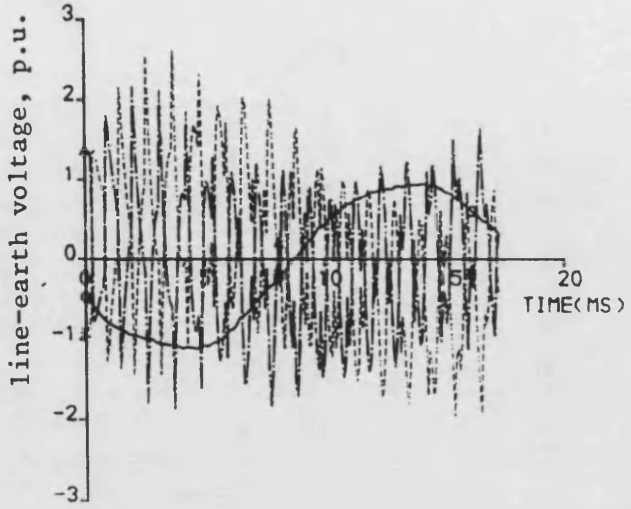

Figure 8.10 Waveforms on the star-side of the transformer, for a solid two-phase-to-earth fault (b-c-earth), fault is at mid point (x = 80Km) and the receiving end is included a realistic source model

——— a-phase
—.— b-phase
----- c-phase

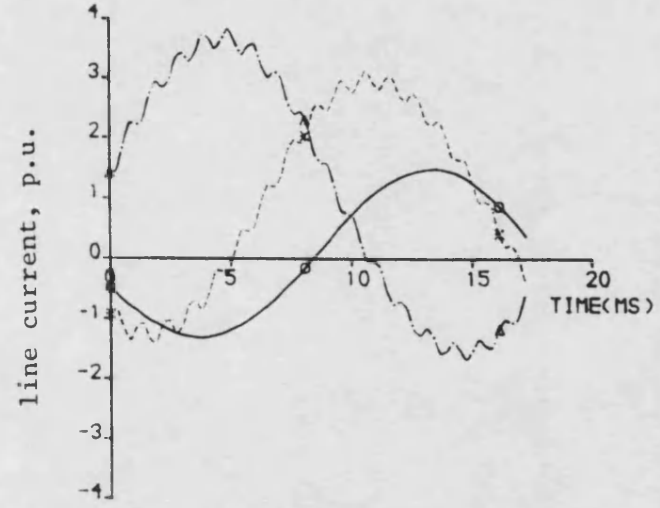

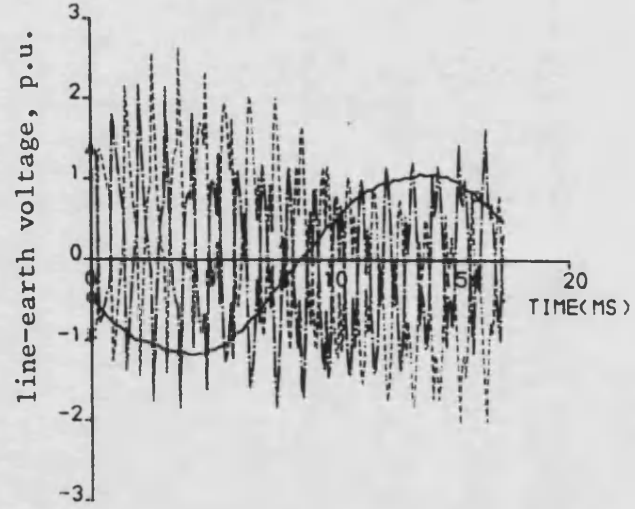

Figure 8.11 Waveforms on the star-side of the transformer, for a solid two-phase-to-earth fault (b-c-earth), fault is at mid point (x = 80Km) and the receiving end is included a simple source model

——— a-phase
—.— b-phase
----- c-phase

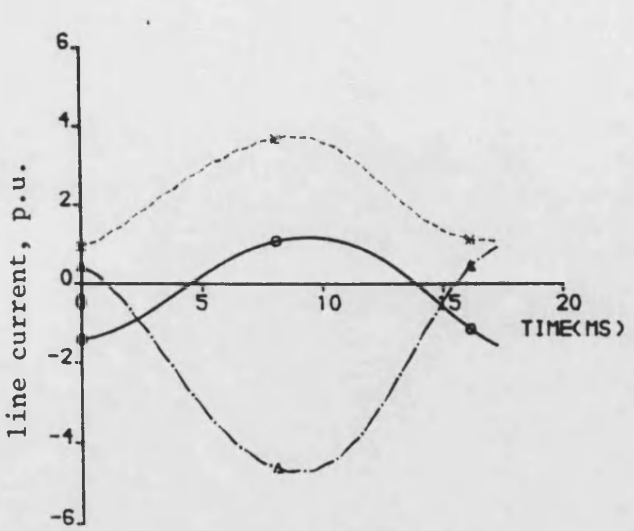

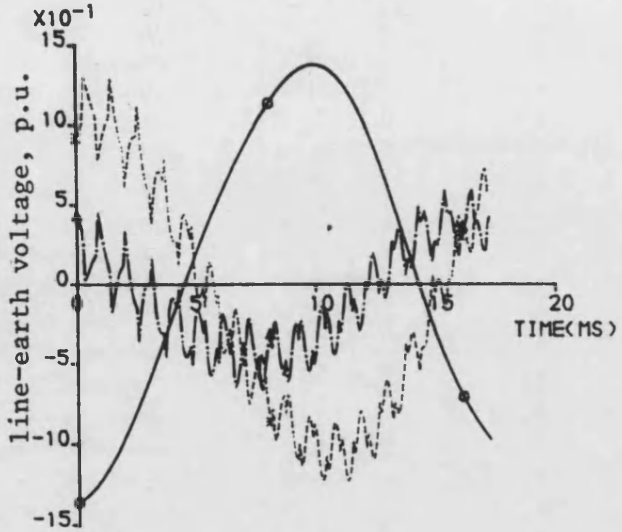

Figure 8.12 Waveforms on the star-side of the transformer for a pure interphase fault (b-c), fault is at mid point (x = 80Km) and the receiving end source is substituted by a s.c.1. = 1200MVA

——— a-phase
—.— b-phase
----- c-phase

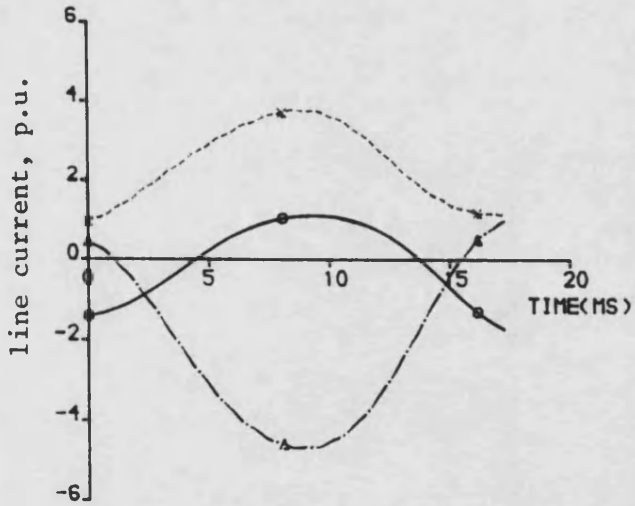

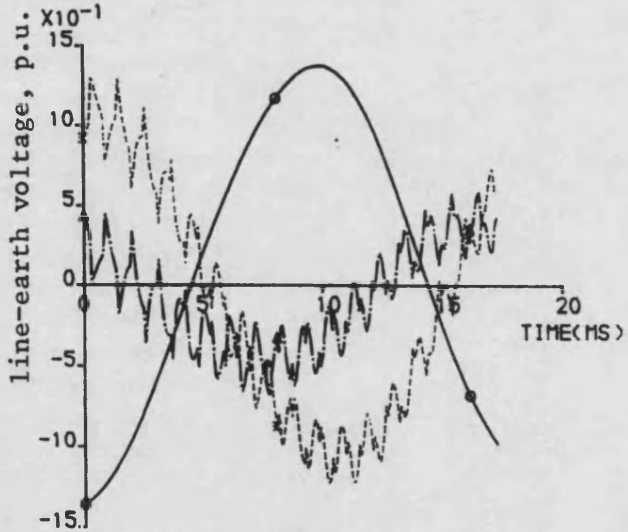

Figure 8.13 Waveforms on the star-side of the transformer for a pure interphase fault (b-c), fault is at mid point (x = 80Km) and the receiving end source is substituted by a s.c.1. = 5000MVA

——— a-phase
—.— b-phase
----- c-phase

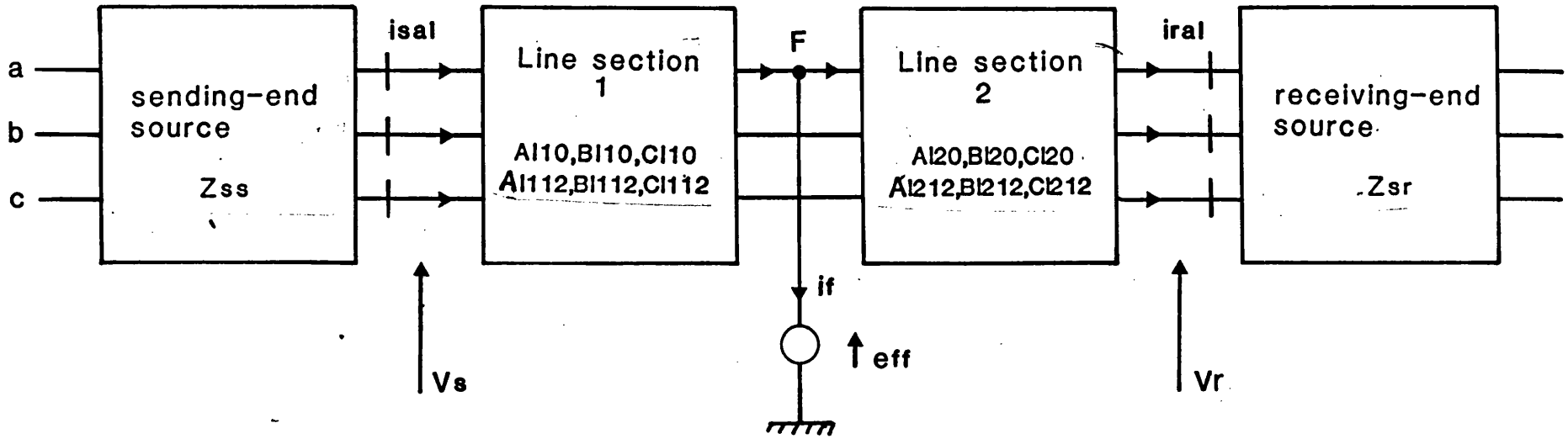

F = Fault point
is - Sending end currents (time varying steady state currents and transient currents)
ir Receiving end currents (" " " " ")
Vs Sending end voltages (steady state voltage vectors and transient voltage vectors)
Vr Receiving end voltages (" " " " " ")

Fig. 8.14 Fault Simulation Model

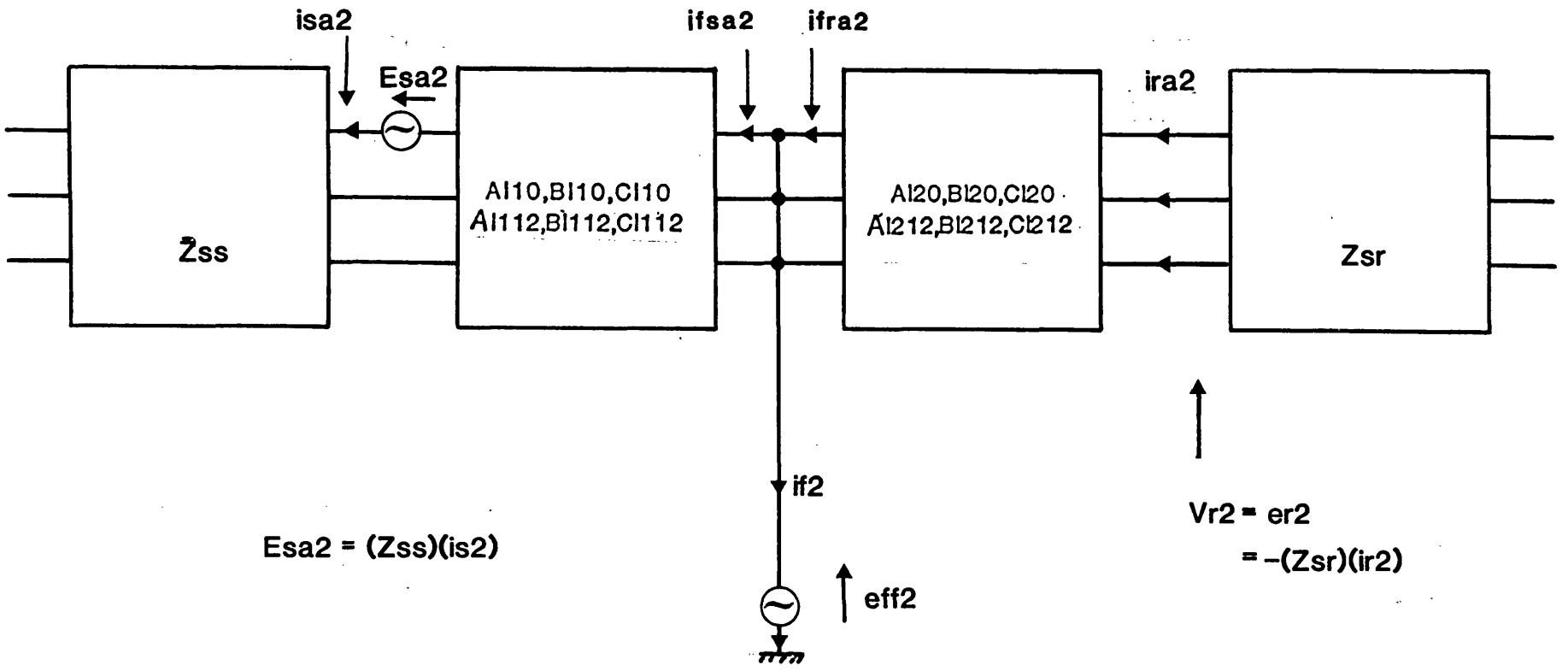

Fig. 8.15 Sending-end a-phase Pole Opening Simulation

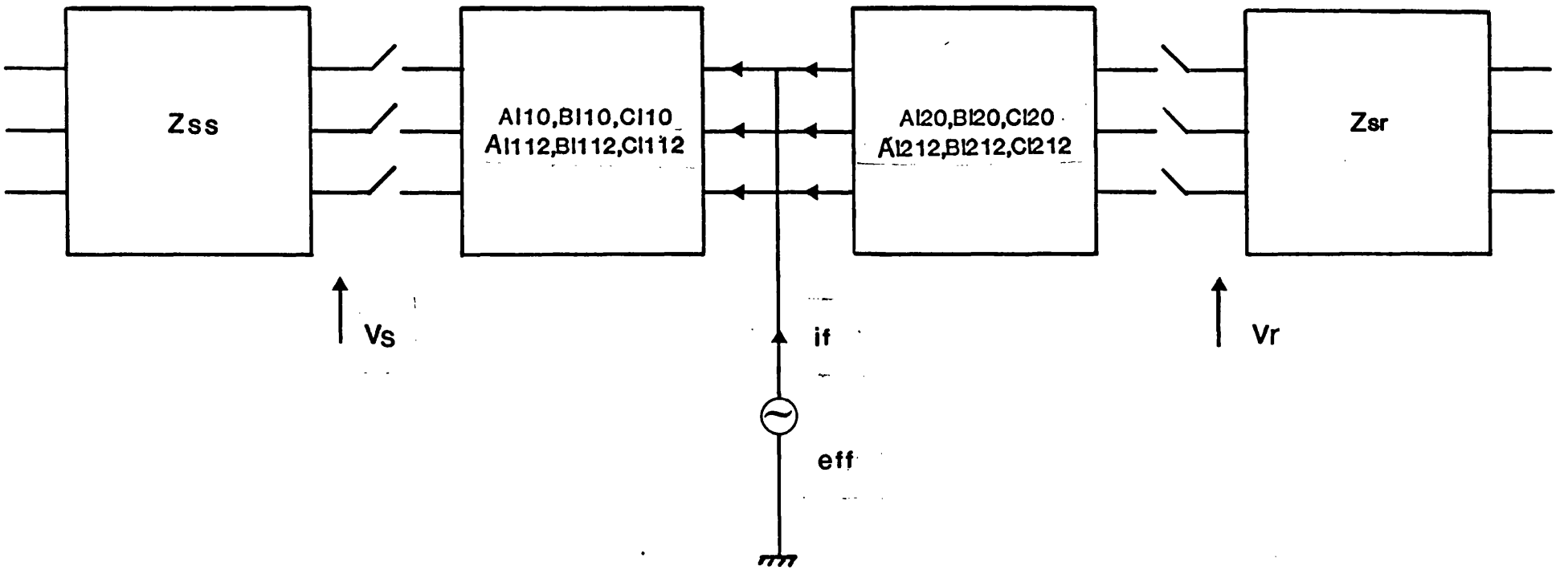

Fig. 8.16 Fault Break-off Simulation

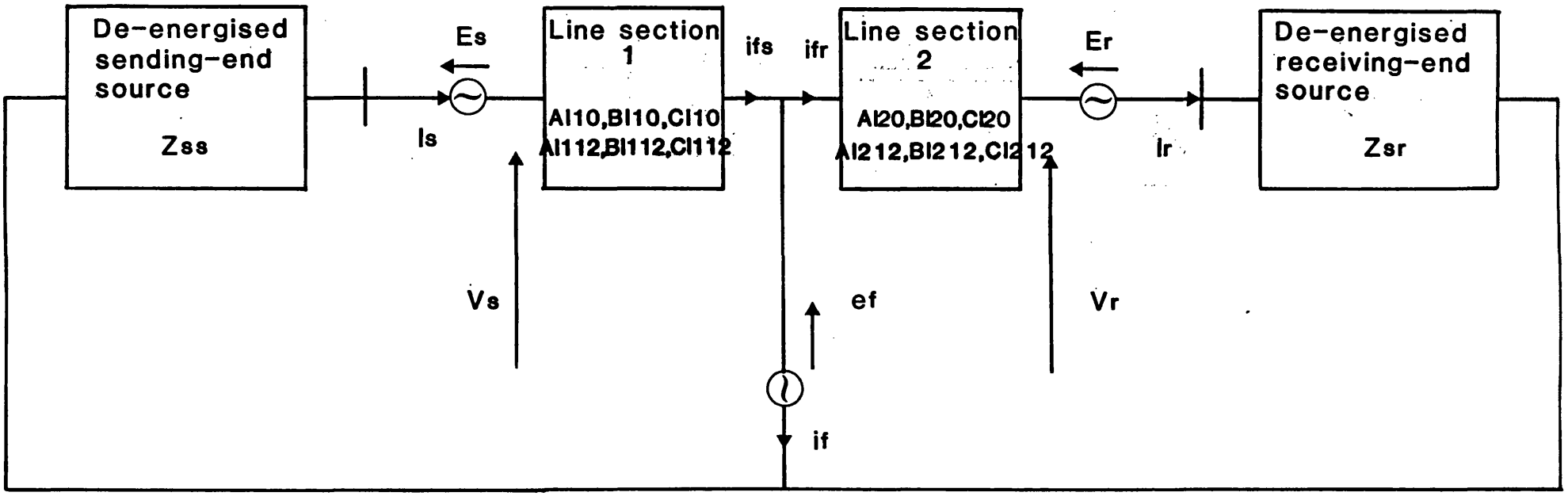

Fig. 8.17 Superimposed-system Model for Solid Fault

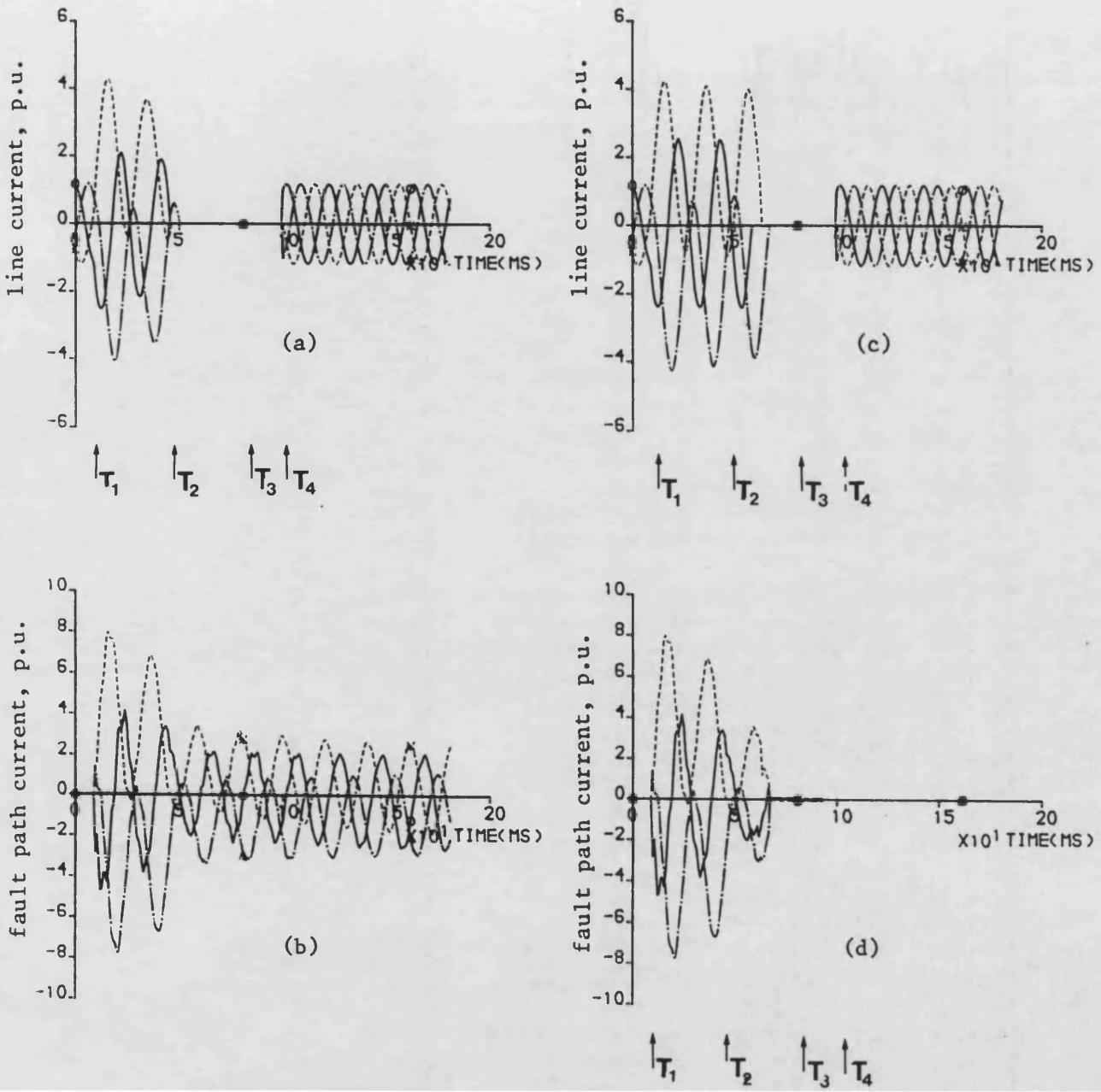

Figure 8.18 Current waveforms associated with three-phase autoreclosure sequences from fault inception (solid three phase fault) up to fault break-off and reclosing.

(a) Sending end currents
(b) Fault path currents from fault inception up to opening three phases at sending end, while the receiving end is not opened
(c) Receiving end currents
(d) Fault path currents from fault inception up to fault break-off

Fault is at mid point (X = 160Km), T_1 = fault inception (10ms), T_2 = breaker contacts at end 's' and end 'r' separate (66ms), T_3 = fault break-off (80ms), T_4 = breaker at end 's' recloses (96ms), breaker at receiving end closes (100ms)

——— a-phase
—.— b-phase
----- c-phase

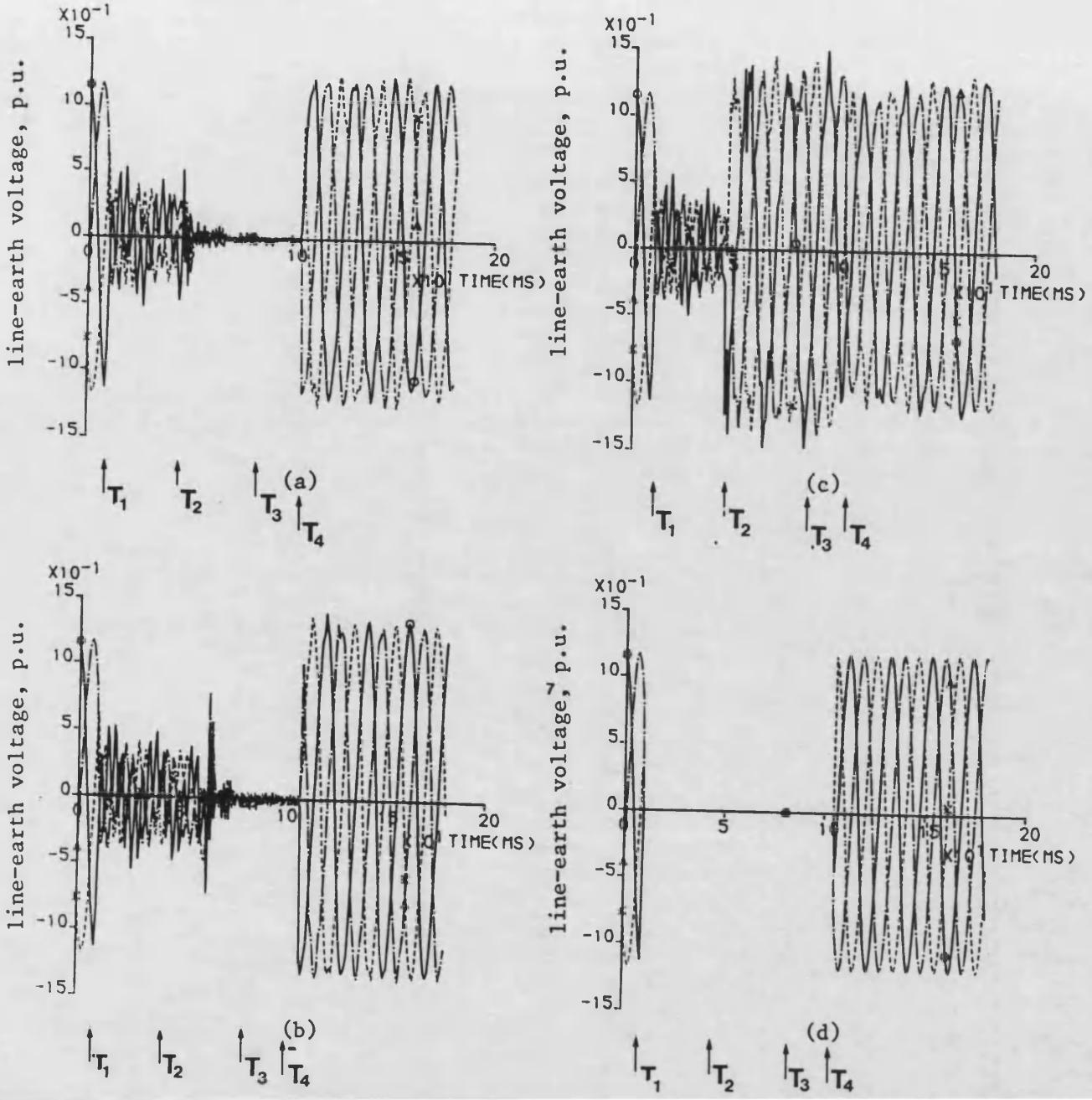

Figure 8.19 Voltage waveforms associated with three-phase autoreclosure sequences from fault inception (solid three phase fault) up to fault break-off and reclosing

(a) Voltages on line side of breaker at sending end
(b) Voltages on line side of breaker at receiving end
(c) Voltages on source side of breaker at sending end
(d) Voltage across the fault path

Fault is at mid point (X = 160Km), T_1 = fault inception (10ms), T_2 = breaker contacts at end 's' and end 'r' separate (66ms), T_3 = fault break-off (80ms), T_4 = breakers at end 's' recloses (96ms), breakers at end 'r' recloses (100ms)

——— a-phase
—.— b-phase
----- c-phase

CHAPTER 9

CONCLUSIONS AND FUTURE WORKS

9.1 General Conclusions

In this work, frequency domain techniques have been developed for realistically modelling a power system comprising a synchronous generator, generator/transformer and a transmission line. The methods are thus attractive for use in power-system studies, in particular fault studies, where it is desired to press as close as possible to the actual response of the system or a system section under investigation.

The techniques developed are frequency domain based and this makes it somewhat simpler to take into account the frequency variant of both the transmission line and source side networks. In particular, the generator on the source side is represented by its true model rather than a lumped impedance approximation based on subtransient reactance. Furthermore, taking into account the frequency variance of the operational parameters of the generator adds more realism to the results obtained. In this respect, it should be mentioned that the rather difficult problem of incorporating frequency variable parameters into the model has been overcome by using curve fitting techniques coupled with carefully chosen polynomial functions.

The computational results obtained from the model developed clearly show the desirability of incorporating a more realistic model of synchronous generators than is afforded by simpler methods based upon subtransient impedance. For example, when using the more exact generator model, complete offsetting of at least one phase current is predicted and this is what happens in practice. This effect is,

however, absent in the case of a system model comprising a simple source. This is particularly so in relation to faults which occur near zero voltage point on wave, where complete offsetting of the currents at the machine terminals and/or the line can occur. As expected, for such types of faults, the travelling waves are less pronounced. It is important to note that for faults which occur near the peak of the prefault voltage, there is close similarity between the responses obtained using a more realistic source model and those obtained using elementary source networks.

When considering the frequency dependent parameters, neglecting the frequency variant of the transmission line parameters mainly affects the high frequency components and has little effect on the low frequency distortions. Computing times are, however, reduced. Taking into acount the frequency variant of the genrator parameters somewhat reduces the high frequency distortion, but the offset in the current waveforms is increased thus affecting the zero crossing points. It is interesting to note that when using frequency response data for the machine as opposed to constant data, the computing time is actually reduced.

As mentioned in the previous chapters, the transformer parameters are more or less constant in the range of frequency considered in this study. The effect of generator/transformer on the transient waveforms is twofold. First of all, as expected, a 30^0 phase shift is produced between the star and delta sides and secondly, although the distortion level in the faulted phase(s) waveforms is somewhat reduced on the delta side (in comparison with the star side), however, the distortion level in the sound phase(s) is increased. The latter is due to the discontinuities created by the delta–star connection.

It is also worth emphasising that when considering frequency invariant generator model, the rotor eddy–current effects cannot be taken into account and this can affect the accuracy of the results. This further emphasises the improtance

of taking frequency dependency of the generator parameters into account when developing the generator model.

In general, the results indicate that the standard model, based on manufacturers data, is inadequate in simulating the fault transient resposne.

Hitherto, the results and the associated discussion has been mainly concerned with how the fault transient waveforms are affected by the accuracy of the model, in particular the source side networks. It is nevertheless interesting to see how various other factors, such as, for example, the power factor, can further affect the fault transient waveforms when considering the very realistic model developed here. For this part of the work, results have been presented for two different systems, a 400kV system comprising a 588MVA generator and a 132kV system comprising 150MVA generator. First of all, considering the former of the two, the results clearly show that if the generator is underexcited (i.e. system operating at a leading power factor) as opposed to an overexcited gtenerator (lagging power factor) the severity of the dc component, in particular in the currents, is increased and this in turn delays the time at which the first zero crossing occurs. For such a system, a slightly higher leading power factor has quite a profound effect on the zero crossing time in that it is increased even further. This can be attributed to the fact that in large machines, since the X:R ratio is high, the dc component becomes quite sensitive to the small voltage changes associated with small changes in the magnitude of the power factor. When considering the lower voltage level second system, it can be seen that the zero crossing times are unaffected by the small changes in the power factor. This is so because in smaller machines, the X:R ratio is comparatively much lower and hence the dc components are unaffected by the change in the magnitude of the power factor.

In this study, methods are also developed to take into account the effects of

inclusion of source-side shunt capacitances in the system model under study. First of all, considering the current waveforms, the results clearly show that the high frequency distortions produced by voltage maximum faults, particularly on the star-side of the transformer, are accentuated by the shunt capacitances which nonetheless have little effect ont he delta-side waveforms. Voltage-minimum-fault current transients are unaffected by the shunt capacitances on either side of the transformer. In the case of the voltage waveforms, the inclusion of the shunt capacitances has little effect on the waveforms.

In this study, modelling techniques are also developed for simulating fault transients on a double-end fed system using realistic source side networks, as opposed to a single end fed feeder connected to an infinite busbar. It should be mentioned that whilst the techniques for modelling a double-end system with simplified source side networks using phase-co-ordinates are relatively simple to develop, however, when true models of generator, generator/transformer are used to represent the sources, frequency shifted symmetrical components have to be employed and these make the modelling techniques significantly more complex.

The results obtained from the new model developed are verified by comparing with those obtained for the previously developed single end fed system. This can of course be easily done by treating the remote end busbar terminated in very large capacity. A limited study presented clearly shows that fault transient waveforms at any end (sending or receiving) are unaffected by the accuracy of the remote-end source side representation.

A computer technique is also outlined for simulating conditions following the complete sequences associated with three-phase autoreclosure.

Such techniques are especially important in modern protection relay design as

its performance can be assessed not only during the initial fault inception period but throughout the fault clearance and subsequent reclosure periods. Some interesting results which illustrate the transients produced during the discontinuitites associated with the various sequences are presented.

9.2 Suggestions and Future Work

The work presented in this thesis forms the basis for future investigation to study the transient performance of a system which includes generators, transformers and ehv transmission line, for the purposes of system design and further development of new equipments such as protection schemes. However, certain aspects of the work are beyond the scope of the present work but nonetheless can be carried out in the future. These are outlined below:

9.2.1 Inclusion of arc resistance

In the present study, provision has been made for representing the fault arc path by a constant resistance. However, for a more realistic consideration, a non-linear arc resistance model may be inserted into the system model.

9.2.2 Using single-pole and three-pole autoreclosure theory for different faults

In this thesis, three-pole autoreclosure techniques have been utilised to clear faults for three-phase fault conditions only. Simillar studies in the future could involve single-pole or three-pole autoreclosure techniques to simulate the electrical transient phenomena associated with asymmetric faults such as phase-to-earth and two-phase-earth faults.

9.2.3 Inclusion of automatic voltage regulator

The AVR has a significant effect on the ac component of fault current in that it becomes large compared to the dc component and thus causing early zero crossing to occur. In the system studies here, this plant item has not been included. The inclusion of an AVR can be done by modifying the frequency domain impedance matrix of the system to include the superimposed field voltage associated with an AVR.

9.2.4 Possibility of including the magnetising components of the generator/transformer

It is possible to make use of a more exact representation of the transformer by including the magnetising effects. This would involve adding the shunt components as separate elements between the transformer model used and the transmission line. It is also possible to split the transformer to primary and secondary circuits where the star-side incorporates the magnetising component.

9.2.5 Studying the effect of frequency dependent parameters of the transformer

Although in this study the effect of frequency dependent parameters of synchronous machine and transmission line have ben incorporated into the model for fault transient studies, however, due to the range of frequency considered in this work, the transformer parameters are assumed to be constant. However, for studies which require a knowledge of very high frequency transients, such as surge phenomena, the transformer parameters then become frequency dependent and hence inclusion of frequency variant of transformer parameters to study the electromangetic transients becomes essential. Here it should be noted that as in the case of generator and transmission line, the use of the frequency domain

techniques makes it somewhat easier to incorporate the frequency dependency of transformer parameters.

9.2.6 Inclusion of the interturn capacitance and mutual inductances

In the present work, when studying the effects of shunt capacitances on the transient waveforms at relaying point, the interturn elements such as mutual inductances, capacitance and conductance between turns are neglected. However, for more accuracy, the winding should be treated as an infinite number of identical coils connected in series, in which each coil may be represented by an equivalent circuit which includes an inductance, turn to ground capacitance (as studied in this work), mutual inductance and capacitance between turns. These can be added to the system model to predict more accurately the transient behaviour of the machine and the corresponding transformer.

9.2.7 Inclusion of surge diverters in the system

At the higher transmission line voltage levels, increasing use is being made of surge diverters to closely control the magnitude of system overvoltages. Consequently, there is a need for further development of the present model, whereby surge diverters can be included in transient overvoltage calculations on transmission systems in order that the interaction between the surge diverter and the system could be studied.

9.2.8 The possibility for multimachine study

The multimachine problem has been mathematically solved using Laplace techniques and Forward and Backward components of $Ku^{(10)}$. In this work we have shown a close relationship between Laplace and modified Fourier Transforms

and Forward/Backward and symmetrical components. Hence an extension of Ku's approach is directly possible using the frequency domain techniques for incorporating a multimachine model on the source side.

9.2.9 Studies for double or parallel transmission lines

In this study, a single circuit three phase system has been considered. The present fault simulation techniques presented can be easily extended for studying the behaviour of a double or parallel system. It should be mentioned that the effect of paralleling transmission lines is to produce zero sequence mutual impedance effects which are of partricular importance in distance protection relays, especially during earth faults[69,70]. Such effects can be more accurately modelled using frequency domain analysis.

APPENDIX 1

STEADY STATE OPERATION WITH REGARD TO GENERAL EQUATIONS

With reference to equations (2.23) the general equations are:

$$
\begin{aligned}
e_d &= -(R+pL_d)\,i_d + w_o L_q \cdot i_q + M_{af} \cdot p i_{fd} + M_{af} \cdot p i_{kd} - w_o M_{aq} \cdot i_{kq} \\
e_q &= -w_o L_d \cdot i_d - (R+pL_q)\,i_q + w_o M_{af} \cdot i_{fd} + w_o M_{af} \cdot i_{kd} + M_{aq} \cdot p i_{kq} \\
e_{fd} &= -(3/2) M_{af} \cdot p i_d + (R_{fd}+pL_{ff})\,i_{fd} + M_{af} \cdot p i_{kd}
\end{aligned}
\qquad \ldots \text{(A.1.1)}
$$

The above relationships can therefore be simplified by substituting p=0, speed equal to "w_o" and using the synchronous reactances X_d, X_q, it then follows that:

$$
\begin{aligned}
e_d &= -R \cdot i_d + w_o L_q \cdot i_q \\
e_q &= -R \cdot i_q - w_o L_d \cdot i_d + w_o M_{af} \cdot i_{fd} \\
e_{fd} &= R_{fd} \cdot i_{fd}
\end{aligned}
\qquad \text{where} \quad
\begin{cases}
w_o L_q = X_q \\
w_o L_d = X_d \\
w_o M_{af} = X_{md}
\end{cases}
$$

By replacing $w_o L_q$, $w_o L_d$, $w_o M_{af}$ by X_q, X_d, X_{md}:

$$
\begin{aligned}
e_d &= -R \cdot i_d + X_q \cdot i_q \\
e_q &= -R \cdot i_q - X_d \cdot i_d + X_{md} \cdot i_{fd} \\
e_{fd} &= R_{fd} \cdot i_{fd}
\end{aligned}
\qquad \ldots \text{(A.1.2)}
$$

and also from equations (2.34):

$$
E = E_d + jE_q = [e_d/\mathrm{sqrt}(2)] - j[e_q/\mathrm{sqrt}(2)]
$$

substituting from equation A.1.2 we have:

$$E = [-R(i_d - ji_q) + X_q \cdot i_q - jX_d \cdot i_d - jX_{md} \cdot i_{fd}]/\text{sqrt}(2)$$

in which:

$$i_d/\text{sqrt}(2) = I_d$$

and:

$$i_q/\text{sqrt}(2) = I_q$$

then:

$$E = -R(I_d - jI_q) + X_q \cdot I_q - jX_d \cdot I_d - [jX_{md} \cdot i_{fd}/\text{sqrt}(2)]$$

Under no load conditions, ($I_d = I_q = 0$):

$$E = E_{oc} = -jX_{md} \cdot i_{fd}/\text{sqrt}(2)$$

where E_{oc} is the open circuit voltage and X_{md} is the magnetising reactance in the direct axis.

The above analysis shows that for steady state operation, there is a direct relationship between the axes value of voltage and current. With reference to equations (2.33):

$$e_d = \text{sqrt}(2)E_{rms} \cdot \text{SIN}\delta, \qquad e_q = -\text{sqrt}(2)E_{rms} \cdot \text{COS}\delta$$

Equating these to equation A.1.2 gives:

$$\begin{aligned} \text{sqrt}(2)E_{rms}.\text{SIN}\delta &= X_q.i_q - R.i_d \\ -\text{sqrt}(2)E_{rms}.\text{COS}\delta &= -X_d.i_d - R.i_q + X_{md}.i_{fd} \\ &= -X_d.i_d - R.i_q - \text{sqrt}(2).E_{oc} \end{aligned}$$

By simplifying the above relations we get:

$$\begin{aligned} i_q &= \text{sqrt}(2)[R(E_{rms}.\text{COS}\delta - E_{oc}) + X_d.E_{rms}.\text{SIN}\delta]/(R^2 + X_d.X_q) \\ i_d &= \text{sqrt}(2)[-R.E_{rms}.\text{SIN}\delta + X_q(E_{rms}.\text{COS}\delta - E_{oc})]/(R^2 + X_d.X_q) \end{aligned}$$

Finally, by neglecting the armature resistance, i.e. (R=0) the following expression for the steady state currents are obtained[12]:

$$\begin{aligned} i_o &= 0 \\ i_d &= \text{sqrt}(2).(-E_{oc} + E_{rms}.\text{COS}\delta)/X_d \qquad \text{. . (A.1.3)} \\ i_q &= \text{sqrt}(2).(E_{rms}.\text{SIN}\delta)/X_q \end{aligned}$$

APPENDIX 2

SYNCHRONOUS MACHINE IN THE MORE COMPLEX FORM

The synchronous machine model which has been considered in chapter 2 is based on one rotor winding in each axis. A brief description of the way in which the machine can be represented in a more complex form, i.e. one field and two damper widings on d-axis and three damper windings on q-axis, is now given,

A.2.1 The required model configuration

As we have analysed in chapter 2, the synchronous machine models are based on the well-known concept of representing the machine in terms of d- and q-axes equivalent circuits.

The structure of the more complex rotor synchronous machine model is shown in Figure A.2.1. It has a field winding and two amortisseur circuits in the d-axis and three amortisseur circuits in the q-axis. The d-axis equivalent circuit accounts for unequal mutual inductances between rotor and stator. The matrix representation of flux linkage in a more complex model generator is as (29):

$$
\begin{array}{c}
 \\ 0 \\ d \\ q \\ fd \\ kd_1 \\ kd_2 \\ kq_1 \\ kq_2 \\ kq_3
\end{array}
\begin{bmatrix} \psi_o \\ \psi_d \\ \psi_q \\ \psi_{fd} \\ \psi_{kd_1} \\ \psi_{kd_2} \\ \psi_{kq_1} \\ \psi_{kq_2} \\ \psi_{kq_3} \end{bmatrix}
=
\begin{array}{c}
\begin{array}{ccccccccc} 0 & d & q & fd & kd_1 & kd_2 & kq_1 & kq_2 & kq_3 \end{array} \\
\begin{bmatrix}
-L_o & 0 & 0 & 0 & 0 & 0 & 0 & 0 & 0 \\
0 & -(M_{ad}+\ell_1) & 0 & M_{ad} & M_{ad} & 0 & 0 & 0 & 0 \\
0 & 0 & -(M_{aq}+\ell_1) & 0 & 0 & 0 & M_{aq} & M_{aq} & M_{aq} \\
0 & -M_{ad} & 0 & (M_{ad}+\ell_{fd}+L_{fkd_1}+L_{fkd_2}) & (M_{ad}+L_{fkd_1}) & (M_{ad}+L_{fkd_1}+L_{fkd_2}) & 0 & 0 & 0 \\
0 & -M_{ad} & 0 & (M_{ad}+L_{fkd_1}) & (M_{ad}+\ell_{kd_1}+L_{fkd_1}) & (M_{ad}+L_{fkd_1}) & 0 & 0 & 0 \\
0 & -M_{ad} & 0 & (M_{ad}+L_{fkd_1}+L_{fkd_2}) & (M_{ad}+L_{fkd_1}) & (M_{ad}+\ell_{kd_2}+L_{fkd_1}+L_{fkd_2}) & 0 & 0 & 0 \\
0 & 0 & -M_{aq} & 0 & 0 & 0 & (M_{aq}+\ell_{kq_1}) & M_{aq} & M_{aq} \\
0 & 0 & -M_{aq} & 0 & 0 & 0 & M_{aq} & (M_{aq}+\ell_{kq_2}) & M_{aq} \\
0 & 0 & -M_{aq} & 0 & 0 & 0 & M_{aq} & M_{aq} & (M_{aq}+\ell_{kq_3})
\end{bmatrix}
\end{array}
\begin{bmatrix} i_o \\ i_d \\ i_q \\ i_{fd} \\ i_{kd_1} \\ i_{kd_2} \\ i_{kq_1} \\ i_{kq_2} \\ i_{kq_3} \end{bmatrix}
$$

. . (A.2.1)

A.2.2 Voltage equations of the more complex rotor machine

The following equations, based on Park's transformation[1], describe the non-linear dynamic performance of a synchronous machine in a d-q reference frame.

By using the following definitions, the voltage equations of a synchronous

machine with a complex rotor will be found.

$$M_{ad}+\ell_1 = L_d \qquad M_{aq}+\ell_1 = L_q$$

$$M_{ad}+\ell_{fd}+L_{fkd_1}+L_{fkd_2} = L_{ff} \qquad M_{ad}+L_{fkd_1} = M'_{ad}$$

$$M_{ad}+\ell_{kd_1}+L_{fkd_1} = L_{kk_1} \qquad M_{ad}+\ell_{kd_2}+L_{fkd_1}+L_{fkd_2} = L_{kk_2}$$

$$M_{ad}+L_{fkd_1}+L_{fkd_2} = M''_{ad} \qquad M_{aq}+\ell_{kq_1} = L_{qq_1}$$

$$M_{aq}+\ell_{kq_2} = L_{qq_2} \qquad M_{aq}+\ell_{kq_3} = L_{qq_3}$$

and:

$$\begin{aligned}
e_o &= p\psi_o - R.i_o \\
e_d &= p\psi_d - w_o\psi_q - R.i_d \\
e_q &= p\psi_q + w_o\psi_d - R.i_d \\
e_{fd} &= p\psi_{fd} + R_{fd}.i_{fd} \\
0 &= p\psi_{kd_1} + R_{kd_1}.i_{kd_1} \qquad \text{. . (A.2.2)} \\
0 &= p\psi_{kd_2} + R_{kd_2}.i_{kd_2} \\
0 &= p\psi_{kq_1} + R_{kq_1}.i_{kq_1} \\
0 &= p\psi_{kq_2} + R_{kq_2}.i_{kq_2} \\
0 &= p\psi_{kq_3} + R_{kq_3}.i_{kq_3}
\end{aligned}$$

Now, by transforming the time variation of the machine voltages and currents into frequency domain by means of the well-known Fourier integral[21], for example:

$$f(jw) = \int_{-\infty}^{\infty} f(t)\exp(-jwt)dt$$

and applying this fact that $f(jw) = f_1(jw).f_2(jw)$, the general equation which relates the current and voltage components in the frequency domain will be as follows:

$$
\begin{array}{c}
 \\
0 \\
d \\
q \\
fd \\
kd_1 \\
kd_2 \\
kq_1 \\
kq_2 \\
kq_3
\end{array}
\begin{bmatrix} e_o(jw) \\ e_d(jw) \\ e_q(jw) \\ e_{fd}(jw) \\ 0 \\ 0 \\ 0 \\ 0 \\ 0 \end{bmatrix}
=
\begin{array}{c}
\begin{array}{ccccc} 0 & d & q & fd & kd_1 \end{array} \\
\begin{bmatrix}
-(R+jwL_o) & 0 & 0 & 0 & 0 \\
0 & -(R+jwL_d) & w_o.L_q & jwM_{ad} & jwM_{ad} \\
0 & -w_o.L_d & -(R+jwL_q) & w_oM_{ad} & w_oM_{ad} \\
0 & -jwM_{ad} & 0 & (R_{fd}+jwL_{ff}) & jwM'_{ad} \\
0 & -jwM_{ad} & 0 & jwM'_{ad} & (R_{kd_1}+jwL_{kk_1}) \\
0 & -jwM_{ad} & 0 & jwM''_{ad} & jwM'_{ad} \\
0 & 0 & -jwM_{aq} & 0 & 0 \\
0 & 0 & -jwM_{aq} & 0 & 0 \\
0 & 0 & -jwM_{aq} & 0 & 0
\end{bmatrix}
\end{array}
$$

$$
\begin{array}{c}
\begin{array}{cccc} kd_2 & kq_1 & kq_2 & kq_3 \end{array} \\
\begin{bmatrix}
0 & 0 & 0 & 0 \\
jwM_{ad} & -w_oM_{aq} & -w_oM_{aq} & -w_oM_{aq} \\
w_oM_{ad} & jwM_{aq} & jwM_{aq} & jwM_{aq} \\
jwM''_{ad} & 0 & 0 & 0 \\
jwM_{ad}' & 0 & 0 & 0 \\
(R_{kd_2}+jwL_{kk_2}) & 0 & 0 & 0 \\
0 & (R_{kq_1}+jwL_{qq_1}) & jwM_{aq} & jwM_{aq} \\
0 & jwM_{aq} & (R_{kq_2}+jwL_{qq_2}) & jwM_{aq} \\
0 & jwM_{aq} & jwM_{aq} & (R_{kq_3}+jwL_{qq_3})
\end{bmatrix}
\end{array}
\begin{bmatrix} i_o(jw) \\ i_d(jw) \\ i_q(jw) \\ i_{fd}(jw) \\ i_{kd_1}(jw) \\ i_{kd_2}(jw) \\ i_{kq_1}(jw) \\ i_{kq_2}(jw) \\ i_{kq_3}(jw) \end{bmatrix}
$$

. . (A.2.3)

It is also assumed that the effect of saturation is to vary only the mutual inductances M_{ad} and M_{aq}. Results in references (29) and (30) have shown that the saturation of the q-axis is appreciably more than that of the d-axis, and for this reason, different saturation characteristics could be used for the two axes, although the saturation effects in our consideration have been neglected.

APPENDIX 3

SOME EFFECTS OF SYNCHRONOUS GENERATOR ROTOR CONSTRUCTION ON ITS OPERATIONAL INDUCTANCE

Investigation into the Northfleet station in the UK[24,25,27], and Ontario hydro station in Canada[22,26,28] has shown that the design and construction of a synchronous machine have a major influence on its electrical characteristics, such as operational inductances. A brief outline of how these characteristics are influenced by different machine design will now be given.

A.3.1 Simple machine with a laminated rotor and only one field winding

For an illustration, the d-axis operational inductance will be used to demonstrate the significance of different rotor designs on the frequency response tests. Figure A.3.1 shows the d-axis equivalent circuit and a plot of Ld(p) for a very simple machine with a laminated rotor and only a field winding, i.e. a single discrete winding on the rotor.

$$T'_{do} = (M_{ad}+L_{fd})/R_{fd}$$

$$T'_{d} = L_{fd}/R_{fd}$$

There are only two breakpoints in the curve. At very low frequencies, $L_d(p) = L_d = M_{ad} + \ell_1$, the unsaturated value of synchronous inductance.

The magnitude of operational inductance begins to drop off, controlled by T'_{do}, which in this case is the time constant of the field winding, and levels off at L'_d, the transient inductance, which is the sum of (ℓ_1) and parallel combination

of M_{ad} and L_{fd}, i.e. $L'_d = \ell_1 + M_{ad} \| L_{fd}$.

A.3.2 Synchronous machine with laminated rotor and a field winding plus one discrete damper winding

Figure A.3.2 represents a machine with a laminated rotor, a field winding and one discrete damper winding, the time constant of the field and damper are widely separated.

$$T'_{do} = (M_{ad}+L_{fd})/R_{fd} \qquad T'_d = L_{fd}/R_{fd}$$
$$T''_{do} = (M_{ad}+L_{kd})/R_{kd} \qquad T''_d = L_{kd}/R_{kd}$$

In this case, there are four breaks in the Ld(p) curve, two produced by the field winding and two by the damper. As before, the magnitude starts out equal to the synchronous inductance at low frequencies and begins to decrease at 20db/decade according to T_{do}', the transient open circuit time constant. It levels off at the transient inductance $L'_d = \ell_1 + M_{ad} \| L_{fd}$. Then, at even higher frequencies when the damper winding comes into play the magnitude goes down again and levels off at the subtransient inductance, $L''_d = \ell_1 + M_{ad} \| L_{fd} \| L_{kd}$. This is the lowest value that $L_d(p)$ will reach using the above equivalent circuit and is also realistic for machine of this type, e.g. hydraulic generators with laminated pole pieces. Note that the time constants associated with the damper winding, T''_{do} and T''_d are inversely proportional to the damper winding resistance. This means that the parts of the $L_d(p)$ curve which is dependent on the damper can move along the frequency axis with changes in the damper winding resistance.

A.3.3 Turbine generator with complex damper design and high resistance damper structure

Turbine generators imply a very different rotor design. There are no insulated laminations to block electric eddy currents in the magnetic iron of the rotor body and, even more important, the field windings are held in slots in the rotor forging by metal wedges. This means that currents can be induced not only in the discrete conductors of the field winding, but also in the multitude of circuits formed by the rotor body and the slot wedges.

Any currents induced in this damper structure (rotor body plus slot wedges) will have a non-uniform radial distribution with the highest current density at the outer surface of the rotor (skin effect). To represent this damper structure correctly, an equivalent circuit with an infinite number of rotor circuits would be required. Even for obtaining a sufficient accuracy for practical purposes, a large number of circuits would be necessary if the complete frequency spectrum were to be modelled and this could have a significant effect on computational efficiency[23]. Increasing the number of rotor circuits increases the number of states and decreases the shortest time constants associated with the models. The reduction in time constant values may require a smaller integration step this, in turn, could significantly increase the computation costs.

Figure A.3.3 illustrates how this complex damper influences the magnitude of the d-axis operational inductance. The field winding has the same effect as in the previous example. However, the region of influence of the damper is introduced by a slope which will ultimately bring the magnitude of the operational inductance down to the stator winding leakage inductance, i.e.:

$$\lim_{p \longrightarrow \infty} L_d(p) = \ell_1 + M_{ad} \| L_{fd} \| L_{kd_1} \| L_{kd_2} \| \ldots\ldots\ldots \| L_{kdn} = \ell_1$$

The less than 20db/decade slope is a natural consequence of the distributed character of the damper structure.

Note that the region of influence of the damper in Figure A.3.3 is well outside the range of frequencies important for stability studies (around 10rad/s). A characteristic such as this is typical of modern turbogenerators with short, segmented slot wedges and no means for enhancing current transfer between adjacent wedges, such as a copper backing strip. The Lambton generators which have been studied in Ontario hydro station are of this type.

An impression of the importance of the slot wedges to the dynamic performance of a turbogenerator can be gained by considering the distribution of transient currents in the damper structure. Ontario hydro group showed that even at frequencies as low as 10rad/s, the depth of penetration of the induced current in the rotor teeth is typically only 2 to 3cm[29], or about the depth of the slot wedges. In the wedge material itself, the depth of penetration is in the order of 6cm at 10rad/s. Thus, it is apparent that high conductivity, non-magnetic slot wedges are potentially capable of dominating the response of the damper structure in the important frequency range around 10rad/s. The extent of this dominance depends on the resistance of the total series current path through the wedges. In some cases such as a machine, which its characteristics are shown in Figure A.3.3, this resistance is relatively high. Each slot contains many wedges and the wedge current has to transfer to and from a rotor tooth to get to the next wedge in the slot. This means that, in addition to the resistance of the current path around the ends of the rotor, there are also two contact resistances in series with each of the many wedges per slot.

A.3.4 Synchronous machine with complex damper design but low resistance damper structure

The Nanticok Machine with a low resistance, which has been tested in Canada is quite different from the previous one. Each slot containing field winding conductors has a single wedge running the full length of the rotor. This means that all of the wedge-to-wedge contact resistances present in a short wedge design are eliminated, leaving only the resistance of the current path around the ends of the rotor in addition to that of the wedges themselves. The effect of this design on the operational inductances can be seen in Figure A.3.4.

The lower resistance of the damper structure has moved its region of influence back along the frequency axis to the point where it is now right in the most of the range of frequencies important to the performance of the generator in stability studies. The presence of a damper structure influence in this frequency range has at least two important consequences to the power system analyst. First, a more detailed generator model will be required to reproduce the gradual slope of $L_d(p)$ through the range of frequencies in which the machine must be accurately modelled. The second is that any change in the resistance of the damper structure will have a significant influence on the parameter of the model. This, of course, is not a problem in machines with high resistance dampers since even a 50% change in resistance would still leave the region of damper influence outside the important frequency range around 10rad/s.

APPENDIX 4

GENERAL SYSTEM EQUATIONS WHEN SHUNT CAPACITANCE IS INCLUDED AT SOURCE SIDE

A.4.1 Generator equivalent circuit for earthed star connected

The windings of rotating machines for transient calculations may be regarded to a good approximation as a lumped series inductance and shunt capacitance to ground (Figure A-4.1). Due to the arrangement of the coils in individual slots, the influence of the mutual capacitance between different parts of the windings is small and can therefore be neglected. The rotor also has, as a rule, little effect upon the surge phenomena as it is shielded by the action of the eddy currents at the surface against the magnetic fields of high frequency.

A.4.2 Transformer equivalent circuit

Neglecting the capacitance between the turns of the windings, the configuration, as shown in Figure A-4.2, for the transformer is quite reasonable for considering the transient phenomena in a system[56].

a) For star-side we have:

C_t = 1/2 (winding capacitance per phase) + bushing capacitance.

b) For delta-side we have:

C_t = winding capacitance per phase + 2 (bushing capacitance)

A.4.3 General equations at machine terminal (delta side)

The resultant currents at each capacitor bank are as follows:

$$i_{ca}' = jw.C_{gt}.v_a'$$
$$i_{cb}' = jw.C_{gt}.v_b' \qquad \ldots (A.4.2)$$
$$i_{cc}' = jw.C_{gt}.v_c'$$

where $C_{gt} = C_g + C_t$ (delta-side)

Equations A.4.1 in a matrix form is:

$$\begin{bmatrix} i_{ca}' \\ i_{cb}' \\ i_{cc}' \end{bmatrix} = \begin{bmatrix} jwC_{gt} & 0 & 0 \\ 0 & jwC_{gt} & 0 \\ 0 & 0 & jwC_{gt} \end{bmatrix} \begin{bmatrix} v_{ma}' \\ v_{mb}' \\ v_{mc}' \end{bmatrix} \qquad \ldots (A.4.2)$$

By transforming the above original phase values into symmetrical component forms we have:

$$\begin{bmatrix} i_{co}' \\ i_{c1}' \\ i_{c2}' \end{bmatrix} = \begin{bmatrix} jwC_{gt} & 0 & 0 \\ 0 & jwC_{gt} & 0 \\ 0 & 0 & jwC_{gt} \end{bmatrix} \begin{bmatrix} v_{mo}' \\ v_{m1}' \\ v_{m2}' \end{bmatrix} \qquad \ldots (A.4.3)$$

Transformation of equation A.4.3 into the frequency domain is affected by noting that the Fourier Transform of a function of time $f(t) = f_1(p).f_2(t)$ is given by:

$$f(jw) = f_1(jw).f_2(jw)$$

where:

$$f_2(jw) = \int_{-\infty}^{\infty} f_2(t).\exp(-jwt).dt \qquad \ldots (A.4.4)$$

It follows that equation A.4.3 transforms to:

$$\begin{bmatrix} i_{co}'(jw) \\ i_{c1}'(jw) \\ i_{c2}'(jw) \end{bmatrix} = \begin{bmatrix} jwC_{gt} & 0 & 0 \\ 0 & jwC_{gt} & 0 \\ 0 & 0 & jwC_{gt} \end{bmatrix} \begin{bmatrix} v_{mo}'(jw) \\ v_{m1}'(jw) \\ v_{m2}'(jw) \end{bmatrix} \qquad \ldots (A.4.5)$$

Frequency-shifted variables are easily obtained by replacing w by $w \pm w_o$ in equation A.4.5 as appropriate. The final form of the equation (omitting the trapped zero sequence component) relating to shifted variables is therefore given as equation A.4.6.

$$\begin{bmatrix} i_{c1}'[j(w+w_o)] \\ i_{c2}'[j(w-w_o)] \end{bmatrix} \xleftarrow{\qquad\qquad} = \begin{bmatrix} j(w+w_o)C_{gt} & 0 \\ 0 & j(w-w_o)C_{gt} \end{bmatrix} \begin{bmatrix} v_{m1}'[j(w+w_o)] \\ v_{m2}'[j(w-w_o)] \end{bmatrix}$$

$$\xrightarrow{\qquad [yc] \qquad}$$

$$\ldots (A.4.6)$$

The total currents is the sum of the machine terminal currents and that provided by the capacitive transference, i.e.

$$\begin{aligned} i_{mc1}'[j(w+w_o)] &= i_{m1}'[j(w+w_o)] + i_{c1}'[j(w+w_o)] \\ i_{mc2}'[j(w-w_o)] &= i_{m2}'[j(w-w_o)] + i_{c2}'[j(w-w_o)] \end{aligned} \qquad \ldots (A.4.7)$$

With reference to equation (5.30) we have:

$$\begin{bmatrix} i_{m1}'[j(w+w_o)] \\ i_{m2}'[j(w-w_o)] \end{bmatrix} = [y_m] \begin{bmatrix} v_{m1}'[j(w+w_o)] \\ v_{m2}'[j(w-w_o)] \end{bmatrix}$$

where:

$$[y_m] = 1/z^2 \begin{bmatrix} -[R+j(w-w_o)L_1(jw)] & j(w+w_oL_2(jw).\exp(j2\lambda) \\ j(w-w_o)L_2(jw).\exp(-j2\lambda) & -[R+j(w+w_o)L_1(jw)] \end{bmatrix}$$

With regard to equation A.4.7, the total current is as follows:

$$\begin{bmatrix} i_{mc_1}'[j(w+w_o)] \\ i_{mc_2}'[j(w-w_o)] \end{bmatrix} = [y_{mc}] \begin{bmatrix} v_{m_1}'[j(w+w_o)] \\ v_{m_2}'[j(w-w_o)] \end{bmatrix}$$

where:

$$[ym_c] = [y_m] + [y_c] =$$

$$\begin{bmatrix} -[R+j(w-w_o)L_1(jw)]/z^2+j(w+w_o)C_{gt} & j(w+w_o)L_2(jw).\exp(j2\lambda)/z^2 \\ j(w-w_o)L_2(jw).\exp(-j2\lambda)/z^2 & -[R+j(w+w_o)L_1(jw)]/z^2+j(w-w_o)C_{gt} \end{bmatrix}$$

. . (A.4.8)

A.4.4 Equations at star-side of the transformer

The capacitive transferred current at each shunt capacitance bank on the star-side is as follows:

$$\begin{aligned} i_{sca}' &= jwC_t.v_{sa}' \\ i_{scb}' &= jwC_t.v_{sb}' \\ i_{scc}' &= jwC_t.v_{sc}' \end{aligned} \quad \text{. . (A.4.9)}$$

and in a matrix form:

$$\begin{bmatrix} i_{sca}' \\ i_{scb}' \\ i_{scc}' \end{bmatrix} - \begin{bmatrix} jwC_t & 0 & 0 \\ 0 & jwC_t & 0 \\ 0 & 0 & jwC_t \end{bmatrix} \begin{bmatrix} v_{sa}' \\ v_{sb}' \\ v_{sc}' \end{bmatrix} \qquad \ldots(A.4.10)$$

Equation A.4.10 can be transformed into symmetrical components by applying appropriate transformation from original phase values to symmetrical components. Thus with reference to equation A.4.4, in the frequency domain we have:

$$\begin{bmatrix} i_{sco}'(jw) \\ i_{sc_1}'(jw) \\ i_{sc_2}'(jw) \end{bmatrix} - \begin{bmatrix} jwC_t & 0 & 0 \\ 0 & jwC_t & 0 \\ 0 & 0 & jwC_t \end{bmatrix} \begin{bmatrix} v_{so}'(jw) \\ v_{s_1}'(jw) \\ v_{s_2}'(jw) \end{bmatrix} \qquad \ldots(A.4.11)$$

The frequency shifted variables can be obtained by replacing w by $w \pm w_o$ in equation A.4.11 as appropriate, and we have:

$$i_{sco}'(jw) = jwC_t . v_{so}'(jw)$$

$$\xleftarrow{\qquad\qquad\qquad\qquad}$$

$$\begin{bmatrix} i_{sc_1}'[j(w+w_o)] \\ i_{sc_2}'[j(w-w_o)] \end{bmatrix} - \begin{bmatrix} j(w+w_o)C_t & 0 \\ 0 & j(w-w_o)C_t \end{bmatrix} \begin{bmatrix} v_{s_1}'[j(w+w_o)] \\ v_{s_2}'[j(w-w_o)] \end{bmatrix}$$

$$\xrightarrow{\qquad [yc'] \qquad}$$

$$\ldots(A.4.12)$$

The total currents at the star-side of the transformer are the sum of the capacitive current and that through the transformer, i.e.

$$\begin{aligned} i_{scco}'(jw) &= i_{so}'(jw) + i_{sco}'(jw) \\ i_{scc_1}'[j(w+w_o)] &= i_{s_1}'[j(w+w_o)] + i_{sc_1}'[j(w+w_o)] \\ i_{scc_2}'[j(w-w_o)] &= i_{s_2}'[j(w-w_o)] + i_{sc_2}'[j(w-w_o)] \end{aligned} \qquad \ldots(A.4.13)$$

Using equation (5.18a), (5.32) and A.4.12 in conjunction with A.4.13 gives:

$$i_{scco}'(jw) = [-1/(r_t+jwL_t) + jwC_t].v_{so}'(jw)$$

$$\begin{bmatrix} i_{scc_1}'[j(w+w_o)] \\ i_{scc_2}'[j(w-w_o)] \end{bmatrix} = [YT_{21}] \begin{bmatrix} v_{m_1}'[j(w+w_o)] \\ v_{m_2}'[j(w-w_o)] \end{bmatrix} + [Y_{T22}+y_c'] \begin{bmatrix} v_{s_1}'[j(w+w_o)] \\ v_{s_2}'[j(w-w_o)] \end{bmatrix}$$

. .(A.4.14)

APPENDIX 5

EVALUATION OF SUPERIMPOSED VOLTAGES AND CURRENTS AT FAULT POINT

In addition to the relations which exist between the voltages and currents at sending and receiving ends with those at the fault point, these voltages and currents as have been considered in chapter 5 are also related to source impedances by:

$$v_{so}'(jw) = -(r_t+jwL_t)\,i_{so}'(jw) \qquad \text{(a)}$$

$$\begin{bmatrix} v_{s_1}'[j(w+w_o)] \\ v_{s_2}'[j(w-w_o)] \end{bmatrix} = -[z_{ss}]_{12} \begin{bmatrix} i_{s_1}'[j(w+w_o)] \\ i_{s_2}'[j(w-w_o)] \end{bmatrix} \qquad \text{(b)}$$

. . (A.5.1)

Also for a simple source model at receiving end we have:

$$v_{ro}'(jw) = (z_{sro})\,i_{ro}'(jw) \qquad \text{(a)}$$

$$\begin{bmatrix} v_{r_1}'[j(w+w_o)] \\ v_{r_2}'[j(w-w_o)] \end{bmatrix} = [z_{sr}]_{12} \begin{bmatrix} i_{r_1}'[j(w+w_o)] \\ i_{r_2}'[j(w-w_o)] \end{bmatrix} \qquad \text{(b)}$$

. . (A.5.2)

Substituting these two equations into equations (8.3) and (8.4), the symmetrical component values of superimposed voltages and currents can be obtained as follows:

For zero sqeuence components from equation (8.3a) we have:

$$e_{ffo}'(jw) = A_{\ell 10} \cdot v_{so}'(jw) - B_{\ell 10} \cdot i_{so}'(jw)$$

which, by replacing $v_{so}'(jw)$ from A.5.1a then becomes:

$$e_{ffo}'(jw) = -A_{\ell 10}(r_t+jwL_t) i_{so}'(jw) - B_{\ell 10} \cdot i_{so}'(jw) =$$
$$-[A_{\ell 10}(r_t+jwL_t)+B_{\ell 10}] i_{so}'(jw) \quad \ldots (A.5.3)$$

Also, from equation (8.3a) for the current we have:

$$-i_{fso}'(jw) = C_{\ell 10} \cdot v_{so}'(jw) - A_{\ell 10} \cdot i_{so}'(jw) =$$
$$= -[C_{\ell 10}(r_t+jwL_t) + A_{\ell 10}] i_{so}'(jw)$$
$$\ldots (A.5.4)$$

Substituting equation A.5.3 into equation A.5.4 then gives:

$$i_{fso}'(jw) = -[C_{\ell 10} \cdot (r_t+jwL_t)+A_{\ell 10}] \cdot [A_{\ell 10} \cdot (r_t+jwL_t)+B_{\ell 10}]^{-1} e_{ffo}'(jw)$$
$$\ldots (A.5.5)$$

Zero sequence components at the receiving end can be obtained by using equation (8.4a):

$$e_{ffo}'(jw) = A_{\ell 20} \cdot v_{ro}'(jw)+B_{\ell 20} \cdot i_{ro}'(jw)$$
$$i_{fro}'(jw) = C_{\ell 20} \cdot V_{ro}'(jw)+A_{\ell 20} \cdot i_{ro}'(jw)$$

By applying equation A.5.2a, here gives:

$$e_{ffo}'(jw) = [A_{\ell 20} \cdot z_{sro}+B_{\ell 20}] \cdot i_{ro}'(jw)$$
$$i_{fro}'(jw) = [C_{\ell 20} \cdot z_{sro}+A_{\ell 20}] i_{ro}'(jw) \quad \ldots (A.5.6)$$

Finally, we have:

$$i_{fro}'(jw) = [C_{\ell 20} \cdot z_{sro} + A_{\ell 20}] \cdot [A_{\ell 20} \cdot z_{sro} + B_{\ell 20}]^{-1} e_{ffo}'(jw) \quad \text{. . (A.5.7)}$$

The positive and negative sequence components at the two ends can be obtained by the same procedure as follows:

From equation (8.3b) we can have:

$$\begin{bmatrix} e_{ff_1}'[j(w+w_o)] \\ e_{ff_2}'[j(w-w_o)] \end{bmatrix} = [A_{\ell 112}] \begin{bmatrix} v_{s_1}'[j(w+w_o)] \\ v_{s_2}'[j(w-w_o)] \end{bmatrix} + [B_{\ell 112}] \begin{bmatrix} -i_{s_1}'[j(w+w_o)] \\ -i_{s_2}'[j(w-w_o)] \end{bmatrix}$$

$$\begin{bmatrix} -i_{fs_1}'[j(w+w_o)] \\ -i_{fs_2}'[j(w-w_o)] \end{bmatrix} = [C_{\ell 112}] \begin{bmatrix} v_{s_1}'[j(w+w_o)] \\ v_{s_2}'[j(w-w_o)] \end{bmatrix} + [A_{\ell 112}] \begin{bmatrix} -i_{s_1}'[j(w+w_o)] \\ -i_{s_2}'[j(w-w_o)] \end{bmatrix}$$

Substituting $v_{s_1}[j(w+w_o)]$ and $v_{s_2}[j(w-w_o)]$ from equation A.5.1 into these two equations gives:

$$\begin{bmatrix} e_{ff_1}'[j(w+w_o)] \\ e_{ff_2}'[j(w-w_o)] \end{bmatrix} = -[A_{\ell 112}][z_{ss}] \begin{bmatrix} i_{s_1}'[j(w+w_o)] \\ i_{s_2}'[j(w-w_o)] \end{bmatrix} - [B_{\ell 112}] \begin{bmatrix} i_{s_1}'[j(w+w_o)] \\ i_{s_2}'[j(w-w_o)] \end{bmatrix}$$

$$= -\left[[A_{\ell 112}][z_{ss}] + [B_{\ell 112}] \right] \begin{bmatrix} i_{s_1}'[j(w+w_o)] \\ i_{s_2}'[j(w-w_o)] \end{bmatrix} \quad \text{. . (A.5.8)}$$

$$\begin{bmatrix} -i_{fs_1}'[j(w+w_o)] \\ -i_{fs_2}'[j(w-w_o)] \end{bmatrix} = -[C_{\ell 112}][z_{ss}] \begin{bmatrix} i_{s_1}'[j(w+w_o)] \\ i_{s_2}'[j(w-w_o)] \end{bmatrix} - [A_{\ell 112}] \begin{bmatrix} i_{s_1}'[j(w+w_o)] \\ i_{s_2}'[j(w-w_o)] \end{bmatrix}$$

$$= -\left[[C_{\ell 112}][z_{ss}] + [A_{\ell 112}] \right] \begin{bmatrix} i_{s_1}'[j(w+w_o)] \\ i_{s_2}'[j(w-w_o)] \end{bmatrix} \quad \text{. . (A.5.9)}$$

Substituting i_{s_1}' and i_{s_2}' from equation A.5.8 into equation A.5.9 gives:

$$\begin{bmatrix} i_{fs_1}'[j(w+w_o)] \\ i_{fs_2}'[j(w-w_o)] \end{bmatrix} = -\left[[C_{\ell_{112}}][z_{ss}]+[A_{\ell_{112}}]\right] \cdot \left[[A_{\ell_{112}}][z_{ss}]+[B_{\ell_{112}}]\right]^{-1} \begin{bmatrix} e_{ff_1}'[j(w+w_o)] \\ e_{ff_2}'[j(w-w_o)] \end{bmatrix} \quad \ldots (A.5.10)$$

A similar procedure can be applied for calculating the receiving end superimposed voltages and currents:

$$\begin{bmatrix} i_{fr_1}'[j(w+w_o)] \\ i_{fr_2}'[j(w-w_o)] \end{bmatrix} = \left[[C_{\ell_{212}}][z_{sr}]+[A_{\ell_{212}}]\right] \cdot \left[[A_{\ell_{212}}][z_{sr}]+[B_{\ell_{212}}]\right]^{-1} \begin{bmatrix} e_{ff_1}'[j(w+w_o)] \\ e_{ff_2}'[j(w-w_o)] \end{bmatrix} \quad \ldots (A.5.11)$$

APPENDIX 6

OPENING AND CLOSING BREAKER SIMULATION

The basis of the method for obtaining the steady-state response of the full system model of Figure 8.1 is expressed in Appendix A5 and this will not be considered here.

The standard superimposed circuit of the full system model of Figure 8.1 is represented by the circuit of Figure 8.17. The basic relationships of equation A.6.1 and A.6.2, with reference to Figure 8.17, are seen to describe the circuit at each end of the line and fault point respectively. Furthermore, the line sections on each side of the fault are most conveniently represented in terms of the polyphase 2-port of A,B,C,D parameters defined in equation A.6.3 and A.6.4.

$$[v_s']_{012} = -[z_{ss}][i_s']_{012} - [E_s]_{012} \quad \ldots (A.6.1)$$

$$[v_r']_{012} = [z_{sr}][i_r']_{012} + [E_r]_{012} \quad \ldots (A.6.2)$$

$$[v_{ff}']_{012} = [e_{ff}']_{012} \text{ (for solid fault)}$$

With reference to equation (8.3) it follows that:

$$\begin{bmatrix} v_{so}'(jw) \\ v_{s_1}'[j(w+w_o)] \\ v_{s_2}'[j(w-w_o)] \\ i_{so}'(jw) \\ i_{s_1}'[j(w+w_o)] \\ i_{s_2}'[j(w-w_o)] \end{bmatrix} = \begin{bmatrix} A_1 & & B_1 \\ & & \\ & & \\ & & \\ & & \\ C_1 & & D_1 \end{bmatrix} \cdot \begin{bmatrix} v_{ffo}'(jw) \\ v_{ff_1}'[j(w+w_o)] \\ v_{ff_2}'[j(w-w_o)] \\ i_{fso}'(jw) \\ i_{fs_1}'[j(w+w_o)] \\ i_{fs_2}'[j(w-w_o)] \end{bmatrix}$$

. . (A.6.3)

where:

$$A_1 = \begin{bmatrix} A_{\ell_{10}} & 0 & 0 \\ 0 & A_{\ell_{111}} & 0 \\ 0 & 0 & A_{\ell_{122}} \end{bmatrix} \qquad B_1 = \begin{bmatrix} B_{\ell_{10}} & 0 & 0 \\ 0 & B_{\ell_{111}} & 0 \\ 0 & 0 & B_{\ell_{122}} \end{bmatrix}$$

$$C_1 = \begin{bmatrix} C_{\ell_{10}} & 0 & 0 \\ 0 & C_{\ell_{111}} & 0 \\ 0 & 0 & C_{\ell_{122}} \end{bmatrix} \qquad D_1 = A_1$$

Moreover, with regard to equation (8.4) it follows that:

$$\begin{bmatrix} v_{ffo}'(jw) \\ v_{ff_1}'[j(w+w_o)] \\ v_{ff_2}'[j(w-w_o)] \\ i_{fro}'(jw) \\ i_{fr_1}'[j(w+w_o)] \\ i_{fr_2}'[j(w-w_o)] \end{bmatrix} = \begin{bmatrix} A_2 & & B_2 \\ & & \\ & & \\ & & \\ & & \\ C_2 & & D_2 \end{bmatrix} \cdot \begin{bmatrix} v_{ro}'(jw) \\ v_{r_1}'[j(w+w_o)] \\ v_{r_2}'[j(w-w_o)] \\ i_{ro}'(jw) \\ i_{r_1}'[j(w+w_o)] \\ i_{r_2}'[j(w-w_o)] \end{bmatrix}$$

. . (A.6.4)

where:

$$A_2 = \begin{bmatrix} A_{\ell 20} & 0 & 0 \\ 0 & A_{\ell 211} & 0 \\ 0 & 0 & A_{\ell 222} \end{bmatrix} \qquad B_2 = \begin{bmatrix} B_{\ell 20} & 0 & 0 \\ 0 & B_{\ell 211} & 0 \\ 0 & 0 & B_{\ell 222} \end{bmatrix}$$

$$C_2 = \begin{bmatrix} C_{\ell 20} & 0 & 0 \\ 0 & C_{\ell 211} & 0 \\ 0 & 0 & C_{\ell 222} \end{bmatrix} \qquad D_2 = A_2$$

Here, $A_{\ell 10}$, $B_{\ell 10}$, $C_{\ell 10}$, $A_{\ell 111}$, $B_{\ell 111}$, . . . and $A_{\ell 20}$, $B_{\ell 20}$, $C_{\ell 20}$, $A_{\ell 211}$, $B_{\ell 211}$, $C_{\ell 211}$, . . . etc., are the line parameters from sending and receiving ends to fault point which has been defined previously in chapter 5.

The four foregoing relationships effectively define a set of simultaneous equations relating the superimposed circuit currents to the associated voltages and this can be shown in the alternative form as follows:

$$\begin{bmatrix} [i_f']_{012} \\ [i_s']_{012} \\ [i_r']_{012} \end{bmatrix} = \begin{bmatrix} Y_1 & Y_2 & Y_3 \\ Y_4 & Y_5 & Y_6 \\ Y_7 & Y_8 & Y_9 \end{bmatrix} \begin{bmatrix} [E_{ff}']_{012} \\ [E_s']_{012} \\ [E_r']_{012} \end{bmatrix} \qquad \ldots (A.6.5)$$

where $i_f = i_{fs} - i_{fr}$ (with regard to the direction shown in Figure 8.17) and $[E_{ff}]_{012} = [V_{ff}]_{012}$. Each submatrix in the admittance relationship of equation A.6.5 is defined in terms of the basic parameters (A_1, B_1, C_1, ... , z_{ss}, z_{sr}, etc.) of the system at any spectral frequency interest as follows:

$$Y_1 = -([(z_{ss}D_1+B_1)^{-1}(A_1+z_{ss}C_1)+(z_{sr}.D_2+B_2)^{-1}(A_2+z_{sr}.C_2)])$$

$$Y_2 = -[z_{ss}D_1-B_1]^{-1}$$

$$Y_3 = [z_{sr}D_2+B_2]^{-1}$$

$$Y_4 = -([z_{ss}+B_1D_1^{-1}]^{-1}\ [A_1 - B_1D_1^{-1}\ C_1])$$

$$Y_5 = -[z_{ss}+B_1D_1^{-1}]$$

$$Y_6 = 0.0$$

$$Y_7 = [(z_{sr}+B_2D_2^{-1})^{-1} (A_2-B_2D_2^{-1} C_2)]$$

$$Y_8 = 0.0$$

$$Y_9 = -(z_{sr}+B_2D_2^{-1})^{-1}$$

It is evident that each of the above submatrices within the whole is a 3x3 matrix and can be obtained by the convenient substitution between equations A.6.1,2,3,4 and that each subvector (E_f, i_f, etc) is a 3x1 column vector representing the voltage or current of individual symmetrical component sequence values, e.g.

$$[E_{ff'}]_{012} = [e_{ff_0'} e_{ff_1'} e_{ff_2'}]$$

The 9x9 admittance matrix of equation A.6.5 is essentially a universal relationship which can be computed and stored at all spectra frequencies of interest at the outset of a particular simulation study. As such, it enables a solution to any of the superimposed circuit models to be obtained in a specially economic manner from a digital processing point of view.

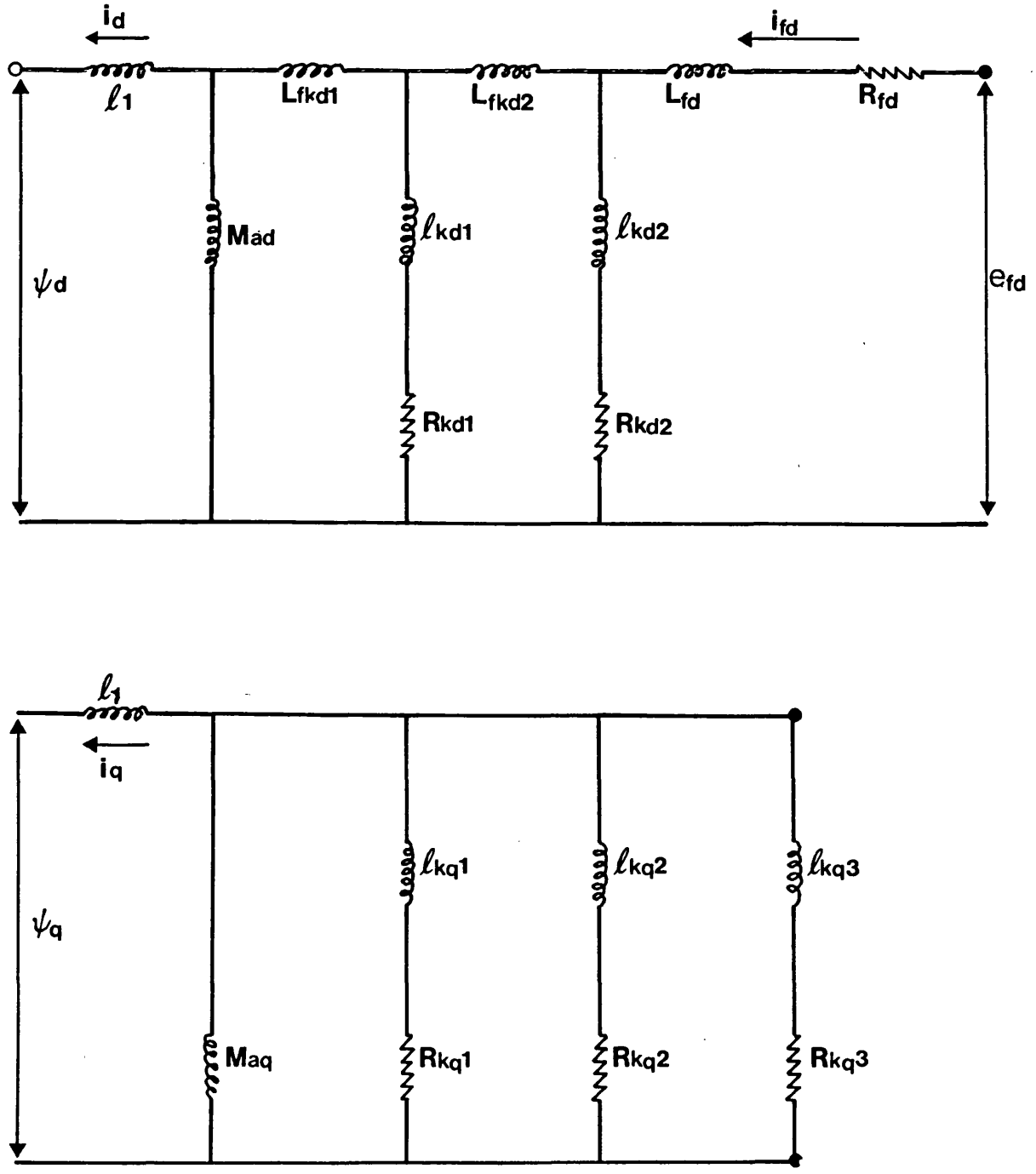

Fig. A-2.1 Structure of the More Complex Model for Representation of the Synchronous Machine

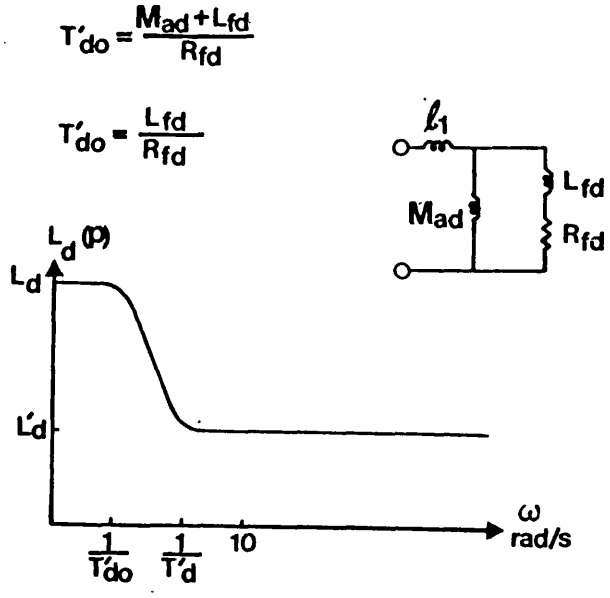

Figure A-3.1

Direct Axis Operational Inductance and Equivalent Circuit for a Machine With a Laminated Rotor and No Damper Winding

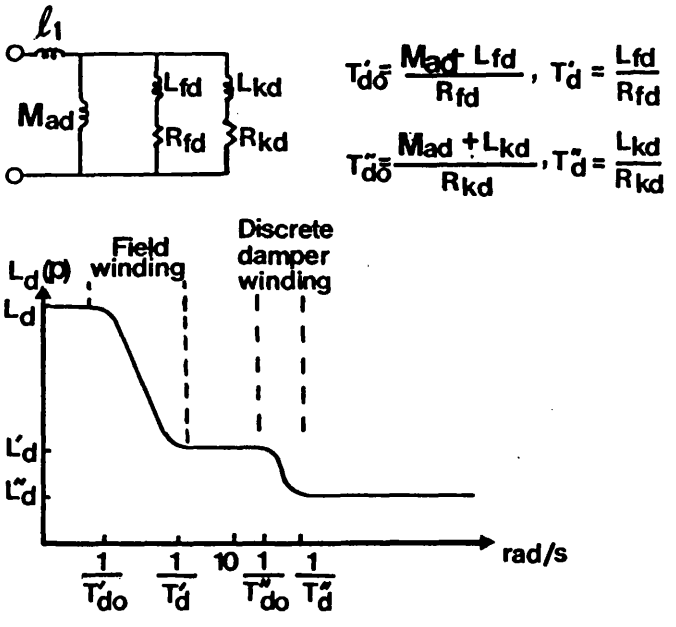

Figure A-3.2

Direct Axis Operational Inductance and Equivalent Circuit for a Machine with a Laminated Rotor and One Discrete Damper Winding

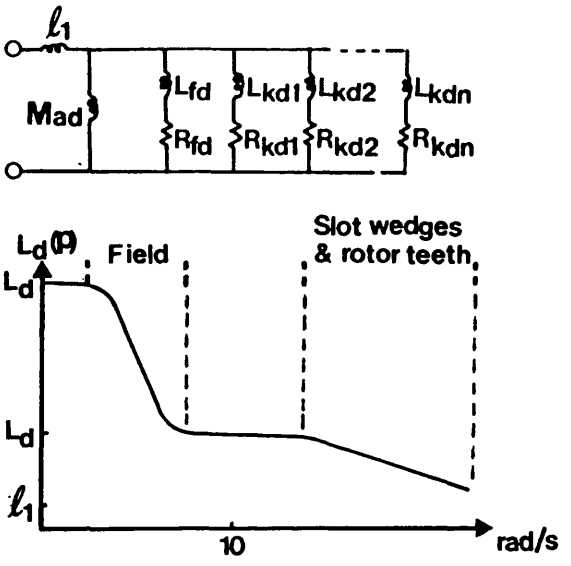

Figure A-3.3

Direct Axis Operational Inductance and Equivalent Circuit for a Turbogenerator with a High Resistance Damper Structure

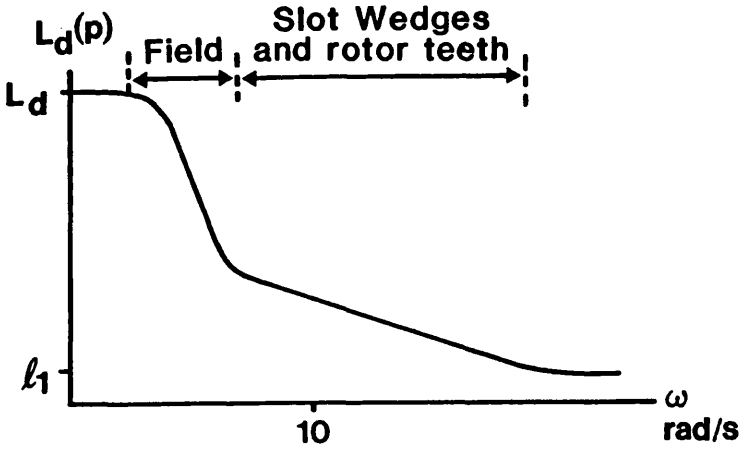

Figure A-3.4 Direct axis operational inductance for a turbogenerator with low resistance damper structure.

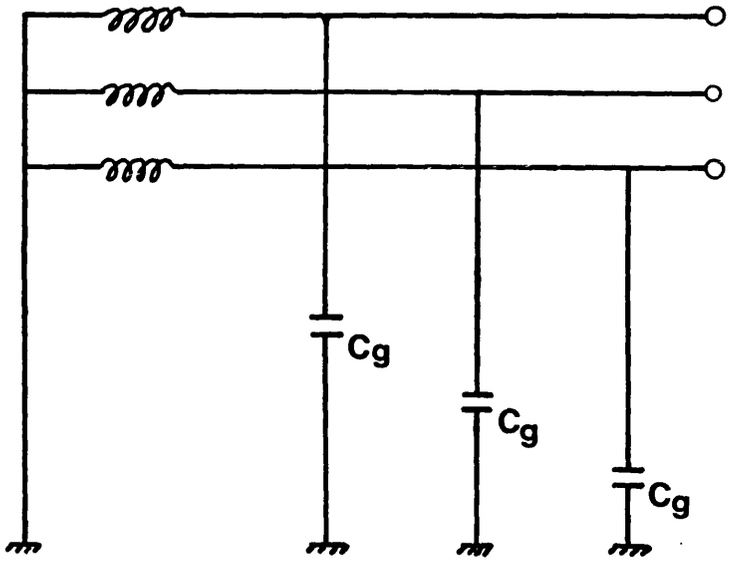

Fig. A-4.1 Generator Equivalent Circuit

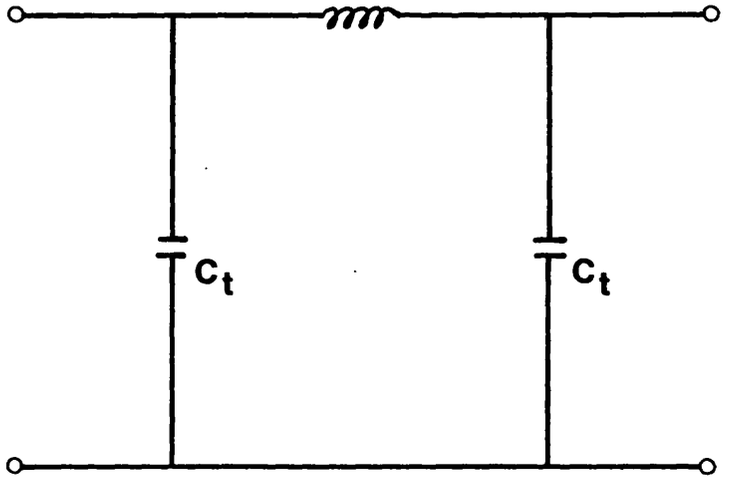

Fig. A-4.2 Transformer Equivalent Circuit

REFERENCES

1. PARK, R.H.: "Tow-reaction theory of synchronous machines generalised method of analysis - part I", AIEE Trans, Vol.48, No.2, pp716-730, 1929.

2. DOHERTY, R.E. and NICKLE, C.A.: "Synchronous machines - parts I and II", AIEE Trans., Vol.45, pp912-947, 1926.

3. CLARKE, E.: "Circuit analysis of AC power system, I and II", John Wiley & Sons Inc., New York, 1950.

4. FORTESCUE, C.L.: "Methods of symmetrical co-ordinates applied to the solution of polyphase networks", AIEE Trans., Vol.137, pp1027-1115, 1918.

5. KU, Y.H.: "Transient analysis of AC machinery", AIEE Trans., Vol.48, pp707-715, 1929.

6. KIMBARK, E.W.: "Power system stability, vol.III", John Wiley & Sons Inc., New York, 1956.

7. ADKINS, B.: "Transient theory of synchronous generator connected to power systems", Proc.IEE, Vol.98, No.2, pp510-523, 1951.

8. RAFIAN, M. and LAUGHTON, M.A.: "Determination of synchronous machine phase co-ordinate parameter", Proc.IEE, Vol.123, No.8, 1976, pp818-824.

9. CRARY, S.B. and DUNGAN, W.E.: "Amortisseur windings for

hydrogenerator", Electrical World, Vol.115, pp.2204-2206, 1941.

10. KU, Y.H.: "Electric energy conversion", The Ronald Press Co., New York, 1959.

11. LEWISE, W.P.: "Solution of network transients using symmetrical components techniques", Proc.IEE, Vol.113, No.12, pp2012-2016, 1966.

12. CONCORDIA, C.: "Synchronous machine", John Wiley & Sons Inc., New York, 1951.

13. ADKINS, B.: "The general theory of electrical machines", John Wiley & Sons Inc. New York, 1962.

14. CONCORDIA, C.: "Relations among transformations used in electrical engineering problems", General Electric Review, pp323-325, 1938.

15. JOHNS, A.T. and AGGARWAL, R.K.: "Digital simulation of faulted ehv transmission lines with particular reference to very high speed protection", Proc.IEE, Vol.123, No.4, pp353-359, 1976.

16. BICKFORD, J.P., SANDERSON, J.V.H., ABDELSALEM, M.M., MOHAMED, S.E.T., MORAIS, S.A. and OLIPADE, O.: "Developments in the calculation of waveforms and frequency spectra for transient fault currents and voltages", Proc.IEE, Vol.127, Pt.C, No.3, pp145-152, 1980.

17. DAY, S.J., MULLINEUX, N. and REED, J.R.: "Development in obtaining transient response using Fourier Transform: Gibbs phenomena on Fourier integral", Int.J.Electric Eng.Edu., 3, pp501-506, 1965.

18. DAY, S.J., MULLINEUX, N. and REED, J.R.: "Development in obtaining transient response using Fourier Transform: use of the modified Fourier Transform", Int.J.Electric Eng Edu., Vol.4, pp31-40, 1966.

19. BICKFORD, J.P., MULLINEUX, N. and REED, J.R.: "Computation of power system transients", IEE Monograph Series 18, Peter Peregrinus Ltd., 1980.

20. IEEE Task Force: "Supplementary definitions and associated test methods for obtaining parameters for synchronous machine stability study simulation", IEEE Trans., PAS-99, pp1625-1633, 1980.

21. BRACEWELL, R.M.: The Fourier Transform and its applications", McGraw Hill, 1965.

22. DANDENO, P.L. and KUNDUR, P.: "Stability performance of 555 MVA turboalternators digital comparisons with system operating tests", IEEE Power Apparatus and System, Vol.93, No.3, pp767-776, 1974.

23. DANDENO, P.L., KUNDUR, P. and PORAY, A.T.: "Recent trends in the analysis and measurement of synchronous machine stability constants", PSCC, England, pp834-842, 1978.

24. SHACKSHAFT, G.: "Generator parameters for stability studies", Cigre, Paper 32-15, 1976.

25. SHACKSHAFT, G. and PORAY, A.T.: "Implementation of new approach to determination of synchronous machine parameters from test", Proc.IEE, Vol.124, No.12, pp1170-1178, 1977.

26. DANDENO, P.L. and PORAY, A.T.: "Development of detailed turbogenerator equivalent circuits from standstill frequency response measurements", IEEE Trans on Power Apparatus and System, Vol.PAS-100, No.4, pp1646-1655, 1981.

27. CHARLTON, A. and SHACKSHAFT, G.: "Comparison of accuracy of methods for studying stability. North-fleet exercise", Electra, No.23, pp9-49, 1972.

28. DANDENO, P.L., HAUTH, R.L. and SCHULZ, R.P.: "Effects of synchronous machine modelling in large scale system studies", IEEE Trans., PAS-92, pp574-582, 1973.

29. COULTES, M.E., DANDENO, P.L., et al: "Determination of synchronous machine stability study constants", Final Report EPRI-EL-1424, Vol.2, 1980.

30. SHACKSHAFT, G. and HENSER, P.B.: "Model of generator saturation for use in power system studies" Proc.IEE, Vol.126, No.8, pp759-763, 1979.

31. LI, K.K.: "The parameters of transformer windings for surge distribution purpose", MSc, Dissertation, UMIST, 1971.

32. LAUGHTON, M.A.: "Analysis of unbalanced polyphase networks by the method of phase co-ordinates, part I, system representation in phase frame of reference", Proc.IEE, Vol.115, No.8, pp1163-1172, 1968.

33. LAUGHTON, M.A.: "Analysis of unbalanced polyphase networks by the method of phase co-ordinates, part II, fault analysis", Proc.IEE, Vol.116, pp857-865, 1969.

34. WEDEPOHL, LM.M: "Application of matrix methods to the solution of travelling-wave phenomena in polyphase system", Proc.IEE, Vol.110, No.12, pp2200-2212, 1963.

35. GALLOWAY, R.H., SHORROCKS, W.B. and WEDEPOHL, L.M.: "Calculation of electrical parameters for short and long polyphase transmission lines", ibid, Vol.111, No.12, pp2051-2059, 1964.

36. SLEMON, G.R., ROBERTSON, S.D.T. and RAMAMOORTY, M.: "High speed protection of power system based on improved power system models:, CIGRE, Paris, Paper 31-09, 1968.

37. WEDEPOHL, L.M.: "Electrical characteristics of polyphase transmission systems with special reference to boundary value calculations at power line carrier frequency", Proc.IEE, Vol.112, No.111, pp2103-2112, 1965.

38. JOHNS, A.T. and EL-KATIB, M.M.T.: "Developments in technique for simulating faults in ehv transmission systems", Proc.IEE, Vol.125, No.3, pp221-229, 1978.

39. URAM, R. and MILLER, R.W.: "Mathematical analysis and solution of transmission-line transients, I - theory", Trans.IEEE, PAS, Vol.83, pp1116-1123, 1964.

40. SCOTT-MAYER, W. and DOMMEL, H.W.: "Numerical modelling of frequency-dependent-line parameters in an electromagnetic transient program", IEEE PAS, pp1401-1409, 1974.

41. JOHNS, A.T. and AGGARWAL, R.K.: "Performance of high speed distance

relays with particular reference to travelling wave effects", Proc.IEE, Vol.124, No.7, pp639-646, 1977.

42. HALL, J.E., CARE, J.M. and LIGHT, B.R.: "Developments in CEGB system requirements for protection", IEE Conf.Publ. 125, pp1-10, 1975.

43. EL-KATIB, M.M.T. and JOHNS, A.T.: "Frequency-domain digital simulation of synchronous generators operating under faulted conditions", Proc.IEE, Vol.124, No.3, pp223-228, 1977.

44. COX, M.G. and HAYES, J.G.: "Curve fitting: a guide and suite of algorithms for the non-specialist user", NPL Report NAC 26, 1973, amended 1979.

45. HAYES, J.G.: "Numerical methods for curve and surface fitting", Bull.Inst.Math.Applcs., Vol.10, pp144-152, 1974.

46. HURLEY, J.D. and SCHWENK, H.R.: "Standstill frequency repsonse modelling and evaluation by field tests on 645 MVA turbogenerator", IEEE Trans. on Power Apparatus and System, Vol.PAS-100, No.2, pp828-836, 1981.

47. COULTS, M.E.: "Standstill frequency response tests", IEEE Trans., pp26-30, 1983.

48. SHACKSHAFT, G.: "New approach to determination of synchronous machine parameters from test", Proc.IEE, Vol.121, No.11, pp1385-1392, 1974.

49. SHACKSHAFT, G. and NEILSON, R.: "Results of stability tests on underexcited 120MW generator", Proc.IEE, Vol.110, No.2, pp175-188, 1972.

50. DWEK, M.G. and PAC SOO M.F.: "The derivation of 50Hz and high frequency parameters of supergrid transformers from low voltage injection test measurements", Sixth Universities Power Engineering Conference, UMIST, 1971.

51. GOSLAND, L.: "Restriking-voltage characteristics under various fault conditions at typical points on the network of a large city supply authority", Journal IEE, Vol.86, pp248-274, 1940.

52. GREENWOOD, A.: "Electrical transients in power system", John Wiley & Sons Inc., New York, 1971.

53. ADJOYE, R.E. and CORNICK, K.J.: "Distributon of switching surges in the line-end coils of cable-connected motors", Electric Power Applications, Vol.2, No.1, pp11-21, 1979.

54. WHITE, E.L.: "Surge-transference characteristics of generator/transformer installations", Proc.IEE, Vol.116, No.4, pp575-587, 1969.

55. HICKLING, G.H. and WINDER, A.I.: "Surge transfer through transformer/generator units", Proc.IEE, Vol.116, No.5, pp788-800, 1969.

56. HELLER, B. and VEVERKA, A.: "Surge phenomena in electrical machines", English translation edited by Vosper, J.S., London, Iliffe Books Ltd., 1968.

57. OWEN, R.E. and LEWISE, W.A.: "Asymmetry characteristic of progressive short-circuit on large synchronous generators", IEEE Trans. on Power Apparatus and Systems, Vol.PAS-90, No.2, pp587-596, 1971.

58. CANAY, M. and WERREN, L.: "Interrupting sudden asymmetric short-circuit currents without zero transition", Brown Boverie Review, 1969.

59. CANAY, M. and KLEIN, H.: "Asymmetric short-circuit currents from generators and the effect of the breaking arc", Brown Boverie Review, 1974.

60. HINDMARSH, J.: "Electrical machines and their applications", Pergamon Press, UK, 1984.

61. HARRIS, M.R., BAYINDIER, N.S. and JACK, A.G.: "Standstill micromachine for turbogenerator parameter studies", Proc.IEE, Vol.134, Pt.C, No.2, pp104-115, 1987.

62. RAMAMOORTY, M.: "Approximate method for including ground effects in wave propagation on transmission lines", Proc.IEE, Vol.120, No.6, pp702-703, 1973.

63. BARRET, P.G. and ROQUEFORT, Y.M.: "Calculation and measurement of frequency response of large turbogenerators in the presence of small disturbances", IEEE Trans., PAS, Vol.92, pp1348-1357, 1973.

64. ROQUEFORT, Y.M.: "Large turbogenerators electric model on-line identification", Fifth Power System Conference, Churchill College, Cambridge, 1975.

65. SRIHARAN, S. and KOH WEE HI ONG: "Synchronous machine modelling by standstill frequency response tests", IEE Trans. on Energy Conversion, Vol.EC-2, No.2, 1987.

66. COOLEY, J. and TUKEY, J.: "An algorithm for the machine calculation of complex Fourier series", Math. of Comput., Vol.19, pp297-301, 1965.

67. BICKFORD, J.P. and ABDEL-RAHMAN, M.H.: "Application of travelling-wave methods to the calculation of transient fault currents and voltages in power system networks", Proc.IEE, Vol.127, Pt.C, No.3, 1980.

68. JOHNS, A.T. and AGGARWAL, R.K.: "Digital simulation of fault autoreclosure sequences with particular reference to the performance evaluation of protection for ehv transmission lines", Proc.IEE, Vol.128, Pt.C, No.4, pp183-195, 1981.

69. WARRINGTON, A.R. VANC.: "Protective relays - their theory and practice", Volume One, London: Chapman & Hall, 1962.

70. WARRINGTON, A.R. VANC.: "Protective relays - their theory and practrice", Volume Two, London: Chapman & Hall, 1969.

71. BARBER, M.D. and GIANNINI, M.: "Simulation of a synchronous generator connected via a delta-star transformer", Proc.IEE, Vol.121, No.12, pp1513-1521, 1974.

72. PARK, R.H.: "Definition of an ideal synchronous machine and formula for the armature flux linkages", General Electric Review, Vol.31, pp332-334, 1928.